E-ISSN: 2148-6247

Turkish Journal of PHARMACEUTICAL SCIENCES

An Official Journal of the Turkish Pharmacists' Association, Academy of Pharmacy

Volume: 19 Issue: 4 August 2022

www.turkjps.org

Emerging Sources Citation Index

PubMed Central PubMed Scopus TR DİZİN

galenos Publishing House

Turkish Journal of
PHARMACEUTICAL SCIENCES

Turkish Journal of
PHARMACEUTICAL SCIENCES

Turkish Journal of
PHARMACEUTICAL SCIENCES

AIMS AND SCOPE

The Turkish Journal of Pharmaceutical Sciences is the only scientific periodical publication of the Turkish Pharmacists' Association and has been published since April 2004.
Turkish Journal of Pharmaceutical Sciences journal is regularly published 6 times in a year (February, April, June, August, October, December). The issuing body of the journal is Galenos Yayinevi/Publishing House level. The aim of Turkish Journal of Pharmaceutical Sciences is to publish original research papers of the highest scientific and clinical value at an international level.
The target audience includes specialists and professionals in all fields of pharmaceutical sciences.
The editorial policies are based on the "Recommendations for the Conduct, Reporting, Editing, and Publication of Scholarly Work in Medical Journals (ICMJE Recommendations)" by the International Committee of Medical Journal Editors (20, archived at http://www.icmje.org/) rules.

Editorial Independence

Turkish Journal of Pharmaceutical Sciences is an independent journal with independent editors and principles and has no commerical relationship with the commercial product, drug or pharmaceutical company regarding decisions and review processes upon articles.

ABSTRACTED/INDEXED IN

PubMed
PubMed Central
Web of Science-Emerging Sources Citation Index (ESCI)
SCOPUS SJR
TÜBİTAK/ULAKBİM TR Dizin
ProQuest
Chemical Abstracts Service (CAS)
EBSCO
EMBASE
GALE
Index Copernicus
Analytical Abstracts
International Pharmaceutical Abstracts (IPA)
Medicinal & Aromatic Plants Abstracts (MAPA)
British Library
CSIR INDIA
GOALI
Hinari
OARE
ARDI
AGORA
Türkiye Atıf Dizini
Türk Medline
UDL-EDGE
J- Gate
Idealonline
CABI

OPEN ACCESS POLICY

This journal provides immediate open access to its content on the principle that making research freely available to the public supports a greater global exchange of knowledge.
Open Access Policy is based on the rules of the Budapest Open Access Initiative (BOAI) http://www.budapestopenaccessinitiative.org/. By "open access" to peer-reviewed research literature, we mean its free availability on the public internet, permitting any users to read, download, copy, distribute, print, search, or link to the full texts of these articles, crawl them for indexing, pass them as data to software, or use them for any other lawful purpose, without financial, legal, or technical barriers other than those inseparable from gaining access to the internet itself. The only constraint on reproduction and distribution, and the only role for copyright in this domain, should be to give authors control over the integrity of their work and the right to be properly acknowledged and cited.

CORRESPONDENCE ADDRESS

All correspondence should be directed to the Turkish Journal of Pharmaceutical Sciences Editorial Board

Post Address: Turkish Pharmacists' Association, Mustafa Kemal Mah 2147.Sok No:3 06510 Çankaya/Ankara, TÜRKİYE
Phone: +90 (312) 409 81 00
Fax: +90 (312) 409 81 09
Web Page: http://turkjps.org
E-mail: turkjps@gmail.com

PERMISSIONS

Requests for permission to reproduce published material should be sent to the publisher.
Publisher: Erkan Mor
Adress: Molla Gürani Mah. Kaçamak Sok. 21/1 Fındıkzade, Fatih, Istanbul, Türkiye
Telephone: +90 212 621 99 25
Fax: +90 212 621 99 27
Web page: http://www.galenos.com.tr/en
E-mail: info@galenos.com.tr

ISSUING BODY CORRESPONDING ADDRESS

Issuing Body : Galenos Yayınevi
Address: Molla Gürani Mah. Kaçamak Sk. No: 21/, 34093 İstanbul, Türkiye
Phone: +90 212 621 99 25 Fax: +90 212 621 99 27
E-mail: info@galenos.com.tr

MATERIAL DISCLAIMER

The author(s) is (are) responsible for the articles published in the JOURNAL.
The editors, editorial board and publisher do not accept any responsibility for the articles.

Publisher Contact
Address: Molla Gürani Mah. Kaçamak Sk. No: 21/1
34093 İstanbul, Türkiye
Phone: +90 (212) 621 99 25 **Fax:** +90 (212) 621 99 27
E-mail: info@galenos.com.tr/yayin@galenos.com.tr
Web: www.galenos.com.tr | **Publisher Certificate Number:** 14521

Publication Date: August 2022
E-ISSN: 2148-6247
International scientific journal published bimonthly.

Turkish Journal of
PHARMACEUTICAL SCIENCES

INSTRUCTIONS TO AUTHORS

Turkish Journal of Pharmaceutical Sciences journal is published 6 times (February, April, June, August, October, December) per year and publishes the following articles:

- Research articles
- Reviews (only upon the request or consent of the Editorial Board)
- Preliminary results/Short communications/Technical notes/Letters to the Editor in every field of pharmaceutical sciences.

The publication language of the journal is English.

The Turkish Journal of Pharmaceutical Sciences does not charge any article submission or processing charges.

A manuscript will be considered only with the understanding that it is an original contribution that has not been published elsewhere.

The Journal should be abbreviated as "Turk J Pharm Sci" when referenced.

The scientific and ethical liability of the manuscripts belongs to the authors and the copyright of the manuscripts belongs to the Journal. Authors are responsible for the contents of the manuscript and accuracy of the references. All manuscripts submitted for publication must be accompanied by the Copyright Transfer Form [copyright transfer]. Once this form, signed by all the authors, has been submitted, it is understood that neither the manuscript nor the data it contains have been submitted elsewhere or previously published and authors declare the statement of scientific contributions and responsibilities of all authors.

Experimental, clinical and drug studies requiring approval by an ethics committee must be submitted to the JOURNAL with an ethics committee approval report including approval number confirming that the study was conducted in accordance with international agreements and the Declaration of Helsinki (revised 2013) (http://www.wma.net/en/30publications/10policies/b3/). The approval of the ethics committee and the fact that informed consent was given by the patients should be indicated in the Materials and Methods section. In experimental animal studies, the authors should indicate that the procedures followed were in accordance with animal rights as per the Guide for the Care and Use of Laboratory Animals (http://oacu.od.nih.gov/regs/guide/guide.pdf) and they should obtain animal ethics committee approval.

Authors must provide disclosure/acknowledgment of financial or material support, if any was received, for the current study.

If the article includes any direct or indirect commercial links or if any institution provided material support to the study, authors must state in the cover letter that they have no relationship with the commercial product, drug, pharmaceutical company, etc. concerned; or specify the type of relationship (consultant, other agreements), if any.

Authors must provide a statement on the absence of conflicts of interest among the authors and provide authorship contributions.

All manuscripts submitted to the journal are screened for plagiarism using the 'iThenticate' software. Results indicating plagiarism may result in manuscripts being returned or rejected.

The Review Process

This is an independent international journal based on double-blind peer-review principles. The manuscript is assigned to the Editor-in-Chief, who reviews the manuscript and makes an initial decision based on manuscript quality and editorial priorities. Manuscripts that pass initial evaluation are sent for external peer review, and the Editor-in-Chief assigns an Associate Editor. The Associate Editor sends the manuscript to at least two reviewers (internal and/or external reviewers). The Associate Editor recommends a decision based on the reviewers' recommendations and returns the manuscript to the Editor-in-Chief. The Editor-in-Chief makes a final decision based on editorial priorities, manuscript quality, and reviewer recommendations. If there are any conflicting recommendations from reviewers, the Editor-in-Chief can assign a new reviewer.

The scientific board guiding the selection of the papers to be published in the Journal consists of elected experts of the Journal and if necessary, selected from national and international authorities. The Editor-in-Chief, Associate Editors may make minor corrections to accepted manuscripts that do not change the main text of the paper.

In case of any suspicion or claim regarding scientific shortcomings or ethical infringement, the Journal reserves the right to submit the manuscript to the supporting institutions or other authorities for investigation. The Journal accepts the responsibility of initiating action but does not undertake any responsibility for an actual investigation or any power of decision.

The Editorial Policies and General Guidelines for manuscript preparation specified below are based on "Recommendations for the Conduct, Reporting, Editing, and Publication of Scholarly Work in Medical Journals (ICMJE Recommendations)" by the International Committee of Medical Journal Editors (20, archived at http://www.icmje.org/).

Preparation of research articles, systematic reviews and meta-analyses must comply with study design guidelines:

CONSORT statement for randomized controlled trials (Moher D, Schultz KF, Altman D, for the CONSORT Group. The CONSORT statement revised recommendations for improving the quality of reports of parallel group randomized trials. JAMA 2001; 285: 1987-91) (http://www.consort-statement.org/);

PRISMA statement of preferred reporting items for systematic reviews and meta-analyses (Moher D, Liberati A, Tetzlaff J, Altman DG, The PRISMA Group. Preferred Reporting Items for Systematic Reviews and Meta-Analyses: The PRISMA Statement. PLoS Med 2009; 6(7): e1000097.) (http://www.prisma-statement.org/);

STARD checklist for the reporting of studies of diagnostic accuracy (Bossuyt PM, Reitsma JB, Bruns DE, Gatsonis CA, Glasziou PP, Irwig LM, et al., for the STARD Group. Towards complete and accurate reporting of studies of diagnostic accuracy: the STARD initiative. Ann Intern Med 2003;138:40-4.) (http://www.stard-statement.org/);

STROBE statement, a checklist of items that should be included in reports of observational studies (http://www.strobe-statement.org/);

MOOSE guidelines for meta-analysis and systemic reviews of observational studies (Stroup DF, Berlin JA, Morton SC, et al. Meta-analysis of observational studies in epidemiology: a proposal for reporting Meta-analysis of observational Studies in Epidemiology (MOOSE) group. JAMA 2000; 283: 2008-12).

Turkish Journal of
PHARMACEUTICAL SCIENCES

INSTRUCTIONS TO AUTHORS

GENERAL GUIDELINES

Manuscripts can only be submitted electronically through the Journal Agent website (http://journalagent.com/tjps/) after creating an account. This system allows online submission and review.

Format: Manuscripts should be prepared using Microsoft Word, size A4 with 2.5 cm margins on all sides, 12 pt Arial font and 1.5 line spacing.

Abbreviations: Abbreviations should be defined at first mention and used consistently thereafter. Internationally accepted abbreviations should be used; refer to scientific writing guides as necessary.

Cover letter: The cover letter should include statements about manuscript type, single-Journal submission affirmation, conflict of interest statement, sources of outside funding, equipment (if applicable), for original research articles.

ETHICS COMMITTEE APPROVAL

The editorial board and our reviewers systematically ask for ethics committee approval from every research manuscript submitted to the Turkish Journal of Pharmaceutical Sciences. If a submitted manuscript does not have ethical approval, which is necessary for every human or animal experiment as stated in international ethical guidelines, it must be rejected on the first evaluation.

Research involving animals should be conducted with the same rigor as research in humans; the Turkish Journal of Pharmaceutical Sciences asks original approval document to show implements the 3Rs principles. If a study does not have ethics committee approval or authors claim that their study does not need approval, the study is consulted to and evaluated by the editorial board for approval.

SIMILARITY

The Turkish Journal of Pharmaceutical Sciences is routinely looking for similarity index score from every manuscript submitted before evaluation by the editorial board and reviewers. The journal uses iThenticate plagiarism checker software to verify the originality of written work. There is no acceptable similarity index; but, exceptions are made for similarities less than 15 %.

REFERENCES

Authors are solely responsible for the accuracy of all references.

In-text citations: References should be indicated as a superscript immediately after the period/full stop of the relevant sentence. If the author(s) of a reference is/are indicated at the beginning of the sentence, this reference should be written as a superscript immediately after the author's name. If relevant research has been conducted in Türkiye or by Turkish investigators, these studies should be given priority while citing the literature.

Presentations presented in congresses, unpublished manuscripts, theses, Internet addresses, and personal interviews or experiences should not be indicated as references. If such references are used, they should be indicated in parentheses at the end of the relevant sentence in the text, without reference number and written in full, in order to clarify their nature.

References section: References should be numbered consecutively in the order in which they are first mentioned in the text. All authors should be listed regardless of number. The titles of Journals should be abbreviated according to the style used in the Index Medicus.

Reference Format

Journal: Last name(s) of the author(s) and initials, article title, publication title and its original abbreviation, publication date, volume, the inclusive page numbers. Example: Collin JR, Rathbun JE. Involutional entropion: a review with evaluation of a procedure. Arch Ophthalmol. 1978;96:1058-1064.

Book: Last name(s) of the author(s) and initials, book title, edition, place of publication, date of publication and inclusive page numbers of the extract cited.

Example: Herbert L. The Infectious Diseases (1st ed). Philadelphia; Mosby Harcourt; 1999:11;1-8.

Book Chapter: Last name(s) of the author(s) and initials, chapter title, book editors, book title, edition, place of publication, date of publication and inclusive page numbers of the cited piece.

Example: O'Brien TP, Green WR. Periocular Infections. In: Feigin RD, Cherry JD, eds. Textbook of Pediatric Infectious Diseases (4th ed). Philadelphia; W.B. Saunders Company;1998:1273-1278.

Books in which the editor and author are the same person: Last name(s) of the author(s) and initials, chapter title, book editors, book title, edition, place of publication, date of publication and inclusive page numbers of the cited piece. Example: Solcia E, Capella C, Kloppel G. Tumors of the exocrine pancreas. In: Solcia E, Capella C, Kloppel G, eds. Tumors of the Pancreas. 2nd ed. Washington: Armed Forces Institute of Pathology; 1997:145-210.

TABLES, GRAPHICS, FIGURES, AND IMAGES

All visual materials together with their legends should be located on separate pages that follow the main text.

Images: Images (pictures) should be numbered and include a brief title. Permission to reproduce pictures that were published elsewhere must be included. All pictures should be of the highest quality possible, in

JPEG format, and at a minimum resolution of 300 dpi.

Tables, Graphics, Figures: All tables, graphics or figures should be enumerated according to their sequence within the text and a brief descriptive caption should be written. Any abbreviations used should be defined in the accompanying legend. Tables in particular should be explanatory and facilitate readers' understanding of the manuscript, and should not repeat data presented in the main text.

MANUSCRIPT TYPES

Original Articles

Clinical research should comprise clinical observation, new techniques or laboratories studies. Original research articles should include title, structured abstract, key words relevant to the content of the article, introduction, materials and methods, results, discussion, study limitations, conclusion references, tables/figures/images and

Turkish Journal of
PHARMACEUTICAL SCIENCES

INSTRUCTIONS TO AUTHORS

acknowledgement sections. Title, abstract and key words should be written in both Turkish and English. The manuscript should be formatted in accordance with the above-mentioned guidelines and should not exceed 16 A4 pages.

Title Page: This page should include the title of the manuscript, short title, name(s) of the authors and author information. The following descriptions should be stated in the given order:

1. Title of the manuscript (Turkish and English), as concise and explanatory as possible, including no abbreviations, up to 135 characters

2. Short title (Turkish and English), up to 60 characters

3. Name(s) and surname(s) of the author(s) (without abbreviations and academic titles) and affiliations

4. Name, address, e-mail, phone and fax number of the corresponding author

5. The place and date of scientific meeting in which the manuscript was presented and its abstract published in the abstract book, if applicable

Abstract: A summary of the manuscript should be written in both Turkish and English. References should not be cited in the abstract. Use of abbreviations should be avoided as much as possible; if any abbreviations are used, they must be taken into consideration independently of the abbreviations used in the text. For original articles, the structured abstract should include the following sub-headings:

Objectives: The aim of the study should be clearly stated.

Materials and Methods: The study and standard criteria used should be defined; it should also be indicated whether the study is randomized or not, whether it is retrospective or prospective, and the statistical methods applied should be indicated, if applicable.

Results: The detailed results of the study should be given and the statistical significance level should be indicated.

Conclusion: Should summarize the results of the study, the clinical applicability of the results should be defined, and the favorable and unfavorable aspects should be declared.

Keywords: A list of minimum , but no more than 5 key words must follow the abstract. Key words in English should be consistent with "Medical Subject Headings (MESH)" (www.nlm.nih.gov/mesh/MBrowser.html). Turkish key words should be direct translations of the terms in MESH.

Original research articles should have the following sections:

Introduction: Should consist of a brief explanation of the topic and indicate the objective of the study, supported by information from the literature.

Materials and Methods: The study plan should be clearly described, indicating whether the study is randomized or not, whether it is retrospective or prospective, the number of trials, the characteristics, and the statistical methods used.

Results: The results of the study should be stated, with tables/figures given in numerical order; the results should be evaluated according to the statistical analysis methods applied. See General Guidelines for details about the preparation of visual material.

Discussion: The study results should be discussed in terms of their favorable and unfavorable aspects and they should be compared with the literature. The conclusion of the study should be highlighted.

Study Limitations: Limitations of the study should be discussed. In addition, an evaluation of the implications of the obtained findings/results for future research should be outlined.

Conclusion: The conclusion of the study should be highlighted.

Acknowledgements: Any technical or financial support or editorial contributions (statistical analysis, English/Turkish evaluation) towards the study should appear at the end of the article.

References: Authors are responsible for the accuracy of the references. See General Guidelines for details about the usage and formatting required.

Review Articles

Review articles can address any aspect of clinical or laboratory pharmaceuticals. Review articles must provide critical analyses of contemporary evidence and provide directions of or future research. Most review articles are commissioned, but other review submissions are also welcome. Before sending a review, discussion with the editor is recommended.

Reviews articles analyze topics in depth, independently and objectively. The first chapter should include the title in Turkish and English, an unstructured summary and key words. Source of all citations should be indicated. The entire text should not exceed 25 pages (A, formatted as specified above).

Turkish Journal of
PHARMACEUTICAL SCIENCES

CONTENTS

Original Articles

Turkish Journal of
PHARMACEUTICAL SCIENCES

CONTENTS

Turk J Pharm Sci 2022;19(4):371-376
DOI: 10.4274/tjps.galenos.2021.29726

ORIGINAL ARTICLE

Cytotoxic and Apoptotic Effects of the Combination of Borax (Sodium Tetraborate) and 5-Fluorouracil on DLD-1 Human Colorectal Adenocarcinoma Cell Line

Ömer Faruk KIRLANGIÇ[1], Ecem KAYA-SEZGİNER[2], Sema ÖREN[3], Serap GÜR[4], Özlem YAVUZ[5], Taner ÖZGÜRTAŞ[5]*

[1]Gazi University, Faculty of Medicine, Department of Medical Biochemistry, Ankara, Türkiye
[2]Ankara University, Faculty of Pharmacy, Department of Biochemistry, Ankara, Türkiye
[3]University of Health Sciences Türkiye, Gülhane Health Sciences Institute Research Center, Ankara, Türkiye
[4]Ankara University, Faculty of Pharmacy, Department of Pharmacology, Ankara, Türkiye
[5]University of Health Sciences Türkiye, Gülhane Training and Research Hospital, Department of Clinical Biochemistry, Ankara, Türkiye

ABSTRACT

Objectives: Colorectal cancer (CRC) remains a crucial health problem due to the toxicity of 5-Fluorouracil (5-FU) as first-line chemotherapy agent for treating CRC. The anticancer effects of boron and its compounds have been shown in various cell lines. This study aimed to examine the cytotoxic and apoptotic effects of borax (sodium tetraborate) alone or along with 5-FU on human CRC cells, DLD-1.

Materials and Methods: Cytotoxicity and apoptosis were determined by 3-(4,5-dimethylthiazolyl-2)-2,5-diphenyltetrazolium bromide (MTT) assay, 4',6-diamidino-2-phenylindole and annexin V/propidium iodide staining.

Results: The results showed that combined treatment revealed a significant time- and concentration-dependent cytotoxic effect on DLD-1 cells compared with borax or 5-FU treatment alone. The combination of borax and 5-FU induced a clear increase in the early apoptotic cell percentage, compared to the cells treated with monotherapies. Additionally, a significant increase in condensed and fragmented nuclei was detected in DLD-1 cells treated with the combination treatment compared with borax or 5-FU alone.

Conclusion: Our current findings suggest that the combination of borax with 5-FU has a strong cytotoxic and apoptotic effect on the human CRC DLD-1 cells.

Key words: Apoptosis, borax, colorectal adenocarcinoma, DLD-1, 5-fluorouracil

INTRODUCTION

Colorectal cancer (CRC) is the second most commonly identified cancer and is the third leading occur in cancer-related deaths in the worldwide.[1] 5-Fluorouracil (5-FU) has been widely used intravenously as the first-line drug for treating both advanced and early stage CRC.[2] However, the patients' low response rates to therapy, development of chemoresistance and serious adverse reactions severely limit the clinical application of 5-FU in advanced CRC.[3-6] Recently, many aggressive adjuvant therapies combined with 5-FU have been developed to overcome clinical resistance.[7,8] The combination of 5-FU and other agents as an advanced-stage CRC treatment has shown success in prolonging patient survival,[9,10] but leads to increased vulnerability of patients to disease relapse together with high costs and some side effects.[10]

Previous clinical studies have demonstrated the possible beneficial effects of high boron intake in lung and prostate cancer.[11,12] Boron, a nutrient element, is present in food and drinking water and categorized as "probably essential" for humans by the World Health Organization.[13] Boron is found

*Correspondence: taner.ozgurtas@sbu.edu.tr, Phone: +90 32 422 23 03, ORCID-ID: orcid.org/0000-0003-1110-6671
Received: 10.06.2021, Accepted: 08.09.2021

abundantly in nature as boric acid (a soluble form of boron) and inorganic salts called borates.[14,15] Sodium tetraborate known as borax is a salt of boric acid.[15] A study by Wei et al.[15] revealed the anticarcinogenic effect of borax in hepatocellular carcinoma. Another boron compound, boric acid inhibited the proliferation of prostate cancer cell lines, DU-145 and LNCaP[16] and MDA-MB-231 human breast cancer cells[17] and inhibited cell growth, apoptosis, and morphological alterations of DU-145 cells.[18] Currently, bortezomib, which is made from boric acid polymers, is used as an anticancer chemotherapeutic agent for treating multiple myeloma cells.[19] Additionally, boron compounds have been used in neutron capture therapy for different types of cancer.[20,21]

The use of natural products along with a conventional chemotherapeutic agent, 5-FU enhanced efficacy in anti-CRC treatment.[2,22,23] Accordingly, the primary aim of this study was to evaluate the effects of borax (sodium tetraborate) combined with 5-FU on the viability and apoptosis of DLD-1 CRC cells.

MATERIALS AND METHODS

Cell culture and chemical treatments

Human colorectal adenocarcinoma DLD-1 cells (CCL-221) were bought from American Tissue Culture Collection (ATCC, Manassas, VA). The cells were cultured in RPMI-1640 medium (Capricorn Scientific, Germany) supplemented with 10% fetal bovine serum (Gibco, USA) in a humidified incubator (Sanyo MCO-20AIC, California, USA) containing 5% CO_2 at 37°C.

Borax was obtained from Sigma-Aldrich (St. Louis, MO, USA), and prepared as 0.25 M stock solution in RPMI-1640 medium (Capricorn Scientific, Germany). 5-FU was diluted with physiological saline solution to obtain 50 mg/mL stock solution. Both aliquots were stored at -20°C until further experiments.

Cell viability assay

Cell viability was determined by 3-(4,5-dimethylthiazolyl-2)-2,5-diphenyltetrazolium bromide (MTT) assay, as described previously.[24] The effect of borax, either alone or with 5-FU, on CRC cell survival was evaluated by cell viability assay using MTT (Sigma-Aldrich, St. Louis, MO, USA). DLD-1 cells were cultured in 96 well plates (2 x 10^3 cells/well) with 100 µL of complete medium. At the end of 24 h incubation, cells were treated with various concentrations of borax (50 to 1000 µM) or 5-FU (5 to 100 µg/mL). In combination treatment, increasing concentrations of borax ranging from 50 to 500 µM were mixed with IC_{50} value of 5-FU (50 µg/mL) and applied to the wells. Upon 24 and 48 h treatment, 20 µL of MTT reagent (5 mg/mL in RPMI) was added to each well. After 4 h incubation at 37°C, culture medium containing MTT was removed, formazan crystals were dissolved in 100 µL isopropanol. The absorbance of the wells was measured at 590 nm in a micro-plate reader (ThermoScientific, USA).

Quantification of apoptotic cells by flow cytometry

Quantitative assessment of the cell apoptosis rate was determined by the Annexin V-FITC Apoptosis Detection Kit (Thermo Scientific, Waltham, MA, USA) in line with manufacturer's protocol. In the experiments, we selected the IC_{50} concentration of borax (500 µM) and 5-FU (50 µg/mL) for 48 h according to the MTT assay. Firstly, DLD-1 cells were cultured in 25 cm^2 flasks with a density of 1 x 10^6/mL and incubated for 24 h. After treating DLD-1 cells with borax or 5-FU alone or a combination of these reagents for 48 h, cells were harvested by trypsinization and washed twice with cold phosphate buffered saline (PBS) *via* centrifugation at 1000 rpm for 3 min. The cell pellets then were resuspended in 100 µL of 1X Annexin binding buffer and 5 µL of FITC-conjugated Annexin V.[25] After the addition of 20 µL of propidium iodide (PI), samples were vortexed gently and 30 min incubation process was initiated in the dark, then 400 µL of 1X Annexin binding buffer was added into each tube. Finally, the number of viable, necrotic, and apoptotic cells quantified by a flow cytometer (BD Bioscience, USA) with CellQuest software for data analysis.

4',6-Diamidino-2-phenylindole (DAPI) staining

DAPI staining was performed on DLD-1 cells treated with borax, 5-FU, and a combination of both to investigate nuclear morphological changes. After 24 and 48 h incubation in 6-well plates at a density of 2.4 x 10^4 (cells/cm^2), the cells were harvested and centrifuged at 1000 rpm for 10 min. Then, cell pellets were rinsed with PBS and fixed using 100 µL of 4% formaldehyde for 10 min at room temperature. The fixed cells were centrifuged at 3000 rpm for 2 min and cell pellets were washed with sterile PBS.[26] Finally, cells were stained with 20 µL DAPI (Thermo Fisher, USA) at room temperature for 20 min in a dark place. After the incubation, the supernatant was discarded by centrifugation at 3000 rpm for 2 min, and 20 µL of sterile PBS was added to the cell pellet. One µL of the final mixture was placed on slides.[26] Morphological changes in cell nuclei were visualized under the Thermo Fisher EVOS M5000 imaging system equipped with a DAPI filter.

Statistical analysis

Statistical analysis was carried out using SPSS 19.0 for Windows (SPSS, Chicago, IL, USA). The numerical parameters were reported as mean ± standard deviation. Differences between the control and treatment groups were examined by one-way ANOVA test for triplicate experimental data. Test results ($p \leq 0.05$) were considered statistically significant.

RESULTS

Cytotoxicity of borax, 5-FU, and their combination in DLD-1 cells

Based on the results of MTT assay, borax (150-1000 µM) or 5-FU (20-100 µg/mL) treatment for 24 and 48 h suppressed DLD-1 cell growth dose and time-dependently ($p<0.05$), with an IC_{50} value of 500 µM and 50 µg/mL for 48 h, respectively (Figure 1). Additionally, the combination of four different concentrations of borax (150, 200, 250, and 500 µM) with IC_{50} concentration of 5-FU (50 µg/mL) for 24 and 48 h displayed strong growth-inhibitory activity in DLD-1 cells compared with control as shown in Figure 2 ($p<0.05$).

The percentage of viable cell amount was 81.5 ± 4.28 at 150 µM borax and 53.7 ± 3.19 at 50 µg/mL 5-FU in DLD-1 cells for 48 h, while it was decreased to 38.59 ± 2.28 in DLD-1 cells treated with a combination of 150 µM borax with 50 µg/mL FU for 48 h (Figure 2).

Analysis of Annexin V-FITC/PI staining

To quantitatively analyze the apoptosis- and necrosis-related cell death, DLD-1 cells were treated with borax or 5-FU alone or in combination for 48 h and stained with Annexin V-PI. As shown in Figure 3, DLD-1 cells treated with borax or 5-FU alone and borax + 5-FU combination demonstrated significantly increased early (Annexin V+/PI-) and late (Annexin V+/PI+) apoptotic cell percentages compared with untreated control cells. Besides, more apoptotic cell death was observed in combined treatment (66.3%) compared with borax (46.8%) or 5-FU (32.2%) alone in DLD-1 cell lines. Based on the flow cytometry results, the percentage of early apoptotic cells in DLD-1 cells treated by borax (25.5 ± 2.1%) was similar to 5-FU (21.8 ± 1.8%) as a common approved anticancer drug. A significantly greater percentage of early apoptotic cells was found in combination treatment (43.9 ± 3.2%) compared to borax or 5-FU alone. These findings demonstrate that borax and 5-FU could mediate DLD-1 cell growth inhibition through the induction of apoptosis.

Analysis of DAPI staining

To clarify whether combination treatment with borax and 5-FU for 48 h induced apoptosis of DLD-1 cells, DAPI staining was

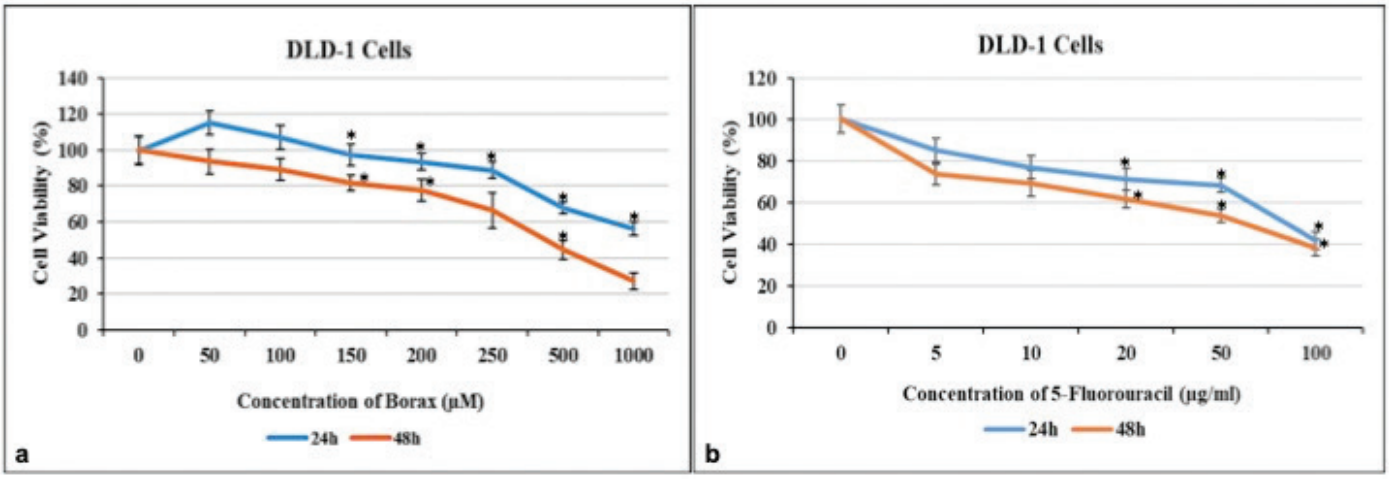

Figure 1. Cytotoxicity of borax (50-1000 µM) and 5-FU (5-100 µg/mL) against DLD-1 cells after 24 and 48 h of treatment. The IC_{50} of borax was 500 µM (a) and the IC_{50} of 5-FU was 50 µg/mL (b) for 48 h. Error bars represent mean ± SD of the three independent experiments

*$p<0.05$ demonstrates the statistical significance between treatment groups and control cells, SD: Standard deviation (n: 3) , 5-FU: 5-Fluorouracil

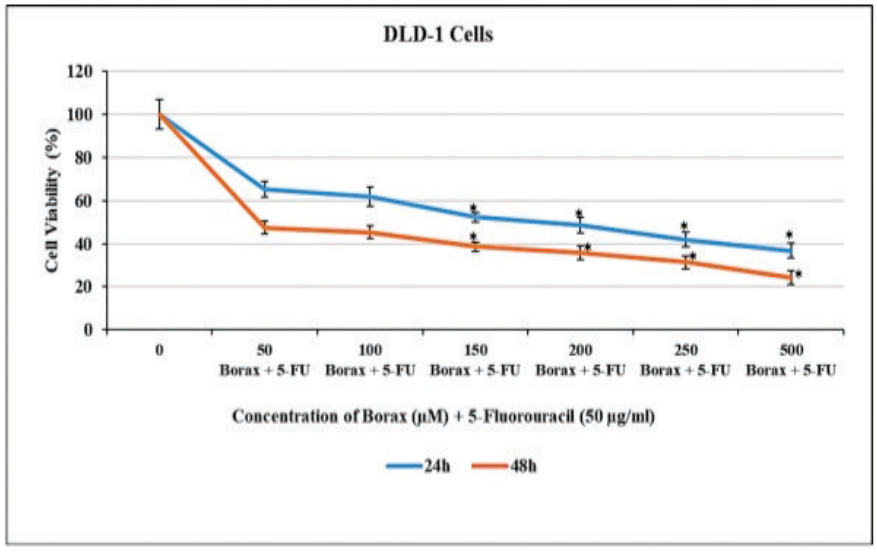

Figure 2. Effects of 5-FU at IC_{50} concentration on the viability of DLD-1 cells after incubation with borax (50, 100, 150, 200, 250 and 500 µM) for 24 and 48 h. Error bars represent mean ± SD of the three independent experiments

*$p<0.05$ demonstrates the statistical significance between treatment groups and control cells, SD: Standard deviation (n: 3), 5-FU: 5-Fluorouracil

conducted. As shown in Figure 4, DLD-1 cells treated with either borax or 5-FU showed fragmented nuclei and cellular disintegration into apoptotic bodies compared with untreated control cells. However, much stronger morphological and apoptotic changes that involve condensed and fragmented nuclei were observed in combination treatment compared with borax or 5-FU alone.

DISCUSSION

No article considers the evaluation of borax, which is a salt of boric acid, on DLD-1 cells with it is cytotoxic and apoptotic effects. In this study, the cytotoxic and apoptotic effects of borax combined with or without 5-FU were investigated on DLD-1 cells. Combined treatment exhibited a more significant reduction in DLD-1 cell viability compared to borax or 5-FU alone in a time and dose-dependent manner. As revealed using different methods (Annexin V-FITC/PI and DAPI staining), it appeared that the anti-proliferative effect of boric acid or 5-FU treatment alone, and their combination on DLD-1 cells is mediated by induction of apoptosis.

In the current study, the concentration of borax between 150 and 1000 µM and 5-FU between 20 and 100 µg/mL reduced the cell proliferation in DLD-1 cells compared with control. Additionally, combination of 150 µM and higher concentrations of borax with 5-FU at 50 µg/mL concentration exerted cytotoxic effects on DLD-1 cells for 24 and 48 h. Similarly, borax treatment inhibited cell proliferation in human hepatocellular carcinoma cell line HepG2.[15] Canturk et al.[27] demonstrated cytotoxic effect of boric

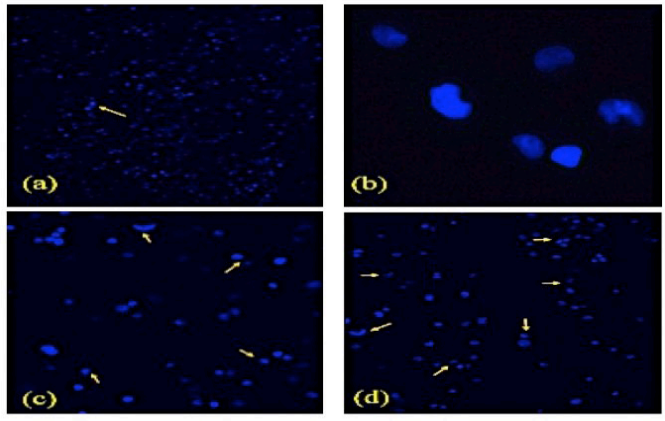

Figure 4. Analysis of DAPI staining. Control group cells (a), DLD-1 cells treated with IC_{50} concentration of borax (500 µM) (b), DLD-1 cells treated with IC_{50} concentration of 5-FU (50 µg/mL) (c), DLD-1 cells treated with borax (500 µM) + 5-FU (50 µg/mL) (d). This was photographed using a confocal inverted microscope with the DAPI filter at magnification of 100X

5-FU: 5-Fluorouracil, DAPI: 4',6-Diamidino-2-phenylindole

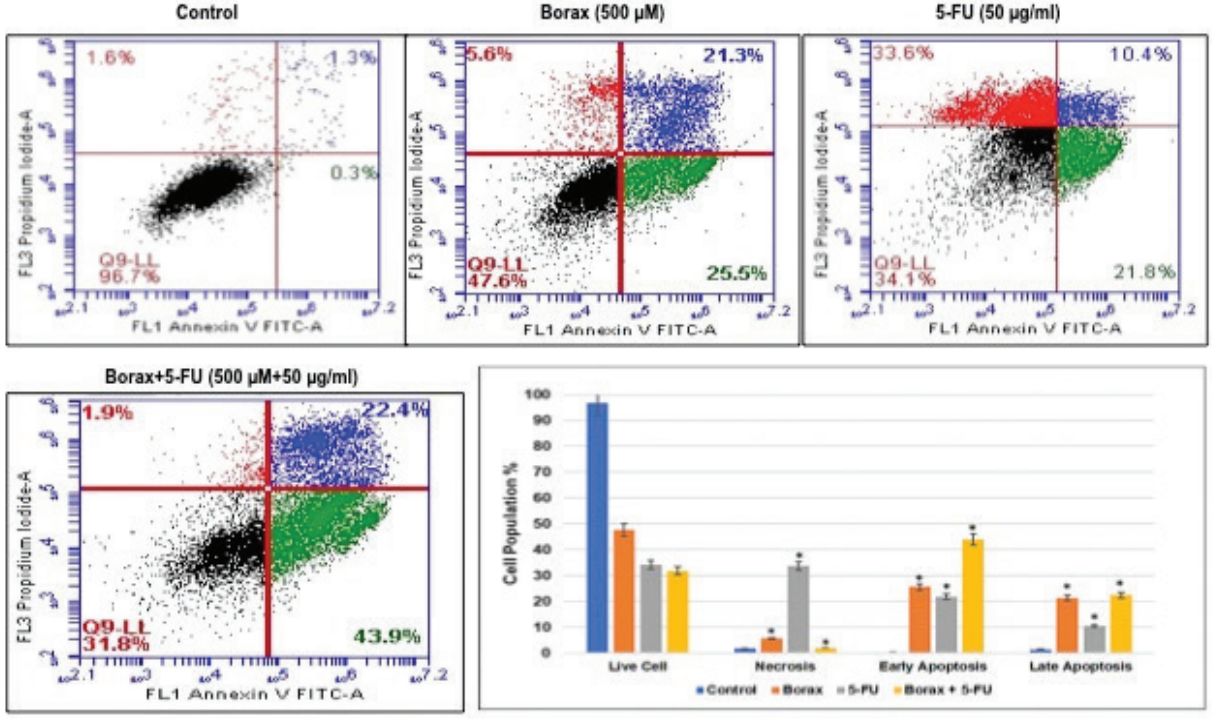

Figure 3. Flow cytometry analysis of DLD-1 cells treated with IC_{50} concentration of borax and 5-FU for 48 h *via* staining with Annexin V-FITC/PI. The lower left quadrant represents viable cells, the lower and upper right quadrant represent early and late apoptotic cells, and the upper left quadrant represents non-viable necrotic cells. Control group cells (a), DLD-1 cells treated with IC_{50} concentration of borax (500 µM) (b), DLD-1 cells treated with IC_{50} concentration of 5-FU (50 µg/mL) (c), DLD-1 cells treated with borax (500 µM) + 5-FU (50 µg/mL) (d). The analysis of viable, necrotic, and early and late apoptotic cells of control DLD-1 cells and those which have been treated with IC_{50} concentration of borax, 5-FU, and both (e). The data present the mean ± SD of three independent experiments

*p<0.05 demonstrates the statistical significance between control cells and treatment groups, SD: Standard deviation (n: 3) , 5-FU: 5-Fluorouracil, PI: Propidium iodide

acid and borax on HL-60 human acute leukemia cell line using MTT. Exposure to boric acid reduced viability of MDA-MB-231 breast cancer cells and DU-145 human prostate cancer cells in a dose-dependent manner.[16,17] Murmu et al.[28] reported that boron compounds inhibited cell growth of myeloid leukemia cell lines (HL-60 and U-937).

According to Annexin V/PI double-staining assay of DLD-1 cells treated with either borax alone (500 µM), 5-FU alone (50 µg/mL) or a combination of the two drugs for 48 h, the early apoptotic rates were 25.5, 21.8, and 43.9%, respectively, compared with the control 0.3%. The percentage of total apoptotic cell amount was 46.8% in the borax-treated group at 500 µM concentration and 32.2% in the 5-FU-treated group at 50 µg/mL concentration. The combined treatment group demonstrated higher percentages of apoptotic cells (66.3%) compared to the either borax or 5-FU treatment alone at 48 h. Similarly, staining of HepG2 cells with Annexin V and PI demonstrated promotion of borax-induced apoptosis.[15] Additionally, a derivative of boric acid, boron oxide, demonstrated significant apoptotic effects for both L929 fibroblast and DLD-1 CRC cell lines.[29] Moreover, borax (a salt of boric acid) and boric acid concentration-dependently induced apoptosis by increasing the expression levels of tumor suppressor p53 gene and decreasing anti-apoptotic Bcl-2 mRNA expression levels in HepG2 human hepatocellular carcinoma cancer cell line.[30] In a previous study by Scorei et al.[17], calcium fructoborate induced apoptosis in MDA-MB-231 breast cancer cells.

To further investigate the apoptotic effects of borax alone or along with 5-FU, DAPI staining was performed. In this study, the induction of apoptosis accompanied by condensed and fragmented nuclei was observed with higher efficiency in DLD-1 cells treated with a combination of borax and 5-FU than monotherapies. Another study demonstrated nuclear fragmentation in boron compound-treated leukemia cells.[27]

CONCLUSION

In conclusion, cancer- and apoptosis-inducing effects of combination of borax and 5-FU were stronger than that of an individual treatment. These results suggest that borax could be a promising adjunct therapeutic agent for CRC by eliminating adverse effects of 5-FU and increasing treatment efficiency. However, further research is needed to identify the underlying molecular mechanisms of borax-induced apoptosis and understand the anticarcinogenic effect of borax in CRC.

Ethics

Ethics Committee Approval: Not necessary.

Informed Consent: There is no requirement for informed consent in the current study.

Peer-review: Externally peer-reviewed.

Authorship Contributions

Concept: Ö.F.K., E.K.S., T.Ö., Design: Ö.F.K., E.K.S., T.Ö., Data Collection or Processing: Ö.F.K., E.K.S., S.Ö., S.G., Ö.Y., T.Ö., Analysis or Interpretation: Ö.F.K., E.K.S., S.Ö., S.G., Ö.Y., T.Ö., Literature Search: Ö.F.K., E.K.S., T.Ö., Writing: Ö.F.K., E.K.S.

Conflict of Interest: No conflict of interest was declared by the authors.

Financial Disclosure: The authors declared that this study received no financial support.

REFERENCES

1. Parkin DM. Global cancer statistics in the year 2000. Lancet Oncol. 2001;2:533-543. Erratum in: Lancet Oncol. 2001;2:596.
2. Hong S, Cai W, Huang Z, Wang Y, Mi X, Huang Y, Lin Z, Chen X. Ginsenoside Rg3 enhances the anticancer effect of 5FU in colon cancer cells *via* the PI3K/AKT pathway. Oncol Rep. 2020;44:1333-1342.
3. Malet-Martino M, Martino R. Clinical studies of three oral prodrugs of 5-fluorouracil (capecitabine, UFT, S-1): a review. Oncologist. 2002;7:288-323.
4. Sanoff HK, Carpenter WR, Freburger J, Li L, Chen K, Zullig LL, Goldberg RM, Schymura MJ, Schrag D. Comparison of adverse events during 5-fluorouracil *versus* 5-fluorouracil/oxaliplatin adjuvant chemotherapy for stage III colon cancer: a population-based analysis. Cancer. 2012;118:4309-4320.
5. Li J, Hou N, Faried A, Tsutsumi S, Kuwano H. Inhibition of autophagy augments 5-fluorouracil chemotherapy in human colon cancer *in vitro* and *in vivo* model. Eur J Cancer. 2010;46:1900-1909.
6. Vodenkova S, Buchler T, Cervena K, Veskrnova V, Vodicka P, Vymetalkova V. 5-Fluorouracil and other fluoropyrimidines in colorectal cancer: past, present and future. Pharmacol Ther. 2020;206:107447.
7. O'Connell MJ. Oxaliplatin or irinotecan as adjuvant therapy for colon cancer: the results are in. J Clin Oncol. 2009;27:3082-3084.
8. Carrato A. Adjuvant treatment of colorectal cancer. Gastrointest Cancer Res. 2008;2(Suppl 4):S42-S46.
9. Pitot HC, Goldberg RM. Future directions in adjuvant therapy for stage III colon carcinoma. Oncology (Williston Park). 2001;15(3 Suppl 5):31-36.
10. Braun MS, Seymour MT. Balancing the efficacy and toxicity of chemotherapy in colorectal cancer. Ther Adv Med Oncol. 2011;3:43-52.
11. Mahabir S, Spitz MR, Barrera SL, Dong YQ, Eastham C, Forman MR. Dietary boron and hormone replacement therapy as risk factors for lung cancer in women. Am J Epidemiol. 2008;167:1070-1080.
12. Cui Y, Winton MI, Zhang ZF, Rainey C, Marshall J, De Kernion JB, Eckhert CD. Dietary boron intake and prostate cancer risk. Oncol Rep. 2004;11:887-892.
13. Del Rosso JQ, Plattner JJ. From the test tube to the treatment room: fundamentals of boron-containing compounds and their relevance to dermatology. J Clin Aesthet Dermatol. 2014;7:13-21.
14. Devirian TA, Volpe SL. The physiological effects of dietary boron. Crit Rev Food Sci Nutr. 2003;43:219-231.
15. Wei Y, Yuan FJ, Zhou WB, Wu L, Chen L, Wang JJ, Zhang YS. Borax-induced apoptosis in HepG2 cells involves p53, Bcl-2, and Bax. Genet Mol Res. 2016;15.
16. Barranco WT, Eckhert CD. Boric acid inhibits human prostate cancer cell proliferation. Cancer Lett. 2004;216:21-29.
17. Scorei R, Ciubar R, Ciofrangeanu CM, Mitran V, Cimpean A, Iordachescu D. Comparative effects of boric acid and calcium fructoborate on breast cancer cells. Biol Trace Elem Res. 2008;122:197-205.
18. Kar F, Hacioglu C, Kacar S, Sahinturk V, Kanbak G. Betaine suppresses cell proliferation by increasing oxidative stress-mediated apoptosis and

inflammation in DU-145 human prostate cancer cell line. Cell Stress Chaperones. 2019;24:871-881.

19. Baker SJ, Ding CZ, Akama T, Zhang YK, Hernandez V, Xia Y. Therapeutic potential of boron-containing compounds. Future Med Chem. 2009;1:1275-1288.
20. Kageji T, Nagahiro S, Kitamura K, Nakagawa Y, Hatanaka H, Haritz D, Grochulla F, Haselsberger K, Gabel D. Optimal timing of neutron irradiation for boron neutron capture therapy after intravenous infusion of sodium borocaptate in patients with glioblastoma. Int J Radiat Oncol Biol Phys. 2001;51:120-130.
21. Takagaki M, Powell W, Sood A, Spielvogel BF, Hosmane NS, Kirihata M, Ono K, Masunaga SI, Kinashi Y, Miyatake SI, Hashimoto N. Boronated dipeptide borotrimethylglycylphenylalanine as a potential boron carrier in boron neutron capture therapy for malignant brain tumors. Radiat Res. 2001;156:118-122.
22. Langner E, Lemieszek MK, Rzeski W. Lycopene, sulforaphane, quercetin, and curcumin applied together show improved antiproliferative potential in colon cancer cells *in vitro*. J Food Biochem. 2019;43:12802.
23. Carriere PP, Kapur N, Mir H, Ward AB, Singh S. Cinnamtannin B-1 inhibits cell survival molecules and induces apoptosis in colon cancer. Int J Oncol. 2018;53:1442-1454.
24. Alper M, Kockar F. IL-6 upregulates a disintegrin and metalloproteinase with thrombospondin motifs 2 (ADAMTS-2) in human osteosarcoma cells mediated by JNK pathway. Mol Cell Biochem. 2014;393:165-175.
25. Singh S, Chitkara D, Mehrazin R, Behrman SW, Wake RW, Mahato RI. Chemoresistance in prostate cancer cells is regulated by miRNAs and Hedgehog pathway. PLoS One. 2012;7:e40021.
26. Sarkhosh-Inanlou R, Molaparast M, Mohammadzadeh A, Shafiei-Irannejad V. Sanguinarine enhances cisplatin sensitivity *via* glutathione depletion in cisplatin-resistant ovarian cancer (A2780) cells. Chem Biol Drug Des. 2020;95:215-223.
27. Canturk Z, Tunali Y, Korkmaz S, Gulbaş Z. Cytotoxic and apoptotic effects of boron compounds on leukemia cell line. Cytotechnology. 2016;68:87-93.
28. Murmu N, Ghosh P, Gomes A, Mitra S, Das M, Besra SE, Majumdar J, Bhattacharya S, Sur P, Vedasiromoni JR. Antineoplastic effect of new boron compounds against leukemic cell lines and cells from leukemic patients. J Exp Clin Cancer Res. 2002;21:351-356.
29. Albuz Ö, Dülger D, Tunali BÇ, Aydin F, Yalçin S, Türk M. Effects of B2O3 (boron trioxide) on colon cancer cells: our first-step experience and *in vitro* results. Turk J Biol. 2019;43:209-223.
30. El-Hefny IM, Al Senosy NK, Hozayen WG, Ahmed AE, Diab A, Basal WT. Evaluation of the cytotoxicity and apoptotic induction in human liver cell lines exposed to three food additives. Recent Pat Food Nutr Agric. 2020;11:193-201.

Turk J Pharm Sci 2022;19(4):377-382
DOI: 10.4274/tjps.galenos.2021.96493

ORIGINAL ARTICLE

In Vitro Antioxidant and Enzyme Inhibition Activity of *Tanacetum argyrophyllum* (K. Koch) Tzvelev var. *argyrophyllum* Extract

Nuraniye ERUYGUR[1]*, Kevser TABAN AKÇA[2], Osman ÜSTÜN[2], Mehmet TEKİN[3]

[1]Selçuk University, Faculty of Pharmacy, Department of Pharmacognosy, Konya, Türkiye
[2]Gazi University, Faculty of Pharmacy, Department of Pharmacognosy, Ankara, Türkiye
[3]Trakya University, Faculty of Pharmacy, Department of Pharmaceutical Botany, Edirne, Türkiye

ABSTRACT

Objectives: *Tanacetum* L. belongs to Asteraceae family and is represented by 46 species in Türkiye. *Tanacetum* genus is known for its insecticide and insect repellent effect. *T. argyrophyllum* contains sesquiterpene lactone derivatives. These compounds are responsible for its various activities, especially cytotoxic, antitumor, phytotoxic, antimicrobial, antiviral, and antifungal activity. There are not enough biological activity studies on the plant that are likely to have a wide variety of activities in terms of the compounds it contains. The aim of the present study is to evaluate various biological activities of 80% aqueous methanol extract prepared from aerial parts of *T. argyrophyllum* (K. Koch) Tzvelev var. *argyrophyllum* collected from Sivas province of Turkey.

Materials and Methods: Antioxidant activity of the methanol extract was determined by 2,2'-diphenyl-1-picryl-hydrazyl and 2,2-azinobis (3-ethyl benzothiazoline-6-sulfonic acid) radical scavenging activity, total phenolic, and total flavonoid content tests. Acetylcholinesterase (AChE) and butyrylcholinesterase (BChE) inhibitory activities were investigated *via* Ellman's spectrometric method.

Results: Total phenolic content was found as 71.67 mg/gallic acid equivalent g and total flavonoid content was 25.225 mg/quercetin equivalent g on a dry extract weight basis. In this work, AChE, BChE, and α-glycosidase enzymes were inhibited by the extract of *T. argyrophyllum* var. *argyrophyllum*. IC_{50} values for these enzymes were found as 266.79 µg/mL for AChE and 176.91 µg/mL for BChE. Also, the α-glycosidase activity exhibited a dose-dependent manner with increasing concentration.

Conclusion: According to the results, *T. argyrophyllum* var. *argyrophyllum* can be used as an ingredient of functional foods as well as herbal products for diabetic and Alzheimer's disease patients.

Key words: *Tanacetum argyrophyllum* var. *argyrophyllum*, antioxidant, acetylcholinesterase, butyrylcholinesterase, antidiabetic

INTRODUCTION

Asteraceae family has approximately 1535 genera around the world, while 138 genera and 1186 species in Türkiye.[1] The genus *Tanacetum* L. is one of the largest genera in this family and is represented by 46 species, 18 subspecies, and 5 varieties, where its 26 taxa are endemic to Türkiye.[2] Several members of *Tanacetum* include medicinally important taxa. According to recent literature, essential oils and extracts of *Tanacetum* species have antiinflammatory, antibacterial, antifungal, anti-Alzheimer, and insecticidal effects.[3] Various biological activities are thought to associate with sesquiterpene lactone content of *Tanacetum* species.[4] The interest in the *Tanacetum* species is increasing day by day due to the fact that it is effective against many diseases due to it is powerful secondary metabolites such as essential oil, sesquiterpenes, sesquiterpene lactones, flavonoids, coumarins, tannins, and sterols.[5,6] However, there are not enough studies on the biological activity of *Tanacetum argyrophyllum* (K. Koch) Tzvelev var. *argyrophyllum* except for their antimicrobial activity.[7]

This study was presented as an oral lecture at the International Symposium on Medicinal, Aromatic and Dye Plants, Malatya, Turkey, 2017.

***Correspondence:** nuraniye.eruygur@selcuk.edu.tr, **Phone:** +90 332 223 34 65, **ORCID-ID:** orcid.org/0000-0002-4674-7009
Received: 07.04.2021, **Accepted:** 14.09.2021

Alzheimer's disease (AD) is a neurological disorder characterized by decreased cognitive functions, daily activities, behavioral changes, and psychiatric symptoms.[8] Acetylcholine is a neurotransmitter released from the synapse of neurons and the biochemical changes in AD are closely related to the reduction of acetylcholine levels in the brain neurons.[9] Acetylcholinesterase (AChE) has become impressive in drug design studies. Cholinesterase inhibitors are commonly used in AD therapy; however, they can have serious side effects such as gastrointestinal disturbances, fatigue or depression.[10] The drawbacks of these licensed drugs have pushed researchers to find new and potential inhibitors of AChE and butyrylcholinesterase (BChE) from plants that have therapeutic properties.

Diabetes mellitus is a metabolic disease marked by an excessive increase in blood glucose levels, which is regulated by α-glucosidase and α-amylase enzymes. α-Amylase initiates carbohydrate digestion by hydrolyzing polysaccharide 1,4-glycosidic linkages to disaccharides. α-Glucosidase converts disaccharides into monosaccharides, which causes blood glucose levels to increase after meals.[11] α-Glucosidase inhibitors (AGIs) are a new class of antidiabetic medicines that can control blood sugar levels by inhibiting glycosidase competitively and preventing sugar breakdown. However, AGI drugs are not satisfactory because of fewer in their numbers, lower bioavailability, and gastrointestinal problems.[12] Therefore, there is a need to research out new and safer AGI inhibitor drugs from natural products.

In the literature review, there are not enough biological activity studies on the *T. argyrophyllum* var. *argyrophyllum*. Therefore, the aim of this study was to evaluate the antioxidant, anti-AChE, anti-BChE, α-glucosidase, and α-amylase activity of *T. argyrophyllum* var. *argyrophyllum* methanol extract *in vitro*. Total phenolic content (TPC) and total flavonoid content (TFC); as well as 2,2-azinobis (3-ethyl benzothiazoline-6-sulfonic acid) diammonium salt (ABTS) and 2,2'-diphenyl-1-picryl-hydrazyl (DPPH) radical scavenging assays, were used to assess the antioxidant capacity. AChE and BChE inhibition methods were used to determine the anti-Alzheimer activity. α-Glucosidase and α-amylase enzyme inhibition approaches were used to assess the anti-diabetic activity.

MATERIALS AND METHODS

Chemicals

DPPH, ABTS, butylated hydroxy anisole (BHA), α-glucosidase (from *Saccharomyces cerevisiae*, type I, lyophilized powder), AChE (from electric eel type-VI-S, EC 3.1.1.7) and BChE (from horse serum, EC 3.1.1.8), 5,5'-dithiobis (2-nitrobenzoic) acid (DTNB), acetylthiocholine iodide (AChI), butyrylthiocholine chloride (BChC), and galantamine were obtained from Sigma Chemicals Co. (St. Louis, MO, USA). All of the other chemicals used were of analytical grade.

Plant material

The plant material was gathered from a natural habitat during the flowering period. Locality data of collection: Turkey- B6 Sivas: Şerefiye to Suşehri, of Abdiağa Çeşmesi, steep slope, 39° 59' 41,2" N, 37° 43' 45,7" E, 1529 m, June 27, 2016, M. Tekin 1739. The dried specimens were preserved at the Sivas Cumhuriyet University, Faculty of Science Herbarium, Department of Biology, Sivas, Türkiye. Taxonomical identification was done based on the Flora of Türkiye (Davis, 1966) by botanist Dr. Mehmet Tekin, Trakya University (Edirne, Türkiye), Department of Pharmaceutical Botany.

Preparation of the extract

The plant's aerial parts were dried at room temperature. Then, the dried materials were grounded to powder using a laboratory type mill and macerated with methanol:water: 80:20 (v/v) for 24 h at room temperature. The extracts were filtered and the solvent was removed by rotary evaporation at 40°C. This extraction process was repeated with the residue three times (24 h x 3). Extract obtained from the process was held at +4°C until it was used.

Antioxidant activity

Determination of total phenolic content

TPC was determined as gallic acid equivalent (GAE) according to the procedure.[13] In a test tube, 2.5 mL of 7.5% sodium carbonate solution and 2.5 mL of 0.1 N Folin-Ciocalteu's reagent were combined with 500 µL of test solution (2 mg/mL). After vortexing, the tubes were left in the dark for 2 h and the absorbance was measured using a ultraviolet-visible (UV-vis) spectrophotometer (Shimadzu, UV-VIS 1800, Japan) at 730 nm. The extract's TPC was calculated as mg GAE *per* gram of dry extract.

Estimation of total flavonoid content

TFC was measured by a colorimetric method using aluminum chloride according to the procedure of Yang et al.[14] and the results were given in milligrams of quercetin equivalent (QE) *per* gram of dry extract. TFC was calculated using an equation derived from the normal concentration-response graph of quercetin.

DPPH radical scavenging activity

DPPH radical scavenging capacity of the extract and standards (BHA and BHT) was evaluated using the previously described method with slight modifications.[15] Various concentrations of test sample (100 µL) were combined with 100 µL of methanol containing DPPH (0.1 mM) and incubated at 25°C for 30 min in the dark. The absorbance was read with a UV-vis spectrophotometer at 517 nm. Percentage of inhibition was found according to the formula:

% inhibition= $(A_0-A_t)/A_0*100$,

where A_0 represents the absorbance of the control without sample and A_t represents the absorbance of test solution.

ABTS radical scavenging assay

The assay of $ABTS^{\bullet+}$ radical cation decolorization was used to assess radical scavenging activity of the extract according to the method of Re et al.[16] The stock solution of $ABTS^{\bullet+}$ was generated by mixing 2.45 mmol/L potassium persulfate with

7 mmol/L ABTS. The mixture stood for in the dark at room temperature for 12-16 h. Diluting the stock with methanol yielded an $ABTS^{\bullet+}$ working solution; the absorbance was 0.70 ± 0.02 at 734 nm. 100 µL sample solution was combined with 100 µL of $ABTS^{\bullet+}$ working solution and incubated for 7 min at 25°C. A UV-vis spectrophotometer set to 734 nm was used to read the absorbance of the mixture.

Determination of anticholinesterase inhibition activity

The inhibitory activities of AChE and BChE were determined using Ellman's spectrophotometric method[17] with minor modifications. In a 96 well-plate, 0.14 mL of 0.1 mM sodium phosphate buffer (pH 8.0), 0.02 mL test sample, and 0.02 mL AChE (0.22 U/mL) or BChE (0.1 U/mL) solution were combined and incubated at 25°C for 15 min before adding 10 µL of 0.5 mM DTNB. The reaction was started with the addition of 10 µL of 0.71 mM AChI or 0.2 mM BChC to the mixture. The substrate's hydrolysis was estimated at 412 nm. By comparing the reactions of the samples with a blank, the percentage inhibition of AChE/BChE was calculated.

Antidiabetic activity

Inhibition of α-glucosidase

Inhibitory activity of the extract against α-glucosidase was measured using the method reported by Abirami et al.[18] Test sample (50 µL) was combined with 0.1 mL of 0.1 M phosphate buffer (pH 6.8) and 0.1 mL of 1 U/mL α-glucosidase solution and incubated for 5 min at 25°C. After pre-incubation, 0.1 mL of 5 mM *p*-nitrophenyl-*α-D*-glucopyranoside solution was applied to the reaction mixture, which was then incubated for 10 min at 25°C. The absorbance at 405 nm was then measured and percent inhibition of α-glucosidase was estimated.

Inhibition of α-amylase

Inhibitory activity of the extract against α-amylase was investigated using the method reported by Ademiluyi and Oboh.[19] After boiling 0.5 g potato starch in 0.1 L phosphate buffer (pH 6.8) for 5 min, the substrate was cooled to 25°C. In a 96 well plate, 20 µL of samples in different concentrations, 50 µL of 0.1 M phosphate buffer (pH 6.8) and 10 µL of 2 U/mL α-amylase solution were applied, and the mixture was incubated at 37°C for 15 min. Following the preincubation, 20 µL of starch solution was added. Then, 100 µL of 3,5-dinitrosalicylic acid was added to the mixture as a coloring reagent and left in hot water for 10 min. Then, the absorbance was read using a microplate reader (Epoch, USA) at 540 nm, and acarbose was used as a positive control.

Statistical analysis

The results are presented as mean ± standard deviation (SD) of three parallel measurements. The analysis of variance was carried out with Graphpad prism software 7.0 (USA). Significant differences between means were determined using the student's *t*-test with $p<0.05$ considered significant.

RESULTS AND DISCUSSION

As part of our study on the biological activity of medicinal plants growing in Sivas province (Türkiye), *in vitro* antioxidant, anticholinesterase, and antidiabetic potential of an endemic species, *i.e. T. argyrophyllum* var. *argyrophyllum* was investigated. This research is the first to report on different biological activity investigations of *T. argyrophyllum* var. *argyrophyllum* except for its essential oil.

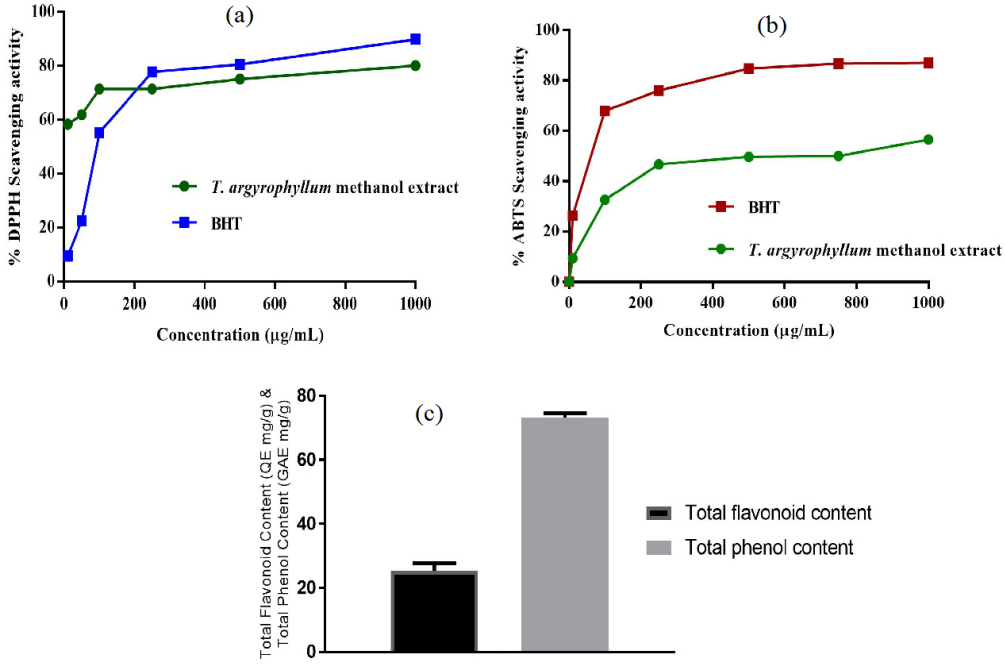

Figure 1. Total antioxidant activity results of *Tanacetum argyrophyllum* var. *argyrophyllum* aqueous methanol extract by DPPH, ABTS, TPC, and TFC methods
DPPH: 2,2'-Diphenyl-1-picryl-hydrazyl, ABTS: 2,2-Azinobis (3-ethyl benzothiazoline-6-sulfonic acid) diammonium salt, TPC: Total phenolic content, TFC: Total flavonoid content

In vitro antioxidant activity

Antioxidant activity of the aqueous methanol extract prepared from the aerial part of *T. argyrophyllum* var. *argyrophyllum* was evaluated using different *in vitro* methods. Total flavonoid and phenolic contents, as well as DPPH free radical and ABTS cation radical decolorization methods were used to assess the antioxidant activity. The results are given in Figure 1. Considering the antiradical activity, *T. argyrophyllum* var. *argyrophyllum* aqueous methanol extract exerted a remarkable DPPH scavenging effect, even stronger than that of standard (BHT) from 250 to 1000 µg/mL concentration. As for ABTS radical-scavenging effect, the aqueous methanol extract of *T. argyrophyllum* var. *argyrophyllum* demonstrated concentration-dependent activity; but showed lower radical scavenging activity than the reference (BHT).

Calibration equations were calculated as Y= 0.0066x + 0.1146 (R^2= 0.9981) for TPC generated from gallic acid and Y= 0.0023x + 0.1247 (R^2= 0.9971) for TFCs prepared from quercetin. Results of total phenol and flavonoid contents in the extract are shown in Figure 1. The aqueous methanol extract obtained from the aerial part of *T. argyrophyllum* var. *argyrophyllum* was found to contain total phenol amount (71.67 mg/GAE g) as GAE and TFC (25.225 mg/QE g) as QE on the dry weight basis of the extract. Wu et al.[20] identified phenolic compounds of *T. parthenium* and 3,5-, 4,5- and 3,4-di-*O*-caffeoylquinic acids were characterized as major compounds causing potent antioxidant activity of the plant. In another study, methanol extracts of three *T. densum* subspecies were screened for their antioxidant activities and a positive correlation was found between their TPC and antioxidant activity.[21] Herein, flavonoid and phenolic compounds, which may be found in the methanol extract are supposed to be responsible for the antioxidant activity of *T. argyrophyllum* var. *argyrophyllum*.

Anticholinesterase inhibition assay

AChE and BChE inhibitory activities of *T. argyrophyllum* var. *argyrophyllum* aqueous methanol extract was determined by Ellman's spectrophotometric method. The extract was tested at different concentrations (10, 100, 250, 500, 1000, and 2000 µg/mL), the concentration-enzyme inhibition graph was generated, and compared with the standard (galantamine) (Figure 2). A lower IC_{50} value indicates higher enzyme inhibition activity. IC_{50} values of the extract were obtained 266.79 µg/mL for AChE, 176.91 µg/mL for BChE. As can be seen from the antioxidant activity results, enzyme inhibition activity seems to be in

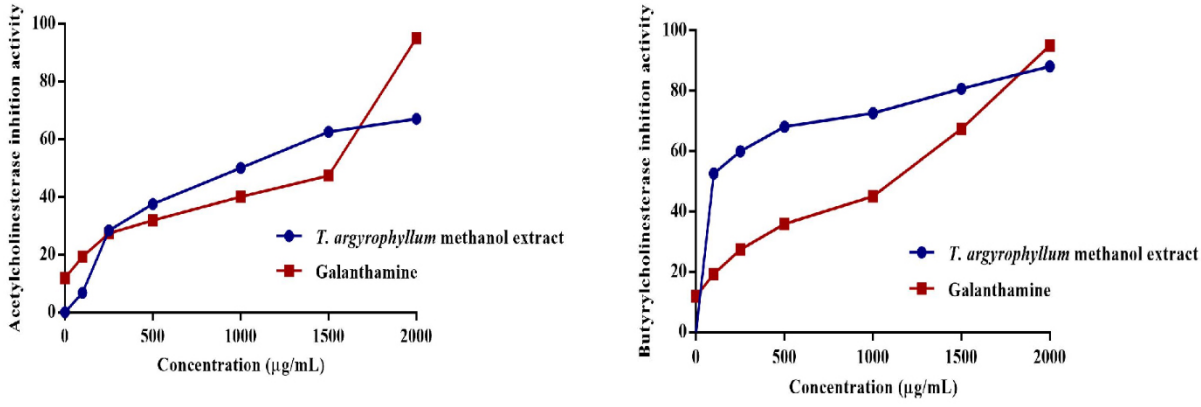

Figure 2. AChE and BChE inhibitory results of *Tanacetum argyrophyllum* var. *argyrophyllum* aqueous methanol extract with reference compound (galantamine)

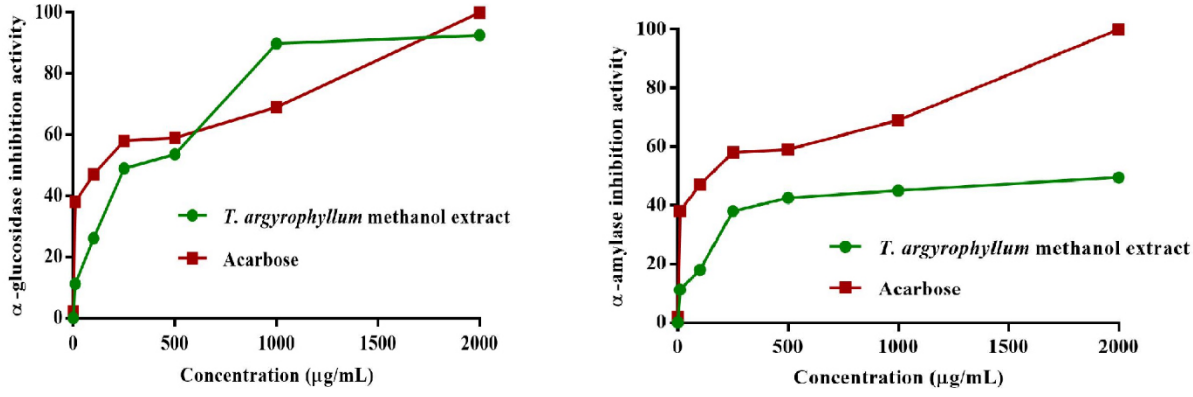

Figure 3. α-Glucosidase and α-amylase inhibitory results of *Tanacetum argyrophyllum* var. *argyrophyllum* aqueous methanol extract with reference compound (acarbose)

accordance with total phenols and flavonoids contained. Wszelaki et al.[22] observed that the methanolic and hexane extracts of *T. parthenium* Sch. Bip. ranged from 32.4% to 40.9% against AChE and BChE at a concentration of 400 µg/mL. Orhan et al.[23] investigated different *Tanacetum* taxa for their cholinesterase inhibitory activity and found that the leaf of *T. argenteum* (Lam.) Willd. subsp. *flabellifolium* (Boiss. & Heldr.) Grierson had the highest inhibition of 96.68% at 100 µg/mL concentration against AChE, while *T. argyrophyllum* var. *argyrophyllum* showed the best inhibition of 63.81% against BChE. However, parthenolide, the main constituent of *Tanacetum* taxa has demonstrated lower inhibition activity against both enzymes. It can be concluded that the major compound parthenolide found in most *Tanacetum* taxa may not be active principle for their anticholinesterase activity or it can exert its activity by synergistic effect with other secondary metabolites. AChE inhibitory activity was tested on the essential oil of *T. densum* (Labill.) Heywood ssp. *sivasicum* Hub. - Mor. & Grierson and *T. mucroniferum* Hub. - Mor. & Grierson. Pure oil showed 100% inhibition, however, dilutions demonstrated lower inhibition.[24] In another study on *T. vulgare* L. root, polyacetylenes were identified as the active zone for its antibacterial, antioxidant, and AChE inhibitory effects by HPTLC combined with *in situ* effect-directed analysis and spectrometric techniques.[25]

Antidiabetic activity assays

Inhibition of α-amylase contributes to improving the symptoms of type-2 diabetes by delaying or cutting glucose absorption because of slowing starch digestion. While the primary goal of α-amylase inhibition is to reduce the rate, at which maltose and glucose are produced from starch, this enzyme can slow down the function of α-glucosidase by eliminating the substrate.[26] *T. argyrophyllum* var. *argyrophyllum* aqueous methanol extract concentration-dependently inhibited both α-glucosidase and α-amylase activity *in vitro* (IC_{50} of 234.77 ± 1.76 µg/mL and 806.68 ± 2.36 µg/mL, respectively) compared with the positive control (acarbose) (Figure 3). A previous study on antidiabetic and enzyme inhibition properties of *T. praeteritum* (Horw.) Heywood essential oil revealed that the oil has a noteworthy inhibitory activity with IC_{50} of 0.89 ± 0.13 mg/mL against porcine pancreatic α-amylase.[27] In another study, *T. poteriifolium* ethyl acetate extract exhibited inhibition in α-glucosidase (23.67 mmol acarbose equivalent/g extract)[28] *T. nubigenum*, a Himalayan medicinal plant from India, showed potent stimulation of glucose uptake with + 61.2% in C_2Cl_2 myotubes. Also, ethanol extract of *T. nubigenum* decreased blood glucose level significantly in STZ induced Sprague-Dawley rats (15.5%).[29]

CONCLUSION

According to the literature review, this study is the first investigation of *T. argyrophyllum* var. *argyrophyllum* in terms of antioxidant and enzyme inhibitory activities. This study showed that the aqueous methanol extract possessed polar compounds, which are rich in phenolic and flavonoid compounds, have strong antiradical, AChE, BChE, and AGI activity, while it demonstrated moderate α-amylase inhibitory activity. This work will provide important scientific data for further phytochemical and biological activity-guided studies on the polar extract of *T. argyrophyllum* var. *argyrophyllum* to identify active principles that are attributed to the strong activity. However, to identify the active phytochemicals responsible for the antioxidant and enzyme inhibition activity, bioactivity-guided chromatographic fractionation and isolation must be performed.

ACKNOWLEDGMENTS

The authors want to thank the Sivas Cumhuriyet University Faculty of Pharmacy and Advanced Technology Research Center for providing laboratory facilities. This study was partly funded by Sivas Cumhuriyet University Scientific Research Project (CUBAP no: ECZ26 and ECZ31).

Ethics

Ethics Committee Approval: Not required.

Informed Consent: Not applicable.

Peer-review: Externally peer-reviewed.

Authorship Contributions

Concept: N.E., Design: N.E., Data Collection or Processing: N.E., K.T.A., O.Ü., M.T., Analysis or Interpretation: N.E., K.T.A., O.Ü., M.T., Literature Search: N.E., K.T.A., Writing: N.E., K.T.A.

Conflict of Interest: No conflict of interest was declared by the authors.

Financial Disclosure: This study was partly funded by the Sivas Cumhuriyet University Scientific Research Projects (CUBAP no: ECZ26 and ECZ31).

REFERENCES

1. Davis, HP. Flora of Turkey and The East Aegean Islands. Edingburgh; Edinburgh University Press; 1982.
2. Güner A. Türkiye Bitkileri Listesi, Damarlı Bitkiler (1st ed). İstanbul; Nezahat Gökyiğit Botanik Bahçesi Yayınları; 2012.
3. Akpulat HA, Tepe B, Sokmen A, Daferera D, Polissiou, M. Composition of the essential oils of *Tanacetum argyrophyllum* (K. Koch) Tzvelev. var. *argyrophyllum* and *Tanacetum parthenium* (L.) Schultz Bip. (Asteraceae) from Turkey. Biochem Syst Ecol. 2005;33:511-516.
4. Gören N, Arda N, Çaliskan Z. Chemical characterization and biological activities of the genus *Tanacetum* (Compositae). Stud Nat Prod Chem. 2002;27:547-658.
5. Kumar V, Tyagi, D. Chemical composition and biological activities of essential oils of genus *Tanacetum* - a review. J Pharmacogn Phytochem. 2013;2:159-163.
6. Abad MJ, Bermejo P, Villar A. An approach to the genus *Tanacetum* L. (Compositae): phytochemical and pharmacological review. Phyther Res. 1995;9:79-92.
7. Polatoglu K, Demirci F, Demirci B, Gören N, Can Baser KH. Antimicrobial activity and essential oil composition of a new *T. argyrophyllum* (K. Koch) Tzvelev var. *argyrophyllum* chemotype. J Oleo Sci. 2010;59:307-313.
8. Öztürk M, Duru ME, Kivrak S, Mercan-Doğan N, Türkoglu A, Özler MA. *In vitro* antioxidant, anticholinesterase and antimicrobial activity studies on

three *Agaricus* species with fatty acid compositions and iron contents: a comparative study on the three most edible mushrooms. Food Chem Toxicol. 2011;49:1353-1360.

9. Aktumsek A, Zengin G, Guler GO, Cakmak YS, Duran A. Antioxidant potentials and anticholinesterase activities of methanolic and aqueous extracts of three endemic *Centaurea* L. species. Food Chem Toxicol. 2013;55:290-296.
10. Orhan IE, Sezer Senol F, Ercetin T, Kahraman A, Celep F, Akaydin G, Sener B, Dogan M. Assessment of anticholinesterase and antioxidant properties of selected sage (*Salvia*) species with their total phenol and flavonoid contents. Ind Crops Prod. 2013;41:21-30.
11. Poovitha S, Parani M. *In vitro* and *in vivo* α-amylase and α-glucosidase inhibiting activities of the protein extracts from two varieties of bitter gourd (*Momordica charantia* L.). BMC Compl Alternative Med. 2016;16(Suppl 1):185.
12. Liu S, Yu Z, Zhu H, Zhang W, Chen Y. *In vitro* α-glucosidase inhibitory activity of isolated fractions from water extract of qingzhuan dark tea. BMC Compl Alternative Med. 2016;16:1-8.
13. Ainsworth EA, Gillespie KM. Estimation of total phenolic content and other oxidation substrates in plant tissues using Folin-Ciocalteu reagent. Nat Protoc. 2007;2:875-877.
14. Yang H, Dong Y, Du H, Shi H, Peng Y, Li X. Antioxidant compounds from propolis collected in Anhui, China. Molecules. 2011;16:3444-3455.
15. Wang H, Gao XD, Zhou GC, Cai L, Yao WB. *In vitro* and *in vivo* antioxidant activity of aqueous extract from *Choerospondias axillaris.* Food Chem. 2008;106:888-895.
16. Re R, Pellegrini N, Proteggente A, Pannala A, Yang M, Rice-Evans C. Antioxidant activity applying an improved ABTS radical cation decolorization assay. Free Radic Biol Med. 1999;26:1231-1237.
17. Ellman GL, Courtney KD, Andres V Jr, Feather-Stone RM. A new and rapid colorimetric determination of acetylcholinesterase activity. Biochem Pharmacol. 1961;7:88-95.
18. Abirami A, Nagarani G, Siddhuraju P. *In vitro* antioxidant, anti-diabetic, cholinesterase and tyrosinase inhibitory potential of fresh juice from *Citrus hystrix* and *C. maxima* fruits. Food Sci Hum Wellness. 2014;3:16-25.
19. Ademiluyi AO, Oboh G. Soybean phenolic-rich extracts inhibit key-enzymes linked to type 2 diabetes (α-amylase and α-glucosidase) and hypertension (angiotensin I converting enzyme) *in vitro*. Exp Toxicol Pathol. 2013;65:305-309.
20. Wu C, Chen F, Wang X, Wu Y, Dong M, He G, Galyean RD, He L, Huang G. Identification of antioxidant phenolic compounds in feverfew (*Tanacetum parthenium*) by HPLC-ESI-MS/MS and NMR. Phytochem Anal. 2007;18:401-410.
21. Tepe B, Sokmen A. Screening of the antioxidative properties and total phenolic contents of three endemic *Tanacetum* subspecies from Turkish flora. Bioresour Technol. 2007;98:3076-3079.
22. Wszelaki N, Kuciun A, Kiss AK. Screening of traditional European herbal medicines for acetylcholinesterase and butyrylcholinesterase inhibitory activity. Acta Pharm. 2010;60:119-128.
23. Orhan IE, Tosun F, Gülpınar AR, Kartal M, Duran A, Mihoglugil F, Akalgan D. LC-MS quantification of parthenolide and cholinesterase inhibitory potential of selected *Tanacetum* L. (Emend. Briq.) taxa. Phytochem Lett. 2015;11:347-352.
24. Polatoğlu K, Servi H, Yücel Yücel Y, Nalbantsoy A. Cytotoxicity acetylcholinesterase inhibitory and PRAP activities of the essential oils of selected *Tanacetum* L. species. Nat Volatiles & Essent Oils. 2015;2:11-16.
25. Móricz ÁM, Ott PG, Morlock GE. Discovered acetylcholinesterase inhibition and antibacterial activity of polyacetylenes in tansy root extract *via* effect-directed chromatographic fingerprints. J Chromatogr A. 2018;1543:73-80.
26. Jemaa HB, Jemia AB, Khlifi S, Ahmed HB, Slama FB, Benzarti A, Elati J, Aouidet A. Antioxidant activity and a-amylase inhibitory potential of *Rosa canina* L. Afr J Tradit Complement Altern Med. 2017;14:1-8.
27. Özek G. Chemical diversity and biological potential of *Tanacetum praeteritum* subsp. *praeteritum* essential oils. JOTCSA. 2018;5:493-510.
28. Zengin G, Cvetanović A, Gašić U, Stupar A, Bulut G, Şenkardes I, Dogan A, Sinan KI, Uysal S, Aumeeruddy-Elalfi Z, Aktumsek A, Mahomoodally MF. Modern and traditional extraction techniques affect chemical composition and bioactivity of *Tanacetum parthenium* (L.) Sch.Bip. Ind Crops Prod. 2020;146:112202.
29. Khan MF, Rawat AK, Khatoon S, Hussain MK, Mishra A, Negi DS. *In vitro* and *in vivo* antidiabetic effect of extracts of *Melia azedarach, Zanthoxylum alatum*, and *Tanacetum nubigenum*. Integr Med Res. 2018;7:176-183.

Turk J Pharm Sci 2022;19(4):383-390
DOI: 10.4274/tjps.galenos.2021.50432

ORIGINAL ARTICLE

Evaluation of the Effect of Ethyl Acrylate-Methyl Methacrylate Copolymer in Racecadotril Dispersible Tablet

Onur PINARBAŞLI*, Burcu BULUT, Gülistan Pelin GURBETOĞLU, Nurdan ATILGAN, Nagehan SARRAÇOĞLU, Asuman AYBEY

ILKO Pharmaceuticals, Research and Development Center, Ankara, Türkiye

ABSTRACT

Objectives: Racecadotril is an anti-diarrheal drug that has the indication to reduce the secretion of water and electrolytes into the intestine. It has an unpleasant taste, when administered orally. The presenting study developed a pharmaceutical racecadotril dispersible tablet, which masked the unpleasant taste using wet granulation method. For this reason, the effect of the number of ethylacrylate-methylmethacrylate copolymers (Eudragit® NE 30D) in taste masking and *in vitro* dissolution of the finished product was investigated.

Materials and Methods: Taste-masked racecadotril granules were prepared using Eudragit® NE 30D and the ratio between the amounts of racecadotril and Eudragit® NE 30D involved in the formulation was optimized. The products obtained in the dispersible tablet dosage form were evaluated in terms of taste and *in vitro* dissolution studies. *In vitro* dissolution profiles of the products obtained in this study were compared with reference product Tiorfan® granules for oral suspension manufactured by Bioprojet Pharma (Paris, France). A method of apparatus II (paddle), 900 mL, pH 4.5 acetate buffer + 1% sodium dodecyl sulfate (SDS) and 100 rpm at 37.0 ± 0.5°C was adopted.

Results: Results of the studies have shown that the formulation should have Eudragit® NE 30D higher than 1% by weight of racecadotril to satisfy the taste-masking ability and the formulation should have Eudragit® NE 30D equal or lower than 10% by weight of racecadotril to have better release characteristic to be compatible with reference product.

Conclusion: Our results demonstrated that a chemically long-term stable racecadotril dispersible tablet product, whose taste is efficiently masked using wet granulation method with an acceptable release profile was obtained with Eudragit® NE 30D ratio higher than 1% and equal or lower than 10% by weight of racecadotril. The developed formulation can increase patient compliance.

Key words: Racecadotril, dispersible tablet, wet granulation, ethyl acrylate-methyl methacrylate copolymers, taste-masking

INTRODUCTION

Racecadotril, which is also known as acetorphan, is a specific inhibitor of enkephalinase for use for treating acute diarrhea.[1-3] Diarrhea, a worldwide critical disease, occurs, when the bowel movements are unable to absorb or actively release fluid, which is loose, watery stools during bowel movements. According to the information released by the World Health Organization, the mortality rate for children under the age of 5 caused by acute diarrhea is estimated at 1.8 million *per* year.[4] Racecadotril active substance reduces excessive secretion of water and electrolytes into the intestinal lumen by preventing the degradation of endogenous opioids (enkephalins).[3,5,6] The efficacy and safety of the specified active substance used orally have been proven in children and adults with acute watery diarrhea.[6] Furthermore, racecadotril has an unpleasant taste, which results in poor patient compliance when administered orally, particularly in the case of children.[2] It is well-known that oral route is commonly used for pediatric patients with solid or liquid dosage forms. Since racecadotril is a hydrophobic active agent, it is difficult to describe in suspension dosage forms. This is why the suspension form is not preferred for formulation development since the active ingredient is water repellent.

*Correspondence: opinarbasli@ilko.com.tr, Phone: +90 312 248 68 00, ORCID-ID: orcid.org/0000-0001-7091-683X
Received: 25.06.2021, Accepted: 17.09.2021

Considering solid dosage forms used in pharmaceutical industry, there are tablets (fast dissolving tablets, dispersible tablets, chewable, immediate release and delayed release), capsules, chewable gums, and powders for oral suspension and granules for oral suspension.

The commercially available product, Tiorfan® granules, for oral suspension with dosage forms of 30 mg and 10 mg produced by Bioprojet Pharma (Paris, France) was used as a reference product to compare *in vitro* dissolution studies of the developed racecadotril dispersible tablets. Characteristic of the formulation is that the racecadotril granulate prepared with a suitable carrier is coated and mixed with a sweetener. Acrylate and methacrylate polymers, especially Eudragit® NE 30D, are stated as coating agents. According to the procedure, firstly, racecadotril granulate is prepared with a little sugar, it is coated with a coating agent; the coated granule is mixed with the remaining sugar, aerosil and sweetener and then filled into a sachet.[7]

Eudragit® NE 30 D is a polymer consisting of methyl methacrylate and ethyl acrylate monomers in a ratio of 2:1, with a low glass transition temperature of -8˚C and a minimum film formation temperature of 5˚C.[8]

Many active substances can be expressed in conventional solid dosage forms, especially capsule and tablet forms, but tablet and capsule forms are not preferred as dosage forms for pediatric patients.[2] Difficulty in swallowing of solid dosage forms in pediatric and geriatric patients can be overcome by developing dispersible tablets that can be dissolved, dispersed or mixed in food, milk or water before administration. These dispersible tablets are suitable dosage form for infants, toddlers, children, and adults. Since dispersible tablets have significant advantages over solid and liquid dosage forms, they are preferable for pediatric usage. Some of the advantages of the solid drugs are listed as being easily portable, providing a range of doses, masking the unpleasent taste, having better adherence. Also, since it remains solid during transportation and storage, the stability of the product is maintained and it turns into a liquid state within a few minutes after dispersion and provides ease of use.[9] It is seen because of these studies that, dispersible tablets improve the efficacy, safety, and compatibility of treatments in infants, toddlers and children.

Solid dispersion technology is a method used to improve the solubility of poor aqueous soluble drugs and hence to achieve an improvement in their bioavailability.[10,11] However, this technology is also known for its ability to mask the taste of bitter-tasting active ingredients. The granules containing the drug substance are obtained by solidification of the molten mixture or evaporation of the solvent. Different methods are also used for the preparation of solid dispersions, such as melting method, solvent method, melting solvent method, melt extrusion method, lyophilization technique, melt agglomeration process, the use of surfactant, electro, spinning, and super critical fluid technology. However, one of the known drawbacks of solid dispersion method is the difficulty in removing the solvent and the cost of preparation of the process compared to other methods.[2,12] In addition to these, the major disadvantage of solid dispersion is related to the degradation that occurs in stability. Exposure to moisture and temperature under stability conditions has a high degrading effect on the products obtained from solid dispersion.[10]

The most important and critical problem in pediatric drugs is the accuracy of the applied dose, which is caused by the unpleasant taste of the product[9] racecadotril can be developed into a dispersible tablet form with taste masking properties in a simple and easy method of wet granulation to overcome the problem of providing a suitable pediatric dosage form that allows for administrating an unpleasant taste drug substance to children. Therefore, taste masking and correct dose with acceptable release are key issues in the current study. The objective of the present study was to develop pharmaceutical compositions comprising racecadotril, whose taste is masked using the wet granulation method, for treating diarrhea.

MATERIALS AND METHODS

Materials

Racecadotril (API grade) was obtained from Symed Labs Limited (India). Eudragit® NE 30D (Evonik, Germany), pregelatinized starch (Colorcon, USA), mannitol (Merch, Germany), aspartame (Vitasweet), kollidon CL (Basf, Germany), acesulfame K (Suzhou, China), strawberry flavor (Firmenich, Switzerland), and sodium stearyl fumarate (JRS Pharma, Germany) were used as inactive ingredients in formulations.

Analytical grades of potassium dihydrogen phosphate (Merck, Germany), phosphoric acid (*ortho*-phosphoric acid 85%, Merck, Germany), and acetonitrile (J.T. Baker, Poland) were used in high performance liquid chromatography (HPLC) analysis. Quantitative stability indicating HPLC test methods were performed on a Shimadzu HPLC System (Shimadzu, Kyoto, Japan) equipped with the separations module and variable wavelength ultraviolet-detector and running with LC solution software. Deionized distilled water was obtained from Millipore water purification system (Millipore Corp., Bedford, MA, USA) and used throughout this study.

Reference product, Tiorfan® granules, for oral suspension produced by Bioprojet Pharma (Paris, France) was purchased.

Analytical method and validation studies

The content of racecadotril for assay studies and *in vitro* dissolution studies were determined spectrophotometrically by an HPLC method at 210 nm using a Shimadzu HPLC System (Shimadzu, Kyoto, Japan). HPLC method with a quaternary pump, autosampler, and diode array detector (DAD) was used during analytical method development and validation for finished product assay and *in vitro* dissolution testing. The separation was achieved using an ODS-3V C18 5 µm column (4.6 mm × 250 mm) using a mobile phase of buffer:acetonitrile (35:65). Buffer was prepared by dissolving 1.0 g of potassium dihydrogen phosphate in a 1 L of deionized water and adjusted to pH 2.5 with phosphoric acid. The granules and tablets to be analyzed were dissolved using the solvent consisting

of buffer:acetonitrile (1:1) mixture. Flow rate was 1.0 mL/min and the signal was monitored at a wavelength of 210 nm. The analytical method of racecadotril was validated for specificity, selectivity, sensitivity, linearity, recovery, accuracy, and precision parameters. Other than statistical evaluation of *f2*, there was no statistical data analysis.

Formulation studies

Due to lack of water solubility of the active ingredient, *i.e.* racecadotril, and inability to press tablets using the direct compression method, it was decided to use the wet granulation production method in a high shear mixer (Pilotmix 150T) for this study.

Granules comprising racecadotril were obtained using wet granulation production method in high shear mixer using Eudragit® NE 30D copolymer. The aim of using Eudragit® NE 30D copolymer was to mask the unpleasent taste of the racecadotril. The granulation process was followed by a drying step with a fluidized bed dryer (HDGC 100) at a maximum of 70˚C temperature. The final blend is obtained by adding other excipients and finally tablet compression is carried out. The unit formula of racecadotril dispersed tablet is given in Table 1.

After the formulation was approximately determined during the pre-formulation, studies were conducted to determine the ratio between Eugragit® NE 30D and racecadotril. To optimize the unit formula of the taste-masked racecadotril granules prepared using wet granulation technique, six formulations (F1-F2-F3-F4-F5-F6) having different weight percent ratios of Eudragit® NE 30D to racecadotril (0.67%, 1%, 2%, 5%, 10%, 12%, respectively) were prepared the following unit formula and prepared as dispersible tablet.

Granules comprising racecadotril, whose taste is masked by being subjected to wet granulation, are used as intermediate products in the preparation of oral pharmaceutical compositions such as tablet, dispersible tablet, and suspension. The granules obtained in this study are blended with the specified excipients and compressed in the form of dispersible tablets. All the dispersible tablet products prepared (F1-F6) were first tested with organoleptic taste properties to determine if the unpleasent taste of racecadotril was masked, and then other quality control tests were performed.

Content uniformity studies

Content uniformity of the final granule mixture

Granules comprising racecadotril are manufactured with wet granulation method and then obtained granules are compressed as tablets. Content uniformity of the final granule mixture was carried out by withdrawing at least 10 random samples taken from different parts like top, center, bottom, and wall locations. Samples selected were dissolved with the solvent in flask and filtered into 0.45 µm polytetrafluoroethylene (PTFE) and transferred to a vial. The prepared vials were tested for racecadotril content using a validated HPLC method mentioned in the analytical methods and validation study section.

Content uniformity of the tablets

Tablets were randomly selected from the beginning, middle, and end of each compression run. Ten tablets were tested for their content uniformity using the validated HPLC method. Each selected tablet is dissolved with the solvent in flask and filtered into 0.45 µm PTFE and transferred to the vial. The prepared vials were tested for racecadotril content using a validated HPLC method mentioned in the analytical methods and validation study section. According to 10 individual assay results, acceptance value (AV) is calculated. Final product content uniformity had to meet European Pharmacopeia (EP) (2.9.40) requirements as the L1 criteria state that 10 samples should be tested and the AV should be equal to or lower than 15.[13]

Disintegration time testing

Disintegration testing was performed in accordance with EP monograph for tablet disintegration. This test is provided to determine, whether tablets or capsules disintegrate within the prescribed time, when placed in a liquid medium at the experimental conditions. Six tablets were tested for each batch and the mean result was reported. Disintegration time testing

Table 1. Unit formulas of racecadotril 30 mg dispersible tablet used in the study

Ingredients	F1	F2	F3	F4	F5	F6
	(mg)					
Racecadotril	30.0	30.0	30.0	30.0	30.0	30.0
Eudragit® NE 30D	0.2	0.3	0.6	1.5	3.0	3.6
Aspartam	10.0	10.0	10.0	10.0	10.0	10.0
Kollidon CL	30.0	30.0	30.0	30.0	30.0	30.0
Mannitol	126.0	125.9	125.6	124.7	123.2	122.6
Acesulfame K	4.0	4.0	4.0	4.0	4.0	4.0
Pregelatinized starch	26.0	26.0	26.0	26.0	26.0	26.0
Strawberry flavor	9.0	9.0	9.0	9.0	9.0	9.0
Sodium stearyl fumarate	4.8	4.8	4.8	4.8	4.8	4.8
Total	**240.0**	**240.0**	**240.0**	**240.0**	**240.0**	**240.0**

was performed by adding a tablet to a beaker of water at 37 ± 0.5°C and recording the time for the tablet to become fully disintegrated.

In vitro dissolution studies

Comparative dissolution studies in three different dissolution media were conducted to demonstrate *in vitro* dissolution behavior between reference product of Tiorfan® 30 mg granules for oral suspension (produced by Bioprojet Pharma, Paris/France) and test products of racecadotril dispersible tablet (F1-F6). The dissolution tests were carried out with a Distek Evolution 6300 dissolution tester. Since there is not any available *in vitro* dissolution method specified by the Food and Drug Administration (FDA) or pharmacopeias for racecadotril, *in vitro* dissolution method was developed using in-house method. The used dissolution method is Apparatus II (Paddle), a volume of 900 mL, pH 4.5 acetate buffer + 1% sodium dodecyl sulfate (SDS) and 100 rpm at 37.0 ± 0.5°C. In addition to pH 4.5 media, dissolution studies were conducted at two other dissolution mediums (0.1 N HCl + 1% SDS and pH 6.8 phosphate buffer + 1% SDS). Racecadotril has poor water solubility, which is measured as 28.98 µg/mL.[14] In addition to water solubility, the solubility of racecadotril was reported as 327.7 µg/mL in pH 4.5 acetate buffer, 61.75 µg/mL in 0.1 N, HCl and 50.86 µg/mL in pH 6.8 phosphate buffer. Furthermore, the solubility of racecadotril is 587.8 µg/mL in phosphate buffer pH 6.8 with 0.75% SLS.[2] Surfactants play an important role in the dissolution preparations, and the solubility studies carried out mediums of pH 4.5, pH 6.8 and 0.1 N HCl with 1% SDS provide sink conditions for used mediums. At pre-determined time intervals (10, 15, 20, 30, 45, 60 min), 2 mL of the release medium is withdrawn and an equal volume of medium is added instead. The sample withdrawn from the medium is filtered and analyzed using a validated HPLC method at 210 nm to determine the amount of dissolved racecadotril.

To achieve effective bioavailability and provide *in vitro-in vivo* correlation, it is expected that at least about 80% of the total amount of racecadotril have dissolved after 45 minutes of measurement and at least about 90% of the total amount of racecadotril after 60 min of measurement at given pH 4.5 acetate buffer + 1% SDS dissolution medium.

The dissolution profiles were compared; the dissolution profiles obtained were evaluated using the similarity factor (*f2*).[15] According to the Eurpean Medicines Evaluation Agengy (EMEA) and FDA Guidelines; dissolution similarity may be determined using the *f*2 statistic as follows:

$$f2 = 50.\log\left[\frac{100}{\sqrt{1+\frac{\sum_{t=1}^{t=n}\left[\overline{R}(t)-\overline{T}(t)\right]2}{n}}}\right] \quad \text{equation (1)}$$

In this equation [equation (1)] *f*2 is the similarity factor, n is the number of time points, R(t) is the mean percent reference drug dissolved at time t after initiation of the study; T(t) is the mean percent of test drug dissolved at time t after initiation of the study. For both reference and test formulations, percentage dissolution should be determined. An *f2* value between 50 and 100 suggests that the two dissolution profiles are similar.[15]

Stability studies

The selected formulation with proper taste and *in vitro* dissolution results was investigated according to the requirements of ICH stability guidelines.[16] For this purpose, tablets were packed with ALU-ALU blister primary packaging and stored in stability cabinets for 6 months at 40 ± 2°C/75% ± 5% relative humidity (RH) (accelerated conditions) and for 24 months at 25 ± 2°C/60% ± 5% RH (long term conditions). At determined time intervals, the test products were evaluated from the specifications such as assay, related substances, and dissolution tests with using validated HPLC method.

RESULTS

Validation studies of analytical method

The analytical method to determine content (assay) of racecadotril in quantification tests and *in vitro* dissolution tests was developed and validated using HPLC system. The assay and *in vitro* dissolution test method of the finished product validations were completed successfully as to specificity, linearity, stress, precision, accuracy, recovery, and robustness. Calibration curve for racecadotril ranged from 0.0067 mg/mL to 0.04 mg/mL and linearity determination coefficients between concentrations and areas were higher than 0.99 (r^2 >0.99) for both assay and *in vitro* dissolution analysis. Also, the recovery of racecadotril was 99.5 ± 1.15% for assay and 98.9 ± 0.90% for dissolution tests; both are in 95% confidence interval. The methods specified according to the method validation test results were shown to be specific for racecadotril and meet all the requirements for validation.

Formulation

In this study, unpleasent taste of racecadotril was masked by wet granulation method with six formulations prepared using Eudragit® NE 30D in different concentrations. Content uniformity test was applied to the prepared granules. Then, dispersible tablets were compressed from these granules and content uniformity test was also applied to these tablets.

Critical process parameters were evaluated in this study, considering into account the known critical steps during granule preparation using the wet granulation process. Two different critical process parameters were determined as 5 min of granulation time with adjusted to the solution delivery rate. First critical parameter is drying temperature and air flow during drying. The drying process was accomplished in two studies; at 50°C and 80 m^3/h and at 70°C and 120 m^3/h drying temperature and air flow. Proper results could not be obtained because the desired moisture content of 2.0% could not be achieved in the study where the drying temperature and air flow rate was low (50°C and 80 m^3/h); and the dissolution profile was obtained lower than reference product in the dissolution studies carried

out in pH 4.5 + 1% SDS medium. The desired moisture content of below 2.0% was obtained with the granules dried at 70°C and the desired particle size of granules was obtained at 120 m^3/h air flow rate. In dissolution studies conducted in pH 4.5 + 1% SDS medium, it was observed that the dissolution profile showed a similar profile to reference product. Second critical parameters are sieving and sieve opening. Sieves with 0.8 mm and 1.5 mm sieve openings were used to reveal the difference in the obtained product. The small sieve opening and sufficient sieving speed enabled the particle size to be reduced to the desired size and in this case, a similar dissolution profile was obtained with reference product for the dissolution studies carried out in pH 4.5 + 1% SDS medium.

After tablet pressing, tests such as appearance, tablet dimensions, friability, disintegration time, hardness, average weight, and weight distribution were applied and all results were found in accordance with the specifications. pH of the water-dispersed tablet was tested and found to be 7.3, which is similar to reference product.

Content uniformity results of racecadotril at final granules and tablet are given in Table 2. According to the results of the content uniformity of the granules and tablets, both of them met the content uniformity specifications. The contents of racecadotril in the granules and tablets tested were found to be in the range of 97.0 - 103.0% with having L1 values lower than 15, as shown in Table 2.

Table 2. Content uniformity results of racecadotril at final granule mixture and tablet (n: 10)

	Final granules					
Sample	**F1**	**F2**	**F3**	**F4**	**F5**	**F6**
1	101.5	101.2	100.3	102.3	100.6	100.4
2	100.9	98.5	101.1	100.4	101.6	102.6
3	99.6	97.6	99.5	98.8	99.5	98.4
4	98.4	102.5	98.6	100.4	97.9	100.5
5	97.6	101.6	97.9	101.5	99.1	102.6
6	99.1	99.5	100.6	103.6	100.6	101.5
7	100.8	99.4	101.5	99.5	101.5	100.6
8	101.1	98.5	98.6	100.4	98.4	98.7
9	99.5	101.5	101.6	101.6	99.4	99.5
10	102.3	102.1	100.9	99.8	98.1	100.4
Average	**100.1**	**100.2**	**100.1**	**100.8**	**99.7**	**100.5**
SD[a]	**1.48**	**1.74**	**1.33**	**1.43**	**1.35**	**1.43**
RSD[b] %	**1.48**	**1.73**	**1.33**	**1.42**	**1.36**	**1.43**
	Tablet					
Sample	**F1**	**F2**	**F3**	**F4**	**F5**	**F6**
1	101.5	99.8	99.7	99.3	102.3	99.6
2	103.5	101.6	100.5	101.4	100.5	100.5
3	98.5	100.4	102.6	100.6	100.6	101.6
4	99.5	102.3	101.2	102.7	98.5	102.6
5	99.4	100.5	98.6	103.6	100.1	98.6
6	100.5	99.1	98.4	98.5	99.5	99.5
7	101.6	98.3	101.5	101.6	98.6	97.6
8	97.5	102.3	100.5	102.4	98.4	100.5
9	98.9	99.6	98.1	100.5	100.5	102.5
10	100.6	102.5	97.6	100.4	101.6	100.4
Average	**100.2**	**100.6**	**99.9**	**101.1**	**100.1**	**100.3**
SD[a]	**1.76**	**1.48**	**1.66**	**1.56**	**1.32**	**1.61**
RSD[b] %	**1.75**	**1.47**	**1.66**	**1.54**	**1.32**	**1.60**

[a]SD: Standard deviation, [b]RSD: Relative standard deviation

Taste-masking studies

In this study, six formulations with variable concentrations of Eudragit® NE 30D were subjected to human taste tests to mask the unpleasant taste of racecadotril using the wet granulation method. Since taste is an important issue in the administration of drugs containing bitter active substances in the oral administration system, the solution to this problem is the main purpose of this study.

According to human taste test performed on all products prepared (F1-F6), it was observed that the taste of the products prepared with the F1 formulation was still bitter. In other words, racecadotril could not be masked at a sufficient level. As a consequence, the bitter taste of the racecadotril compound is not masked, if the percentage ratio between Eudragit® NE 30D and racecadotril is below 1%.

The products obtained from the F2-F6 formulations developed have confirmed the acceptability of the bitter taste of racecadotril by taste masking by human taste test. According to the taste evaluation results, it was shown that an effective taste mask formulation was achieved using Eudragit® NE 30D higher than 1% by weight of racecadotril.

Since the product is a dispersible tablet and is intended for pediatric patients, the most important step is efficient taste masking. For this reason, if the necessary coating process is not sufficient to mask the bitter taste of racecadotril, then, the issues in patient compliance occur.

In vitro dissolution studies

In vitro dissolution behavior of formulations (F2-F6) prepared with different concentrations of Eudragit® NE 30D by using wet granulation method was examined in pH 4.5 acetate buffer + 1% SDS buffer, 0.1 N HCl + 1% SDS and pH 6.8 phosphate buffer + 1% SDS mediums. The corresponding profiles at pH 4.5 acetate buffer + 1% SDS buffer are shown in Figure 1 and the similarity factors (f_2) calculated for three mediums are given in Table 3 by comparison with reference product Tiorfan® 30 mg granules for oral suspension.

In comparison with the formulations prepared in this study, F4 formulation appears to have lower and slower release, and only about 80% of the drug dissolved within 60 min. According to *in vitro* dissolution results, when the percentage ratio between Eudragit® NE 30D copolymer and racecadotril is higher than 10% (F6), total amount dissolved after 45 min is under 80% (76.3%) and total amount dissolved after 60 min is around 80%, which means dissolution does not complete.

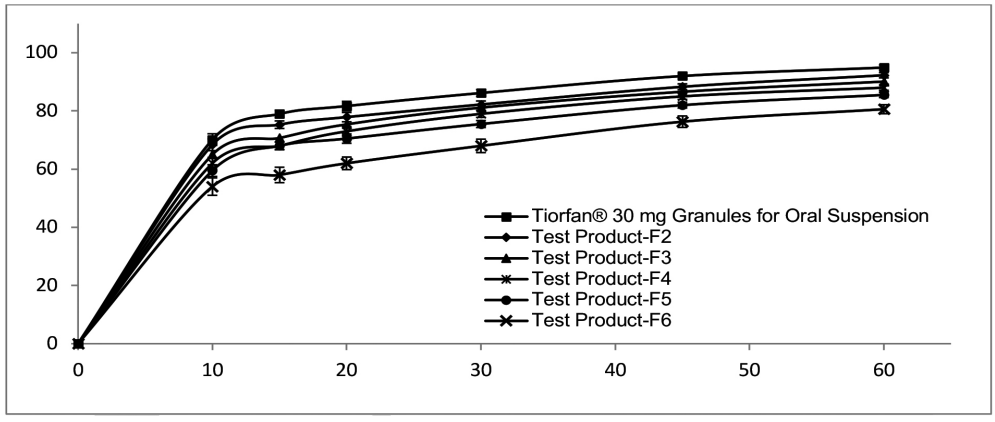

Figure 1. *In vitro* % released racecadotril *vs.* time profiles from the test products (F2-F6) and reference product of Tiorfan® 30 mg granules for oral suspension (SXE1159) in pH 4.5 acetate buffer + 1% SDS medium (mean ± SD, n: 12)

SDS: Sodium dodecyl sulfate, SD: Standard deviation

Table 3. The summary of similarity factor (f_2). test products (F2-F6) *vs.* reference product-Tiorfan® 30 mg granules for oral suspension (Bioprojet Pharma, Paris/France)

f_2 (similarity factor)			
Products	**pH 4.5 acetate + 1% SDS**	**0.1 N HCl + 1% SDS**	**pH 6.8 phosphate buffer + 1% SDS**
F2 *vs.* reference product	f_2: 74	f_2: 66	f_2: 68
F3 *vs.* reference product	f_2: 63	f_2: 57	f_2: 56
F4 *vs.* reference product	f_2: 56	f_2: 52	f_2: 53
F5 *vs.* reference product	f_2: 51	f_2: 52	f_2: 51
F6 *vs.* reference product	f_2: 39	f_2: 45	f_2: 41

SDS: Sodium dodecyl sulfate

Table 4. Stability results for test product F2 initially and after 6 months at 40 ± 2˚C and 75% ± 5% RH storage condition and 24 months at 25 ± 2˚C and 60 ± 5% storage condition (mean ± SD, n: 6)

		Time point		
Initially		**After 6 months at 40˚C**	**After 24 months at 25˚C**	
Taste		Complies	Complies	Complies
Disintegration time (at 37˚C water)		Lower than 3 minutes	Lower than 3 minutes	Lower than 4 minutes
Assay	**Racecadotril**	99.6 ± 0.78%	96.2 ± 1.3%	98.5 ± 0.60%
Related substance	**Total imp.**	0.09%	0.46%	0.37%
Dissolution*	**After 45 minutes**	88 ± 1.6%	82 ± 3.1%	81 ± 2.4%
pH**		7.27	7.30	7.33

*Apparatus II (Paddle), 900 mL, pH 4.5 acetate buffer + 1% sodium dodecyl sulfate and 100 rpm at 37.0 ± 0.5˚C. **Dispersed in one glass of water. RH: Relative humidity, SD: Standard deviation

The results obtained confirmed that there were acceptable similarities between the test products (F2-F5) and reference products for various dissolution mediums under comparison; as a result, *f2* values of all dissolution media are higher than 50 (Table 3). The comparative dissolution rate profiles show that reference product and the test products having a percentage ratio of Eudragit® NE 30D to racecadotril lower than 10% gave similar dissolution profiles.

As *in vitro* dissolution is related to the *in vivo* properties of the product, the bioavailability will be lower in products due to lower values in their dissolution profiles. Primarily to achieve desired dissolution profile and related to achieve effective bioavailability; the percentage ratio between Eudragit® NE 30D copolymer and racecadotril should be lower than 10%.

According to taste and *in vitro* dissolution results, the percentage ratio range of Eudragit® NE 30D copolymer should be higher than 1% and equal or lower than 10% by weight of the amount of racecadotril.

Test product F2 was found to be the most suitable in all formulations in the taste masking and *in vitro* dissolution studies; therefore, stability studies continued with this formulation.

Stability studies

Test product F2 (the best formulation among the others) was further studied with stability studies. In a further aspect of the invention, the unit dosage form of formulation according to the invention is physically and chemically stable. Stability of the tablets can be measured at accelerated and at long term storage conditions for periods of several months. Experiments can be performed at different temperatures and humidity. The oral pharmaceutical compositions of this invention, which are prepared according to Test product F2, were subjected to accelerated stability studies at 40 ± 2˚C/75% ± 5 RH (accelerated conditions) and 25 ± 2˚C/60% ± 5% RH (long term conditions). The stability results are given in Table 4.

DISCUSSION

This study aimed to demonstrate the effect of Eudragit® NE 30D concentrations in the dispersible tablet formulation on taste-masking and on the *in vitro* dissolution profile of racecadotril by using wet granulation technique. The analytical HPLC method was validated successfully; with results obtained the method has been used in *in vitro* dissolution tests and other stability tests. In this study, six formulations with variable concentrations of Eudragit® NE 30D were prepared by wet granulation method and evaluated for taste and *in vitro* drug release. The results of the taste assessment showed that by providing a minimum ethyl acrylate-methyl methacrylate copolymer ratio of 1% by weight of racecadotril quantity, an appropriate taste-masked formulation, was achieved. If the ratio between ethyl acrylate-methyl methacrylate copolymer and racecadotril is under 1%, bitter taste of the racecadotril compound is not masked. Since the product is a dispersible tablet and developed for pediatric patients, effective taste masking is a critical process. Due to bitter taste of racecadotril, if the coating process is not sufficient, problems in patient compliance may occur.

Maximum ratio of ethyl acrylate-methyl methacrylate copolymer to racecadotril should be 10% by weight so that the amount of dissolved racecadotril resulting from an *in vitro* dissolution study in 45 min is at least about 80% of the total amount of active ingredient. According to stability test results, racecadoril dispersible tablets were found to be stable in terms of assay, impurity, and dissolution results at 40 ± 2˚C and 75 ± 5% RH conditions for 6 months and at 25 ± 2˚C and 60 ± 5% RH conditions for 24 months.

CONCLUSION

This study confirms the feasibility of developing a racecadotril dispersible tablet formulation using wet granulation method and shows the effect of Eudragit® NE 30D on the taste and dissolution properties of the drug product.

REFERENCES

1. Lecomte JM. An overview of clinical studies with racecadotril in adults. Int J Antimicrob Agents. 2000;14:81-87.
2. Singhvi G, Gampa G, Yadav N, Kumar V, Ukawala R. Design and evaluation of rapidly disintegrating tablets of racecadotril with enhanced *in vitro* dissolution achieved by solid dispersion technique. Indian J Pharm Edu Res. 2013;47:56-63.
3. Vishwakarma AK, Pant I, Patel MK, Pandey A. Formulation, development and optimization of fast dissolving oral film of racecadotril. Int J Indig Herbs Drugs. 2018;3:1-6.
4. Proposal for the inclusion of racecadotril in the WHO model list of essential medicines. Bioprojet Pharma, May 2007. Available form: http://www.bioprojet.fr
5. Matheson AJ, Noble S. Racecadotril. Drugs. 2000;59:829-835; discussion 836-837.
6. Salazar-Lindo E, Santisteban-Ponce J, Chea-Woo E, Gutierrez M. Racecadotril in the treatment of acute watery diarrhea in children. N Engl J Med. 2000;343:463-467.
7. Dry powder formulation comprising racecadotril. Patent EP1294372B1.
8. Zheng W, McGinity JW. Influence of Eudragit NE 30 D blended with eudragit L 30 D-55 on the release of phenylpropanolamine hydrochloride from coated pellets. Drug Dev Ind Pharm. 2003;29:357-366.
9. Ali AA, Charoo NA, Abdallah DB. Pediatric drug development: formulation considerations. Drug Dev Ind Pharm. 2014;40:1283-1299.
10. Das SP, Verma S, Saha P. Fast dissolving tablet using solid dispersion technique: a review. Int J Curr Pharml Res. 2017;9:1-4.
11. Yoshida T, Kurimoto I, Yoshihara K, Umejima H, Ito N, Watanabe S, Sako K, Kikuchi A. Aminoalkyl methacrylate copolymers for improving the solubility of tacrolimus. I: evaluation of solid dispersion formulations. Int J Pharm. 2012;428:18-24.
12. Douroumis D. Practical approaches of taste masking technologies in oral solid forms. Expert Opin Drug Deliv. 2007;4:417-426.
13. Madathilethu J, Roberts M, Peak M, Blair J, Prescott R, Ford JL. Content uniformity of quartered hydrocortisone tablets in comparison with mini-tablets for paediatric dosing. BMJ Paediatrics Open. 2018;2:1-7.
14. Semalty M, Panchpuri M, Singh D, Semalty A. Cyclodextrin inclusion complex of racecadotril: effect of drug-β-cyclodextrin ratio and the method of complexation. Curr Drug Discov Technol. 2014;11:154-61.
15. Guideline on the investigation of bioequivalence. EMEA 2010 CPMP/EWP/QWP/1401/98 Rev. European Medicines Agency. London, USA.
16. ICH Harmonized tripartite guideline stability testing of new drug substances and products Q1A(R2), 2003.

Turk J Pharm Sci 2022;19(4):391-399
DOI: 10.4274/tjps.galenos.2021.48961

ORIGINAL ARTICLE

Preparation and Characterization of Chitosan and Inclusive Compound-Layered Gold Nanocarrier to Improve the Antiproliferation Effect of Tamoxifen Citrate in Colorectal Adenocarcinoma (Caco-2) and Breast Cancer (MCF-7) Cells

Yahia KAHLOUS[1], Vijayaraj Kumar PALANIRAJAN[1]*, Melbha STARLIN[1], Jeetendra Singh NEGI[1], Shiau-Chuen CHEAH[2]

[1]UCSI University, Faculty of Pharmaceutical Sciences, Department of Pharmaceutical Technology, Kuala Lumpur, Malaysia
[2]UCSI University, Faculty of Medicine and Health Sciences, Department of Biochemistry, Kuala Lumpur, Malaysia

ABSTRACT

Objectives: Cancer diseases have been linked to a huge number of causes that led to deaths in this century along with cardiovascular and lung diseases. Most death-leading types of cancer are colon, lung, breast, and prostate cancers. Due to the remarkable properties of gold (Au) nanocarrier, they are used to deliver and improve tamoxifen (Tam) citrate activity in Caco-2 and MCF-7 cells.

Materials and Methods: In this study, preparation of Au nanoparticles (NPs), zeta-potential and size, high resolution transient electron microscopy (HRTEM), high-performance liquid chromatography, ultraviolet-visible spectra, fluorescence microscopy, fourier infrared spectroscopy, and real-time cellular analysis xCELLigence technology were investigated.

Results: The zeta-average size of the Tam- β-cyclodextrin (β-CD)-hyaluronic acid (HA)-chitosan (Chi)-Au nanocomposite is 82.02 nm with a negative zeta potential of -23.6. Furthermore, HRTEM images showed that, successful formulation of polymer shell around Au core and the Au NP shape is mostly spherical, triangle and irregular. Furthermore, the fluorescence microscope image showed proper cellular uptake of the Tam-β-CD-HA-Chi-Au nanocomposite in MCF-7 and Caco-2 cells. Additionally, Tam-β-CD-HA-Chi-Au nanocomposite significantly improved the cytotoxic activity of Tam citrate on Caco-2 cells. IC_{50} value of Tam reduced from 8.55 µM to 5.32 µM, after 48 h of incubation time (p value <0.00001).

Conclusion: This study showed that Tam-β-CD-HA-Chi-Au nanocomposite is a potential nanocarrier for delivering the drug to Caco-2 and MCF-7 cancer cells, since it has improved Tam citrate activity on colorectal cancer cells. After all, the developed formula showed more effect on Caco-2 than MCF-7. The prepared nanocomposite could be used to improve the cancer therapy in clinical trials.

Key words: Chitosan gold nanoparticles, tamoxifen citrate and β-cyclodextrin, MCF-7 cell line and Caco-2 cell line, cytotoxicity and cellular uptake, Xcelligence RTCA systems

INTRODUCTION

Cancer diseases have been linked to a huge number of causes that lead to death in this era, along with cardiovascular and lung diseases.[1] Generally, cancer has widely spread in the last few years, the number of cancer patients in America alone reaches, around 1,806,590 patients.[2] Most death-leading types of cancer are colon, lung, breast, and prostate cancers. Among various cancer types, colorectal cancer has a high prevalence in the United States, with 147.950 new patients and 53.200 expected deaths. Approximately 104.610 patients were identified with

*Correspondence: vijayarajkumar_p@yahoo.com, Phone: +60103782399, ORCID-ID: orcid.org/0000-0003-1129-7084
Received: 19.05.2021, Accepted: 17.09.2021

colon cancer and 43.340 were identified with rectal cancer during 2020.[3] The potential causes of colon cancer may be sporadic, hereditary, or caused by the development of ulcerative colitis and Crohn's disease.[4]

Tamoxifen citrate (Tam) is most frequently used for treating breast cancer by preventing the estrogen hormone from binding to its receptors.[5] Therapeutic dose of the Tam was 10 mg 40 mg/day, while 15.2 mg of Tam citrate is equivalent to 10 mg Tam. Tumors are generally associated with irregular blood vessels with the ability to increase permeation and poor lymphatic drainage that contributes to the retention inside tumors.[6] This enhanced permeability and retention effect could be utilized by nanoparticles (NPs) to localize inside solid tumours.[7] Various nanocarriers formulations have been developed to improve chemotherapy.[8] Doxil and myocet (doxorubicin liposomes) were the first class therapeutics to be approved for cancer therapy.[9] Other promising nanocarriers either approved or in clinical trials are nab-paclitaxel (albumin NPs),[10] SMANCS, CRLX-101 (campthothecin NPs) and NK-105 (paclitaxel micelle).[11] Moreover, nanocarriers could be decorated with targeting ligands for a specific receptor in the tumour cells to improve cellular uptake.[12] Few nanocarriers for targeted drug delivery are also in clinical trials such as MM302 (HER-2 targeting), MBP-426 (TfR-targeting), and BIND-014 (PSMA-targeting).[13] In addition to therapeutic benefits, nanocarriers could also be used in cancer diagnosis. Inorganic NPs and particularly gold (Au) NPs have extensively been extensively used extensively to improve diagnosis of cancer tissue.[14]

An issue to be addressed with current chemotherapy is its ineffectiveness against multidrug resistant cancer cells.[15] Specifically, resilience against structurally and systematically unrelated drugs is the primary concern in cancer treatment.[1] Cancer cells acquire resistance mainly due to the overexpression of drug efflux proteins, DNA repair activation, and apoptotic signaling modification.[16] High interstitial fluid pressure of tumour stroma also hinders drug penetration that results in the development of drug resistance due to less drug exposure.[17] Furthermore, multidrug resistant cancer cells strongly reduce the internalization of drugs across the cell membrane with the help of P-glycoprotein efflux pumps.[18] Recently, scientists have started to use several unique characteristics of the extracellular tumour microenvironment like acidic extracellular pH, specific enzymes, and hypoxia condition. Chitosan (Chi) is derived from chitin by the deacetylation process. The polymer is considered Chi, when the degree of acetylation is less than 50%, which is soluble in acidic solutions.[19] Moreover, Chi has increased usage due to its cationic nature and mucoadhesive properties due to it is improved drug absorption capability.[20] Chi NPs not only can deliver hydrophilic and hydrophobic molecules but also to stabilize pharmaceutical ingredients against enzymatic degradation and thus improve the bioavailability and prolong the drug action.[21] This study attempts to develop a NP drug delivery system using β-cyclodextrin (β-CD)-based inclusion complexes to enhance the cellular uptake of nanocarriers and increase the internalization of Tam inside the cancer cells and improve its efficacy.

MATERIALS AND METHODS

Materials

Au (III) chloride 99% (Sigma-Aldrich, USA), Chi low molecular weight (Sigma-Aldrich,USA), β-CD >97% (Sigma-Aldrich, USA), sodium citrate tribasic dihydrate (Sigma-Aldrich, USA), hyaluronic acid (HA) sodium salt (Sigma-Aldrich, USA), Tam citrate (Sigma-Aldrich, USA), sodium tripolyphosphate (TPP) 85% (Sigma-Aldrich, USA), Dulbecco's Modified Eagle's Medium (DMEM) (ATCC, USA), phosphate-buffered saline (PBS) (ATCC, USA), trypsin-EDTA solution (ATCC, USA), penicillin-streptomycin solution (ATCC, USA), fetal bovine serum (ATCC, USA), trypsin-EDTA solution (ATCC, USA), Caco-2 (ATCC HTB-37, USA), and MCF-7 (ATCC HTB22™, USA) cell lines.

Preparation of Tam: β-CD inclusion compound

Tam: β-CD inclusion compound was prepared in a 1:1 M ratio. Briefly, Tam and β-CD, 10 mg for each, were completely

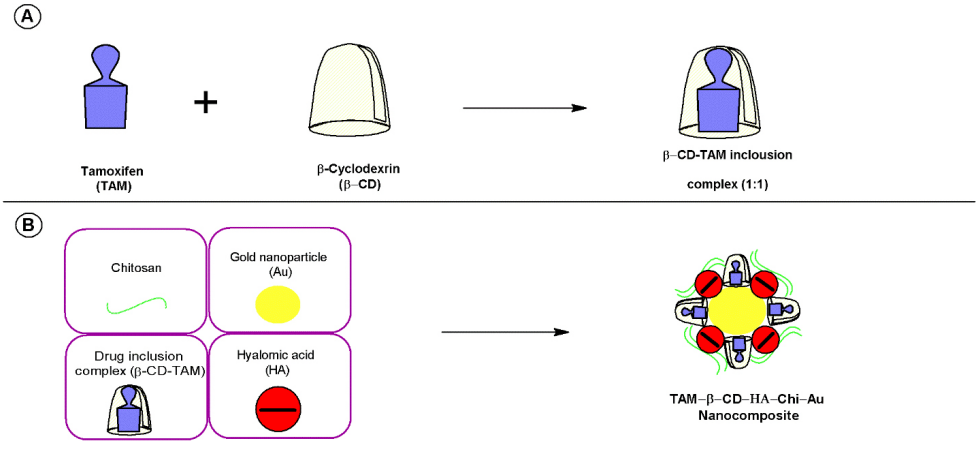

Figure 1. A schematic diagram describing the preparation steps of both β-CD-Tam inclusion complex (A) and Tam-β-CD-HA-Chi-Au nanocomposite (B)
β-CD: β-Cyclodextrin, Tam: Tamoxifen, HA: Hyaluronic acid, Chi: Chitosan, Au: Gold

dissolved in (2:1, v/v) a mixture of methanol and 30% of ammonium hydroxide. The solution was filtered through a 0.45 µ membrane filter and the filtrate was evaporated under reduced pressure and dried in a vacuum oven (80˚C and 695 ± 69 mbar) (Figure 1A).[22,23]

Preparation of gold nanoparticles

In brief, 2.5 mL of chloroauric acid ($HAuCL_4$) solution (1 $mg.mL^{-1}$) was mixed with 20 mL ultrapure water and the solution temperature was maintained at 80˚C under magnetic stirring at 350 rpm. Then, Au NPs were formed by adding 1 mL of sodium citrate tribasic dihydrate solution (7 $mg.mL^{-1}$) and stirring was continued until the colour of the solution changed to purple.

Preparation of chitosan-gold nanoparticles

Chi-Au NPs were prepared by adding 0.2 mL Chi solution (0.5 $mg.mL^{-1}$) and 2.5 mL of $HAuCL_4$ solution (1 $mg.mL^{-1}$) along with 19.8 mL of ultrapure water at 80˚C and 700 rpm. Then, 1 mL of sodium citrate tribasic dihydrate solution (7.5 $mg.mL^{-1}$) was added to the obtained solution and the stirring was continued until the colour of the solution changed to dark blue.

Preparation of Tam-β-CD-HA-Chi-Au nanocomposite

Briefly, 12.5 mL of $HAuCL_4$ solution (1 $mg.mL^{-1}$) was mixed with 1 mL Chi solution (0.5 $mg.mL^{-1}$) and 97.5 mL of ultrapure water was added under stirring at 500 rpm and a temperature of 65˚C for 30 min. Then, 2.5 mL of Tam-β-CD inclusion compound and 500 µg of HA were added to the solution. Finally, the formation of NPs was achieved by adding 3.66 mL of sodium citrate tribasic dihydrate solution (15 $mg.mL^{-1}$) along with 1.84 mL of TPP solution (1 $mg.mL^{-1}$) to the obtained solution under continuous stirring. The resulting NPs were centrifuged at 13,000 rpm, dried by vacuum oven (80˚C and 695 ± 69 mbar), and used for further studies.

Determination of particle size, zeta-potential and polydispersity index

Zeta-potential of Tam-β-CD-HA-Chi-Au nanocomposite was measured by Doppler anemometry using zeta-sizer (Malvern instrument, Malvern, UK) at 25˚C. Around 2 mL samples were filtered by 0.20 µm syringe filter and then filled in the zeta cell for measuring the size and charge of the nanocomposite.

High resolution transient absorption microscopy (HRTEM)

HRTEM was conducted using a JEM-2100F microscope. The structure and morphology of Tam-β-CD-HA-Chi-Au nanocomposite were determined. The sample was sonicated for 15 min. Then, one drop of the sample was placed on an HRTEM grid and maintained at room temperature of 4′,6-diamidino-2-phenylindole (DAPI) until it was completely dry. After that, morphology of the nanocomposite was observed and high-quality images were taken.

Ultraviolet-visible (UV-visible) spectra

Optical properties of the Au NP solutions were determined using a double beam spectrophotometer by scanning the spectra from 200 to 800 nm. Sodium citrate tribasic dihydrate and TPP solution were used as the blank and ultrapure water was used as the solvent. Au NPs, Chi-Au NPs, and Tam-β-CD-HA-Chi-Au nanocomposite solutions were characterized as well. Fourier transform infrared spectroscopy (FTIR) spectrometers.

All spectra of the samples were taken by the Thermo Fisher Scientific Nicolet iS5 spectrophotometer (Wisconsin, USA), using OMNIC Software from 1000 to 4000 cm^{-1} at a data acquisition rate of 2 cm^{-1} *per* point.

Determination of encapsulation and loading efficiency

To assess the encapsulation and loading efficiency (EE) of Au NPs, 5 mg of Tam-loaded Au NPs were dissolved in methanol, then filtered and centrifuged for 30 min at 13,000 rpm.[24,25] The amount of Tam in the supernatant was determined by HPLC and the EE was calculated using the following equation:[26]

$$EE\ (\%) = \frac{(\text{total Tamoxifen citrate content} - \text{free Tamoxifen citrate content})}{\text{total Tamoxifen citrate content}} \times 100$$

equation 1

Chromatographic conditions

The HPLC system used for this study was a Waters 2487 dual λ absorbance detector equipped with Water 1515 Isocratic HPLC Pump and Supelco® analytical column with 15 cm x 4.6 mm *i.d.*; 5 µm particle size. The mobile phase for gradient elution was composed of a solution of acetic acid and 1% of ammonium acetate in methanol (1:99) at 1.5 $mL.min^{-1}$ flow.[27] 10 µL of the sample was injected into the chromatographic system.

Cell culture

MCF-7 (ATCC HTB22™) and Caco-2 (ATCC HTB-37) cells were routinely kept in DMEM containing 1% penicillin-streptomycin at 37˚C and 10% fetal bovine serum in 5% CO_2 and 95% air.

Dynamic assessment of cytotoxic effect of Tam-β-CD-HA-Chi-Au nanocomposites on Caco-2 and MCF-7 cells using real-time cell analysis

In this study, real-time cellular analysis (RTCA) xCELLigence technology was chosen for screening the cytopathic effect of the nanocomposite by monitoring the cellular impedance of the cells in real-time during the complete time course of the experiment.[24] Background measurements were taken from the wells by adding 50 µL of DMEM media to E-plates 16. Then, MCF-7 and Caco-2 cells were seeded and plated at a density of $1x10^4$ cells/well in fresh DMEM medium grown overnight at 37˚C and 5% CO_2 to reach the log phase, then incubated with Tam, Tam-β-CD-Au NPs, and Tam-β-CD-HA-Chi-Au nanocomposite (each complex contained 23.69, 35.69, and 47.55 µM Tam) or medium alone, and cell responses were monitored by taking RTCA DP instrument (ACEA Biosciences Inc., USA) readings every single 5 min for 24 h and every 30 min for 48 h. Kinetic profile of the cellular responses, the reduction in cell index, and IC_{50} values as *per* each complex were taken accordingly against their respective concentrations.[25]

Preparation of rhodamine 6G-labeled Tam-β-CD-HA-Chi-Au nanocomposite

The vacuum-dried Tam-β-CD-HA-Chi-Au nanocomposite was redispersed in 5 mL dimethyl sulfoxide solution followed by the

addition of rhodamine 6G and 0.5 mL NaOH (0.1 M) was dissolved in methanol at 10.0 mg.mL^{-1} concentration. The nanocomposites were incubated with rhodamine 6G solution for 24 h in the dark at environmental temperature. The prepared rhodamine-labelled Tam-β-CD-HA-Chi-Au nanocomposites were collected by centrifugation and washed 3 times with methanol until the free rhodamine 6G could not be seen in the supernatant. Then, Tam-β-CD-HA-Chi-Au nanocomposites were resuspended in 5 mL PBS after centrifugation.

Cellular uptake assessment of Tam-β-CD-HA-Chi-Au nanocomposites by fluorescence microscopy

A Zeiss Axio Vert.A1 inverted microscope (Carl Zeiss, Germany) outfitted with HBO 50 W mercury vapor lamp and exciter/emitter filter combinations were used. Filter 38 (495 nm excitation and 517 nm emission) was used to observe FITC stained cellular membrane with green. Filter 43 (550 nm excitation and 573 nm emission) was used to observe rhodamine-labelled Tam-β-CD-HA-Chi-Au nanocomposites with red and filter 49 (359 nm excitation and 457 nm emission) was used to observe DAPI stained cells with blue. MCF-7 and Caco-2 cells were seeded at a density of 1x10^5 cells/well. Then, the cells were shifted to centrifuge tubes containing serum free medium supplemented with rhodamine-labelled Tam-β-CD-HA-Chi-Au nanocomposites (100 µg.mL^{-1}) and kept in the dark place for 6 h. Instantly after 6 h, the cells were washed several times with PBS and fixed by 100 µL of 37% formaldehyde, then left at environmental temperature for 10 min followed by additional washing steps. The cells were centrifuged at 4000 rpm and the supernatant was discarded. Then, 10 µL of DAPI stain (1 µg.mL^{-1}) and 10 µL of FITC stain (60 µg.mL^{-1}) were added. The cells were kept in the dark place for 20 min. Finally, the cells were centrifuged and separated, then resuspended in 20 µL of PBS and 1 µL of cell suspension was placed onto a glass slide, then the slide was coated with a coverslip.[28] The images of the cells were captured, under standardized setting and contact time, a fluorescence microscope and Zen 2010 software (Blue Edition) was used for image analysis.

Statistical analysis

The one-way ANOVA was used to determine the significant differences between the means of three Tam-β-CD-HA-Chi-Au nanocomposite concentrations.

RESULTS AND DISCUSSION

Preparation of Tam-β-CD-HA-Chi-Au nanocomposite

Tam-β-CD-HA-Chi-Au nanocomposites were prepared as described by Turkevich et al.[29] with modification. Chi was used to offer sufficient surface area for loading the drug and improve drug delivery; hence, it was chosen to be mixed with Au (III) chloride.[30] Then, ultrapure water was added under stirring at 500 rpm and at a temperature of 65°C for 30 min, followed by the addition of Tam-β-CD inclusion compound to improve Tam solubility. HA was added to enhance tumour permeability and NP retention[31,32] along with TPP solution, which was used as cross-linker to form electrostatic attraction between the positively charged Chi and negatively charged TPP.[33] Finally, due to the reduction properties of sodium citrate tribasic dihydrate, it was added to sodium citrate tribasic dihydrate to achieve the formation of Au NPs (Figure 1B) and it resulted in the repositioning and rigidization of both inclusion compound and Chi on the superficial of Au NPs to form Tam-β-CD-HA-Chi-Au nanocomposite.[29,34]

Particle size, zeta potential, and polydispersity index (PDI) determination

Average size of the prepared NPs was 12.31 nm with -46.4 mV zeta potential for Au NPs, 21.66 nm with -37.7 mV zeta potential for Chi-Au NPs and 82.02 nm with -32.6 mV zeta potential and PDI 0.107 (Figure 2A, B) for Tam-β-CD-HA-Chi-Au nanocomposite (Table 1). Setyawati et al.[35] stated that the size of their Au NPs was 11 nm. Moreover, Regiel-Futyra et al.[36] reported that the size of Chi-Au NPs was 26 nm, which is similar to our average size of Chi-Au NPs. However, Kang and Ko[37] prepared docetaxel cationic lipid-coated Au NPs with a size of about 70 nm, which is smaller than the size of our Tam-β-CD-HA-Chi-Au nanocomposite.

High resolution transmission electron microscope studies

HRTEM images revealed that the Au occupied the central position, and a layer of polymer surrounding the Au NPs that indicate a successful formulation of Au NPs and a layer of Chi and inclusion complex was deposited on the surface of NPs (Figure 3C). Figure 3A, B presents different Au NP shapes including spherical, hexagonal and irregular shapes. Regiel-Futyra et al.[36] reported that most of their Au NPs were in spherical shape. However, previous research reported the presence of irregular NPs with an average size of 33 nm.[38]

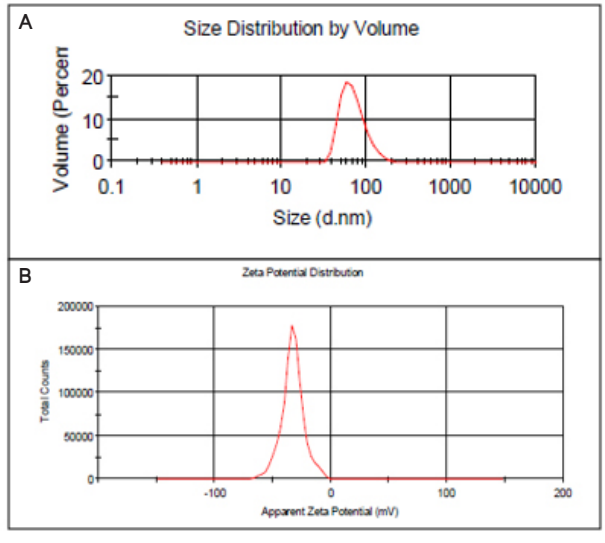

Figure 2. Size distribution of Tam-β-CD-HA-Chi-Au nanocomposite by volume (A), zeta potential distribution of Tam-β-CD-HA-Chi-Au nanocomposite (B)

β-CD: β-Cyclodextrin, Tam: Tamoxifen, HA: Hyaluronic acid, Chi: Chitosan, Au: Gold

UV-vis spectra

The reduction of $HAuCL_4$ to Au NPs was confirmed by UV spectroscopy, by scanning the spectra from 200 to 800 nm (Figure 4D). The UV-Vis spectra of gold nanoparticles (GNPs) revealed maximum absorbance at 233 and 529 nm, which indicated that the $HAuCL_4$ was converted to Au NPs. Whereas, when Chi was incorporated with GNPs, the result showed a shifting in λ_{max} from 233 to 243 and from 529 to 527 nm. Noticeably, this shifting in λ_{max} changed colour form purple (GNPs) to light violet (Chi-GNPs) (Figure 4A, B). However, the maximum absorbance of Tam-β-CD-HA-Chi-Au nanocomposite was at 221 and 527 nm with a dark violet (Figure 4C) (Table 2).

Determination of encapsulation efficiency

As previously described, the encapsulation EE of Au NPs can be calculated using equation (1), which was found to be 94.97%.

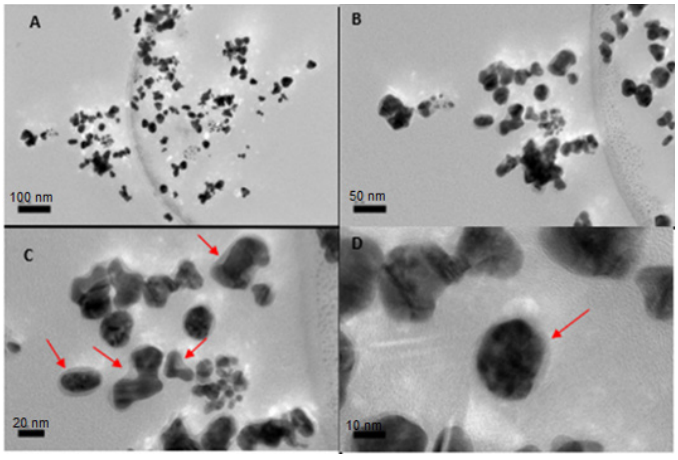

Figure 3. Images of Tam-β-CD-HA-Chi-Au nanocomposite. A and B show different Au NP shapes including spherical, hexagonal and irregular. C and D show the successful formation of Chi and the inclusion complex layer that surrounded the Au NPs

β-CD: β-Cyclodextrin, Tam: Tamoxifen, HA: Hyaluronic acid, Chi: Chitosan, Au: Gold, NPs: Nanoparticles

FTIR characterization

A comparison was made of several FTIR spectra of analyzed samples to confirm the complex formation between Au NPs, Chi-Au NPs, inclusive compound, and Tam-β-CD-HA-Chi-Au nanocomposite. Figure 5B reveals that the characteristic peak

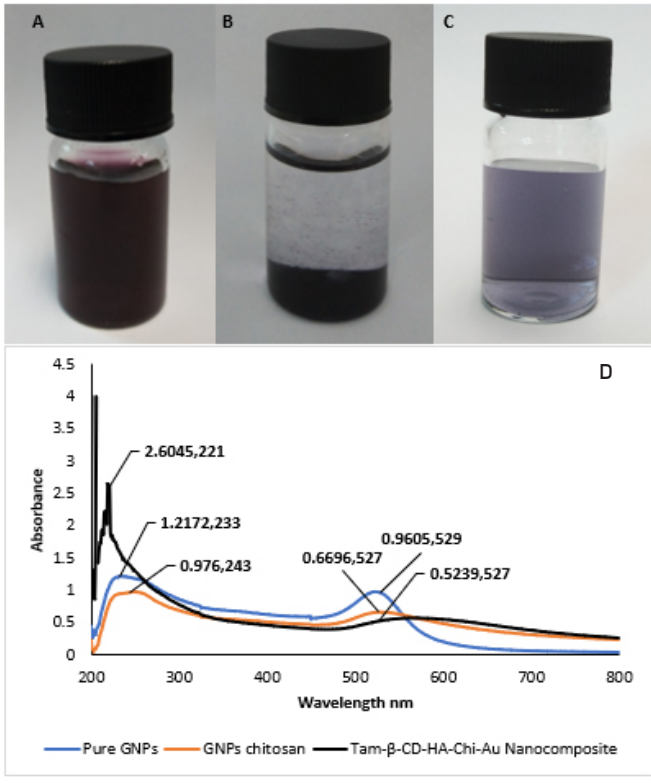

Figure 4. GNPs (A), Chi-GNPs (B), Tam-β-CD-HA-Chi-Au nanocomposite (C), absorption spectra of GNPs. The results demonstrated the correlation between the shift in l_{max} and the formation of NPs (D)

β-CD: β-Cyclodextrin, Tam: Tamoxifen, HA: Hyaluronic acid, Chi: Chitosan, Au: Gold, NPs: Nanoparticles, GNP: Gold nanoparticles

Table 1. Mean particle size, zeta potential, and polydispersity index of the prepared gold nanoparticle

Parameters	Au NPs	Chi-Au NPs	Tam-β-CD-HA-Chi-Au nanocomposite
Mean particle size	12.31	21.66	82.02
Zeta potential	-46.4	-37.7	-32.6
PDI	0.544	0.557	0.107

β-CD: β-Cyclodextrin, Tam: Tamoxifen, HA: Hyaluronic acid, Chi: Chitosan, Au: Gold, PDI: Polydispersity index, NPs: Nanoparticles

Table 2. The shift in λ_{max} between GNPs, Chi-GNPs, and Tam-β-CD-HA-Chi-Au due to change in the chemical composition in nanocomposite is shown in Figure 4

Nanoparticles	Absorbance (nm)
GNPs	233 and 529
Chi-GNPs	243 and 527
Tam-β-CD-HA-Chi-Au nanocomposite	221 and 527

β-CD: β-Cyclodextrin, Tam: Tamoxifen, HA: Hyaluronic acid, Chi: Chitosan, Au: Gold, GNPs: Gold nanoparticles

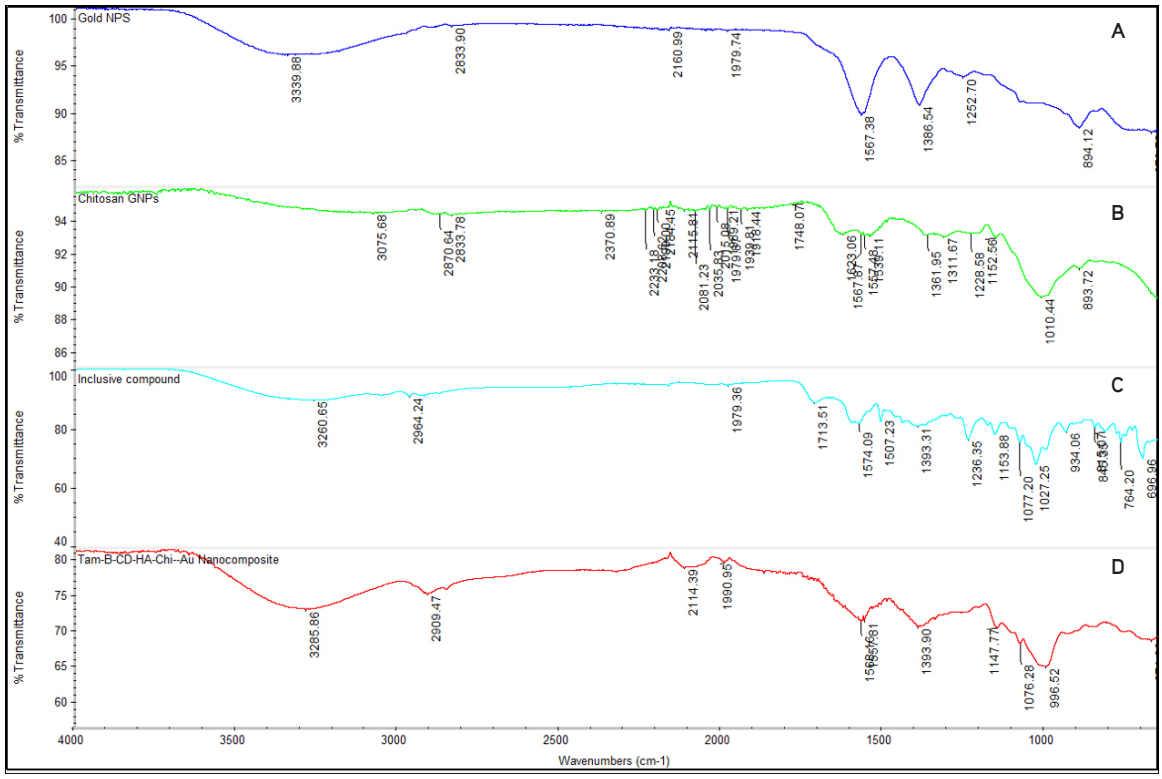

Figure 5. FTIR spectrum of Au NPs (A), Chi NPs (B), inclusion complex (C) and Tam-β-CD-HA-Chi-Au nanocomposite (D)

FTIR: Fourier transform infrared spectroscopy, β-CD: β-Cyclodextrin, Tam: Tamoxifen, HA: Hyaluronic acid, Chi: Chitosan, Au: Gold, NPs: Nanoparticles

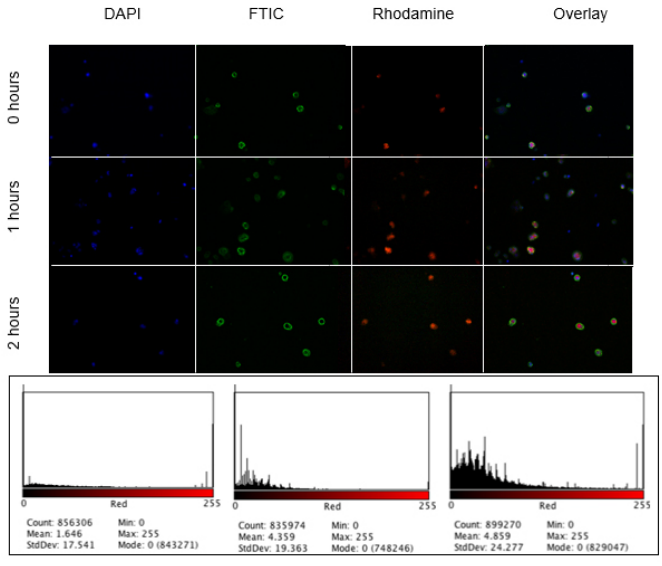

Figure 6. Rhodamine incorporated Tam-β-CD-HA-Chi-Au nanocomposite uptake by Caco-2 cells. Caco-2 cells were analysed by fluorescence microscopy after 0 h, 1 h and 2 h of incubation with Tam-β-CD-HA-Chi-Au nanocomposite (A). The red-light intensity due to rhodamine incorporated Tam-β-CD-HA-Chi-Au nanocomposite represents the cellular uptake of the developed formulation at 0 h (B), 1 h (C) and 2 h (D)

β-CD: β-Cyclodextrin, Tam: Tamoxifen, HA: Hyaluronic acid, Chi: Chitosan, Au: Gold, NPs: Nanoparticles

of Chi at 1645 cm^{-1} disappeared and two new peaks appeared at 1623 cm^{-1} and 1567 cm^{-1}. This disappearance of the peaks can be explained by the attribution of the band to the linkage of the phosphoric and ammonium ions. This new band at 1623 cm^{-1} was due to N-H vibrations in NH^{3+} ion, which showed the occurrence of the cross-linking between Chi and TPP and confirmed the formation of the polyelectrolyte complex. However, the characteristic peaks of Tam in the inclusion complex entirely vanished showing characteristic peaks at 1393 cm^{-1} (coupled in plane bending of CH_2), 2964 cm^{-1} (asymmetric stretching from CH_2), and at 3260 cm^{-1} (asymmetric and symmetric stretching of OH). Figure 5C indicates that the Tam molecule was entirely inserted into the β-CD cavity. In Figure 5D, none of the characteristic peaks of Tam nor β-CD were observed as the inclusive compound was loaded into the NPs, but only the characteristic peaks of Chi and Au NPs were observed with slight shifting due to the surface interaction between Chi and Au NPs.

Cellular uptake of Tam-β-CD-HA-Chi-Au nanocomposite using fluorescence microscopy techniques

The objective of fluorescence microscope imaging was to confirm the cellular uptake of NPs by Caco-2 and MCF-7 cells. As shown in Figure 6A, rhodamine stained the NPs with a red and DAPI stained the nucleus with a blue, whereas fluorescein isothiocyanate stained the cellular membrane with a green. According to the data presented in Figure 6A, Caco-2 cellular uptake of Tam-β-CD-HA-Chi-Au nanocomposite is time-

dependent. The fluorescence microscopy indicated that the Tam-β-CD-HA-Chi-Au nanocomposite had entered the cancer cell and was localized near the nucleus. In other words, there was a portion of the Tam: β-CD-HA-Chi-Au nanocomposite was taken up by the cell and got localized next to the nucleus. Additionally, fluorescence images showed a punctuated staining pattern due to intracellular aggregates of the nanocomposites.

Hence, cellular uptake of the prepared Tam-β-CD-HA-Chi-Au nanocomposite was efficiently improved by Chi properties such as mucoadhesive and absorption enhancement. Moreover, the cellular uptake was also quantified by measuring the red light (due to rhodamine-labelled NPs) intensity *per* cell and as shown in Figures 6B-D (Table 3). These observations suggested that the light intensity is directly correlated with the incubation time, indicating that the developed formulation improved the cellular uptake of NPs in time-dependent manner. However, as shown in Figure 7, Tam-β-CD-HA-Chi-Au nanocomposites did not appear at zero hour, indicating that absorption did not occur. However, at 1 h and 2 h, MCF-7 cellular uptake of Tam-β-CD-HA-Chi-Au nanocomposite was time-dependent with a slight improvement in cellular uptake.

Cytotoxicity of Tam-β-CD-HA-Chi-Au nanocomposite on Caco-2 cells and MCF-7

In this study, Caco-2 and MCF-7 cell lines were used to investigate cytotoxicity of Tam-β-CD-HA-Chi-Au nanocomposite on cancer cells and the cellular impedance of the cells was monitored by an RTCA DP instrument. Figure 8A presents dose-dependent cytotoxicity of Tam-β-CD-HA-Chi-Au nanocomposite on the Caco-2 cell line. Tam-β-CD-HA-Chi-Au nanocomposite significantly improved the cytotoxic activity of Tam since the half maximal IC_{50} value of Tam decreased from 8.55 μM to 5.32 μM after 48 h of incubation time (*p* value <0.00001). Since the intestinal epithelium of the small and large intestines is normally surrounded by goblet cells which secrete a thick layer of mucus around them, was postulated that the improvement in the cytotoxicity over time is due to the mucoadhesive and absorption enhancement properties of Chi. A similar study has shown that the keratinocyte growth (FGF7) FGF7: β-CD: Everolimus complex has a significant cytotoxicity on Caco-2 cells and has improved the antiproliferative effect of everolimus. In other words, FGF7: β-CD: Everolimus complex succeeded in reducing the IC_{50} value of everolimus from 9.65 μM to 1.87 μM.[39]

Table 3. The intake of rhodamine-incorporated Tam-β-CD-HA-Chi-Au nanocomposite deviation for 0 h, 1 h, and 2 h is shown in Figure 6

Time	0 h (h)	1 h (h)	2 h (h)
Intake of rhodamine-incorporated Tam-β-CD-HA-Chi-Au nanocomposite	856306 ± 17.541	835975 ± 19.363	899272 ± 24.277

β-CD: β-Cyclodextrin, Tam: Tamoxifen, HA: Hyaluronic acid, Chi: Chitosan, Au: Gold

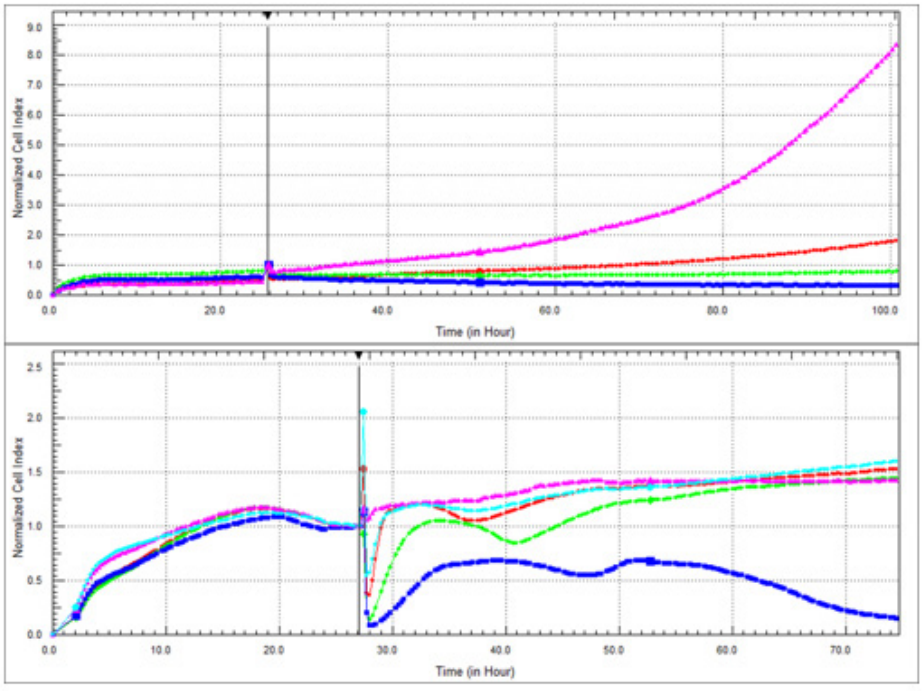

Figure 7. Rhodamine incorporated Tam-β-CD-HA-Chi-Au nanocomposite uptake by MCF-7 cells was analysed by fluorescence microscopy after 0 h, 1 h, and 2 h of incubation with Tam-β-CD-HA-Chi-Au nanocomposite. The red-light intensity due to rhodamine incorporated Tam-β-CD-HA-Chi-Au nanocomposite represents the cellular uptake of the developed formulation at 0 h, 1 h, and 2 h

β-CD: β-Cyclodextrin, Tam: Tamoxifen, HA: Hyaluronic acid, Chi: Chitosan, Au: Gold

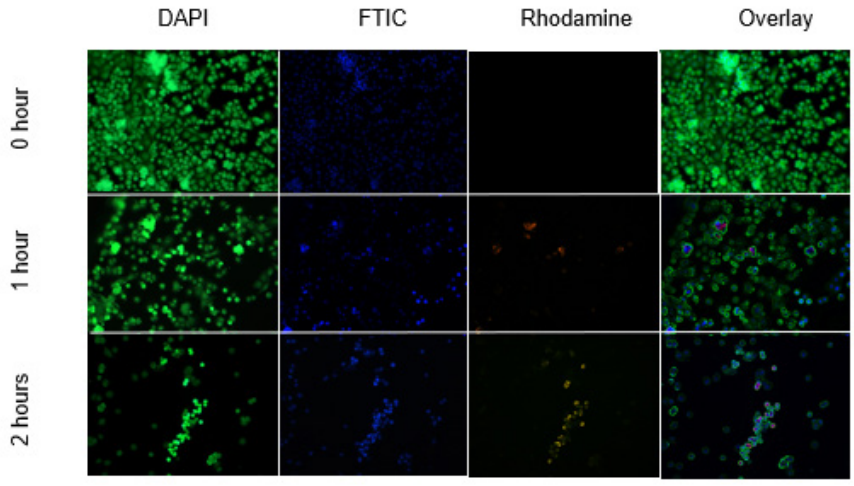

Figure 8. The cytotoxicity of Tam-β-CD-HA-Chi-Au nanocomposite on Caco-2 cells is shown by the RTCA DP instrument (8A). Cells were seeded and incubated with DMEM media (1A), 23.69 μM of Tam-β-CD-HA-Chi-Au nanocomposite (2A), 35.62 μM of Tam-β-CD-HA-Chi-Au nanocomposite (3A), 47.55 μM of Tam-β-CD-HA-Chi-Au nanocomposite (4A). The cytotoxicity of Tam-β-CD-HA-Chi-Au nanocomposite on MCF-7 cells is shown by the RTCA DP instrument (8B). Cells were seeded incubated with DMEM medium (pink), 2.15 μg of Tam-β-CD-HA-Chi-Au nanocomposite (red), 3.23 μg of Tam-β-CD-HA-Chi-Au nanocomposite (green), 4.31μg of Tam-β-CD-HA-Chi-Au nanocomposite (dark blue), cells incubated with DMSO (light blue)

β-CD: β-Cyclodextrin, Tam: Tamoxifen, HA: Hyaluronic acid, Chi: Chitosan, Au: Gold, RTCA: Real-time cellular analysis xCELLigence, DMEM: Dulbecco's Modified Eagle's Medium, DMSO: Dimethyl sulfoxide

On the other hand, no improvement in Tam cytotoxicity was observed, when the nanocomposite was tested on the MCF-7 cell line as the IC_{50} value of Tam was 6.48 μM, which is lower than nanocomposite 68.6 μM, after 48 h of incubation time. It is mainly due to the lack of mucus lining around MCF-7 cells, which prevents the adhesion of the nanocomposite to the cell surface and reduces the cellular uptake, and consequently affects the cytotoxicity of Tam (Figure 8B).

CONCLUSION

Tam-β-CD-HA-Chi-Au nanocomposite was prepared successfully, which exhibited an average size of 82.02 nm with -23.6 mV zeta potential. Au occupied the central position and a layer of polymer was surrounding Au NPs that indicates a successful formulation of Au NPs, and a layer of Chi and the inclusion complex was deposited on the surface of the NPs. Furthermore, Tam-β-CD-HA-Chi-Au nanocomposite (equivalent to 5.32 μM of Tam citrate) significantly improved the cytotoxic activity and cellular uptake of Tam on Caco-2 cells. However, the developed formula showed more effect on Caco-2 than MCF-7. In conclusion, this study showed that Tam-β-CD-HA-Chi-Au nanocomposite is a potential nanocarrier to deliver the drug to cancer cells, due to its improved Tam activity on colorectal cancer cells.

ACKNOWLEDGMENTS

This project is supported by Fundamental Research Grant Scheme (reference code: FRGS/1/2021/SKK0/UCSI/02/5), Ministry of Higher Education and Pioneer Scientists Incentive Fund Under Centre of Excellence in Research, Value Innovation and Entrepreneurship, (project code: Proj-In- FPS-017) UCSI University, Malaysia.

Ethics

Ethics Committee Approval: There is no requirement for ethical approval.

Informed Consent: Not applicable.

Peer-review: Externally peer-reviewed.

Authorship Contributions

Concept: V.K.P., Design: V.K.P., J.S.N., Data Collection or Processing: Y.K., V.K.P., M.S., J.S.N., S.S.C., Analysis or Interpretation: Y.K., V.K.P., M.S., J.S.N., S.S.C., Literature Search: Y.K., M.S., J.S.N., Writing: Y.K., V.K.P.

Conflict of Interest: No conflict of interest was declared by the authors.

Financial Disclosure: The authors declared that this study received no financial support.

REFERENCES

1. Li R, Xie Y. Nanodrug delivery systems for targeting the endogenous tumor microenvironment and simultaneously overcoming multidrug resistance properties. J Control Release. 2017;251:49-67.
2. Bromma K, Chithrani DB. Advances in gold nanoparticle-based combined cancer therapy. Nanomaterials (Basel). 2020;10:1671.
3. Siegel RL, Miller KD, Goding Sauer A, Fedewa SA, Butterly LF, Anderson JC, Cercek A, Smith RA, Jemal A. Colorectal cancer statistics, 2020. CA Cancer J Clin. 2020;70:145-164.
4. Zhao Y, Hu X, Zuo X, Wang M . Chemopreventive effects of some popular phytochemicals on human colon cancer: a review. Food Funct. 2018;9:4548-4568.
5. Howell A, Dowsett M. Recent advances in endocrine therapy of breast cancer. BMJ. 1997;315:863-866.
6. Maeda H, Nakamura H, Fang J. The EPR effect for macromolecular drug delivery to solid tumors: improvement of tumor uptake, lowering of

systemic toxicity, and distinct tumor imaging *in vivo*. Adv Drug Deliv Rev. 2013;65:71-79.

7. Bertrand N, Wu J, Xu X, Kamaly N, Farokhzad OC. Cancer nanotechnology: the impact of passive and active targeting in the era of modern cancer biology. Adv Drug Deliv Rev. 2014;66:2-25.
8. Nazir S, Hussain T, Ayub A, Rashid U, MacRobert AJ. Nanomaterials in combating cancer: therapeutic applications and developments. Nanomedicine. 2014;10:19-34.
9. Barenholz Y. Doxil®-the first FDA-approved nano-drug: lessons learned. J Control Release. 2012;160:117-134.
10. Reynolds C, Barrera D, Jotte R, Spira AI, Weissman C, Boehm KA, Pritchard S, Asmar L. Phase II trial of nanoparticle albumin-bound paclitaxel, carboplatin, and bevacizumab in first-line patients with advanced nonsquamous non-small cell lung cancer. J Thorac Oncol. 2009;4:1537-1543.
11. A Phase III Study of NK105 in Patients With Breast Cancer: US National Library of Medicine. Available from: https://clinicaltrials.gov/ct2/show/NCT01644890?term
12. Silva JM, Videira M, Gaspar R, Préat V, Florindo HF. Immune system targeting by biodegradable nanoparticles for cancer vaccines. J Control Release. 2013;168:179-199.
13. Shi J, Kantoff PW, Wooster R, Farokhzad OC. Cancer nanomedicine: progress, challenges and opportunities. Nat Rev Cancer. 2017;17:20-37.
14. Thakor AS, Jokerst J, Zavaleta C, Massoud TF, Gambhir SS. Gold nanoparticles: a revival in precious metal administration to patients. Nano Lett. 2011;11:4029-4036.
15. Koushik O, Rao Y, Kumar P, Karthikeyan R. Nano drug delivery systems to overcome cancer drug resistance-a review. J Nanomed Nanotechnol. 2016;7:378.
16. Li W, Zhang H, Assaraf YG, Zhao K, Xu X, Xie J, Yang DH, Chen ZS. Overcoming ABC transporter-mediated multidrug resistance: molecular mechanisms and novel therapeutic drug strategies. Drug Resist Updat. 2016;27:14-29.
17. Haley B, Frenkel E, eds. Nanoparticles for drug delivery in cancer treatment. Urologic Oncology: Seminars and original investigations; 2008: Elsevier.
18. Creixell M, Peppas NA. Co-delivery of siRNA and therapeutic agents using nanocarriers to overcome cancer resistance. Nano Today. 2012;7:367-379.
19. Akpan EI, Gbenebor OP, Adeosun SO, Cletus O. Solubility, degree of acetylation, and distribution of acetyl groups in chitosan. Handbook of Chitin and Chitosan. 2020:131-164.
20. Yu S, Xu X, Feng J, Liu M, Hu K. Chitosan and chitosan coating nanoparticles for the treatment of brain disease. Int J Pharm. 2019;560:282-293.
21. Shariatinia Z. Pharmaceutical applications of chitosan. Adv Colloid Interface Sci. 2019;263:131-194.
22. Priotti J, Baglioni MV, García A, Rico MJ, Leonardi D, Lamas MC, Menacho Márquez M. Repositioning of anti-parasitic drugs in cyclodextrin inclusion complexes for treatment of triple-negative breast cancer. AAPS PharmSciTech. 2018;19:3734-3741.
23. SreeHarsha N, Hiremath JG, Chilukuri S, Aitha RK, Al-Dhubiab BE, Venugopala KN, Alzahrani AM, Meravanige G. An approach to enhance dissolution rate of tamoxifen citrate. Biomed Res Int. 2019;2019:2161348.
24. Vijayakumar A, Baskaran R, Jang YS, Oh SH, Yoo BK. Quercetin-loaded solid lipid nanoparticle dispersion with improved physicochemical properties and cellular uptake. AAPS PharmSciTech. 2017;18:875-883.
25. Zhang Y, Li Z, Zhang K, Yang G, Wang Z, Zhao J, Hu R, Feng N. Ethyl oleate-containing nanostructured lipid carriers improve oral bioavailability of *trans*-ferulic acid ascompared with conventional solid lipid nanoparticles. Int J Pharm. 2016;511:57-64.
26. Subedi RK, Kang KW, Choi HK. Preparation and characterization of solid lipid nanoparticles loaded with doxorubicin. Eur J Pharm Sci. 2009;37:508-513.
27. de Santana DP, Braga RMC, Strattmman R, Albuquerque MM, Bedor DCG, Leal LB, da Silva JA. Reversed phase HPLC determination of tamoxifen in dog plasma and its pharmacokinetics after a single oral dose administration. Quim Nova. 2008;31:47-52.
28. Spötl L, Sarti A, Dierich MP, Möst J. Cell membrane labeling with fluorescent dyes for the demonstration of cytokine-induced fusion between monocytes and tumor cells. Cytometry. 1995;21:160-169.
29. Turkevich J, Stevenson PC, Hillier J. A study of the nucleation and growth processes in the synthesis of colloidal gold. Discuss Faraday Soc. 1951;11:55-75.
30. Nivethaa EAK, Dhanavel S, Narayanan V, Vasu CA, Stephen A. An *in vitro* cytotoxicity study of 5-fluorouracil encapsulated chitosan/gold nanocomposites towards MCF-7 cells. RSC Advances. 2015;5:1024-1032.
31. Mattheolabakis G, Milane L, Singh A, Amiji MM. Hyaluronic acid targeting of CD44 for cancer therapy: from receptor biology to nanomedicine. J Drug Target. 2015;23:605-618.
32. Prabhakar U, Maeda H, Jain RK, Sevick-Muraca EM, Zamboni W, Farokhzad OC, Barry ST, Gabizon A, Grodzinski P, Blakey DC. Challenges and key considerations of the enhanced permeability and retention effect for nanomedicine drug delivery in oncology. Cancer Res. 2013;73:2412-2417.
33. Rampino A, Borgogna M, Blasi P, Bellich B, Cesàro A. Chitosan nanoparticles: preparation, size evolution and stability. Int J Pharm. 2013;455:219-228.
34. Abdulkin P, Precht TL, Knappett BR, Skelton HE, Jefferson DA, Wheatley AE. Systematic control of size and morphology in the synthesis of gold nanoparticles. Part Part Syst Charact. 2014;31:571-579.
35. Setyawati MI, Tay CY, Bay BH, Leong DT. Gold nanoparticles induced endothelial leakiness depends on particle size and endothelial cell origin. ACS Nano. 2017;11:5020-5030.
36. Regiel-Futyra A, Kus-Liśkiewicz M, Sebastian V, Irusta S, Arruebo M, Stochel G, Kyzioł A. Development of noncytotoxic chitosan-gold nanocomposites as efficient antibacterial materials. ACS Appl Mater Interfaces. 2015;7:1087-1099.
37. Kang JH, Ko YT. Lipid-coated gold nanocomposites for enhanced cancer therapy. Int J Nanomedicine. 2015;10 Spec Iss(Spec Iss):33-45.
38. Bindhu MR, Umadevi M. Silver and gold nanoparticles for sensor and antibacterial applications. Spectrochim Acta A Mol Biomol Spectrosc. 2014;128:37-45.
39. Maki MAA, Cheah SC, Bayazeid O, Kumar PV. Cyclodextrin inclusion complex inhibits circulating galectin-3 and FGF-7 and affects the reproductive integrity and mobility of Caco-2 cells. Sci Rep. 2020;10:17468.

Turk J Pharm Sci 2022;19(4):400-407
DOI: 10.4274/tjps.galenos.2021.65087

ORIGINAL ARTICLE

In Vitro Anti-Aging Potential Evaluation of *Maclura pomifera* (Rafin.) Schneider 80% Methanol Extract with Quantitative HPTLC Analysis

Timur Hakan BARAK[1]*, İnci KURT CELEP[2], Tuğba Buse ŞENTÜRK[1], Hilal BARDAKCI[1], Engin CELEP[2]

[1]Acıbadem Mehmet Ali Aydınlar University, Faculty of Pharmacy, Department of Pharmacognosy, Istanbul, Türkiye
[2]Yeditepe University, Faculty of Pharmacy, Department of Pharmacognosy, Istanbul, Türkiye

ABSTRACT

Objectives: *Maclura pomifera* (Rafin.) Schneider is a widespread species all around the world, which is also frequently cultured for ornamental purposes. Previous studies revealed that *M. pomifera* fruits are rich in prenylated isoflavonoids, exhibit noteworthy biological activities, and have probable benefits, particularly, when applied topically. Considering that phenolic compounds are important sources in the development of anti-aging cosmetic products, this study investigated the anti-aging potential of *M. pomifera* 80% methanolic extract (MPM) by evaluating antioxidant and extracellular matrix degrading enzymes inhibiting activity.

Materials and Methods: For this study, the inhibitory potential of 80% MPM against different enzymes associated with the aging process was evaluated. Given the unequivocal role of oxidative stress in aging, *in vitro* antioxidant tests were employed as well. Moreover, osajin was determined as the major bioactive isoflavonoid of the sample by high performance thin layer chromatography analysis.

Results: Results of the mechanistically different antioxidant assays exhibited notable antioxidant potential of the extract. Inhibition potential of MPM against hyaluronidase, collagenase, and elastase enzymes, which are directly linked to acceleration of the aging process, was investigated and results revealed that MPM inhibited the aforementioned enzymes explicitly. MPM had notable phenolic and flavonoid content; 113.92 ± 2.26 mg gallic acid equivalent/g and 66.41 ± 0.74 mg QE/g, respectively. When total antioxidant capacity assays were considered, it is possible to suggest that MPM is a promising anti-aging agent.

Conclusion: As a result, this study discloses that extracts of fruits of *M. pomifera* have significant anti-aging potential and may be used for this purpose.

Key words: *Maclura pomifera*, anti-aging, antioxidants, HPTLC, osajin

INTRODUCTION

Likewise, all organs, human skin undergoes various physiological changes with advancing age.[1] Two classes of aging exit: intrinsic aging is controlled by genetics and extrinsic aging is the natural result of physiological modifications due to damaging effects of environmental factors like ultraviolet (UV) radiation, chemical toxins, and smoking.[1,2] Vascular and glandular structure degradation, fibrous tissue loss, and decreasing cell regeneration are fundamental factors of aging,[3] which lead to increment in tissue degeneration, wrinkles, and decrement of extracellular matrix (ECM).[4]

As the largest organ, the skin has several roles such as protection, regulation of the body temperature, and detection of senses.[5] The skin consists of epidermis, dermis, and subcutaneous tissue and is the first barrier between human body and outer environment.[6,7] ECM is the largest unit of the dermis and supports growth and elasticity by presenting a structural scaffold.[8] Collagen, elastin, and fibronectin, which are formed by dermal fibroblasts, constitute ECM, are fused with proteoglycans.[5] Collagen is a basic protein comprising approximately 25-35% of all protein content in the body, and is found in the extracellular space of various types of animal

*Correspondence: thakanbarak@gmail.com, Phone: +90 216 500 44 44, ORCID-ID: orcid.org/0000-0002-7434-3175
Received: 07.09.2021, Accepted: 17.09.2021

connective tissues.[3] One of the major causes of skin aging and wrinkle formation is the alteration of collagen structure.[1] Elastin is a protein, which confers a unique physiological elasticity to the skin, and is present in several connective tissues.[6] Skin hydration, keeping the skin smooth, moist and lubricated are important factors that prevent skin aging and a major glycosaminoglycan (GAG), hyaluronic acid, plays a vital role in these activities.[8] This pivotal constituents are degradation by hyaluronidase, collagenase, and elastase enzymes, thus, leading to an acceleration of skin aging. Moreover, exposure to microorganisms, pollution, ionizing radiation, chemicals, and toxins leads to the formation of reactive oxygen species (ROS) and it is harmful consequences accelerate skin aging.[9] ROS can initiate complex molecular pathways and as a result, collagenase, elastase, and hyaluronidase activity may be increased, leading to detectable ECM breakdown and skin texture modifications.[10] For the reasons mentioned, novel natural agents, which decline ROS formation and inhibit ECM degrading proteases, may delay skin-ageing process.[11]

Maclura pomifera (Rafin.) Schneider belongs to Moraceae or the mulberry family, and is also known as the osage orange tree, cultivated almost all around the world.[12] *M. pomifera* has several biological activities such as antibacterial, antifungal, antiviral, cytotoxic, antitumor, estrogenic, and antimalarial[13] due to its prenylated isoflavones, *i.e.* osajin and pomiferin, which are considered major metabolites of the fruits.[14] In anti-aging cosmetic production, phenolic compounds are significant natural sources. Thus, there is a growing interest in studying phenolic compound rich plants such as *M. pomifera* for such activities. In previous studies, it was found that isoflavones of *Maclura* increase the expression levels of collagen, elastin, and fibrillin comparable or superior to equivalent concentrations of retinol. Hence, it may be assumed that *Maclura* isoflavones are potent ECM protein stimulants.[15] Considering these data, the aim of this study is to investigate the anti-aging potential of *M. pomifera* 80% methanolic extract (MPM) by exploring its potential for antioxidant bioactivity and inhibiting ECM degrading enzymes. Additionally, quantitative analysis of the major bioactive component of the extract, osajin was measured by high performance thin layer chromatography (HPTLC) and total phenolic content and total flavonoid content assays were conducted for more accurate understanding of the phenolic profile. The results show that *M. pomifera* might be a valuable source of anti-aging products.

MATERIALS AND METHODS

Chemicals

All enzymes, chemicals, and references employed in the tests were afforded by Sigma Chemical Co. (St. Louis, MO, USA). The quality of all chemicals was of analytical grade.

Plant material

The fruits of *M. pomifera* were collected from Uşak, Türkiye, in May, 2020. Dr. Hilal Bardakcı carried out the botanical identification procedure of the plant samples. A voucher sample of the plant was deposited at Acıbadem University, Herbarium of Faculty of Pharmacy (ACUPH 00002).

Preparation of extracts

The fruits were separated into small pieces and passed through a blender. The fruits (6.45 kg) were macerated with 3125 mL of 80% methanol (MeOH) by using a shaking device for three days at room temperature in a dark place. The macerate was filtered and this procedure was repeated twice. The filtrates obtained were gathered together and, then, methanol was evaporated in a rotary evaporator. The crude methanolic extract was lyophilized (the yield was 204.37 g, 3.16%) and stored at -20°C (MPM).

Quantification procedure of the major bioactive compounds by HPTLC

All chemicals and reagents used were of analytical grade. Chloroform ($CHCl_3$) and ethyl acetate (EtOAc) were purchased from Sigma-Aldrich. Commercially available standard of osajin was purchased from Sigma-Aldrich (SMB 00092). HPTLC analyses were performed on 20 cm × 10 cm glass HPTLC silica gel 60 F_{254} plates (Merck, Darmstadt, Germany). Osajin content in MPM was determined by a CAMAG HPTLC analytical system. Mobile phase used in the current study was previously described by Bozkurt et al.[16] during the isolation of active principles of *M. pomifera*. 10 mg/mL MeOH extract was used as the analysis test solution. A standard stock solution (0.5 mg/mL) of osajin was prepared using 2 mL of acetone. A working solution with 50 µg/mL concentration of standard compound was prepared by dilution with acetone from the stock solution. Each sample was filtered through a 0.45 µm syringe filter. 10 µL of the extract along with at least five different concentrations of the standard solution (3.3-4.7 µL) were applied in the form of bands of 8 mm length on silica gel glass HPTLC plates 60 F254 with CAMAG Automatic TLC Sampler IV. Developments were carried out in CAMAG Automatic Developing Chamber-2 (ADC-2) and the mobile phase was $CHCl_3$:EtOAc [8:2 (v/v)]. Chamber was saturated for 10 min and the plate was preconditioned for 5 min before the development. Humidity was controlled by ADC-2 using $MgCl_2$ (33% RH) for 10 min. Densitometric evaluation was carried out using a CAMAG TLC Scanner IV in fluorescence mode. The slit dimension was maintained at 5 × 0.2 mm, micro and the scanning speed was set at 20 mm/s. Standard contents were obtained by comparing area under receiver operating characteristic curves (AUCs) with the calibration curve of standards at 280 nm. The presence of standards in the extract was assured by comparison of both retention factors (R*f*) and overlaying UV spectra of each extract and standards. The quantity of osajin was determined by comparison of the intensity of diffusely reflected light from the extract and fractions with the standard compound.

Osajin content in crude plant extract was measured using HPTLC-densitometry. R*f* value of osajin standard was found to be 0.556. The occurrence of osajin in test samples was verified by comparison of their R*f* values and overlapping their UV spectra (Figure 1). Quantification was afforded by

comparing AUCs of samples with the calibration curve obtained using the standard compound osajin. The calibration function was y=2.268*10-8x. The correlation coefficient (R) and the coefficient of variation of the calibration function were 0.998% and 1.06%, respectively. HPTLC analysis showed that MPM contains 0.22% (w/w) osajin. Results of the HPTLC study are given in Table 1.

Phenolic profile assay

Total phenolic content assay

The assay was performed to evaluate total phenolic contents of the samples in accordance with Folin-Ciocalteu's method, as previously used by Kurt-Celep et al.[17] 20 µL of freshly diluted sample solutions were mixed with 75 µL Na_2CO_3 (20%) and 100 µL FCR (Folin-Ciocalteu reagent) diluted with H_2O (1:9). After incubation for 30 min at 45˚C, the absorbance of the mixtures was read spectrophotometrically at 765 nm. The results were expressed as mg gallic acid equivalents (GAE) *per* g of extract.

Total flavonoid content assay

Measurement of total flavonoid contents of the fractions was done as a method previously reported by Bardakci et al.[18] Concisely, freshly prepared 1 M CH_3COONa and 10% $AlCl_3$ were mixed with the samples. Then, 30 min of incubation of the mixtures was performed at room temperature and in the dark. After incubation process, the absorbance was calculated at 415 nm. The results were asserted as mg quercetin equivalents (QE) in 1 g of sample.

Determination of in vitro antioxidant activity

2,2-Diphenyl-1-picrylhydrazyl (DPPH) radical scavenging activity test

To determine DPPH radical scavenging activity, a combination of freshly diluted sample solutions (various concentrations prepared from 1 mg/mL stock solution) and methanolic DPPH solution (100 mM) were done. After the incubation interval at room temperature for 45 min, the absorbance was read at 517

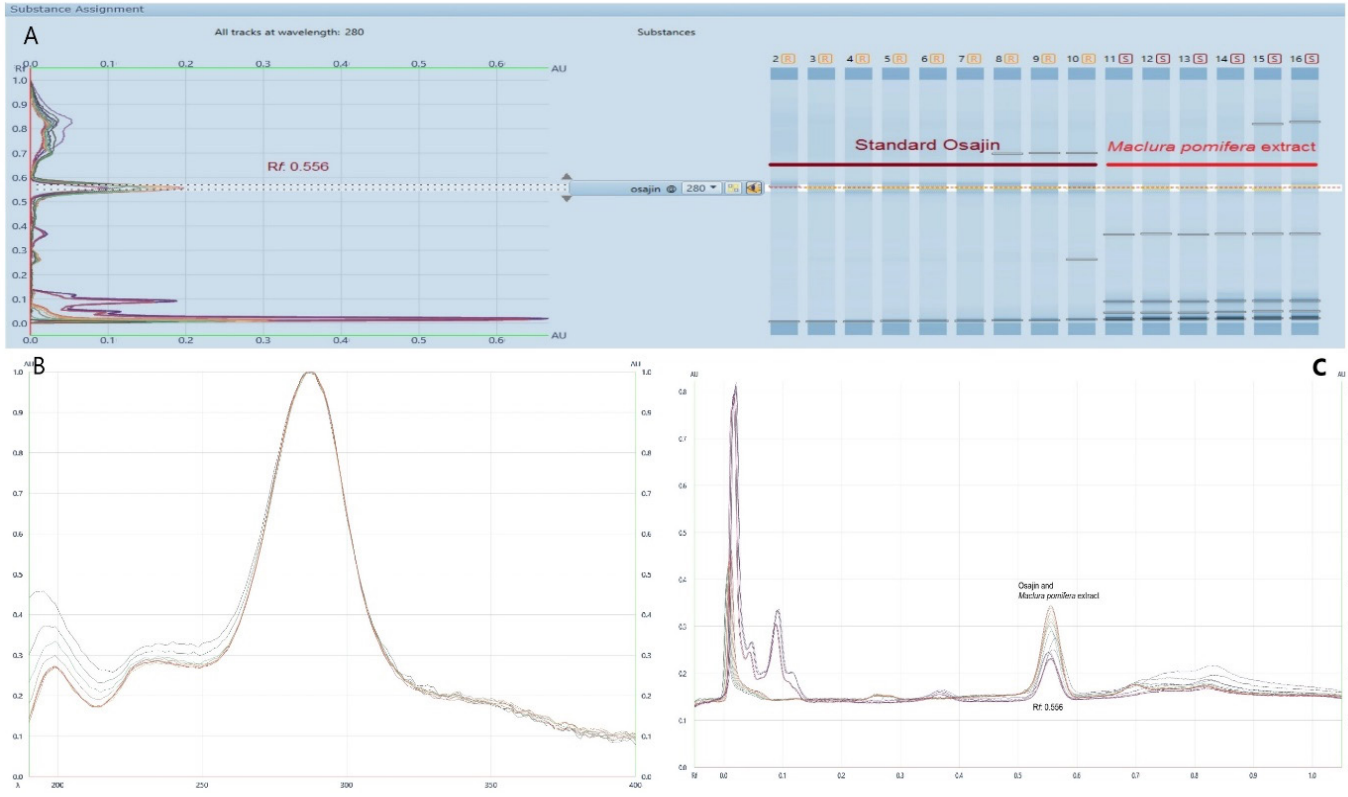

Figure 1. (A) HPTLC chromatogram of standard osajin and test samples at 280 nm. (B) Overlapped UV spectra osajin and *Maclura pomifera* extract. (C) HPTLC chromatogram of standard osajin and test samples at 280 nm

HPTLC: High performance thin layer chromatography, UV: Ultraviolet

Table 1. Spectrophotometric determination of phenolic profile and HPTLC quantification of MPM

	Total phenolic content[A]	Total flavonoid content[B]	Osajin content (%)[C]
MPM[D]	113.92 ± 2.26	66.41 ± 0.74	0.22 ± 0.01

[A]Results were expressed as the mean of triplicates ± standard deviation and as mg gallic acid equivalents in 1 g sample.
[B]Results were expressed as the mean of triplicates ± standard deviation and as mg quercetin equivalents in 1 g sample.
[C]Quantification data of osajin in MPM[D] by HPTLC analysis.
[D]MPM: 80% Methanolic extract of *Maclura pomifera* (Rafin.) Schneider.

nm. Butylated hydroxy toluene (BHT) was used as reference compound to acquire a calibration curve. IC_{50} values of results were stated as µg/mL.[19]

Ferric reducing antioxidant power (FRAP) test

To obtain FRAP reagent, 25 mL of 300 mM acetate buffer (pH 3.6), 2.5 mL TPTZ [2,4,6-tris (2-pyridyl)-s-triazine] and 2.5 mL of $FeCl_3.6H_2O$ (20 mM) were mixed. After that, 10 mL of the sample was added to 260 mL of FRAP reagent and diluted to 300 mL with distilled water in a 96 well-plate. After incubating for 30 min at 37°C, the measurement of absorbance was performed at 593 nm. BHT was used as reference compound. Ferrous chloride solution (0.252 mM) was used to obtain a standard curve and the results were given as mM $FeSO_4$ in 1 g dry extract.[20]

Cupric-reducing antioxidant capacity (CUPRAC) test

CUPRAC test was estimated according to the method described before by Barak et al.[21] Equal volumes of 10 mM $CuSO_4$, neocupraine, and ammonium acetate buffer (85 mL) were mixed in a 96 well plate. After that, 51 mL of distilled water and 43 mL of sample solutions were added to the mixture, respectively. After incubation for 20 min, the absorbance was read at 450 nm. The results were stated as mg ascorbic acid equivalent in 1 g dry extract.

Determination of total antioxidant capacity (TOAC) test

Total antioxidant capacity test was calculated according to the phosphomolybdenum method explained earlier by Barak et al.[22] Firstly, to obtain TOAC solution; 28 mM sodium phosphate monobasic, 4 mM ammonium molybdate and 600 mM H_2SO_4 were mixed. Then, 300 µL of TOAC solution were mixed with 30 µL of sample solutions in a 96 well plate. After the incubation period at 95°C for 90 min, the absorbance was read at 695 nm. Ascorbic acid was used to obtain a standard curve and the results were calculated as mg Trolox equivalents in 1 g dry extract.

Inhibitory activity on skin aging-related enzymes

Anti-collagenase activity

To measure anti-collagenase activity of MPM, 50 mM tricine buffer solution (pH: 7.5) was prepared (400 mM NaCl and 10 mM $CaCl_2$). *Clostridium histolyticum* (ChC - EC. 3.4.23.3) was used as the source of collagenase, which was dissolved in the 50 mM tricine buffer solution to achieve an initial concentration of 0.8 U/mL. 2 mM of *N*-[3-(2-furyl) acryloyl]-Leu-Gly-Pro-Ala (FALGPA) dissolved in tricine buffer was used as substrate. The extracts were incubated with collagenase enzyme in buffer solution for 15 min before adding the substrate to start the reaction. Final reaction mixture comprised a total volume of 150 µL; tricine buffer, 0.8 mM FALGPA, 0.1 units of ChC, and 25 µL MPM. Water was used for the blank results. After addition of the substrate, measurement of absorbance was done immediately. Positive controls performed epigallocatechin gallate (EGCG).[23]

Anti-elastase activity

Evaluation of MPM for anti-elastase activity was carried out using 0.2 mM tris-HCl buffer solution (pH: 8.0). A stock solution of elastase (P.E., E.C. 3.4.21.36) obtained from porcine pancreas was prepared with distilled water at a concentration of 3.33 mg/mL. *N*-Succinyl-Ala-Ala-*p*-nitroanilide (AAAPVN) to used as substrate was dissolved in a buffer solution (1.6 mM). MPM extract was incubated with 1 µg/mL of PE for 15 min at 37°C before substrate addition. At the end of 15 min pre-incubation, 0.8 mM AAAPVN substrate was added to the enzyme mixture containing 1 mg/mL plant extract and incubation was performed again for 15 min at 37°C. While using 0.25 mg/mL EGCG as positive control, this test sample contains the same volume of EGCG instead of MPM, and the test setup was repeated. Following the incubation periods, measurements were taken at 4 different time points for 5 to 30 minutes by Thermo Scientific Multiskan SkyHigh Microplate Spectrophotometer at 365 nm excitation and 410 nm emission.[24, 25]

Anti-hyaluronidase activity

Anti-hyaluronidase activity was performed by modifying the method described by Kolayli et al.[26] and Lee et al.[3] Firstly, the commercially-purchased hyaluronidase (EC 3.2.1.35, Sigma-Aldrich) was dissolved in 0.02 M phosphate buffer (pH: 3.5) containing NaCl and bovine serum albumin. Then, hyaluronic acid, an appropriate substrate of the enzyme, was prepared in acetate buffer (0.1 M, pH: 3.5) and made ready for use. The assay mixture consisting of 20 µL of MPM at a concentration of 1 mg/mL, 10 µL of hyaluronidase and 60 µL of 0.1 M acetate buffer was pre-incubated for 20 min at 37°C. After the incubation time, 10 µL of hyaluronic acid was added to the mixture and incubated again at 37°C for 20 min. At the end of the total incubation time, measurements were made at different time points by Thermo Scientific Multiskan SkyHigh Microplate Spectrophotometer at 600 nm. The blank group did not contain enzyme in the experimental setup, while the control group did not contain the extract. The percent of anti-hyaluronidase activity was calculated using the following equation:

Anti-aging activities (%)= [(Abs of control - Abs of sample)/ Abs of control] × 100

Statistical analysis

Anti-elastase, anti-collagenase, and anti-hyaluronidase activity experiments included in this study were repeated three times independently. The statistical difference was analyzed using the *t*-test of the GraphPad Prism 8 software ($p \leq 0.05$).

RESULTS AND DISCUSSION

Determination of anti-aging potential

Elastin, collagen, and hyaluronic acid are known contents of ECM, which have pivotal roles for young appearance of the skin. Elastin is a vital protein for maintaining the elastic properties of the skin, consequently decrement of elastin in ECM leads to acceleration in the aging process.[27] Previous literature clearly indicates the direct link between wrinkling and aging of skin with lowered amounts of elastin.[28] Hyaluronic acid is a hydrophobic GAG molecule, which is depolymerized *via* hyaluronidase. Hyaluronic acid is crucial to keep the skin smoothness and moisture stable; hence, it has been shown that excessive

breakdown leads to drying and wrinkling to the skin.[29] Through aging process with time, decreased level of collagen causes thinning on dermis, which is considered a distinctive indication under microscopic examination.[30] It was precisely indicated that delaying breakdown of collagen *via* collagenase inhibitors consequently intervals the wrinkling and aging of skin structure.[5] Considering this information, substances that inhibit elastase, collagenase, and hyaluronidase have noteworthy potential for anti-aging products. Previous studies have demonstrated that various isoflavonoids exhibit significant inhibitory bioactivity against aforementioned enzymes. Addotey et al.[31] showed that four different isoflavonoids inhibited hyaluronidase up to 61.2%. Kim et al.[32] have shown that an isolated isoflavonoid from *Glycyrrhiza uralensis* Fisch., licoricidine, has significant elastase inhibitory activity. IC_{50} value of licoridine was calculated as 61.2 ± 4.2 µM while oleanolic acid was calculated 131.4 ± 11.4 as reference compound. Results indicated that isoflavonoids might inhibit elastase enzyme. Consistent with aforementioned study, Kim et al.[33] studied nine different prenylated isoflavonoids, exceedingly related structures with osajin, isolated from roots of *Flemingia philippinensis* Merr. & Rolfe. Researchers reported that five of the prenylated isoflavones had potent inhibition activity against neutrophil elastase, IC_{50} values diversified between 1.9-12.0 µM, while IC_{50} value of oleanolic acid was 28.4 µM. In another study, Ergene Öz et al.[34] investigated *in vitro* inhibitory activity of five isoflavonoids isolated from roots of *Ononis spinoza* L. against hyaluronidase, collagenase, and elastase. Hyaluronidase inhibitory activity of the isoflavones was reported to be between 22.08-45.58%, while, at the same concentration, tannic acid showed 88.32% inhibition. Collagenase inhibition results were calculated between 20.41-28.49% and elastase inhibition was measured as 20.47-46.88%. EGCG was used as reference for both assays and the inhibition activities at the same concentration were measured as 41.18% and 84.64%, respectively. Another study investigated topical treatments of pomiferin directly isolated from *M. pomifera*.[15] Pomiferin is a prenylated isoflavonoid, which can be found in *M. pomifera* fruits and its molecular structure exceedingly resembles that of osajin. Investigators reported that pomiferin exhibited potent ECM protein stimulation activity by increasing collagen and elastin that is superior or equivalent to the reference compound, retinol. All mentioned studies revealed that isoflavones are moderate to potent inhibitors of these enzymes and have significant potential as natural anti-aging materials.

In this study, *in vitro* hyaluronidase, collagenase, elastase inhibitory activities of MPM were investigated for determination of antiaging potential. A comparative assay was conducted for collagenase inhibition assay at two time points, *e.g.* 20 and 40 min, for both MPM and the reference compound, EGCG. The results demonstrated that collagenase inhibition activity increased with time. 1 mg/mL MPM showed 84.55 ± 1.99% inhibition, while 250 µg/mL EGCG showed 84.66 ± 1.83% after 20 min of incubation. Inhibitory bioactivity was amplified through

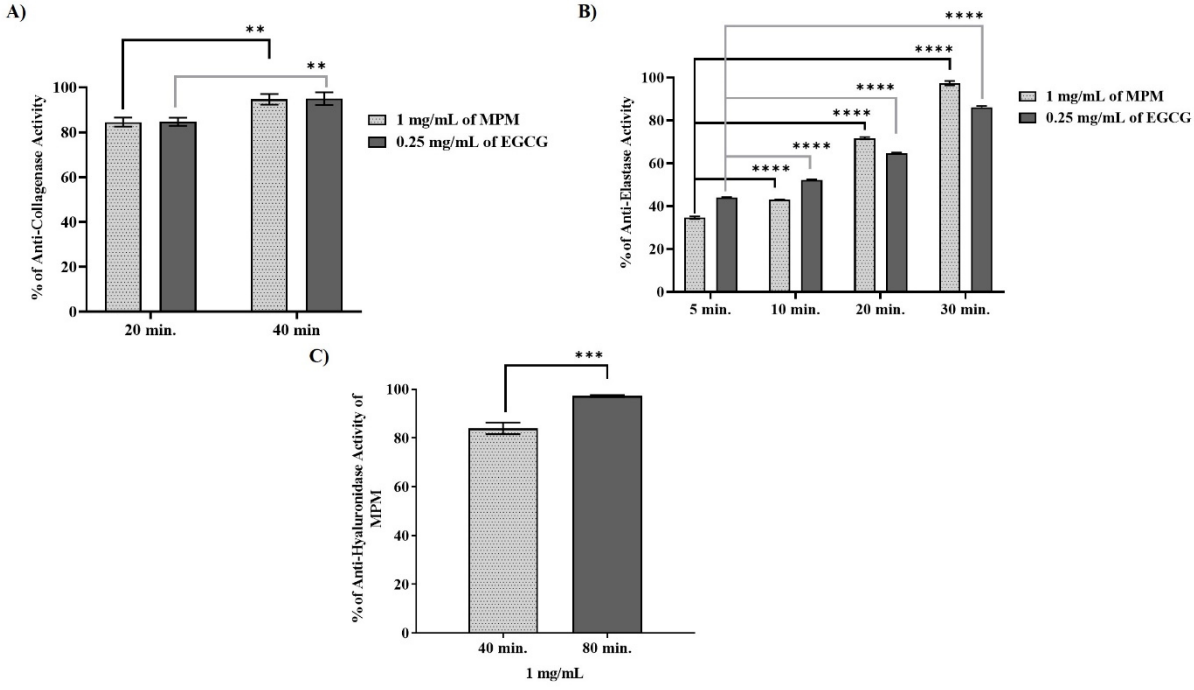

Figure 2. (A) The percent anti-collagenase activity of MPM at a 1 mg/mL concentration at the end of 20 and 40 minutes is presented. In the statistical analysis, the $p \leq 0.01$ value was symbolized with **. % of Anti-elastase activity of 1 mg/mL MPM was shown in (B), and **** was meant $p \leq 0.0001$. EGCG was used as positive control in anti-collagenase and anti-elastase assays (A and B). (C) was shown that % of the anti-hyaluronidase activity of 1 mg/mL MPM at two different time points (at the end of the 40 and 80 minutes). $p \leq 0.001$ value was symbolized with ***

MPM: *Maclura pomifera* 80% methanolic extract, EGCG: Epigallocatechin gallate

time, after 40 min MPM and EGCG inhibited collagenase 94.68 ± 2.42% and 94.98 ± 2.81%, respectively. Consistent with the literature, MPM exhibited significant inhibition activity against elastase. Results were measured for four time points (5, 10, 20, and 30 min) and demonstrated increment over time (Figure 2). EGCG (250 µg/mL) was used as reference and inhibition activity increased at every time point (44.07 ± 0.00%, 52.19 ± 0.00%, 64.69 ± 0.00% and 86.21 ± 0.00%, respectively). Meanwhile MPM in 1 mg/mL concentration exhibited higher enhancement and inhibition activity, which raised from 34.70 ± 0.57% to 97.40 ± 1.04% from 5 min to 30 min. Similarly, 1 mg/mL MPM inhibited hyaluronidase enzyme significantly after 40 min incubation. 83.91 ± 2.36% inhibition was measured following 40 min, after that 80 min of incubation, inhibition rate amplified to 97.19 ± 0.45%. When entire enzyme inhibition assays were considered, results noticeably demonstrated that MPM may be a valuable natural anti-aging agent and may be used in the contents of various anti-aging products; thus, *M. pomifera* may gain extra economic importance.

Determination of antioxidant potential

Numerous exogenous and endogenous factors lead to skin aging *via* various mechanisms. A majority of these factors are directly or indirectly affected by ROS formation in the ECM of the skin.[35] Since the skin covers the outer part of our body, it encounters significant amounts of UV irradiation in daily life. Thus, majority of the skin problems such as sunburn, hyperpigmentation, and skin carcinogenesis originate or are related to direct effects of UV radiation. Likewise, photoaging is an additional consequence of its hazardous properties.[36] Moreover, UV light generates ROS formation and, consequently, oxidative stress in skin tissue, which is one of the most important mechanisms that leads to photoaging.[37] It was hypothesized that since excessive ROS formation causes premature skin aging, agents with a significant antioxidative capacity may be a valuable tool against the perilous effects of UV radiation. Accordingly, clinical studies show that topical antioxidant usage has a protective effect on the skin.[38]

After the interlink between topical antioxidant usage and postponement of skin aging, which is well established in previous literature, examining *in vitro* antioxidant potential of MPM provides valuable information for it is anti-aging potential, when applied topically. Earlier literature clearly demonstrated that extracts with a high number of isoflavonoids might be valuable antioxidants. In a previous study, isoflavonoid-rich extract of *F. macrophylla* extract reduced UVB-induced skin damage by scavenging ROS.[39] Santos and Silva[40] indicated that prenylated isoflavonoids have important antioxidant potential due to their flavonoid moiety and an additive effect of prenyl sidechain. Antioxidant potential of extracts and isoflavonoids of *M. pomifera* was evaluated in a previous study. Results demonstrated that the hydroalcoholic extract and pure osajin showed significant activity on DPPH, FRAP, and TOAC assays, eventhough pomiferin and ethyl acetate fractions showed higher activity.[41] For this study, DPPH radical scavenging activity, FRAP, CUPRAC, and TOAC assays were conducted for comprehensive determination of *in vitro* antioxidant potential of MPM (Table 2). MPM exhibited significant DPPH radical scavenging activity, where IC_{50} value was measured 1998.86 ± 0.02. FRAP and TOAC assays also resulted with notable metal-reducing activity, 0.191 ± 0.01 mM $FeSO_4$/DE and 114.43 ± 0.02 AAE/g DE, respectively. These findings were consistent with the previous study published by Orhan et al.[41] CUPRAC assay was conducted on *M. pomifera* fruit extracts for the first time to our knowledge. Correspondingly, MPM showed noteworthy copper-reducing activity in the CUPRAC assay, where results were measured as 73.928 ± 0.01 AAE/g DE. When total antioxidant capacity assays were considered, it is possible to suggest that MPM is a promising anti-aging agent.

Phenolic profile and HPTLC analysis

Isoflavonoids are phenolic substances, which are known as plant constituents responsible for various noteworthy biological activities such as antioxidant, anticancer, and against gynecological problems.[42] Previous studies evidently demonstrated that prenylated isoflavonoids are major phenolic compounds in *M. pomifera* fruits.[43] Numerous studies identified osajin and pomiferin as the major ingredients of *M. pomifera* fruits, which are primarily accountable for it is biological activities.[12] Osajin and pomiferin are highly similar prenylated isoflavonoids that only differ with one hydroxyl group.[44] Previous reports demonstrated conflictual results for osajin and pomiferin contents of *M. pomifera* fruits. Kartal et al.[45] developed an LC-MS method for determination of osajin and pomiferin in *M. pomifera,* which were collected from Ankara province of Türkiye. The results demonstrated that pomiferin content was slightly higher than osajin content in different parts of the fruit samples. In another study, *M. pomifera* fruit samples were collected from different regions of Midwest and Southern United States and osajin and pomiferin contents were measured *via* a novel HPLC analysis method. Results showed that geographic differences lead to significant alterations of isoflavonoid amounts in samples.[46] Tsao et al.[47] determined osajin and pomiferin content of the fruits collected from Canada

Table 2. *In vitro* antioxidant activity of MPM

	DPPH scavenging activity[A]	FRAP[B]	CUPRAC[C]	Total antioxidant capacity[C]
MPM[D]	1998.86 ± 8.02	0.191 ± 0.01	73.928 ± 0.004	114.43 ± 0.02

[A]Results were expressed as the mean of triplicates ± standard deviation and IC_{50} value of the reference compound "butylated hydroxytoluene" in DPPH scavenging activity is found to be 975.11 ± 4.16.
[B]Results were expressed as the mean of triplicates ± standard deviation and as Mm $FeSO_4$ equivalents in 1 g sample.
[C]Result was expressed as the mean of triplicates ± standard deviation and as ascorbic acid equivalents in 1 g sample.
[D]MPM: 80% methanolic extract of *Maclura pomifera* (Rafin.) Schneider.
DPPH: 2,2-Diphenyl-1-picrylhydrazyl, FRAP: Ferric-reducing antioxidant power, CUPRAC: Cupric-reducing antioxidant capacity

and found that pomiferin content was slightly higher than osajin content. In contrast, Hwang et al.[48] summarized several studies that found osajin amount higher than pomiferin amount in various extracts. It can be claimed that osajin and pomiferin contents of *M. pomifera* fruits are exceptionally variable with geographic differences and extraction techniques due to their decidedly analogous chemical structure. For this study, the amount of MPM was measured *via* HPTLC analysis, for the first time to our knowledge. Results of the analysis showed that osajin is the predominant ingredient of MPM which were collected from Uşak province, 0.22% of the sample consisted of osajin (Table 1). Furthermore, to achieve further assessment of phenolic profile of MPM, total phenolic and total flavonoid content assays were conducted. Results showed that MPM had notable phenolic and flavonoid content as follows; 113.92 ± 2.26 mg GAE/g and 66.41 ± 0.74 mg QE/g, respectively. Results of phenolic profile evaluation showed that MPM might be a prominent candidate as a novel natural anti-aging agent.

CONCLUSION

Even though studies investigating the topical implementation of *M. pomifera* fruits are relatively new, attention in this manner is increasing with encouraging reports. Therefore, this study was aimed to describe a comprehensive evaluation of possible anti-aging potential of *M. pomifera* fruit extract. HPTLC analysis used for *M. pomifera* fruits for determination of isoflavonoid content for the first time to our knowledge, along with *in vitro* studies for determining total phenolic profile. Results showed that osajin is the major ingredient of the samples. Additionally, *in vitro* antioxidant potential of the extract was assessed with four different assays and results demonstrated a significant antioxidant potential of MPM. Additionally, inhibitory activity against the enzymes, which are related to the aging process, was measured and it was seen that MPM had notable enzyme inhibition activity. In conclusion, this study provides information, which may lead to production of novel skincare products.

Ethics

Ethics Committee Approval: Ethics committee approval is not required for the study.

Informed Consent: Not necessary.

Peer-review: Externally peer-reviewed.

Authorship Contributions

Concept: T.H.B., T.B.Ş., H.B., Design: T.H.B., İ.K.C., E.C., Data Collection or Processing: T.H.B., İ.K.C., H.B., Analysis or Interpretation: T.H.B., İ.K.C., Literature Search: T.H.B., T.B.Ş., Writing: T.H.B., E.C.

Conflict of Interest: No conflict of interest was declared by the authors.

Financial Disclosure: This study was supported by Acıbadem Mehmet Ali Aydınlar University Commision of Scientific Projects (no: 2020/02/07).

REFERENCES

1. Hwang E, Park SY, Yin CS, Kim HT, Kim YM, Yi TH. Antiaging effects of the mixture of *Panax ginseng* and *Crataegus pinnatifida* in human dermal fibroblasts and healthy human skin. J Ginseng Res. 2017;41:69-77.
2. Ganceviciene R, Liakou AI, Theodoridis A, Makrantonaki E, Zouboulis CC. Skin anti-aging strategies. Dermatoendocrinol. 2012;4:308-319.
3. Lee H, Hong Y, Tran Q, Cho H, Kim M, Kim C, Kwon SH, Park S, Park J, Park J. A new role for the ginsenoside RG3 in antiaging *via* mitochondria function in ultraviolet-irradiated human dermal fibroblasts. J Ginseng Res. 2019;43:431-441.
4. Rouvrais C, Bacqueville D, Patrick B, Haure MJ, Duprat L, Coutanceau C, Castex-Rizzi N, Duplan H, Mengeaud V, Bessou-Touya S. Assessment of antiaging properties of retinaldehyde, delta-tocopherol glucoside and glycylglycine oleamide combination. J Invest Dermatol. 2017;137(Suppl 2):S303.
5. Bravo K, Alzate F, Osorio E. Fruits of selected wild and cultivated Andean plants as sources of potential compounds with antioxidant and anti-aging activity. Ind Crops Prod. 2016;85:341-352.
6. Yepes A, Ochoa-Bautista D, Murillo-Arango W, Quintero-Saumeth J, Bravo K, Osorio E. Purple passion fruit seeds (*Passiflora edulis* f. *edulis* Sims) as a promising source of skin anti-aging agents: enzymatic, antioxidant and multi-level computational studies. Arab J Chem. 2021;14:102905.
7. Rittié L, Fisher GJ. UV-light-induced signal cascades and skin aging. Ageing Res Rev. 2002;1:705-720.
8. Duque L, Bravo K, Osorio E. A holistic anti-aging approach applied in selected cultivated medicinal plants: a view of photoprotection of the skin by different mechanisms. Ind Crops Prod. 2017;97:431-439.
9. Manjia NJ, Njayou NF, Joshi A, Upadhyay K, Shirsath K, Devkar VR, Moundipa FP. The anti-aging potential of medicinal plants in Cameroon-*Harungana madagascariensis* Lam. and *Psorospermum aurantiacum* Engl. prevent *in vitro* ultraviolet B light-induced skin damage. Eur J Integr Med. 2019;29:100925.
10. Pujimulyani D, Suryani CL, Setyowati A, Handayani RAS, Arumwardana S, Widowati W, Maruf A. Cosmeceutical potentials of *Curcuma mangga* Val. extract in human BJ fibroblasts against MMP1, MMP3, and MMP13. Heliyon. 2020;6:e04921.
11. Stavropoulou MI, Stathopoulou K, Cheilari A, Benaki D, Gardikis K, Chinou I, Aligiannis N. NMR metabolic profiling of Greek propolis samples: comparative evaluation of their phytochemical compositions and investigation of their anti-ageing and antioxidant properties. J Pharm Biomed Anal. 2021;194:113814.
12. Filip S, Djarmati Z, Lisichkov K, Csanadi J, Jankov RM. Isolation and characterization of *Maclura* (*Maclura pomifera*) extracts obtained by supercritical fluid extraction. Ind Crops Prod. 2015;76:995-1000.
13. Saloua F, Eddine NI, Hedi Z. Chemical composition and profile characteristics of osage orange *Maclura pomifera* (Rafin.) Schneider seed and seed oil. Ind Crops Prod. 2009;29:1-8.
14. Veselá D, Kubínová R, Muselík J, Zemlicka M, Suchý V. Antioxidative and EROD activities of osajin and pomiferin. Fitoterapia. 2004;75:209-211.
15. Gruber JV, Holtz R, Sikkink SK, Tobin DJ. *In vitro* and *ex vivo* examination of topical pomiferin treatments. Fitoterapia. 2014;94:164-171.
16. Bozkurt İ, Dilek E, Erol HS, Çakir A, Hamzaoğlu E, Koç M, Keleş ON, Halici MB. Investigation on the effects of pomiferin from *Maclura pomifera* on

indomethacin-induced gastric ulcer: an experimental study in rats. Med Chem Res. 2017;26:2048-2056.

17. Kurt-Celep İ, Celep E, Akyüz S, İnan Y, Barak TH, Akaydın G, Telci D, Yesilada E. *Hypericum olympicum* L. recovers DNA damage and prevents MMP-9 activation induced by UVB in human dermal fibroblasts. J Ethnopharmacol. 2020;246:112202.
18. Bardakci H, Cevik D, Barak TH, Gozet T, Kan Y, Kirmizibekmez H. Secondary metabolites, phytochemical characterization and antioxidant activities of different extracts of *Sideritis congesta* P.H. Davis et Hub.-Mor. Biochem Syst Ecol. 2020;92:104120.
19. Celep E, Seven M, Akyüz S, İnan Y, Yesilada E. Influence of extraction method on enzyme inhibition, phenolic profile and antioxidant capacity of *Sideritis trojana* Bornm. South African J Bot. 2019;121:360–365.
20. Bardakcı H, Barak TH, Özdemir K, Celep E. Effect of brewing material and various additives on polyphenolic composition and antioxidant bioactivity of commercial *Tilia platyphyllos* Scop. infusions. J Res Pharm. 2020;24:133-141.
21. Barak TH, Celep E, İnan Y, Yesilada E. Influence of *in vitro* human digestion on the bioavailability of phenolic content and antioxidant activity of *Viburnum opulus* L. (European cranberry) fruit extracts. Ind Crops Prod. 2019;131:62-69.
22. Barak TH, Celep E, İnan Y, Yeşilada E. *In vitro* human digestion simulation of the bioavailability and antioxidant activity of phenolics from *Sambucus ebulus* L. fruit extracts. Food Biosci. 2020;37:100711.
23. Ersoy E, Eroglu Ozkan E, Boga M, Yilmaz MA, Mat A. Anti-aging potential and anti-tyrosinase activity of three *Hypericum* species with focus on phytochemical composition by LC-MS/MS. Ind Crops Prod. 2019;141:111735.
24. Lee KK, Kim JH, Cho JJ, Choi JD. inhibitory effects of 150 plant extracts on elastase activity, and their anti-inflammatory effects. Int J Cosmet Sci. 1999;21:71-82.
25. Itoh S, Yamaguchi M, Shigeyama K, Sakaguchi I. The anti-aging potential of extracts from *Chaenomeles sinensis*. Cosmetics 2019;6:21.
26. Kolayli S, Can Z, Yildiz O, Sahin H, Karaoglu SA. A comparative study of the antihyaluronidase, antiurease, antioxidant, antimicrobial and physicochemical properties of different unifloral degrees of chestnut (*Castanea sativa* Mill.) honeys. J Enzyme Inhib Med Chem. 2016;31(Suppl 3):96-104.
27. Korkmaz B, Horwitz MS, Jenne DE, Gauthier F. Neutrophil elastase, proteinase 3, and cathepsin G as therapeutic targets in human diseases. Pharmacol Rev. 2010;62:726-759.
28. Akazaki S, Nakagawa H, Kazama H, Osanai O, Kawai M, Takema Y, Imokawa G. Age-related changes in skin wrinkles assessed by a novel three-dimensional morphometric analysis. Br J Dermatol. 2002;147:689-695.
29. Barla F, Higashijima H, Funai S, Sugimoto K, Harada N, Yamaji R, Fujita T, Nakano Y, Inui H. Inhibitive effects of alkyl gallates on hyaluronidase and collagenase. Biosci Biotechnol Biochem. 2019;73:2335-2337.
30. Chung JH, Kang S, Varani J, Lin J, Fisher GJ, Voorhees JJ. Decreased extracellular-signal-regulated kinase and increased stress-activated MAP kinase activities in aged human skin *in vivo*. J Invest Dermatol. 2000;115:177-182.
31. Addotey JN, Lengers I, Jose J, Gampe N, Béni S, Petereit F, Hensel A. Isoflavonoids with inhibiting effects on human hyaluronidase-1 and norneolignan clitorienolactone B from *Ononis spinosa* L. root extract. Fitoterapia. 2018;130:169-174.
32. Kim KJ, Xuan SH, Park SN. Licoricidin, an isoflavonoid isolated from *Glycyrrhiza uralensis* Fisher, prevents UVA-induced photoaging of human dermal fibroblasts. Int J Cosmet Sci. 2017;39:133-140.
33. Kim JY, Wang Y, Uddin Z, Song YH, Li ZP, Jenis J, Park KH. Competitive neutrophil elastase inhibitory isoflavones from the roots of *Flemingia philippinensis*. Bioorg Chem. 2018;78:249-257.
34. Ergene Öz B, Saltan İşcan G, Küpeli Akkol E, Süntar İ, Bahadır Acıkara Ö. Isoflavonoids as wound healing agents from *Ononidis radix*. J Ethnopharmacol. 2018;211:384-393.
35. Azevedo Martins TE, de Oliveira Pinto CAS, de Oliveira AC, Robles Velasco MV, Gorriti Guitiérrez AR, Cosquillo Rafael MF, Huamani Tarazona JP, Retuerto-Figueroa MG. Contribution of topical antioxidants to maintain healthy skin-a review. Sci Pharm. 2020;88:27.
36. Krutmann J, Schroeder P. Role of mitochondria in photoaging of human skin: the defective powerhouse model. J Investig Dermatol Symp Proc. 2009;14:44-49.
37. Dong KK, Damaghi N, Picart SD, Markova NG, Obayashi K, Okano Y, Masaki H, Grether-Beck S, Krutmann J, Smiles KA, Yarosh DB. UV-induced DNA damage initiates release of MMP-1 in human skin. Exp Dermatol. 2008;17:1037-1044.
38. Oresajo C, Pillai S, Manco M, Yatskayer M, McDaniel D. Antioxidants and the skin: understanding formulation and efficacy. Dermatol Ther. 2012;25:252-259.
39. Chiang HM, Chiu HH, Liao ST, Chen YT, Chang HC, Wen KC. Isoflavonoid-rich flemingia macrophylla extract attenuates UVB-induced skin damage by scavenging reactive oxygen species and inhibiting MAP kinase and MMP expression. Evid Based Complement Alternat Med. 2013;2013:696879.
40. Santos CMM, Silva AMS. The antioxidant activity of prenylflavonoids. Molecules. 2020;25:696.
41. Orhan IE, Sezer Senol F, Demirci B, Dvorska M, Smejkal K, Zemlicka M. Antioxidant potential of some natural and semi-synthetic flavonoid derivatives and the extracts from *Maclura pomifera* (Rafin.) schneider (osage orange) and its essential oil composition. Turkish J Biochem. 2016;41:403-411.
42. Křížová L, Dadáková K, Kašparovská J, Kašparovský T. Isoflavones. Molecules. 2019;24:1076.
43. Su Z, Wang P, Yuan W, Grant G, Li S. Phenolics from the fruits of *Maclura pomifera*. Nat Prod Commun. 2017;12:1743-1745.
44. Orazbekov Y, Ibrahim MA, Mombekov S, Srivedavyasasri R, Datkhayev U, Makhatov B, Chaurasiya ND, Tekwani BL, Ross SA. Isolation and biological evaluation of prenylated flavonoids from *Maclura pomifera*. Evid Based Complement Alternat Med. 2018;2018:1370368.
45. Kartal M, Abu-Asaker M, Dvorska M, Orhan I, Zemlicka M. LC-DAD-MS method for analysis of pomiferin and osajin, major isoflavones in *Maclura pomifera* (Rafin.) Schneider. Chromatographia 2009;69:325-329.
46. Darji K, Miglis C, Wardlow A, Abourashed EA. HPLC determination of isoflavone levels in osage orange from the Midwest and southern United States. J Agric Food Chem. 2013;61:6806-6811.
47. Tsao R, Yang R, Young JC. Antioxidant isoflavones in osage orange, *Maclura pomifera* (Raf.) Schneid. J Agric Food Chem. 2003;51:6445-6451.
48. Hwang HS, Winkler-Moser JK, Tisserat B, Harry-O'kuru RE, Berhow MA, Liun SX. Antioxidant activity of osage orange extract in soybean oil and fish oil during storage. J Am Oil Chem Soc. 2021;98:73-87.

Turk J Pharm Sci 2022;19(4):408-415
DOI: 10.4274/tjps.galenos.2021.04874

ORIGINAL ARTICLE

Atazanavir-Loaded Crosslinked Gamma-Cyclodextrin Nanoparticles to Improve Solubility and Dissolution Characteristics

Darshana DHABLIYA, Shagufta Abdul Qaiyum KHAN*, Minal UMATE, Bhavana RAUT, Dilesh SINGHAVI

Institute of Pharmaceutical Education and Research, Maharashtra, India

ABSTRACT

Objectives: Atazanavir sulfate (AS), a Biosafety Cabinet (BCS) class II antiretroviral drug, shows dissolution rate-limited bioavailability, therefore, it is necessary to improve its solubility and oral bioavailability. The present investigation is intended to improve the aqueous solubility by developing AS-loaded nanoparticles (ASNPs). Additionally, the immediate release formulation of AS capsules has gastrointestinal side effects such as nausea and abdominal pain, cardiovascular side effect, *e.g.* abnormal cardiac conduction, toxic effects on kidney and liver such as nephrolithiasis, hyperbilirubinemia, and jaundice. Therefore, ASNPs were designed to release the drug slowly for 12 h, so that these side effects could be reduced.

Materials and Methods: ASNPs were prepared using gamma-cyclodextrin (γ-CD) and the crosslinker dimethyl carbonate were characterized by differential scanning calorimetry (DSC) and X-ray diffraction (XRD) to check the crystal characteristics of AS upon entrapment in NPs. Entrapment efficiency (EE), particle size, morphology, solubility, and dissolution behavior were also determined.

Results: EE%, particle size, and zeta potential varied from 14.38 ± 0.16 to 75.97 ± 0.28%, 65.4 ± 1.25 nm to 439.6 ± 2.21 nm, and 28.3 ± 0.1 mV to 41.0 ± 0.3 mV, respectively. XRD and DSC confirmed the transformation of the crystalline AS to amorphous in NPs. There was 11.717 folds rise in AS solubility in water from NPs. The formulation having AS: γ-CD, 1:1 at 10 mg/mL, depicted 88.55 ± 0.58, 91.23 ± 0.80, and 86.8 ± 0.65% drug release in water, acid buffer, and phosphate buffer, respectively, in 12 h.

Conclusion: Solubility enhancement could be attributed to the decrease in crystallinity of atazanavir, when dispersed in NPs.

Key words: Atazanavir sulfate, gamma-cyclodextrin, nanoparticle solubility, dissolution behavior

INTRODUCTION

The poor solubility of potent therapeutics is a major concern in the development of their effective dosage forms because they show dissolution rate-limited bioavailability. One of the challenging tasks in the drug development process of such drugs is to improve the aqueous solubility in order to enhance their bioavailability. The bioavailability of Biosafety Cabinet (BCS) II drugs may be enhanced by increasing solubility and dissolution rate of the drug in the gastrointestinal fluid, as for rate-limiting step is drug release from the dosage form and solubility in the gastric fluid and not the absorption; so increasing the solubility will consequently improve the bioavailability.[1-3]

The important techniques that increase the oral bioavailability of drugs with low aqueous solubility include micronization, nanosizing, co-crystallization, solid-lipid nanoparticles (SLNs), microemulsion, self-emulsifying drug delivery system, self-microemulsifying drug delivery systems, and liposomes.[4,5] The saquinavir-loaded poly(alkylcyanoacry-late)/HPβCD nanoparticles (NP) prepared by Boudad et al.[6] increased apparent solubility of saquinavir by 400 folds compared with free saquinavir. Sawant et al.[7] have studied *in vitro* and *ex vivo* characteristics of valsartan-loaded SLNs. They reported improvement in the bioavailability of valsartan and suggested that SLNs can bypass the first-pass metabolism, enhance

*Correspondence: shaguftakhan17@rediffmail.com, Phone: +07152-240284, ORCID-ID: orcid.org/0000-0002-2827-7939
Received: 02.05.2021, Accepted: 17.09.2021

lymphatic absorption, and improve solubility as well as bioavailability.[7] Hu et al.[8] prepared lapatinib ditosylate solid dispersions (SDs) using solvent rotary evaporation and hot melt extrusion for solubility and dissolution enhancement. SDs prepared by rotary evaporation showed 29 folds enhancement of solubility of lapatinib ditosylate compared with SDs prepared by hot-melt extrusion.

AS, an antiretroviral drug belongs to the BCS class II. Because of poor solubility and dissolution rate, it has poor oral bioavailability (60-68%) (accessed 12 Jan 2018) https://www.drugbank.ca/drugs/DB01072. Atazanavir is an azapeptide HIV-1 protease inhibitor that prevents the formation of mature virions through the selective inhibition of viral Gag and Gag-Pol polyprotein processing in HIV-1-infected cells.[9] Because of its promising effect, atazanavir is the drug of choice for resisting HIV infection. However, its therapeutic efficacy is low on oral administration because of its poor bioavailability. Polymeric NPs provide a high surface area and can reduce the crystallinity, therefore, can improve the solubility of the poorly water-soluble drugs. In a study, atazanavir was loaded on eudragit RL -100 NPs to improve its oral bioavailability.[10]

In this investigation, gamma-cyclodextrin (γ-CD) is used to prepare NPs because atazanavir sulfate (AS) is a moderately large molecular weight drug (802.93 Da), for which the cavity size of γ-CD would be appropriate (accessed 12 Jan 2018) https://www.drugbank.ca/salts/DBSALT000426.

Wang et al.[11] prepared an inclusion complex of nystatin with γ-CD, which sufficiently increased the water solubility and storage stability of nystatin. In addition to solubility enhancement, crosslinked NPs would sustain the atazanavir release, which could reduce the gastrointestinal side effects caused by its immediate release in the stomach. Bristol Myers Squibb Company. Princeton, NJ 08543, USA. Reyataz product information (accessed April 30, 2021). Available from the following: https://packageinserts.bms.com/pi/pi_reyataz.pdf.

MATERIALS AND METHODS

Material

AS was obtained as a gift from Acebright (India) Pharma Pvt. Ltd., Bangalore, γ-CD was gifted by Wacker Chemie AG. Ashland Inc., USA, dimethyl carbonate (DMC), dimethyl formamide (DMF), and potassium chloride were supplied by LOBA Chemie, Pvt. Ltd., Mumbai India. All other chemicals used in this study were of analytical grade and obtained from LOBA Chemie, Pvt. Ltd., Mumbai.

Preparation of ASNPs

The ASNPs were prepared by the crosslinking method. Varying amounts of γ-CD and AS were dissolved in 30 mL DMF. To the solution, 1 mL triethylamine followed by 15 mL DMC was added and refluxed at 80°C for 3 h to allow the reaction to occur. The reaction mixture was allowed to cool and the formed NPs were separated by centrifugation at 10,000 rpm (Model C-24BL, Remi Motors Ltd, Mumbai, India) and freeze-dried.[12]

Saturation solubility determination

An excess amount of ASNPs was added to 10 mL of water/acid buffer pH 1.2 or phosphate buffer pH 6.8 in the amber-colored vials and kept under stirring for 48 h at 25 ± 0.5°C. The resultant suspensions were then centrifuged at 10,000 rpm and supernatants were analyzed at 279 nm (λmax of AS in water and phosphate buffer) for water and phosphate buffer pH 6.8 and at 246 nm (λmax of AS in acid buffer) for acid buffer pH 1.2 respectively (model UV 2401 PC, Shimadzu Corporation, Kyoto, Japan).

The results were compared to the saturation solubility of AS in water, acid buffer pH 1.2, and phosphate buffer pH 6.8 respectively and the solubility enhancement ratio was calculated.[13-15]

Characterization of ASNPs

Determination of drug loading capacity and percent entrapment efficacy (EE)

100 mg ASNPs was stirred in 100 mL of acid buffer pH 1.2 for 48 h, centrifuged and the supernatant was analyzed at 246 nm for AS.[16,17]

Drug-loading capacity and percent EE were calculated according to the following equations:

$$\textit{Drug loading capacity} = \frac{\textit{weight of drug entrapped in nanoparticles}}{\textit{total weight of drug}} \times 100 \quad (1)$$

$$\%\ \textit{Encapsulation efficiency} = \frac{\textit{Actual drug content in nanoparticles}}{\textit{Therotical drug content}} \times 100 \quad (2)$$

Determination of particle size and zeta potential

The particle size, polydispersity index, and zeta potential of ASNPs were determined using Zetasizer (model-ZS90, Malvern Instrument Ltd., Worcestershire, UK) after appropriate dilution.[10,18]

Solid state characterization

Solid-state characterization by fourier transformed infrared spectroscopy (FTIR), differential scanning calorimetry (DSC) and X-ray powder diffraction (XRPD)

FT spectroscopy was done to check the changes in drug upon NP formation. AS, γ-CD, physical mixture of AS and γ-CD, and ASNPs were compressed with a small quantity of KBr and scanned between 4000 and 400 cm^{-1} (model-8400S, Shimadzu Asia Pacific Pvt. Ltd., Singapore) (Figure 1).[19]

For DSC, AS, γ-CD, physical mixture of AS and γ-CD and ASNPs were scanned between 30 and 300°C with the temperature rise at the rate of 10°C/min under the nitrogen environment (model- DSC 620, DSC Seiko nanotechnology, country) (Figure 2).[20,21]

XRPD of these samples was performed at a voltage of 40 kV and 30 mA with a scanning rate of 2°C/min (model- XRD-7000, Shimadzu, Japan) (Figure 3).[22,23]

Surface morphology study using scanning electron microscopy (SEM)

The surface morphology of ASNPs was probed to examine the surface characteristics of particles. ASNPs were diluted and an aliquot of the diluted preparation was dried. The dried ASNPs were mounted on the double-sided conductive metallic stud. The sample was then coated by ion coating with platinum by sputter coater for 40 sec in the vacuum at a current intensity of 40 mA. The sample was viewed by SEM (model-S-3700N, Hitachi, Japan) using a secondary electron detector with an accelerating voltage of 15 kV and a working distance of 2 mm. Images of SEM were digitally captured using Quartz PCI digital imaging software (Quartz Imaging Corporation, British Columbia, Canada) (Figure 4).[24-26]

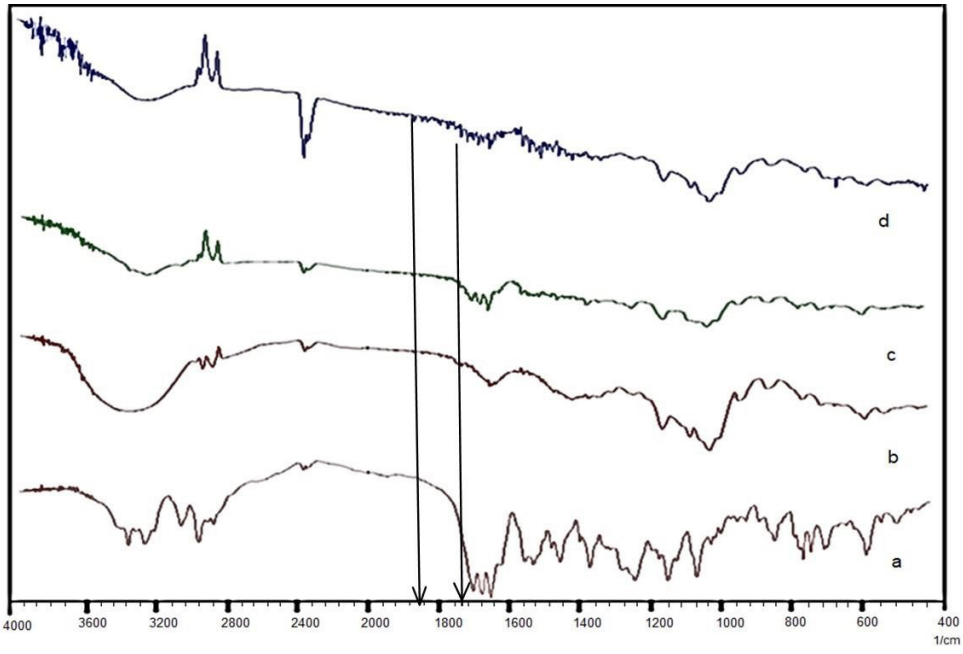

Figure 1. FTIR of a) AS; b) γ-CD; c) Physical mixture of atazanavir sulfate and γ-CD; d) ASNPs

FTIR: Fourier transformed infrared spectroscopy, γ-CD: Gamma-cyclodextrin, ASNPs: Atazanavir sulfate-loaded nanoparticles

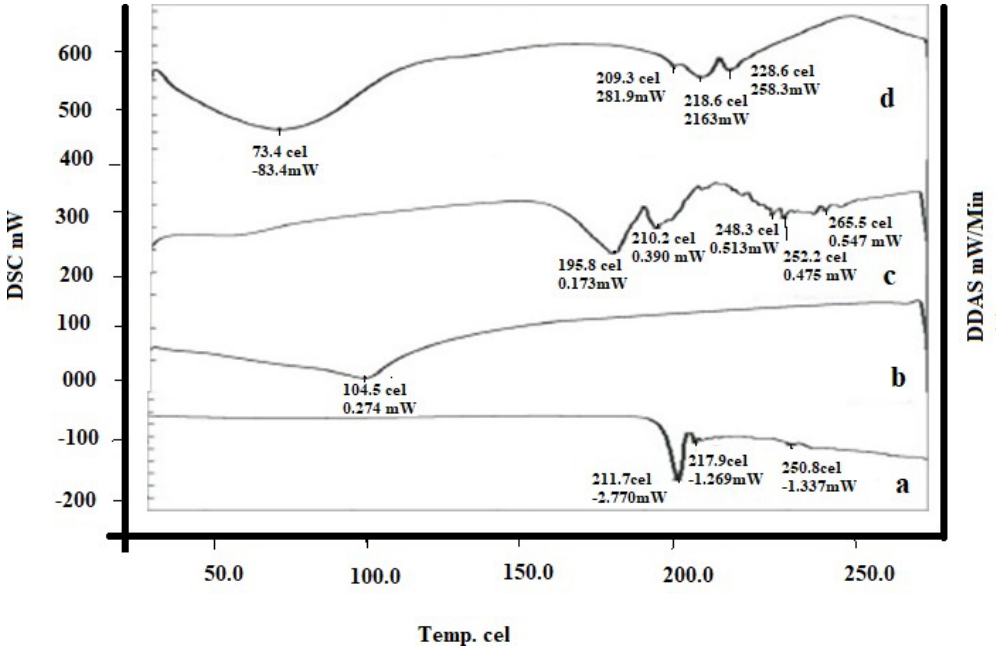

Figure 2. DSC thermogram of a) AS; b) γ-CD; c) Physical mixture of atazanavir sulfate and γ-CD; d) ASNPs

DSC: Differential scanning calorimetry, γ-CD: Gamma-cyclodextrin, ASNPs: Atazanavir sulfate-loaded nanoparticles

In vitro release studies

To elucidate the effect of different dissolution media on the drug release, *in vitro* dissolution testing of ASNPs was performed for 12 h in water, acid buffer pH 1.2, and phosphate buffer pH 6.8 using the dialysis method. NPs equivalent to 15 mg of AS were placed in an activated cellulose dialysis bag containing 2 mL of the dissolution medium, which was sealed from both ends. The dialysis bag was then suspended through the shaft of the USP apparatus (type I), from which the basket was removed into the jar containing 900 mL dissolution medium maintained at 37 ± 0.5°C under stirring at 100 rpm. Samples were withdrawn at the pre-determined intervals and analyzed at 279 nm for water and phosphate buffer, and 246 nm for the acid buffer, respectively.[27,28]

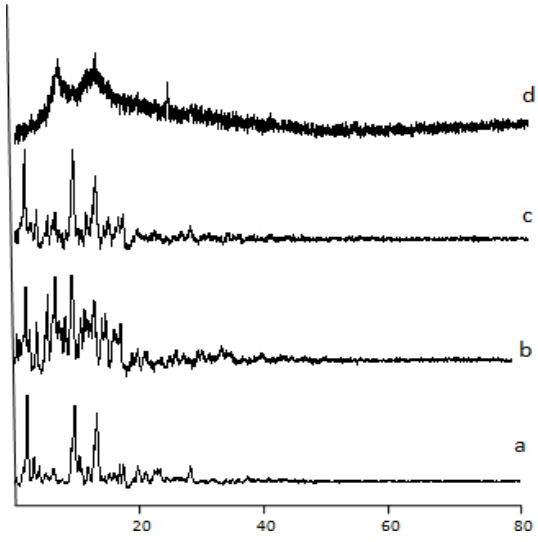

Figure 3. XRD diffractogram of a) Atazanavir sulfate; b) γ-CD; c) Physical mixture of atazanavir sulfate and γ-CD; d) Batch F5 of ASNPs

XRD: X-ray diffraction, γ-CD: Gamma-cyclodextrin, ASNPs: Atazanavir sulfate-loaded nanoparticles

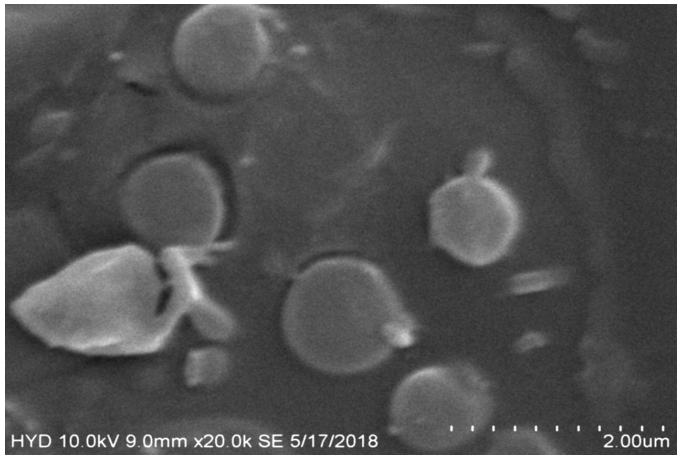

Figure 4. SEM image of batch (F5) of ASNPs

SEM: Scanning electron microscopy, ASNPs: Atazanavir sulfate-loaded nanoparticles

ASNPs wrapped in aluminum foil were placed at 25 ± 2°C and 60 ± 5% RH for 6 months in the stability chamber (model- HTC-3003, Wadegati™ Labe Quip (P) Ltd., Andheri (E), Mumbai, India). Every month, ASNPs were analyzed for physical changes, drug-loading capacity, particle size, and zeta potential.[10]

Statistical analysis

Comparison was done by ANOVA followed by Bartlett's test using Graph Pad Prism 7.0. $p<0.5$ was considered to be significant difference between groups.

RESULTS AND DISCUSSION

Formulation of ASNPs

ASNPs were successfully obtained by the crosslinking method. NPs were prepared by varying the ratios of drug: γ-CD and by varying the concentrations of drug and γ-CD at a constant volume of DMC.

Cross-linked CD was obtained by reacting CD with a carbonyl compound DMC. The reaction is essentially performed out with an excessive carbonyl compound, in the polar aprotic solvent DMF. The presence of an absorption band between 1750 cm^{-1} to 1860 cm^{-1} in the FTIR of ASNPs as marked by the arrows in the Figure 1d, is due to the carbonyl (C=O) group. The absence of this absorption band in the FTIR of the physical mixture (Figure 1c) confirms the successful cross-linked CD network formation in the NPs.

Evaluation of polymeric nanoparticles

Drug-loading capacity and % EE

As shown in Table 1, drug-loading capacity of ASNPs (batches F1 to F9) ranged from 6.73 ± 0.3 to 37.98 ± 0.4%, while percentage EE was between 14.38 ± 0.2 and 75.97 ± 0.3%. Formulation F5 prepared from the 1:1 ratio of AS and γ-CD at 10 mg/mL concentration had the maximum drug-loading capacity (37.98 ± 0.4) and % EE (75.97 ± 0.3). With the increase in drug and polymer concentration up to 10 mg/mL and their ratio 1:1, both drug loading capacity, and % EE increased, possibly because of the compact crosslinked network formation. Maximum drug- loading was obtained at 10 mg/mL γ-CD because at this concentration, the number of OH groups of γ-CD to be crosslinked with DMC to form CD-C-O bond would be optimum, however, at lower γ-CD concentrations than this. Availability of OH groups to participate in crosslinking would be insufficient causing loose network formation and low EE. Higher entrapment in densely crosslinked NPs suggests entrapment of AS both within CD cavity and between the crosslinked network. Similar findings were reported by Singh et al.[29] at higher γ-CD than 10 mg/mL, DMC becomes insufficient to crosslink the available OH groups, forming a weak network with consequent low EE.

Particle size and zeta potential

The average particle size of ASNPs (batch F1 to F9) was between 65.4 ± 1.3 nm and 439.6 ± 2.2 nm as shown in Table 1. It could be noted that the particle size was influenced by the concentration of γ-CD. At higher levels of γ-CD, there was a greater viscosity increase after reflux, ensuing bigger particles.

ASNPs displayed positive zeta potential in the range 20.6 ± 0.2 mV to 41.0 ± 0.3 mV. The zeta potential of batch F5 was 40.3 ± 0.3 mV representing excellent stability of NPs. A high zeta potential was sufficient to keep particles separate from each other due to electrostatic repulsion. A positive zeta potential was due to the basic nature of AS. Polydispersity index of ASNPs in the range from 0.162 ± 0.02 to 0.439 ± 0.01 shows good homogeneity.

Solid state characterization

FTIR, DSC, and XRD

The FTIR spectrum of AS showed a sharp peak at 3313.48 cm^{-1} due to NH stretching, 2873.74 cm^{-1} due to CH stretching, 1701.10 cm^{-1} due to C=O stretching, 1515.94 cm^{-1} due to C=C stretching, 1242.07 cm^{-1} due to S=O stretching and 1124.42 cm^{-1} due to CN stretching (Figure 1a). All the bands were found intact in the FTIR spectrum of the physical mixture of AS and γ-CD indicating no interaction of the drug with the polymer. FTIR of ASNPs revealed additional absorption peaks from 1750 cm^{-1} to 1860 cm^{-1} (Figure 1d), which were absent in the spectra of both γ-CD and the physical mixture. These peaks indicated the carbonyl bonds between the γ-CD molecules.[30] The absence of characteristic peak of AS at 3313.48 cm^{-1} in the spectrum ASNPs indicated hydrogen bond formation between AS and hydroxyl groups of CD. Broadening of characteristic peaks of AS in the NPs suggests the formation of hydrogen bond formation between AS and CD.

The DSC thermograms of AS showed a sharp endothermic peak at 211.7°C corresponding to it is melting point. AS in the current investigation is the type A polymorphic form as it is DSC is similar to the DSC of AS identified by Kim et al.[31], in which it was revealed that the melting endotherm starts at 169°C, peaks at 200°C and extends to about 225°C. In the physical mixture of drug with γ-CD, the endothermic peak of the drug was retained at 195.8°C and 210.2°C. ASNPs depicted the endothermic peak at 209°C and 218°C due to the melting of atazanavir. The thermal behavior seems similar to that one revealed by Kim et al.[31] in their pioneering investigations on AS. Thus, AS was intact in the NPs.

XRD of AS showed characteristic sharp and intense peaks at 2θ= 11°, 13°, 18°, 21°, and 34° (Figure 3a) due to it is crystalline nature, while characteristic peaks of AS had completely disappeared in the NPs, which confirms the conversion of the crystalline drug into an amorphous form upon NP formation. The XRD of γ-CD (Figure 3b) showed sharp peaks up to 20° because it is crystalline, but in the NPs, its peaks were lost. This could be due to the participation of it is hydroxyl groups in the crosslinking with DMC. The crosslinking leads to the formation of irregular arrangements and tortuous structure.[29]

Surface morphology study

From the SEM images of ASNPs, it could be noted that NPs were almost spherical, uniform with a smooth surface.

Saturation solubility

The saturation solubility of AS in water, acid buffer (pH 1.2), and phosphate buffer (pH 6.8) was found to be 0.0046 ± 0.0003 mg/mL, 0.310 ± 0.008 mg/mL, and 0.0025 ± 0.0004 mg/mL respectively (Table 2). The saturation solubility of ASNPs increased from 5.13 to 11.71 folds in water, 0.99 to 1.167 folds in the acid buffer (pH 1.2), and 2.72 to 20.12 folds in the phosphate buffer (pH 6.8). With increasing concentration of γ-CD, solubility of the drug also increased. ASNPs with AS: γ-CD (1:2) showed the highest solubility compared to the combinations with a lower level of γ-CD. The change in the crystalline form to amorphous form upon NP formation with γ-CD as revealed in the XRD in addition to the formation of small-sized NPs, was responsible for the improvement in the solubility of the drug.

In vitro drug release

Percent cumulative drug release from ASNPs F1 to F9 batches is shown in Figure 5a to 5c in water, acid buffer (pH 1.2) and phosphate buffer (pH 6.8), respectively. Drug release after 12 h from ASNP batch F5 in water, acid buffer (pH 1.2), and phosphate buffer (pH 6.8) was found to be 88.55 ± 0.3%, 91.23 ± 0.2%, and 86.8 ± 0.2%, respectively.

Batches that had a concentration of γ-CD 10 mg/mL or more were found to produce a higher dissolution rate. At these concentrations of γ-CD, when drug:CD ratio was 1:2, the

Table 1. Composition of ASNPs and their characteristics

Batches	Atazanavir sulphate (mg/mL)	Gamma cyclodextrin (mg/mL)	Ratio of drug: Polymers	%Drug- loading capacity*	% EE*	Particle size (nm)	Polydispersity index (PDI)
F1	5	2.5	1:0.5	9.62 ± 0.2	14.38 ± 0.2	65.4 ± 1.25	0.162 ± 0.01
F2	5	5	1:1	12.59 ± 0.4	25.18 ± 0.3	73.7 ± 1.5	0.185 ± 0.02
F3	5	10	1:2	6.73 ± 0.3	20.17 ± 0.7	92.5 ± 1.7	0.204 ± 0.01
F4	10	5	1:0.5	31.25 ± 0.3	46.75 ± 0.8	81.6 ± 1.3	0.283 ± 0.01
F5	10	10	1:1	37.98 ± 0.4	75.97 ± 0.3	99.7 ± 1.9	0.310 ± 0.01
F6	10	20	1:2	15.73 ± 0.3	47.16 ± 0.5	141.6 ± 1.6	0.354 ± 0.02
F7	15	7.5	1:0.5	17.75 ± 0.2	26.55 ± 0.2	104.4 ± 1.5	0.381 ± 0.01
F8	15	15	1:1	34.70 ± 0.4	69.40 ± 0.2	136.3 ± 1.3	0.407 ± 0.00
F9	15	30	1:2	19.96 ± 0.5	59.83 ± 0.4	439.6 ± 2.2	0.439 ± 0.01

*Represents mean ± standard deviation (n: 3). EE: Entrapment efficiency, ASNPs: Atazanavir sulfate-loaded nanoparticles

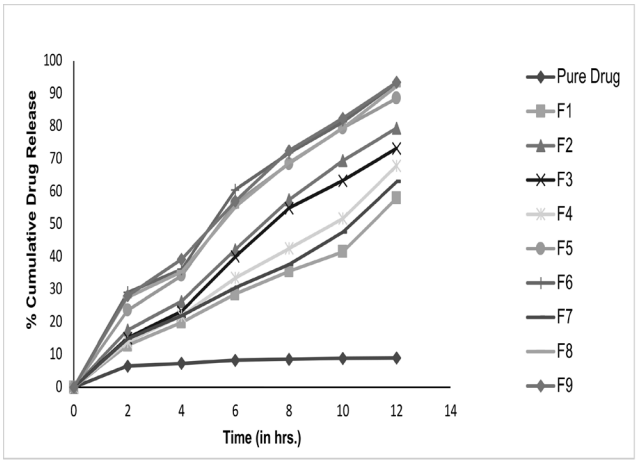

Figure 5a. *In vitro* dissolution profile of pure drug and ASNPs (batch F1 to F9) in water

ASNPs: Atazanavir sulfate-loaded nanoparticles

highest dissolution rate was found. This was because of the greater solubility increase in AS due to the greater masking of hydrophobic groups of AS within the nanochannels at this ratio.[32]

Initial burst release is seen in each media, because of the rapid release of the adhered AS on the surface of NPs. The AS release rate was highest in the acid buffer, because of the basic character of AS. However, the dissolution study clearly indicates that the drug release rate in water, as well as phosphate buffer, was significantly (unpaired *t*-test, $p<0.05$) higher than that in free AS in these media. Additionally, the drug release rate in these media is similar to the dissolution rate in the acid buffer. The dissolution profiles of batch F5 in the three dissolution media were found to be similar when compared using F2 values. For dissolution profiles in water *vs.* acid buffer, F2 was 57.24, in water *vs.* phosphate buffer, F2 was 86.01 and in acid buffer *vs.* phosphate buffer, F2 was 57.72, respectively. Therefore, it can be conclusively said that pH-independent drug release could be achieved from NPs although, the solubility of

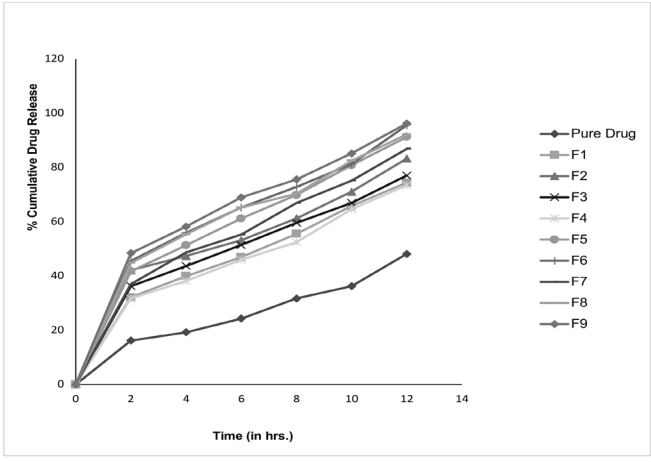

Figure 5b. *In vitro* dissolution profile of pure drug and ASNPs (batches F1 to F9) in HCl buffer (pH 1.2)

ASNPs: Atazanavir sulfate-loaded nanoparticles

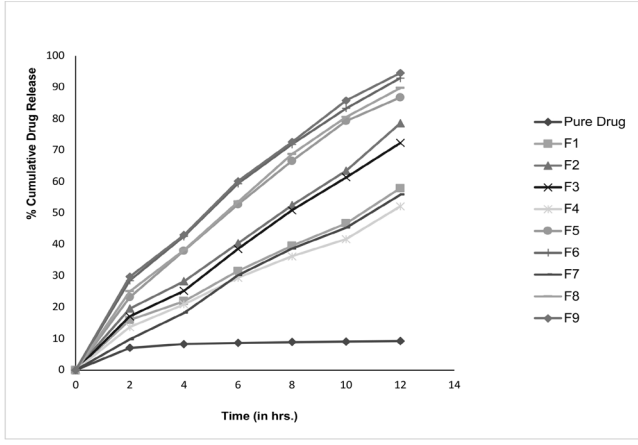

Figure 5c. *In vitro* dissolution profile of pure drug and ASNPs (batches F1 to F9) in phosphate buffer (pH 6.8)

ASNPs: Atazanavir sulfate-loaded nanoparticles

Table 2. Saturation solubility of formulations at different

Batch	Solubility (mg/mL) *		
	Water (mg/mL)	Phosphate buffer (pH 6.8) (mg/mL)	HCl buffer (pH 1.2) (mg/mL)
Pure drug	0.0046 ± 0.0003	0.0025 ± 0.0004	0.310 ± 0.008
F1	0.0236 ± 0.0006	0.0068 ± 0.0006	0.308 ± 0.007
F2	0.0256 ± 0.0005	0.0083 ± 0.0005	0.314 ± 0.006
F3	0.0277 ± 0.0007	0.0095 ± 0.0005	0.319 ± 0.005
F4	0.0289 ± 0.0003	0.0106 ± 0.001	0.340 ± 0.009
F5	0.0365 ± 0.001	0.0253 ± 0.0007	0.351 ± 0.004
F6	0.0539 ± 0.0008	0.0503 ± 0.0006	0.362 ± 0.005
F7	0.0241 ± 0.0004	0.0092 ± 0.0004	0.324 ± 0.008
F8	0.0316 ± 0.0008	0.0121 ± 0.0006	0.349 ± 0.006
F9	0.0347 ± 0.0007	0.0184 ± 0.0007	0.357 ± 0.002

*Represents mean ± standard deviation (n: 3)

free AS is higher in the acidic condition. This could be achieved because of the solubility enhancing capability of γ-CD NPs irrespective of the medium. A uniform sustained release over 12 h by the ASNPs can be a viable way to reduce side effects associated with the immediate releaseof AS.

Stability study

Batch F5 with the highest drug loading capacity and EE with high zeta potential and considerable homogeneity and small size were considered optimum and kept for stability testing for 6 months at 25 ± 2˚C and 60 ± 5% RH. The batch showed insignificant differences in the drug content (p= 0.73), % EE (p= 0.77), particle size (p= 0.53), zeta potential (p= 0.52) and *in vitro* drug release (p>0.5), when analyzed by ANOVA followed by Bartlett's test using Graph Pad Prism 7.0.

CONCLUSION

AS-loaded polymeric NPs were successfully prepared using the crosslinking method. γ-CD was found to be effective in entrapping moderately large molecular weight drug AS and improving its solubility, for which other CDs could not have possibly been so successful owing to their small cavity size. The obtained NPs displayed a significant increase in the dissolution rate of AS irrespective of pH of the medium, which can be considered an important achievement for overcoming it is dissolution rate-limited poor bioavailability. Additionally, as the NPs could sustain the drug release so can alleviate the side effects associated with the AS immediate release. As similar dissolution profiles were obtained in each medium, there is no need to design a gastroretentive formulation of AS, as uniform drug release throughout the GIT over prolonged periods is possible with the prepared NPs in this investigation.

Nevertheless, further *in vivo* studies in animals and humans should be conducted to support the results obtained in this investigation.

Ethics

Ethics Committee Approval: Not required.

Informed Consent: Not required.

Peer-review: Externally peer-reviewed.

Authorship Contributions

Concept: S.A.Q.K., Design: S.A.Q.K., Data Collection or Processing: D.D., Analysis, or Interpretation: S.A.Q.K., Literature Search: D.S., Writing: M.U., B.R., S.A.Q.K.

Conflict of Interest: No conflict of interest was declared by the authors.

Financial Disclosure: The authors declared that this study received no financial support.

REFERENCES

1. Yellela SRK. Pharmaceutical technologies for enhancing oral bioavailability of poorly soluble drugs. J Bioequivalence Bioavailab. 2010;2:28-36.
2. Sharma D, Soni M, Kumar S, Gupta GD. Solubility enhancement - eminent role in poorly soluble drugs. Research J Pharm Tech. 2009;2:220-224.
3. Kumar A, Sahoo SK, Padhee K, Kochar PPS, Sathapathy A, Pathak N. Review on solubility enhancement techniques for hydrophobic drugs. Pharm Glob. 2011;3:1-7.
4. Fahr A, Liu X. Drug delivery strategies for poorly water-soluble drugs. Expert Opin Drug Deliv. 2007;4:403-416.
5. Gomez-Orellana I. Strategies to improve oral drug bioavailability. Expert Opin Drug Deliv. 2005;2:419-433.
6. Boudad H, Legrand P, Lebas G, Cheron M, Duchêne D, Ponchel G. Combined hydroxypropyl-beta-cyclodextrin and poly(alkylcyanoacrylate) nanoparticles intended for oral administration of saquinavir. Int J Pharm. 2001;218:113-124.
7. Sawant KK, Parmar B, Mandal SA, Petkar KC, Patel LD. Valsartan loaded solid lipid nanoparticles: development, characterization and *in vitro* and *ex vivo* evaluation. Int J Pharml Sci Nanotech. 2011;4:1483-1490.
8. Hu XY, Lou H, Hageman MJ. Preparation of lapatinib ditosylate solid dispersions using solvent rotary evaporation and hot melt extrusion for solubility and dissolution enhancement. Int J Pharm. 2018;552:154-163.
9. Robinson BS, Riccardi KA, Gong YF, Guo Q, Stock DA, Blair WS, Terry BJ, Deminie CA, Djang F, Colonno RJ, Lin PF. BMS-232632, a highly potent human immunodeficiency virus protease inhibitor that can be used in combination with other available antiretroviral agents. Antimicrob Agents Chemother. 2000;44:2093-2099.
10. Singh G, Pai RS. Atazanavir-loaded eudragit RL 100 nanoparticles to improve oral bioavailability: optimization and *in vitro*/*in vivo* appraisal. Drug Deliv. 2016;23:532-539.
11. Wang J, Jin Z, Xu X. Gamma-cyclodextrin on enhancement of water solubility and store stability of nystatin. J Incl Phenom Macrocyclic Chem. 2014;78:145-150.
12. Trotta F, Tumiatti W. Cross-linked polymers based on cyclodextrins for removing polluting agents. Available from: https://patentimages.storage.googleapis.com/da/b1/47/521f420ce02a27/US20050154198A1.pdf
13. Wilson B, Samanta MK, Santhi K, Kumar KP, Paramakrishnan N, Suresh B. Poly(*n*-butylcyanoacrylate) nanoparticles coated with polysorbate 80 for the targeted delivery of rivastigmine into the brain to treat Alzheimer's disease. Brain Res. 2008;1200:159-168.
14. Wuyts B, Brouwers J, Mols R, Tack J, Annaert P, Augustijns P. Solubility profiling of HIV protease inhibitors in human intestinal fluids. J Pharm Sci. 2013;102:3800-3807.
15. Berlin M, Ruff A, Kesisoglou F, Xu W, Wang MH, Dressman JB. Advances and challenges in PBPK modeling-analysis of factors contributing to the oral absorption of atazanavir, a poorly soluble weak base. Eur J Pharm Biopharm. 2015;93:267-280.
16. Belgamwar A, Khan S, Yeole P. Intranasal chitosan-g-HP-CD nanoparticles of efavirenz for the CNS targeting. Artif Cells Nanomed Biotechnol. 2018;46:374-386.
17. Yadav SK, Mishra S, Mishra B. Eudragit-based nanosuspension of poorly water-soluble drug: formulation and *in vitro-in vivo* evaluation. AAPS PharmSciTech. 2012;13:1031-1044.
18. Ahmad N, Alam MA, Ahmad R, Naqvi AA, Ahmad FJ. Preparation and characterization of surface-modified PLGA-polymeric nanoparticles used to target treatment of intestinal cancer. Artif Cells Nanomed Biotechnol. 2018;46:432-446. Retraction in: Artif Cells Nanomed Biotechnol. 2020;48:1328.

19. Sahu PL. Indian Pharmacopoeia. The Indian Pharmacopoeia Commission. 2018. Available from: https://www.idma-assn.org/pdf/dr-pl-sahu.pdf

20. Çirpanli Y, Bilensoy E, Doğan AL, Çaliş S. Comparative evaluation of polymeric and amphiphilic cyclodextrin nanoparticles for effective camptothecin delivery. Eur J Pharm Biopharm. 2009;73:82-89.

21. Mu L, Feng SS. A novel controlled release formulation for the anticancer drug paclitaxel (Taxol): PLGA nanoparticles containing vitamin E TPGS. J Control Release. 2003;86:33-48.

22. Sun SB, Liu P, Shao FM, Miao QL. Formulation and evaluation of PLGA nanoparticles loaded capecitabine for prostate cancer. Int J Clin Exp Med. 2015;8:19670-19681.

23. Shaikh J, Ankola DD, Beniwal V, Singh D, Kumar MN. Nanoparticle encapsulation improves oral bioavailability of curcumin by at least 9-fold when compared to curcumin administered with piperine as absorption enhancer. Eur J Pharm Sci. 2009;37:223-230.

24. Win KY, Feng SS. Effects of particle size and surface coating on cellular uptake of polymeric nanoparticles for oral delivery of anticancer drugs. Biomaterials. 2005;26:2713-2722.

25. Merisko-Liversidge E, Sarpotdar P, Bruno J, Hajj S, Wei L, Peltier N, Rake J, Shaw JM, Pugh S, Polin L, Jones J, Corbett T, Cooper E, Liversidge GG. Formulation and antitumor activity evaluation of nanocrystalline suspensions of poorly soluble anticancer drugs. Pharm Res. 1996;13:272-278.

26. Chattopadhyay N, Zastre J, Wong HL, Wu XY, Bendayan R. Solid lipid nanoparticles enhance the delivery of the HIV protease inhibitor, atazanavir, by a human brain endothelial cell line. Pharm Res. 2008;25:2262-2271.

27. Abouelmagd SA, Sun B, Chang AC, Ku YJ, Yeo Y. Release kinetics study of poorly water-soluble drugs from nanoparticles: are we doing it right? Mol Pharm. 2015;12:997-1003.

28. Wilson B, Samanta MK, Santhi K, Kumar KP, Ramasamy M, Suresh B. Chitosan nanoparticles as a new delivery system for the anti-Alzheimer drug tacrine. Nanomedicine. 2010;6:144-152.

29. Singh V, Xu J, Wu L, Guo T, Guo Z, York P, Gref R, Zhang J. Ordered and disordered cyclodextrin nanosponges with diverse physiochemical properties. RSC Adv. 2017;7:23759-23764.

30. Rao MR, Bhingole RC. Nanosponge-based pediatric-controlled release dry suspension of gabapentin for reconstitution. Drug Dev Ind Pharm. 2015;41:2029-2036.

31. Kim S, Lotz BT, Malley MF, Gougoutas JZ, Davidovich M, Srivastava SK. Process for preparıng atazanavir bisulfate and novel forms. US Patent. 2005; US 20050256202A1.

32. Ansari KA, Vavia PR, Trotta F, Cavalli R. Cyclodextrin-based nanosponges for delivery of resveratrol: *in vitro* characterisation, stability, cytotoxicity and permeation study. AAPS PharmSciTech. 2011;12:279-286.

Turk J Pharm Sci 2022;19(4):416-421
DOI: 10.4274/tjps.galenos.2021.26985

ORIGINAL ARTICLE

Impact of a Coronavirus Pandemic on Smoking Behavior in University Students: An Online Survey in Türkiye

Fatma Gül Nur ÇELİK, Göksun DEMİREL*

Çukurova University, Faculty of Pharmacy, Department of Pharmaceutical Toxicology, Adana, Türkiye

ABSTRACT

Objectives: Coronavirus Disease-2019 (COVID-19) pandemic has a massive impact on human health, causing sudden lifestyle changes. As it affects health, determining the lifestyles of university students related to smoking has gained importance. This study provides evidence of change in smoking behavior among university students in Türkiye during the ongoing COVID-19 pandemic.

Materials and Methods: This cross-sectional survey study was conducted *via* an electronic questionnaire approximately 2020-2021 among university students in Türkiye. The study comprised a structured questionnaire that inquired about demographic information; and the Fagerström Test for Nicotine Dependence. The questionnaire was distributed randomly to university students; it required 6 min to complete.

Results: A total of 749 respondents were included in the study, aged between 19 and 35 years (54.8% females). Of 749 participants, 571 health science students (medicine, pharmacy, dentistry, *etc.*) completed the survey. The pre-pandemic and COVID-19 pandemic mean nicotine dependence scores were 3.03 and 2.97, respectively. A difference was seen pre-pandemic (p= 0.002) and during pandemic (p= 0.005) for those studying in health and other departments. Students who had middle socio-economical status had significantly higher nicotine dependence scores pre-COVID-19, compared to during the pandemic (p= 0.027). Compared to pre and during the pandemic, the mean score of dependence was significantly lower in students, whose parents were non-smokers during the pandemic.

Conclusion: In this study, we have provided the first data on the Turkish university student's nicotine dependence changes during the COVID-19 lockdown. The nicotine dependence level may change based on various factors including behavioral changes. Crucial times such as pandemics can affect individuals, thus, smoking addiction can increase. Behavioral support for quitting smoking such as digital platforms, internet, and television programs should also assist to support smokers quitting successfully during this supreme time.

Key words: Smoking behaviors, COVID-19, university students, Türkiye

INTRODUCTION

Smoking tobacco has been accepted to be related to many disease diagnoses, as wide evidence has highlighted the negative effect of nicotine consumption on the respiratory system.[1] Smoking tobacco is an evident risk of immune system diseases and smokers more undefended from many respiratory infections that occur in the respiratory system.[2,3]

Recent studies have shown that smoking is related to the increase in the severity of symptoms and fatality-level hospitalize of the patients with Coronavirus Disease-2019 (COVID-19).[4]

The global COVID-19 pandemic started in the first quarter of 2020 and caused many people to die from lung problems. Because of such drastic outcomes, addiction levels are expected to change because of the changes in social behavior.[5]

Due to COVID-19 pandemic, an unexpected and major change in the lifestyle of the community has appeared with an extreme decline of any form of socialization.[6] Especially, young university

*Correspondence: gdemirel@cu.edu.tr, Phone: +90 555 854 34 30, ORCID-ID: orcid.org/0000-0002-2994-5505
Received: 05.07.2021, Accepted: 20.09.2021

students were going through an overwhelming process, as they had to continue their life in isolation. Self-isolation and social distancing affected university students' rhythm of life especially lifestyle with smoking behavior.

Caused by the pandemic quarantine, with leaving confined indoor to digital education and the limitations of social life could result in boredom, which in turn, is associated with changes in smoking behavior.[7]

Our study must target evaluating the evidence of the changes in smoking behavior among smoker Turkish university students in the process of COVID-19 pandemic and, more importantly, to understand how demographic factors influence these behaviors.

MATERIALS AND METHODS

Survey instrument and dissemination

A web-based, cross-sectional study was conducted using a survey instrument to obtain responses from university students in Turkey between 2020-2021 after obtaining their written informed consent. Approval for the study was obtained from the Republic of Türkiye Ministry of Health-Scientific Research Platform (form number: 2020-11-01T15_03_42) and Çukurova University Non-Interventional Clinical Studies Ethics Committee (project number: GO-105 dated 22.11.2020 and decision number: 55).

A 30-item survey instrument was developed using the Fagerström Nicotine Dependence Test (FTND) and demographic data including COVID-19. The survey was administered to university students and demographic data, nicotine dependency, and knowledge and perceptions related to COVID-19 were obtained. In this survey, both pre and during the COVID-19 dependency levels were questioned.

The developed draft survey instrument was made accessible through a link and was distributed to 10 randomly selected faculty members from different regions to comprehensively assess the content domains of the questionnaire. Regarding their answers, the final version of the survey was reached.

The final version of the survey was administered using the e-mail databases of the universities in Türkiye.

Statistical analysis

The research data were evaluated using SPSS 20.0. The normal distribution assumption was confirmed with the Kolmogorov-Smirnov test and it was seen that the data showed a normal distribution. The descriptive data of the research were evaluated with numbers and percentages. Independent samples *t*-test, paired-samples *t*-test, and one-way ANOVA were used for continuous data. Chi-square test and crosstabs were used for categorical data. A *p* value of 0.05 or less in all tests was considered significant.

RESULTS

Descriptive statistics

The sample for this study consisted of 749 university students in total. The study data from students from 57 universities in 66 provinces in Türkiye are gathered online. The participant students' socio-demographic characteristics are shown in Table 1.

Table 2 includes the descriptive statistics for university students. The average age of the students is 22.1. Pre-COVID-19 pandemic nicotine dependence mean score averaged 3.03; the

Table 1. Frequency distributions

	Frequency (n)	Percentage (%)
Gender		
Female	412	55.0
Male	337	45.0
Living place		
Village	18	2.4
Town	6	0.8
County	237	31.6
City center	488	65.2
Department		
Health departments	571	76.2
Other departments	178	23.8
Economical status		
Very low	10	1.3
Low	63	8.4
Middle	435	58.1
High	215	28.7
Very high	26	3.5
Smoking habits in the family members		
No	193	25.8
Yes	556	74.2
Mandatory quarantine condition due to contact with someone diagnosed with COVID-19		
No	618	82.5
Yes	131	17.5
Having/passing the coronavirus infection		
Yes, I passed it and got through. My last test result was negative	50	6.7
No, I did not experience any symptoms	522	69.7
No, I had a test and my result was negative	128	17.1
Yes, I doubt it, but it was not confirmed by a test	41	5.5
Yes, I had the test and my result was positive	8	1.1

COVID-19: Coronavirus Disease-2019

nicotine dependence mean score during COVID-19 pandemic process was determined as 2.97.

A comparison of nicotine dependence score pre-pandemic and during the pandemic is shown in Table 3. According to the Table, the nicotine dependence scores of female (p<0.001) and male (p<0.001) students, pre and during the pandemic differ statistically significant.

According to the place where students live, nicotine dependence scores pre-COVID-19 (p= 0.014) and during the pandemic (p= 0.003) differ significantly. The nicotine dependence of the students living in the country pre-pandemic differed significantly from that during the pandemic (p= 0.003). A difference was seen pre-pandemic (p= 0.002) and during pandemic (p= 0.005) for those studying in health and other departments.

Students who had middle socio-economical status had significantly higher nicotine dependence scores pre-COVID-19, compared to during the pandemic (p= 0.027). Compared to pre and during the pandemic, the mean score of dependence was significantly lower in students, whose parents were non-smokers during the pandemic (p= 0.017).

For students who had to be in quarantine due to their relatives or family members, their dependency level was significantly higher compared to pre-pandemic (p= 0.011).

Students, who were diagnosed with COVID-19 and had negative results after recovery, had significantly lower levels of dependency compared to pre-COVID-19 (p= 0.40).

The nicotine dependence-level results are summarized in Table 4. Dependence levels pre and during the pandemic showed significant differences (p<0.001). Three hundred thirty two of the students, who self-evaluated at the very low dependence levels on FTND pre-pandemic continued at the same level during the pandemic. However, 10 students' dependence levels have increased to low dependence levels. One hundred thirty two of the individuals, who proclaimed low addiction levels on the FTND pre-pandemic, continued at the same level during the pandemic. Ten students moved to a very low addiction level and 15 students moved to moderate dependence. Six of those proclaiming a high level of addiction in the pre-pandemic moved down to moderate levels during the pandemic.

DISCUSSION

This study was conducted with 749 university students, 571 of whom were health department students. The addiction score averages of the students studying in health departments and studying in other departments before COVID-19 (p= 0.002) and during COVID-19 process (p= 0.005) differ statistically significant.

More than 80% of dependency on tobacco begins between the ages of 10 and 18 with an average age of onset of 14-15. Youth tobacco dependency was similar to that among adults. The signs of addiction are generally correlated with the number of cigarettes smoked *per* day and generally with the smoking was beginning.[8] In 2015, it was found that approximately 20% of youth in the world between the ages of 15 and 24 smoke. An individual who begins using cigarettes before his/her early 20s is more likely to develop an addiction. In this respect, it can have a negative influence on the students educated in the disciplines of healthcare concerning the capacity to refrain from smoking throughout their lives, even more among male students (p= 0.007).[9,10]

The psychological mood caused by COVID-19 pandemics seems to have various sorts of influences on the usage of cigarettes. That is to say, while some users have consumed more than usual, others seem to decrease the density of consumption. The reason behind the increase in consumption level during the quarantine would be social isolation, while the reason behind the decrease in consumption level would be the fear of falling ill.[11]

Because of our study, the addiction score averages of female and male students before (p<0.001) and during the COVID-19 pandemic (p<0.001) differ significantly. Also, the male students had higher nicotine dependence scores compared with female students, both pre and during the pandemic.

Although there were healthcare professionals in the largest risk group during the pandemic period, it was observed that the cigarette addiction levels of the students of the health departments, where most students studying in departments such as medicine, dentistry, pharmacy, and emergency medical technicians were higher than others and remained unchanged during the pandemic period.

Students who had middle socio-economic status had significantly higher nicotine dependence scores pre-COVID-19, compared to during the pandemic (p= 0.027). However, no statistically significant difference was found in students who had high and low socio-economic status in addiction scores or during the pandemic.

Since the occurrence of the COVID-19 pandemic, supreme evidence has shown that smoking tobacco was a risk factor for pandemic.[12] Recent studies have demonstrated that smoking impacts the increase in the risk in terms of the infection of COVID-19[12] and that cigarette users are more prone to the adverse effects after being contaminated.[13] However, the psychosocial effect of the pandemic with related anxiety and stress raised by limitations and fear of illness could lead smokers to continue to use tobacco.[14]

Table 2. Descriptive statistics

	Mean	Standard deviation	Minimum	Maximum
Age	22.12	3.41	19	35
Smoking addiction scores before the pandemic	3.03	2.47	0	9
Smoking addiction scores during the pandemic	2.97	2.59	0	10

Table 3. Pre-pandemic and during the pandemic comparison of smoking addiction scores

	Pre-COVID-19	During COVID-19	Test statistic	*p*
Sex				
Female	2.69 ± 2.42	2.63 ± 2.52	t^a= 1.769	0.073
Male	3.40 ± 2.47	3.35 ± 2.62	t^a= 1.604	0.0110
Test statistic	t^b= -3.789	t^b= -3.632		
p	***p*<0.001**	***p*<0.001**		
Living place				
Village	3.58 ± 2.85	4.14 ± 3.30	t^a= -1.075	0.302
Town	1.66 ± 2.65	1.33 ± 1.36	t^a= 0.598	0.576
Country	2.65 ± 3.38	2.51 ± 2.44	t^a= 2.973	**0.003**
City center	3.20 ± 2.47	3.16 ± 2.61	t^a= 1.161	0.246
Test statistic	*F*= 3.538	*F*= 4.817		
p	**0.014**	**0.003**		
Department				
Other departments	2.87 ± 2.47	2.82 ± 2.58	t^a= 1.820	0.071
Health science department	3.60 ± 2.38	3.50 ± 2.58	t^a= 1.757	0.079
Test statistic	t^b= 3.187	t^b= 2.822		
p	**0.002**	**0.005**		
Economic situation				
Atrocious	3.88 ± 3.44	4.00 ± 4.09	t^a= 0.263	0.799
Bad	3.28 ± 2.34	3.23 ± 2.55	t^a= 0.490	0.626
Middle	2.94 ± 2.40	2.87 ± 2.51	t^a= 2.225	**0.027**
Good	3.00 ± 2.58	2.98 ± 2.69	t^a= 0.464	0.643
Very good	3.77 ± 2.50	3.49 ± 2.53	t^a= 1.781	0.088
Test statistic	*F*= 1.115	*F*= 0.848		
p	**0.348**	**0.495**		
Smoking in the family				
No	2.76 ± 2.44	3.07 ± 2.63	t^a= 2.407	**0.017**
Yes	3.11±2.47	2.62 ± 2.44	t^a= 1.349	0.178
Test statistic	t^b= 1.577	t^b= 1.920		
p	**0.115**	**0.055**		
Mandatory quarantine condition due to contact with someone diagnosed with COVID-19				
No	2.98 ± 2.47	3.24 ± 2.57	t^a= 2.563	**0.011**
Yes	3.16 ± 2.45	2.91 ± 2.59	t^a= 0.257	0.797
Test statistic	t^b= 1.108	t^b= 1.265		
p	**0.268**	**0.206**		
Having/passing the coronavirus infection				
Yes, I passed it and got through. My last test result was negative	3.11 ± 2.53	2.88 ± 2.58	t^a= 2.121	**0.040**
No, I did not experience any symptoms	2.98 ± 2.42	2.93 ± 2.55	t^a= 1.395	0.164
No, I had a test and my result was negative	3.32 ± 2.67	3.24 ± 2.70	t^a= 1.516	0.132
Yes, I doubt it. But it was not confirmed by a test	2.56 ± 2.33	2.46 ± 2.50	t^a= 1.000	0.324
Yes, I had the test and my result was positive	3.50 ± 2.50	3.75 ± 3.57	t^a= 475	0.649
Test statistic	*F*= 0.908	*F*= 0.915		
p	**0.459**	**0.455**		

t^a:Dependent sample *t*-test, t^b: Independent sample *t*-test and *F* test statistic of the analysis of variance. Bold values were statistically significant. COVID-19: Coronavirus Disease-2019

Table 4. Comparison of nicotine dependence levels pre and during the pandemic

Nicotine dependence levels during COVID-19 pandemic n (%)								
		Very low dependence	Low dependence	Moderate dependence	High dependence	Total	Test statistic	*p*
Nicotine dependence levels before the pandemic	Very low dependence	332 (44.3)	10 (1.3)	0	0	342	1356.47	*p*<0.001
	Low dependence	29 (3.9)	136 (18.1)	15 (2)	0	180		
	Moderate dependence	0	15 (2)	143 (19.1)	12 (1.6)	170		
	High dependence	0	0	6 (0.8)	51 (6.8)	57		
Total		361	161	164	63			

COVID-19: Coronavirus Disease-2019

In a large survey of 53,002 individuals in the UK, current smoking was associated with a 1.8 times higher chance of confirmed COVID-19. The same study showed that smokers reported lower respect to guidelines than non-smokers despite the fear of falling into illness seriously. Many users reported that they smoke more than they did previously and that stress is the prominent factor in the increase in smoking.[15]

CONCLUSION

This study has indicated that the smoking behavior of the students receiving education in the various departments of healthcare increased during the pandemic process considering their behavior on the same issue during the pre-pandemics process. Consequently, an increase or decrease in addiction levels can be seen because of isolation from society and anxiety caused by a pandemic. During the COVID-19 pandemic, addictions like smoking need exhaustive management, especially among vulnerable young populations such as quarantined people and individuals, who are at higher risk of smoking and other addictions. Therefore, the relevant healthcare institutions should develop the necessary projections to fight smoking addiction as well as with other substance addictions by taking advantage of the pandemic process.

Ethics

Ethics Committee Approval: Çukurova University Non-Interventional Clinical Studies Ethics Committee (project number: GO-105 dated 22.11.2020 and decision number: 55).

Informed Consent: Informed consent forms have been obtained from all volunteers.

Peer-review: Externally peer-reviewed.

Authorship Contributions

Concept: G.D., Design: G.D., Data Collection or Processing: F.G.N.Ç., G.D., Analysis, or Interpretation: G.D., Literature Search: F.G.N.Ç., Writing: F.G.N.Ç., G.D.

Conflict of Interest: No conflict of interest was declared by the authors.

Financial Disclosure: The authors declared that this study received no financial support.

REFERENCES

1. Strzelak A, Ratajczak A, Adamiec A, Feleszko W. Tobacco smoke induces and alters immune responses in the lung triggering inflammation, allergy, asthma and other lung diseases: a mechanistic review. Int J Environ Res Public Health. 2018;15:1033.
2. World Health Organization (WHO). Smoking and COVID-19: Scientific brief. Available from: https://apps.who.int/iris/handle/10665/332895 Accessed date: June 30, 2020.
3. Han L, Ran J, Mak YW, Suen LK, Lee PH, Peiris JSM, Yang L. Smoking and influenza-associated morbidity and mortality: a systematic review and meta-analysis. Epidemiology. 2019;30:405-417.
4. Umnuaypornlert A, Kanchanasurakit S, Lucero-Prisno DEI, Saokaew S. Smoking and risk of negative outcomes among COVID-19 patients: a systematic review and meta-analysis. Tob Induc Dis. 2021;19:09.
5. Fidancı İ, Aksoy H, Yengil Taci D, Ayhan Başer D, Cankurtaran M. Evaluation of the effect of the COVID-19 pandemic on smoking addiction levels. Int J Clin Pract. 2021;75:e14012.
6. Wang C, Pan R, Wan X, Tan Y, Xu L, Ho CS, Ho RC. Immediate psychological responses and associated factors during the initial stage of the 2019 coronavirus disease (COVID-19) epidemic among the general population in China. Int J Environ Res Public Health. 2020;17:1729.
7. Di Renzo L, Gualtieri P, Pivari F, Soldati L, Attinà A, Cinelli G, Leggeri C, Caparello G, Barrea L, Scerbo F, Esposito E, De Lorenzo A. Eating habits and lifestyle changes during COVID-19 lockdown: an Italian survey. J Transl Med. 2020;18:229.
8. Henningfield JE, Jude NR. Prevention of nicotine addiction: neuropsychopharmacological issues. Nicotine Tob Res. 1999;1(Suppl 1):S41-S48.
9. World No Tobacco Day 2020: protecting youth. Available from: http://www.euro.who.int/en/mediacentre/events/events/2020/05/world-notobacco-day-2020-protecting-youth Accessed date: 15.1.2021.
10. Granja L, Lacerda-Santos T, de Moura Brilhante D, de Sousa Nóbrega Í, Granville-Garcia AF, de França Caldas A Jr, dos Santos JA. Smoking and alcohol consumption among university students of the healthcare area. J Public Health (Berl). 2020;28:45-52.
11. Bommele J, Hopman P, Walters BH, Geboers C, Croes E, Fong GT, Quah ACK, Willemsen M. The double-edged relationship between COVID-19 stress and smoking: implications for smoking cessation. Tob Induc Dis. 2020;18:63.

12. Russo P, Bonassi S, Giacconi R, Malavolta M, Tomino C, Maggi F. COVID-19 and smoking: is nicotine the hidden link? Eur Respir J. 2020;55:2001116.

13. Vardavas CI, Nikitara K. COVID-19 and smoking: a systematic review of the evidence. Tob Induc Dis. 2020:18:20.

14. Stubbs B, Veronese N, Vancampfort D, Prina AM, Lin PY, Tseng PT, Evangelou E, Solmi M, Kohler C, Carvalho AF, Koyanagi A. Perceived stress and smoking across 41 countries: a global perspective across Europe, Africa, Asia and the Americas. Sci Rep. 2017;7:7597.

15. Jackson SE, Brown J, Shahab L, Steptoe A, Fancourt D. COVID-19, smoking and inequalities: a study of 53 002 adults in the UK. Tob Control. 2021;30:e111-e121.

Turk J Pharm Sci 2022;19(4):422-430
DOI: 10.4274/tjps.galenos.2021.57615

ORIGINAL ARTICLE

Development and Characterization of Hygroscopicity-Controlled Sustain Release Formulation of Divalproex Sodium

Saurav ADHIKARI, Uttam BUDHATHOKI*, Panna THAPA

Kathmandu University, Drug Delivery Research Lab, Department of Pharmacy, Dhulikhel, Nepal

ABSTRACT

Objectives: Divalproex sodium (DS), being a hygroscopic drug, requires low humidity during product manufacturing. This study aims to develop a hygroscopicity controlled sustained release formulation of DS that can be manufactured in relatively high humid conditions in facilities lacking dehumidifiers.

Materials and Methods: This study focuses on the role of polyethylene glycol (PEG-8000) and hydroxypropyl methylcellulose (HPMC K100M) as polymers of choice to control hygroscopicity and retard release of DS using solid dispersion technique. In this study, homogeneous solid dispersions containing various ratios of PEG-8000, HPMC K100M, and DS were obtained *via* melt granulation technique. Fifteen different solid dispersions were prepared based on Box-Behnken experimental design created in MiniTab software. The obtained solid dispersions were separately broken down into granules and their hygroscopic properties were determined *via* moisture uptake studies. Granular solid dispersions were then compressed into tablets and their sustained release dissolution profiles were studied as *per* the United States Pharmacopoeia (USP) monograph of DS extended-release tablets. Dissolution profiles of all fifteen formulations were then analyzed in Box-Behnken experimental design under MiniTab software to determine an optimized formulation having low hygroscopic properties as well as required multipoint drug release as *per* USP monograph. The final optimized formulation was prepared and subjected to moisture uptake study to determine its hygroscopicity, dissolution study to determine drug release kinetics and fourier transform infrared (FTIR) and differential scanning calorimetry (DSC) analysis to determine molecular interactions between drug and polymers.

Result: Optimized final formulation yielded granular solid dispersion with 28% less hygroscopicity compared to DS and tablets with an excellent release profile in accordance with USP monograph. FTIR and DSC analysis did not show any significant interaction between DS and components of the solid dispersion.

Conclusion: Optimized formulation from this study can be used to manufacture divalproex extended-release tablets inside facilities lacking dehumidifiers.

Key words: Divalproex sodium, solid dispersion, melt granulation, sustain release

INTRODUCTION

Oral drug delivery is the most preferred and convenient route of administration as the oral route provides maximum active surface area among all drug delivery systems for the administration of various drugs. Usually, conventional dosage forms produce wide fluctuations in the drug concentration in the bloodstream and tissues, causing undesirable toxicity and poor efficiency. These factors and others such as repetitive dosing and unpredictable absorption, lead to the concept of oral sustained release drug delivery systems.[1] Matrix-based system is a type of sustain release systems, where drug is dissolved or dispersed in a support resistant to disintegration. Drug is released from this support through erosion or diffusion. However, the release behavior is usually non-linear with a continuously diminishing release rate due to diffusion resistance or a decrease in effective surface area.[2]

*Correspondence: uttam@ku.edu.np, Phone: +977-11-415100, ORCID-ID: orcid.org/0000-0003-2804-8113
Received: 14.06.2021, Accepted: 20.09.2021

Conventionally, solid dispersion has been defined as "the dispersion of one or more active ingredients in an inert carrier matrix in solid-state prepared by melting (fusion), solvent or melting-solvent method".[3] Solid dispersion has been used in various applications to enhance the *in vitro* release of a drug compared to the conventional dosage form or to prepare water-insoluble drug polymer matrix to yield a modified release dosage form of a drug.[4] It has also been widely used as a technique to mask taste of bitter drugs for application into rapidly disintegrating tablets.[5] Although not widely adopted, another use of this technique is to modify the physical properties of a drug substance, such as conversion of hygroscopic/deliquescent drug into non-hygroscopic product in the form of solid dispersion.[6]

Response surface methodology (RSM) is a systematic way of establishing a relationship between any process input variable (independent variable) and it is response variable (dependent variable) to optimize the process.[7] The independent/input variables are changed in a predefined and controlled manner while the response variables are observed as the output of the process. A relationship between the input and output variables is then established using mathematical models and regression techniques. Once a relationship is established, it can then be used to develop, improve or optimize the product or process. With the help of RSM, a process or product can be optimized using least number of experiments without affecting the accuracy of results. Unfortunately, qualitative variables cannot be optimized.

During an RSM study, the input variables are predefined based on various design of experiment (DoE) such as Plackett-Burman design, Taguchi design, Full-Factorial design, Central composite design (CCD), Box-Behnken design, *etc*. Of these, Taguchi and Plackett-Burman designs are frequently used for screening studies, while Box-Behnken, Central composite, and factorial designs are frequently used for optimization studies.[8]

Divalproex sodium (DS), the model drug for this study, has been prescribed in various ailments such as seizures, bipolar disorder, and migraine headaches.[9] Conventional dosage forms of divalproex need to be administered two to thrice *per* day to achieve desired pharmaceutical response.[10] When administered as extended release dosage form, 8-20% increase in dose is necessary to produce similar bioavailability as conventional dosage form.[9] Despite this limitation, extended release dosage form is preferred owing to its decrease frequency of administration leading to better patient compliance and fewer side effects. Divalproex is available under the brand name, Depakote®, as delayed-release (125, 250, and 500 mg) and extended-release tablets (250 and 500 mg).[11]

Sodium valproate and valproic acid, components of DS, are extremely stable under thermal stress conditions.[12] Sodium valproate remains stable even after exposure to 110°C for 10 days and valproic acid does not show any sign of degradation after exposure to heat, light, and strong aqueous alkali or acid.[12] Reddy et al.[13] conducted force degradation studies in DS during which DS was subjected to an elevated temperature of 85°C for 120 h. After the completion of the thermal stress period, the sample retained 100% chromatographic purity and did not contain any traces of degradation product.

DS is a hygroscopic powder, which makes it a challenging drug to develop into dosage forms under humid conditions.[14] This study aims to ameliorate this problem by transforming DS into hygroscopicity controlled solid dispersion and use it to develop and optimized hygroscopicity controlled sustained release formulation of DS using Box-Behnken design.

MATERIALS AND METHODS

Materials

DS United States Pharmacopoeia (USP) was purchased from ROAQ Chemicals Pvt. Ltd. (India). Polyethylene glycol (PEG-8000) was purchased from LAR-CHEM Industries (India). Hydroxypropyl methylcellulose (HPMC) K100M and lactose monohydrate were purchased from The Dow Chemical Company (USA) and Modern Dairy (China), respectively. Colloidal silicone dioxide (aerosil) was bought from Evonic Industries (Germany).

Preliminary study

Before performing RSM study, a preliminary study was conducted to produce solid dispersion with various ratios of PEG-8000, HPMC K100M and DS using the melt granulation technique. During this study, it was observed that PEG-8000 melted at around 60°C and DS melted around 100°C. To determine its thermal stability DS, it was heated up to 110°C for 30 min and allowed to cool down. Assay of the thermally stressed DS was conducted using liquid chromatography method mentioned in the USP monograph of DS. The results revealed an assay of 99.579% and it is chromatogram (Figure 1) did not show any secondary peak due to degradation product. The absence of secondary peak concurred with the findings of Chang[12] and Reddy et al.[13], suggesting the excellent thermal stability of DS. HPMC K100M did not melt, when it was heated individually, but was readily soluble, when added to the molten mixture of PEG-8000 and DS. When only two components PEG-

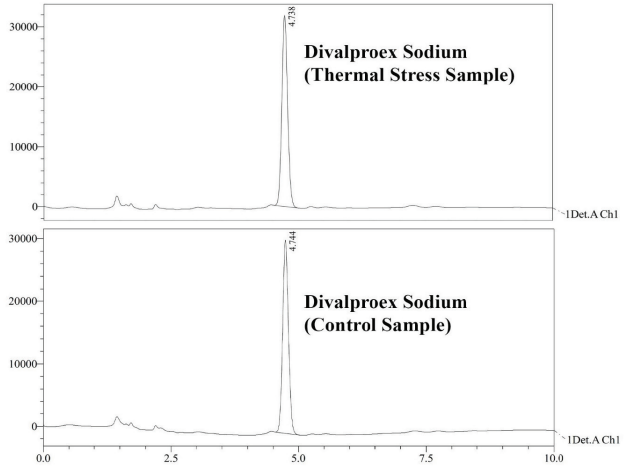

Figure 1. Chromatogram of DS thermal stress sample *vs*. control sample
DS: Divalproex sodium

8000 and DS were used to produce solid dispersion, it produced a homogeneous mixture at 100°C, but phase separation was observed upon cooling, signifying very little molecular interaction between the two. When all three ingredients PEG-8000, HPMC K100M, and DS were melted together, it produced a monophasic homogeneous mixture that did not show any sign of phase separation upon slow and fast cooling (shock cooling). Solid dispersions obtained after cooling were then broken down into granules. Hygroscopic properties of the obtained granular solid dispersion were determined using moisture uptake studies. Extragranullar HPMC K100M was added to the granular solid dispersion and compressed into tablets. Rate of drug release from the obtained tablets was then determined as *per* the USP monograph of DS extended-release tablets.

Based on the results obtained from moisture uptake and dissolution studies, upper and lower control limits of independent variables were set for the RSM.

Design of experiment

Three factors two level (3^2) CCD was used for the optimization of formulation. For this purpose, Minitab 17 software was used. Fifteen different formulations were obtained from the design (Table 1). Each formulation represented an experiment within the Box-Behnken design space. To avoid any potential bias, all experiments were conducted in randomized order (R1 to R15).

Since each formulation obtained from DoE contained a unique amount of PEG-8000, intragranular HPMC K100M and extragranular HPMC K100M, lactose monohydrate was added as diluent in each formulation to produce tablets with uniform weight and thickness (Table 2). Colloidal silicone dioxide (aerosil@0.975%) was used as a lubricating agent in all formulations. The final weight and thickness of tablet were set to be 615 mg and 6.78 ± 0.2 mm, respectively. Dispensing of DS was performed at 25°C and 40% relative humidity (RH). All other steps in the manufacturing process were performed at 25 ± 2°C and 50 ± 5% RH. Statistical analysis was not used in this study.

Preparation of solid dispersion

For the preparation of solid dispersion by fusion technique, following components of each formulation were melted together in a series of steps to produce a single homogeneous phase.

Table 1. Factors and level considered for design of experiment

Levels (mg/Tab)	Factors		
	PEG-8000	Intragranular HPMC K100M	Extragranular HPMC K100M
Lower (-1)	42 mg	66 mg	117 mg
Middle (0)	84 mg	83 mg	133 mg
High (+1)	126 mg	100 mg	150 mg

PEG: Polyethylene glycol, HPMC: Hydroxypropyl methylcellulose

Table 2. Formulation design space created by Box-Behnken experimental design in Minitab

Formulation design space created in Minitab							
Run	PEG	Intragranular HMPC	Extragranular HPMC	DS	Aerosil	Lactose	Final Wt.
R1	84	100	150	250	6	25	615
R2	126	100	133	250	6	0	615
R3	126	83	150	250	6	0	615
R4	42	83	150	250	6	84	615
R5	126	66	133	250	6	34	615
R6	42	66	133	250	6	118	615
R7	126	83	117	250	6	33	615
R8	84	83	133	250	6	59	615
R9	42	100	133	250	6	84	615
R10	84	66	117	250	6	92	615
R11	84	66	150	250	6	59	615
R12	84	83	133	250	6	59	615
R13	42	83	117	250	6	117	615
R14	84	100	117	250	6	58	615
R15	84	83	133	250	6	59	615

All weights are expressed in milligram (mg). PEG: Polyethylene glycol, HPMC: Hydroxypropyl methylcellulose, DS: Divalporex sodium

Step 1: In a small stainless steel vessel, PEG-8000 was added and the container was gradually heated until the PEG melted. When the PEG melted completely, DS was gradually added with continuous stirring.

Step 2: At around 97˚C to 98˚C, DS completely dissolved in PEG giving a transparent hot solution. In this solution, intragranular HPMC K100M was then gradually added with continuous stirring to obtain a translucent hot homogeneous mixture.

Step 3: The hot homogeneous phase obtained during fusion was then poured in stainless steel trays and allowed to cool gradually at room temperature (25˚C). Upon cooling, the molten liquid mass solidified to give a single homogeneous block of solid dispersion.

Preparation of granules

Solid dispersions were separately broken down into granules with the help of Multi Mill fitted with a screen of 1 mm pore size. Any residual material remaining in the Multi Mill was passed through a granulator fitted with a screen of 1 mm pore size to obtain free flowing granular solid dispersion. A small quantity of the obtained granular solid dispersion was subjected to moisture uptake studies and the remaining quantity was then mixed with appropriate amounts of extragranular HPMC K100M, lactose monohydrate, and aerosil as *per* experimental design (Table 2). A precompression study of granules was conducted in granules (Table 3).

Moisture uptake studies

Moisture sorption of compounds can be determined by exposing weighed amounts of compound in dishes placed in sealed desiccators containing saturated salt solutions. Saturated solutions of salts that give defined RH (as a function of temperature) have long been in use.[15]

A thin layer (≈1.5g) of DS and granular solid dispersion were spread in separate glass beakers of capacity 25 mL. The beakers were then placed in a desiccator containing a saturated salt solution that generates desired RH. The desiccator was then stored in a constant temperature chamber (30˚C). At pre-determined time intervals, each sample was removed and covered with aluminum foil to prevent moisture exchange with the environment during weighing process. After being weighing, the dishes were immediately placed back into the desiccator. The net weight gain of each sample after each time interval was calculated and plotted in a graph.

Moisture sorption studies were conducted at RH 52% and RH 75% using saturated salt solutions of magnesium nitrate and sodium chloride, respectively.

Compression into extended-release tablets

The granules for each of the fifteen formulations were lubricated in a double cone blender before being compressed into 7 mm long oval tablets of weight 615 mg and thickness 6.78 ± 0.2 mm.

RESULTS

Evaluation of formulations within the design space

Moisture uptake studies

After exposure of 24 h at RH 75%, granular solid dispersion from all fifteen formulations absorbed a greater amount of moisture compared to DS (Figure 2). It has been reported that

Table 3. Precompression study of granules

Run order	Evaluation of granules				Evaluation of tablets			
	Bulk density	Tapped density	Carr's index	Hausner ratio	Weight variation (mg)	Hardness (kg/cm^2)	Thickness (mm)	Friability (%)
R1	0.417	0.500	16.67	1.200	614.4 ± 4.55	11.04 ± 0.91	6.891 ± 0.034	0.0005
R2	0.449	0.522	14.00	1.163	615.2 ± 3.45	13.57 ± 0.49	6.873 ± 0.066	0.0008
R3	0.435	0.530	18.00	1.220	617.95 ± 2.69	13.25 ± 0.57	6.864 ± 0.075	0.003
R4	0.426	0.519	18.00	1.220	618.55 ± 3.82	13.22 ± 0.48	6.943 ± 0.043	0.0012
R5	0.450	0.536	16.00	1.190	615.6 ± 2.61	11.81 ± 0.48	6.795 ± 0.026	0.0012
R6	0.439	0.535	18.00	1.220	616.9 ± 3.25	11.84 ± 0.46	6.965 ± 0.034	0.0017
R7	0.447	0.545	18.00	1.220	615.95 ± 2.26	12.39 ± 0.42	6.932 ± 0.044	0.0005
R8	0.453	0.526	14.00	1.163	617.1 ± 3.98	11.72 ± 0.84	6.995 ± 0.034	0.0014
R9	0.449	0.535	16.00	1.190	615.05 ± 1.8	12.12 ± 0.66	6.82 ± 0.058	0.0021
R10	0.433	0.528	18.00	1.220	616.45 ± 2.59	12.17 ± 0.35	6.866 ± 0.035	0.0015
R11	0.427	0.508	16.00	1.190	615.2 ± 2.31	12.83 ± 0.32	6.897 ± 0.046	0.0011
R12	0.448	0.534	16.00	1.190	615.6 ± 2.38	11.87 ± 0.59	6.947 ± 0.027	0.0017
R13	0.442	0.514	14.00	1.163	616.75 ± 2.56	11.86 ± 0.48	6.884 ± 0.046	0.0015
R14	0.443	0.527	16.00	1.190	617.05 ± 2.65	12.62 ± 0.38	6.908 ± 0.047	0.0018
R15	0.444	0.528	16.00	1.190	615.85 ± 1.93	12.07 ± 0.35	6.944 ± 0.032	0.0014

HPMC starts swelling at RH greater than 65%.[16] This might be the reason for increased moisture sorption by solid dispersion at RH 75% (Figure 2).

A moisture sorption study at RH 52% was continued for 48 h. At the end of 48 h all fifteen formulations absorbed less moisture compared to DS (Figure 3).

Evaluation of granules and tablets

Granules from all fifteen formulations were evaluated to determine their bulk density, tapped density, Carr's index, and Hausner's ratio. Tablets were evaluated for their weight variation, hardness thickness, friability, dissolution, and assay. Dissolution (dissolution test-2) and assay were performed using respective HPLC methods mentioned under USP monograph of divalproex ER tablets in USP 40.[17]

Final optimized formulation

After the completion of all fifteen experiments within the design space, data obtained from dissolution studies (Table 4 and Figure 4) and moisture sorption studies (Figure 3) were recorded in the Box-Behnken design previously created in MINITAB 17 and analyzed to obtain optimized dissolution parameters (Table 5).

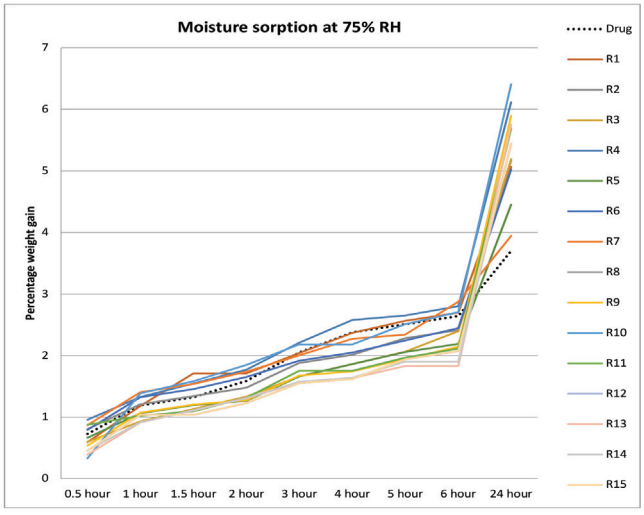

Figure 2. Moisture sorption by various formulations at 75% RH
RH: Relative humidity

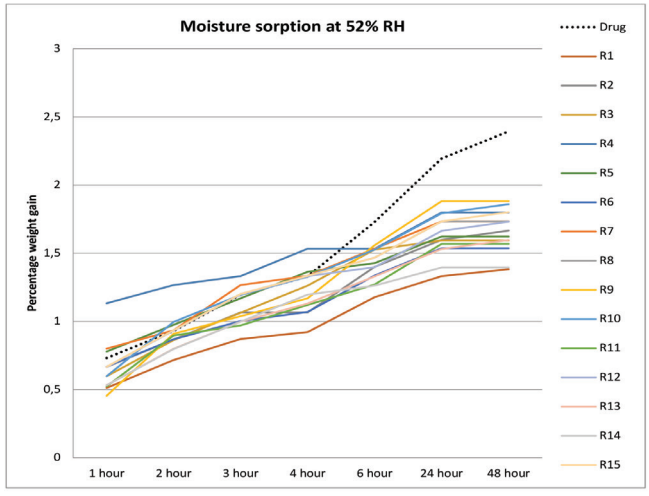

Figure 3. Moisture sorption by various formulations at 52% RH
RH: Relative humidity

Table 4. Dissolution profile and assay of compressed tablets

Run order	Dissolution profile (% release)				Assay (%)
	3rd hour	9th hour	12th hour	21st hour	
R1	29.69 ± 0.25	68.65 ± 1.88	79.99 ± 4.29	99.18 ± 4.42	99.76
R2	29.41 ± 1.09	76.04 ± 2.69	83.95 ± 2.18	101.58 ± 1.97	100.59
R3	20.79 ± 1.84	70.12 ± 2.86	81.8 ± 4.94	92.65 ± 1.21	99.57
R4	21.61 ± 1.04	69.03 ± 2.42	77.97 ± 2.96	92.59 ± 1.43	99.35
R5	28.08 ± 1.31	67.38 ± 3.56	76.17 ± 3.39	96.37 ± 0.38	98.93
R6	28.22 ± 1.25	71.54 ± 1.77	84.8 ± 2.05	95.43 ± 4.24	99.41
R7	31.7 ± 4.43	77.28 ± 2.36	86.3 ± 0.61	99.15 ± 2.16	100.83
R8	29.14 ± 1.27	72.33 ± 0.49	83.14 ± 1.8	99.28 ± 0.85	99.67
R9	27.19 ± 1.48	68.32 ± 3.76	80.69 ± 2.89	104.11 ± 2.11	100.46
R10	33.94 ± 1.33	78.37 ± 2.31	93.74 ± 4.6	107.12 ± 3.13	100.59
R11	26.61 ± 1.44	71.68 ± 2.65	87.04 ± 2.19	103.13 ± 2.19	99.85
R12	29.3 ± 2.09	72.01 ± 1.03	82.55 ± 1.84	99.57 ± 2.48	99.53
R13	28.24 ± 0.68	72.43 ± 1.25	83.42 ± 0.8	105 ± 2.1	101.26
R14	25.72 ± 1.21	70.63 ±1.77	82.62 ± 1.65	98.09 ± 2.63	100.79
R15	29.16 ± 2.29	72.27 ± 0.59	83.32 ± 2.11	99.64 ± 2.39	100.38

Optimized formulation (Tables 6, 7 and Figure 5) obtained from Minitab was manufactured using same process as previous formulations. Moisture sorption of the optimized formulation at 52% RH is shown in Figure 6. The dissolution profile of the optimized formulation was found within the limit of USP (Figure 7).

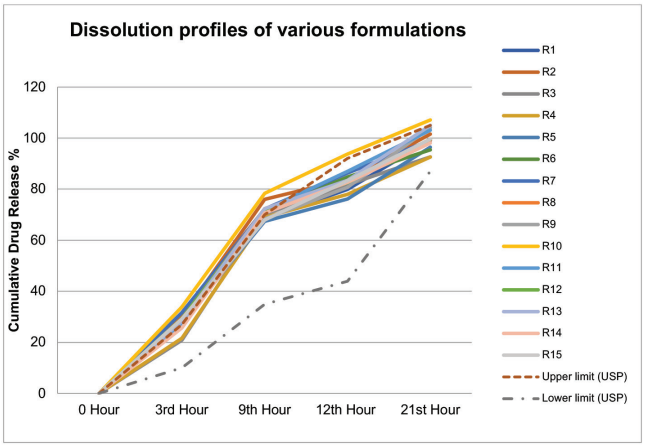

Figure 4. Dissolution profile of tablets before optimization

Table 5. Target dissolution parameters set in Minitab for optimized formulation

3rd hour	24% release
9th hour	65% release
12th hour	78% release
21st hour	95% release

Drug release kinetics

The rate of drug release from the final optimized formulation was fitted into various models of drug release kinetics (Table 8).

Infrared absorption spectroscopy

Infrared absorption spectroscopy was performed on API and the developed solid dispersion (Figure 8 and Table 9).

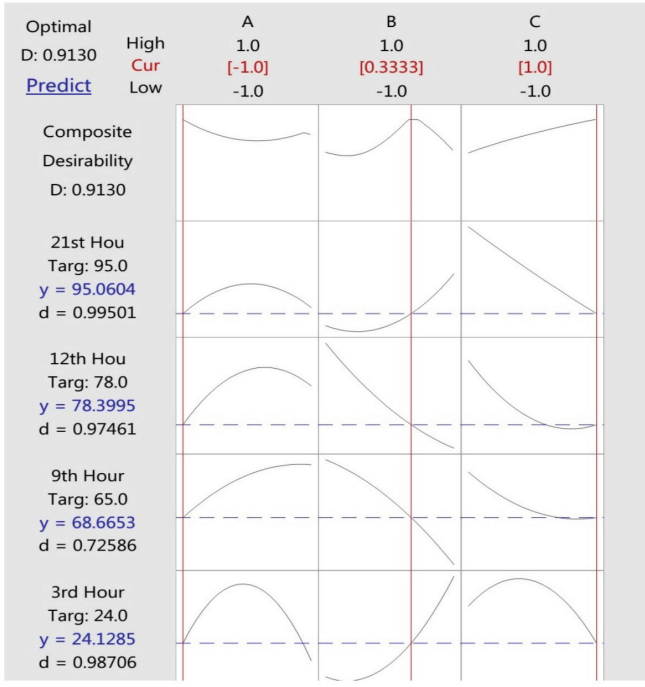

Figure 5. Optimization plot obtained in Minitab

Table 6. Composition given by Minitab for optimized formulation

	PEG (A)	Intragranular HPMC (B)	Extragranular HPMC (C)
Levels in Box-Behnken design	-1	0.33	+1
Actual value	42 mg	88.66 mg	150 mg

PEG: Polyethylene glycol, HPMC: Hydroxypropyl methylcellulose

Table 7. Optimized formulation obtained from Minitab

S. no	Raw material	Quantity (mg)
1	Divalporex sodium	250
2	PEG-800	42
3	HPMC K100M intragranular	88.66
4	HPMC K100M extragranular	150
5	Aerosil	6
6	Lactose monohydrate	78.34
	Total	**615**

PEG: Polyethylene glycol, HPMC: Hydroxypropyl methylcellulose

Differential scanning calorimetry (DSC)

DSC analysis was performed on the final optimized solid dispersion and its individual components (Figure 9).

DISCUSSION

The final optimized formulation when subjected to moisture sorption studies at 52% RH produced granules with 1.71% weight gain at the end of 48 h. During the same period, DS

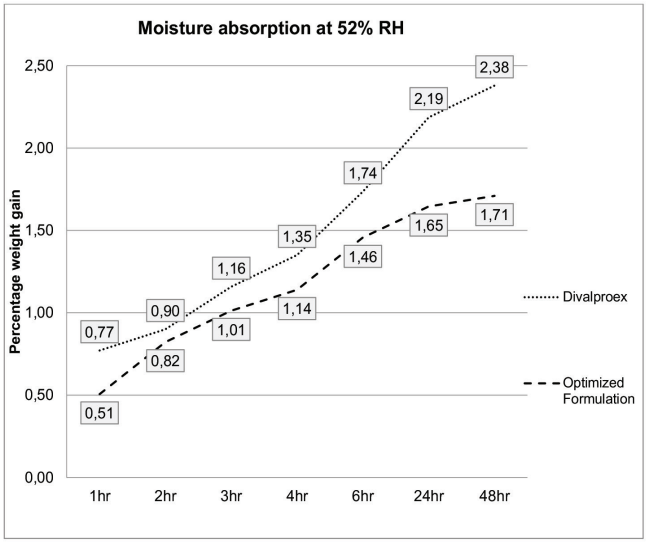

Figure 6. Moisture sorption of optimized formulation at 52% RH

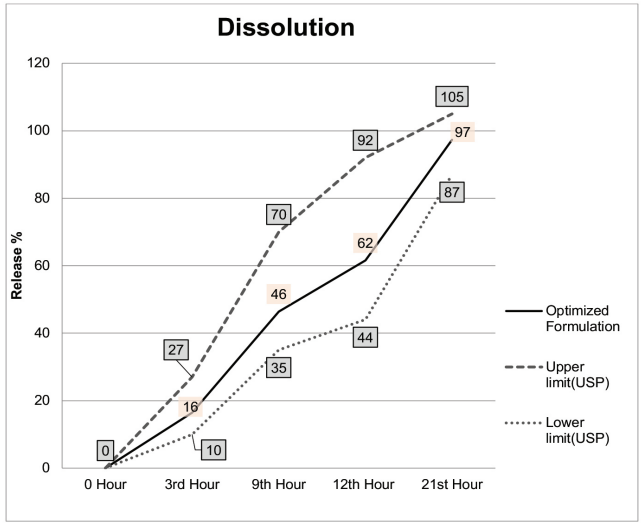

Figure 7. Dissolution profile of optimized formulation
USP: United States Pharmacopoeia

Table 8. Drug release kinetics fitted to various models

S. no	Kinetics	Regression equation	R^2
1	Zero order	y= 4.6439x + 2.5423	0.995
2	First order	y= -0.0727x + 2.1873	0.876
3	Huguchi model	y= 21.087x - 9.5554	0.938
4	Korsmeyer-Peppas	K= 5.689, n= 0.9573	0.9999
5	Hixson-Crowell	y= -0.1526x + 4.8832	0.952

Table 9. Intrepretation of IR spectrum of DS and its solid dispersion

S. no	Wavenumber	Percentage transmittance		Remarks
		Divalproex sodium	DS solid dispersion	
1	2957 cm^{-1}	87.74%	82.26%	Asymmetric C-H stretch of CH3.[18]
2	2933 cm^{-1}	88.50%	83.76%	Asymmetric C-H stretch of CH2.[18]
3	2873 cm^{-1}	91.15%	86.29%	Symmetric C-H stretch of CH3.[18]
4	1689 cm^{-1}	87.75%	83.63%	C=O stretch of valproic acid.[19]
5	1555 cm^{-1}	84.09%	79.64%	C=O stretch of valproate ion.[19]
6	1465 cm^{-1}	88.73%	84.59%	C-H bend/scissoring in CH2.[18]
7	1379 cm^{-1}	84.39%	79.99%	C-H rocking in -CH3.[21]
8	1256 cm^{-1}	82.28%	77.38%	-
9	1217 cm^{-1}	81.69%	77.07%	
10	1107 cm^{-1}	85.60%	73.37%	C-O stretching vibrations in C-O-C bond of PEG.[20]

IR: Infrared spectroscopy, DS: Divalporex sodium, PEG: Polyethylene glycol

gained 2.38%. Hence, the solid dispersion was 28.15% less hygroscopic compared to DS. At the end of 48 h solid dispersion remained free flowing granules, whereas DS had clumped together into a single mass.

Drug release kinetics from the optimized tablet formulation most closely resembles Korsmeyer-Peppas model of drug release with a correlation coefficient r^2= 0.999. The values of K and n in the Korsmeyer-Peppas equation were found to be 5.689 and 0.9573, respectively. Since the value of n is close to 1, we can conclude that the drug release approaches zero order kinetics, which is also evident from the correlation coefficient r^2= 0.995 for zero order approximations (Table 8). In a similar study, Monajjemzadeh et al.[14] produced sustained release formulation of DS *via* a direct compression method using HPMC K100M as rate controlling polymer, where they also found zero order drug release (r^2= 0.995). This implies that release kinetics in both cases were predominantly governed by high solubility and diffusivity of DS, and not by the technology (direct compression *vs*. solid dispersion) used to manufacture the tablets.

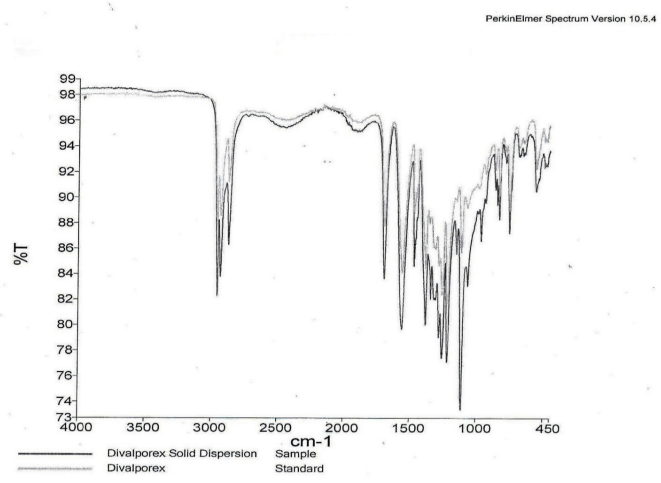

Figure 8. Comparison of IR spectra of DS and DS solid dispersion
DS: Divalproex sodium, IR: Infrared spectroscopy

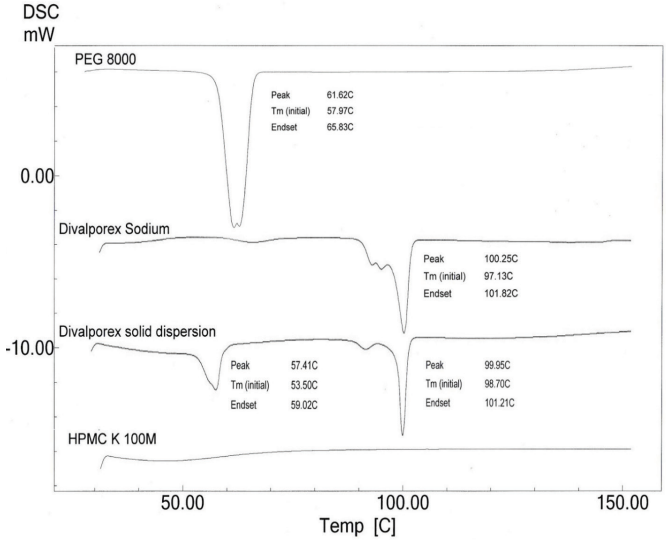

Figure 9. Melting endotherm of DS solid dispersion and its components
DS: Divalporex sodium, DSC: Differential scanning calorimetry

A study on IR spectrum of DS has shown that absorbance at 2957 cm^{-1} is due to asymmetric C-H stretch of CH_3.[18] Another study on IR spectrum of DS has shown that absorbance at 1555 cm^{-1} and 1689 cm^{-1} is associated with carbonyl bonds of sodium valproate and valproic acid, respectively.[19] Any significant interaction between carbonyl groups of divalproex and other components of solid dispersion would mean shift of these frequencies in IR spectrum of DS solid dispersion. This shift is absent and absorption at 1555 cm^{-1} and 1689 cm^{-1} is seen in the IR spectra of DS solid dispersion as well. This implies absence of carbonyl type interaction between DS and other polymers in solid dispersion.

The sharp peak around 99°C in the endotherm of DS represents evaporation of valproic acid.[19] DS and DS solid dispersion both produced identical endothermic peaks at 100.25°C and 99.95°C, respectively. Such close values of T_m imply absence of any molecular forces/interaction between valproic acid and components of the solid dispersion that could have significantly altered the endothermic peak shape or T_m in the endotherm of the DS solid dispersion. This supports the findings from the IR spectrum analysis, which also suggests absence of molecular interaction.

There is a significant difference in IR transmittance at 1107 cm^{-1} between DS (85.60%) and DS solid dispersion (73.37%), 12.23% greater absorption by solid dispersion at 1107 cm^{-1}. Dinç and Guner[20] have reported that absorbance band of PEG at 1107 cm^{-1} is associated with C-O stretch when the C-O bond of PEG is involved in intermolecular hydrogen bonding, suggesting that the C-O bond of PEG in DS solid dispersion is involved in hydrogen bonding possibly with water molecules, resulting in greater absorbance by solid dispersion. This interpretation is also supported by the fact that T_m value in melting endotherm of pure PEG-8000 (61.62°C) has decreased to 57.41°C in endotherm of solid dispersion. Majumdar et al.[21] have observed a similar decrease in T_m value in melting endotherm of PEG due to interactions between water molecule and PEG molecule. This also suggests the presence of interactions between water and PEG molecules in the DS solid dispersion.

Study limitations

X-ray diffraction study could not be performed. This could have enabled a further understanding of molecular interactions and the degree of crystallinity within solid dispersion.

CONCLUSION

DS is present in solid dispersion without any significant molecular interaction between divalproex and polymers of solid dispersion. Moisture present in DS solid dispersion is associated with PEG molecule as evident from shift in T_m of PEG and sharp increase in absorbance by solid dispersion at 1107 cm^{-1}. Since the interaction is absent, the decrease in hygroscopicity of DS solid dispersion compared to DS may be because of PEG/HPMC acting as a barrier between the drug

and moisture. The optimized formulation from this study can be used to manufacture divalproex extended-release tablets inside facilities lacking humidity controlling systems such as dehumidifiers.

Ethics

Ethics Committee Approval: Not required.

Informed Consent: Not required.

Peer-review: Externally peer-reviewed.

Authorship Contributions

Concept: S.A., U.B., P.T., Design: U.B., P.T., Data Collection or Processing: S.A., Analysis, or Interpretation: S.A., U.B., P.T., Literature Search: S.A., U.B., P.T., Writing: S.A., U.B., P.T.

Conflict of Interest: No conflict of interest was declared by the authors.

Financial Disclosure: Part of academic dissertation, thus funded by Department of Pharmacy, Kathmandu University.

REFERENCES

1. Ratnaparkni MP, Gupta Jyoti P. Sustained release oral drug delivery system - an overview. Int J Pharma Res Rev. 2013;2:11-21.
2. Khan GM. Controlled release oral dosage forms: some recent advances in matrix type drug delivery systems. J Med Sci Res. 2001;1:350-354.
3. Chiou WL, Riegelman S. Pharmaceutical applications of solid dispersion systems. J Pharm Sci. 1971;60:1281-1302.
4. Craig DQ. The mechanisms of drug release from solid dispersions in water-soluble polymers. Int J Pharm. 2002;231:131-144.
5. Becker K, Salar-Behzadi S, Zimmer A. Solvent-free melting techniques for the preparation of lipid-based solid oral formulations. Pharm Res. 2015;32:1519-1545.
6. Trivedi JS, Gokhale RD. Solid dispersions comprising a hygroscopic and/or deliquescent drug. 2005; (US 2005/0013856 A1).
7. Fukuda IM, Pinto CFF, dos Santos Moreira C, Saviano AM, Lourenço FR. Design of experiments (DoE) applied to pharmaceutical and analytical quality by design (QbD). Brazilian J Pharm Sci. 2018;54.
8. Bhoop BS, Raza K, Beg S. Developing "optimized" drug products employing "designed" experiments. Chem Ind Dig. 2013;23:70-76.
9. Dutta S, Reed RC. Divalproex to divalproex extended release conversion. Clin Drug Investig. 2004;24:495-508.
10. Phaechamud T, Mueannoom W, Tuntarawongsa S, Chitrattha S. Preparation of coated valproic acid and sodium valproate sustained-release matrix tablets. Indian J Pharm Sci. 2010;72:173-183.
11. Dutta S, Zhang Y, Selness DS, Lee LL, Williams LA, Sommerville KW. Comparison of the bioavailability of unequal doses of divalproex sodium extended-release formulation relative to the delayed-release formulation in healthy volunteers. Epilepsy Res. 2002;49:1-10.
12. Chang ZL. Sodium valproate and valproic acid. Anal Profiles Drug Subst Excipients. 1979;8:529-556.
13. Reddy SR, Reddy KH, Reddy PM, Reddy GA, Kumar MN, Sharma HK. Reliable GC method for related substances in divalproex sodium drug. J Chromatogr Sci. 2017;55:891-898.
14. Monajjemzadeh F, Hamishehkar H, Zakeri-Milani P, Farjami A, Valizadeh H. Design and optimization of sustained-release divalproex sodium tablets with response surface methodology. AAPS PharmSciTech. 2013;14:245-253.
15. Niazi S. Handbook of preformulation: chemical, biological, and botanical drugs. 1st ed. Informa Healthcare; 2007:229-230.
16. Laksmana FL, Kok PJ, Frijlink HW, Vromans H, Van der Voort Maarschalk K. Using the internal stress concept to assess the importance of moisture sorption-induced swelling on the moisture transport through the glassy HPMC films. AAPS PharmSciTech. 2008;9:891-898.
17. Convention USP. U.S. Pharmacopeia National Formulary 2017: USP 40 NF 35. The United States Pharmacopeial Convention, 12601 Twinbrook Parkway, Rockville, MD 20852; 2017.
18. Coates J. Interpretation of infrared spectra, a practical approach. Encycl Anal Chem. Published online 2006.
19. Petrusevski G, Naumov P, Jovanovski G, Bogoeva-Gaceva G, Ng SW. Solid-state forms of sodium valproate, active component of the anticonvulsant drug epilim. ChemMedChem. 2008;3:1377-1386.
20. Dinç CÖ, Guner A. Solid-state characterization of poly(ethylene glycol) samples prepared by solvent cast technique. Bulg Chem Commun. 2017;49:15-20.
21. Majumdar R, Alexander KS, Riga AT. Physical characterization of polyethylene glycols by thermal analytical technique and the effect of humidity and molecular weight. Pharmazie. 2010;65:343-347.

Turk J Pharm Sci 2022;19(4):431-441
DOI: 10.4274/tjps.galenos.2021.83548

ORIGINAL ARTICLE

Molecular Docking Study of Several Seconder Metabolites from Medicinal Plants as Potential Inhibitors of COVID-19 Main Protease

Sinan BİLGİNER[1]*, Sefa GÖZCÜ[2], Zuhal GÜVENALP[3]

[1]Atatürk University, Faculty of Pharmacy, Department of Pharmaceutical Chemistry, Erzurum, Türkiye
[2]Erzincan Binali Yıldırım University, Faculty of Pharmacy, Department of Pharmacognosy, Erzincan, Türkiye
[3]Atatürk University, Faculty of Pharmacy, Department of Pharmacognosy, Erzurum, Türkiye

ABSTRACT

Objectives: Coronaviruses (CoVs) cause infections that affect the respiratory tract, liver, central nervous, and the digestive systems in humans and animals. This study focused on the main protease (M^{pro}) in CoVs (PDB ID: 6LU7) that is used as a potential drug target to combat 2019-CoV. In this study, a total of 35 secondary metabolites from medical plants was selected and docked into the active site of 6LU7 by molecular docking studies to find a potential inhibitory compound that may be used to inhibit Coronavirus Disease-2019 (COVID-19) infection pathway.

Materials and Methods: The chemical structures of the ligands were obtained from the Drug Bank (https://www.drugbank.ca/). AutoDockTools (ADT ver. 1.5.6) was used for molecular docking studies. The docking results were evaluated using BIOVIA Discovery Studio Visualizer and PyMOL (ver. 2.3.3, Schrodinger, LLC).

Results: Pycnamine, tetrahydrocannabinol, oleuropein, quercetin, primulic acid, kaempferol, dicannabidiol, lobelin, colchicine, piperidine, medicagenic acid, and narcotine is found to be potential inhibitors of the COVID-19 M^{pro}. Among these compounds, pycnamine, which was evaluated against COVID-19 for the first time, showed a high affinity to the COVID-19 M^{pro} compared with other seconder metabolites and reference drugs.

Conclusion: Our results obtained from docking studies suggest that pycnamine should be examined *in vitro* to combat 2019-CoV. Moreover, pycnamine might be a promising lead compound for anti-CoV drugs.

Key words: COVID-19, molecular docking, pycnamine, seconder metabolites

INTRODUCTION

Coronaviruses (CoVs) cause disorders in both the respiratory tract and the digestive system in humans and animals.[1] During an epidemic in Wuhan, China at the end of 2019, the new CoV strain was identified and named 2019-nCoV. In a very short time, this newly emerging virus spread to almost all countries and the disease is officially named as Coronavirus Disease-2019 (COVID-19) by World Health Organization (WHO).[2] According to WHO's COVID-19 Weekly Epidemiological Update Report released on May 11, 2021, the number of confirmed cases reached 157,362,408 including 3,277,834 deaths in the world as of May 9, 2021.[3]

Currently, there are several vaccines for COVID-19, but no antiviral drugs are available for specific treatment of COVID-19. However, some antiviral drugs such as lopinavir, ritonavir, remdesivir, and nelfinavir have been using to prevent further complications and organ damage caused by COVID-19.[4] Among all these drugs, nelfinavir, which has been used in clinics, was found as the most potential inhibitor drug against COVID-19 main protease (M^{pro}) based on its docking score according to the docking studies conducted by Xu et al.[5] In docking studies, M^{pro} is used as a potential drug target to combat 2019-CoV.[6-8]

Secondary metabolites obtained from medicinal plants and their semi-synthetic derivatives have been widely used in new

*Correspondence: sinanbilginer25@yahoo.com, Phone: +90 536 357 40 46, ORCID-ID: orcid.org/0000-0001-5676-2045
Received: 06.08.2021, Accepted: 24.09.2021

drug development. Therefore, the use of secondary metabolites purified from medicinal plants in drug development against severe acute respiratory syndrome (SARS)-CoV becomes important.[9] There are many studies reporting the antiviral effects of many compounds with alkaloid,[10-12] flavonoid,[13,14] monoterpene,[15-19] sesquiterpene lactone,[20,21] saponoside,[22,23] and aryl alkene[24,25] structures.

In this study, the potential innhibitory effects of alkaloids (atropine, caffeine, castanospermine, codeine, ephedroxane, hygrine, cuscohygrine, colchicine, lobeline, tussilagine, punicalagin, papaverine, pycnamine, piperidine, scopolamine, morphine, narcotine, pelletierine, ricinine), cannabinoids (cannabidiol and tetrahydrocannabinol), monoterpenes (citral A, thymol, oleuropein, and harpagoside), sesquiterpene lactone, *e.g.* artemisinin, saponins (primulic acid and medicagenic acid), aryl alkene (aromatic ketone), *e.g.* gingerol, and flavonoids (quercetin and kaempferol) were investigated on 2019-CoV Pro *via* molecular docking studies. We hope that the findings of this study will contribute to drug research to combat COVID-19 and direct the researchers working in this field to further designs.

MATERIALS AND METHODS

Experimental in silico part

The 2019-CoV M^{pro} (PDB ID: 6LU7) structure was obtained from The Protein Data Bank (PDB, https://www.rcsb.org/). The pdb file of the 6LU7 protein was prepared using chain A and transferred to AutoDockTools (ADT ver. 1.5.6). Water molecules of the structures were removed and only polar hydrogen and Kollman charges were added to the proteins. Finally, the pdbqt files of the proteins were saved.[26]

Chemical structures of the ligands were obtained from the Drug Bank (https://www.drugbank.ca/). The ligands unavailable in the Drug Bank were drawn in ChemDraw (Professional, version 19.0.1.28), passed to ChemDraw 3D (professional, version 19.0.1.28) and minimized. Torsion of the ligands was examined and then the files of the ligands were saved as pdbqt format by AutodockTools (ADT ver. 1.5.6).

The active site of the 6LU7 was defined using BIOVIA Discovery Studio Visualizer (v20.1.0.19295). AutoDockTools (ADT ver. 1.5.6) was used for molecular docking studies. Lamarckian genetic algorithm with local search was used as a search engine, with 10 runs. The active site of the protein was defined by a grid box of 60 x 60 x 60 points. Ten conformers of the ligands were considered to evaluate the docking results. Finally, the conformer with the lowest binding free energy was evaluated by BIOVIA Discovery Studio Visualizer and PyMOL (ver. 2.3.3, Schrodinger, LLC).[26]

Statistical analysis

No statistical analysis was used in this study.

RESULTS

CoVs cause infections that affect the respiratory tract, liver, central nervous and the digestive systems in humans and animals.[27] This study focused on the M^{pro} in CoVs (PDB ID: 6LU7) that is used as a potential drug target to combat 2019-CoV. 6LU7 has been structured in PDB and has been publicly available since early February, 2020. To date, this M^{pro} (6LU7) has been studied by different groups to find potential inhibitors that can stop this enzyme activity and, thus, the replication of CoVs.[8,27,28]

Nelfinavir, lopinavir, indinavir, and ritonaviprotease inhibitory drugs, of which ritonavir and lopinavir is proposed for treating SARS and MERS.[29] In an *in vitro* study by Yamamoto et al.[29], nelfinavir was reported to strongly inhibit the replication of SARS-CoV in Vero E6 cells.[30] However, in an *in silico* study by Xu et al.[5], nelfinavir was identified as the most potent inhibitor against COVID-19 with a binding free energy score. In our study, nelfinavir, lopinavir, indinavir, and ritonavir were used as standard drugs for comparison.

In this study, 35 secondary metabolites from medical plants were selected and docked into the active site of 6LU7. Docking studies were performed by AutoDockTools (ADT ver. 1.5.6). Table 1 shows the binding free energy scores of all selected molecules. The native ligand for 6LU7 is *n*-[(5-methylisoxazol-3-yl) carbonyl]alanyl-l-valyl-*n*~1~-(1r,2z)-4-(benzyloxy)-4-oxo-1-[[(3r)-2-oxopyrrolidin-3-yl] methyl]but-2-enyl)-l-leucinamide. According to the results presented in Table 1, the binding free energy scores of the compounds were between -11.30 kcal/mol and -4.13 kcal/mol. We investigated pycnamine, tetrahydrocannabinol, oleuropein, quercetin, primulic acid, kaempferol, cannabidiol, lobeline, colchicine, piperidine, medicagenic acid, and narcotine as potential inhibitors of the COVID-19 M^{pro} because to the binding free energy scores of -11.30, -9.10, -9.06, -8.94, -8.94, -8.70, -8.52, -8.30, -8.28, -7.74, -7.71, and -7.60 kcal/mol, respectively.

Analysis of docking results and interactions with six of these compounds are presented in Tables 2 and 3. Table 2 shows the analysis of molecular docking results (binding energy/Gibbs Energy, ligand efficiency, inhibition constant, intermolecular energy, and Van der Waals-H Bond desolvation energy) for the compounds with binding energies less than -7.60 kcal/mol, which is similar to the binding free energy of ritonavir.

Table 3 shows 2D and 3D visualizations of interactions between 6LU7 and the compounds presented in Table 2. According to Table 3, which shows interactions between compounds and 6LU7, nelfinavir forms H-bonds with the amino acids Gly143, His163, Thr190, Gln189 of 6LU7. Lopinavir forms H-bonds with the amino acids His41, Cys145, Gln189, and Glu166. Indinavir realizes H-bonds with the amino acid, *i.e.* Asn142, while ritonavir, the latest standard drug, forms H-bonds with the amino acids His164 and Glu166. When the interactions of the seconder metabolites in Table 3 are evaluated, the following results are seen: pycnamine forms H-bond with the amino acid, *i.e.* Glu166. Tetracannabinol forms H-bonds with the amino acids Glu166, Cys145. Oleuropein realizes H-bonds with the 6LU7 amino acids, *e.g.* His41, Thr26, Gly143, Glu166, and Thr190. Quercetin realizes H-bonds with 6LU7 amino acids, *e.g.* Glu166, Thr190, and His164.

Table 1. Binding free energy scores of the compounds

Compounds	Binding free energy (kcal/mol)	Compounds	Binding free energy (kcal/mol)
Pycnamine	-11.30	Harpagoside	-6.82
Tetrahydrocannabinol	-9.10	Atropine	-6.70
Oleuropein	-9.06	Punicalagin	-6.63
Quercetin	-8.94	Couscohygrin	-6.41
Primulic acid	-8.94	Gingerol	-6.27
Kaempferol	-8.70	Ephedroxan	-5.96
Cannabidiol	-8.52	Tussulagin	-5.91
Lobeline	-8.30	Castanospermine	-5.90
Colchicine	-8.28	Pelletierin	-5.30
Piperidine	-7.74	Citral-A	-4.98
Medicagenic acid	-7.71	Thymol	-4.95
Narcotine	-7.60	Caffeine	-4.64
Butylscopolamine	-7.42	Hygrin	-4.55
Hyoscyamine	-7.39	Ricinin	-4.51
Reticuline	-7.29	Ivermektin	-4.13
Papaverine	-7.16	Native ligand	-7.96
Codeine	-7.07	Nelfinavir*	-10.70
Artemisinin	-7.03	Lopinavir*	-8.95
Scopolamine	-6.97	Indinavir*	-8.73
Morphine	-6.88	Ritonavir*	-7.81

*Nelfinavir, lopinavir, indinavir, and ritonavir are HIV protease inhibitor drugs

Table 2. Molecular docking results analysis of compounds with low binding energy scores and the drugs used in clinic

Compounds	Binding energy (kcal/mol)	Ligand efficiency	Inhibition constant	Intermolecular energy	Van der Waals-H Bond desolvation energy
Pycnamine	-11.30	-0.25	5.21 nM	-12.20	-11.85
Tetrahydrocannabinol	-9.10	-0.40	214.2 nM	-10.59	-10.58
Oleuropein	-9.06	-0.25	229.87 nM	-13.23	-12.96
Quercetin	-8.94	-0.41	277.84 nM	-9.24	-9.13
Primulic acid	-8.94	-0.12	279.96 nM	-14.01	-13.70
Kaempferol	-8.70	-0.41	422.9 nM	-8.99	-8.88
Cannabidiol	-8.52	-0.37	570.21 nM	-10.01	-9.97
Lobeline	-8.30	-0.33	821.52 nM	-10.09	-9.98
Colchicine	-8.28	-0.29	-856.99 nM	-9.77	-9.66
Piperidine	-7.74	-0.37	2.11 μM	-8.64	-8.58
Medicagenic acid	-7.71	-0.21	2.21 μM	-9.50	-9.66
Narcotine	-7.60	-0.25	2.69 μM	-8.79	-8.42
Nelfinavir	-10.70	-0.27	14.45 nM	-12.78	-12.72
Lopinavir	-8.95	-0.19	275.32 nM	-13.72	-13.55
Indinavir	-8.73	-0.19	400.34 nM	-12.90	-12.33
Ritonavir	-7.81	-0.16	1.9 μM	-13.47	-13.39

Table 3. Two-dimensional and three-dimesnsional interaction diagrams for several compounds

No	Compound	2D representation of compounds-6LU7 interactions	3D representation of compounds-6LU7 interactions
1	Pycnamine	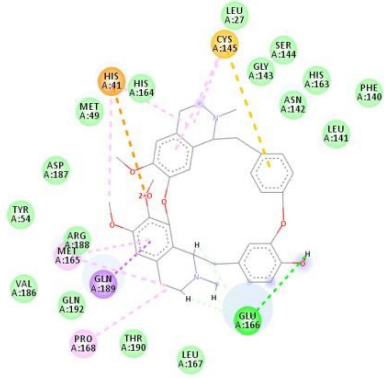	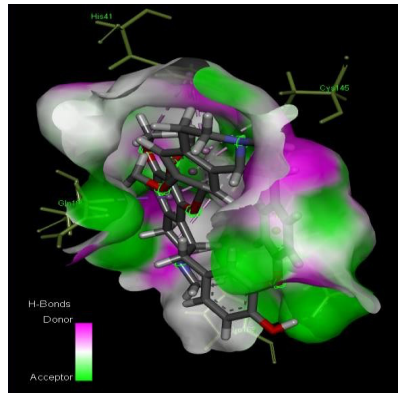
2	Tetrahydrocannabinol	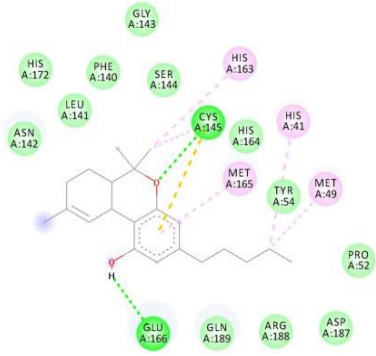	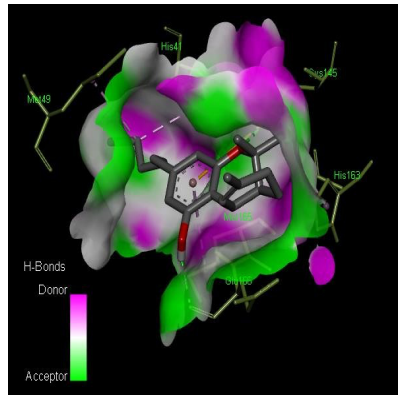
3	Oleuropein	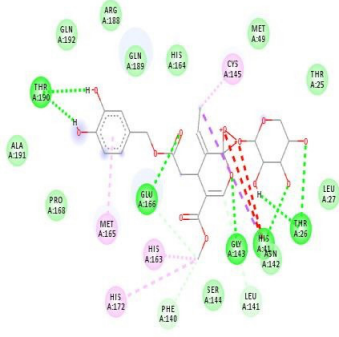	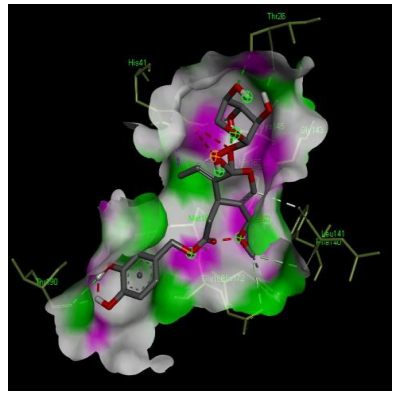
4	Quercetin	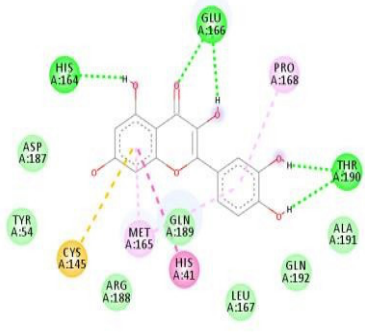	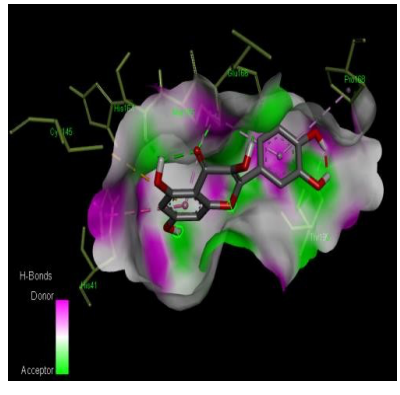

5	Primulic acid	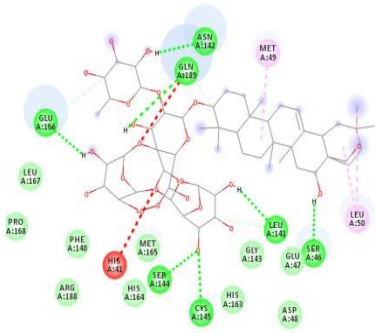	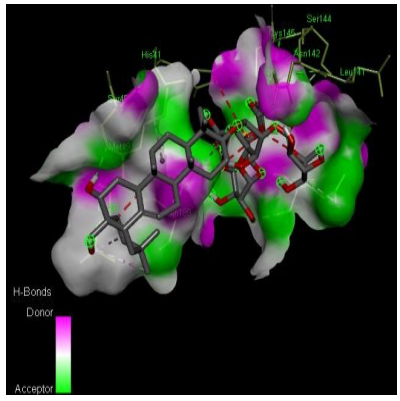
6	Kaempferol	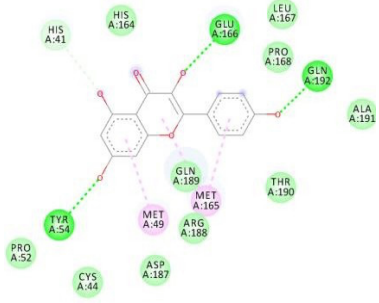	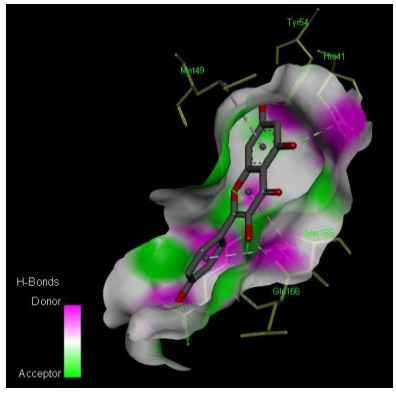
7	Cannabidiol	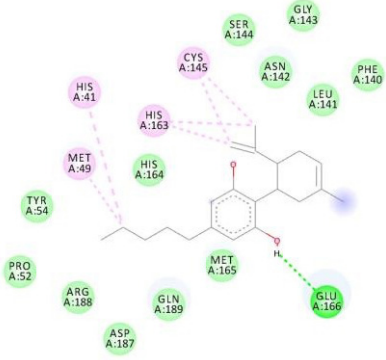	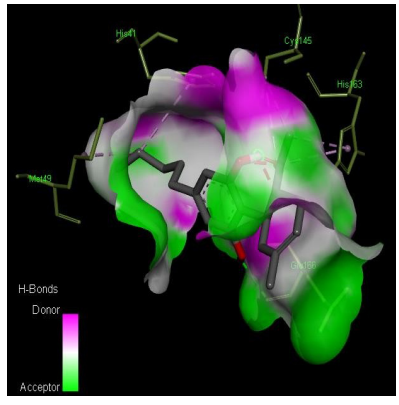
8	Lobeline	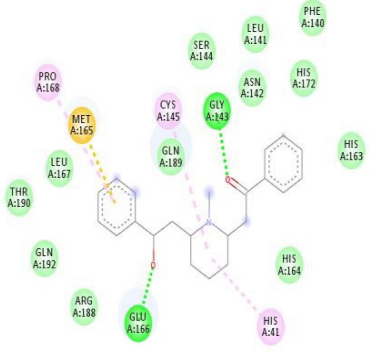	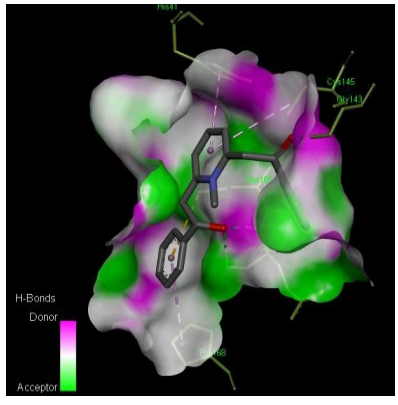

9	Colchicine	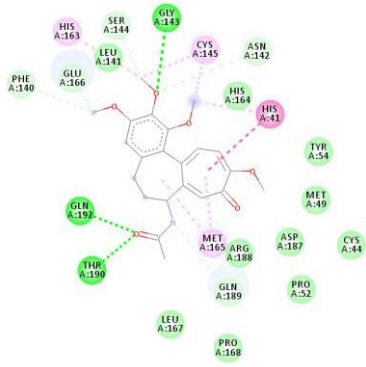	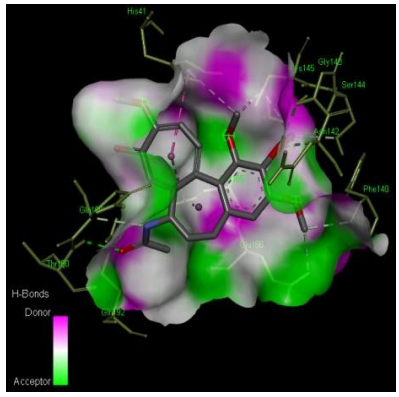
10	Piperidine	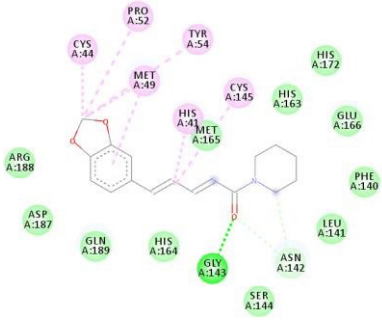	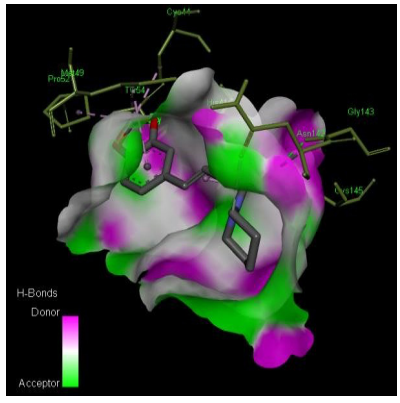
11	Medicagenic acid	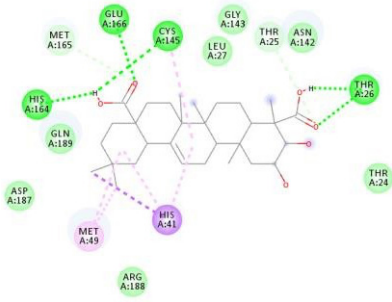	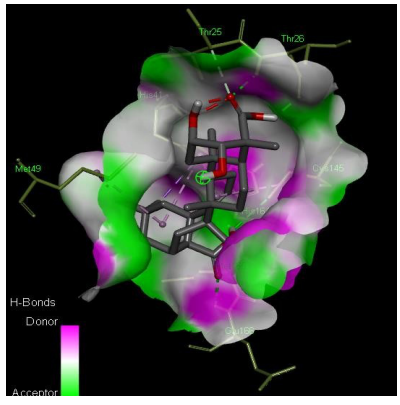
12	Narcotine	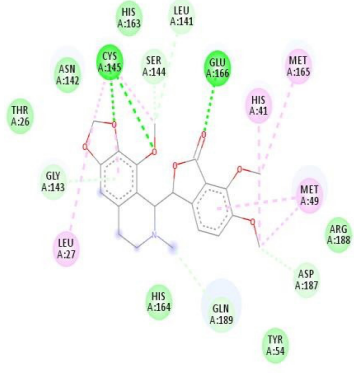	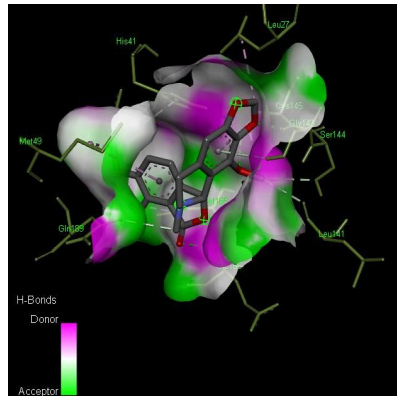

13	Nelfinavir	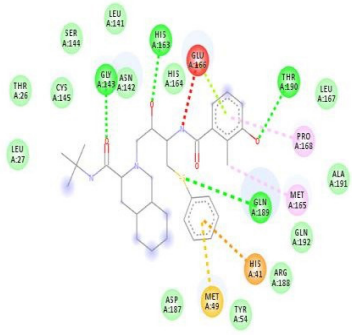	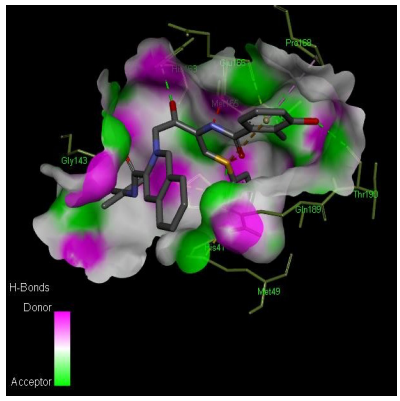
14	Lopinavir	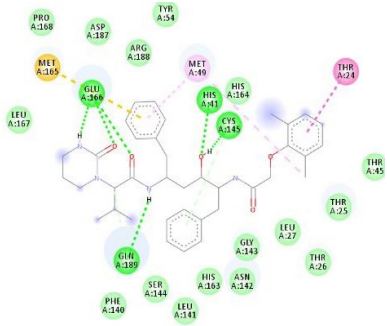	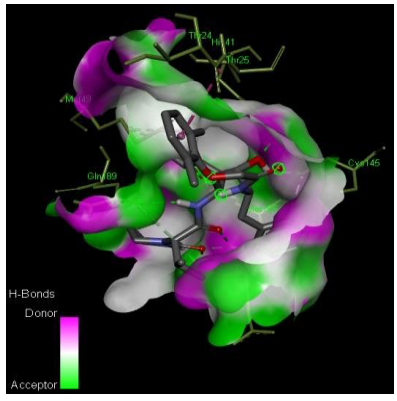
15	Indinavir	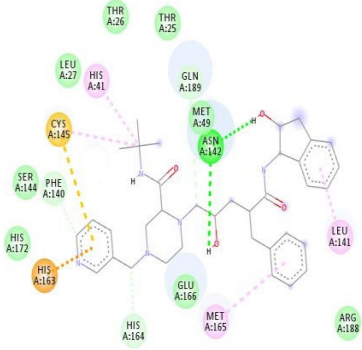	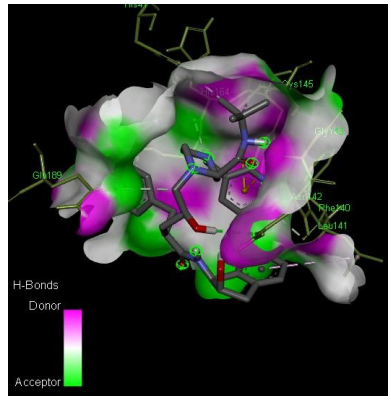
16	Ritonavir	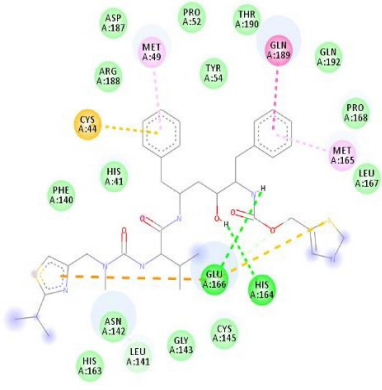	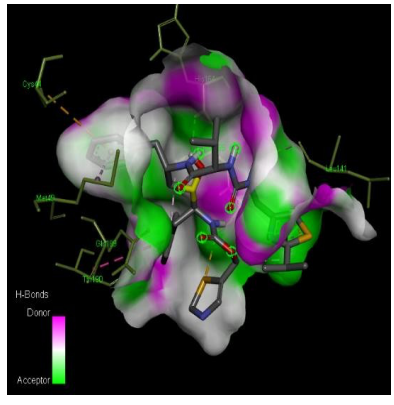

Primulic acid forms H-bonds with the amino acids, *e.g.* Ser46, Ser144, Glu166, Gln189, Asn142, Cys145, and Leu141. Kaempferol forms H-bonds with the 6LU7 amino acids, *e.g.* Tyr54, Glu166, and Gln192. Dicannabidiol realizes H-bond with the 6LU7 amino acid, *i.e.* Glu166. Lobelin realizes H-bonds with the amino acids, *e.g.* Gly143 and Glu166. Colchicine realizes H-bonds with the amino acids, *e.g.* Gly143, Thr190, Gln189, and Gln192. Piperidine forms H-bonds with the amino acids, *e.g.* Gly143 and Asn142. Medicagenic acid forms H- bonds with the amino acids, *e.g.* Thr26, Cys145, Glu166, and His164. Narcotine realizes H- bonds with the 6LU7 amino acids, *e.g.* Cys145 and Glu169. The results presented in Table 3 suggest that the M^{pro} Glu166 plays a crucial role in drug interactions. Besides, the other amino acids, *e.g.* Asn142, Gln189, Cys145, and Thr26 are also predicted to play roles in drug interactions, as reported in previous studies.[8,27]

According to the results in Tables 1 and 2, the most impressive compound of our study is pycnamine with a score of -11.30 kcal/mol, which is higher than that of nelfinavir. When the results in Table 2 are evaluated, it is seen that pycnamine has a predicted inhibition constant value (5.21 nM) approximately 3 times lower than that of nelfinavir (14.45 nM). According to pycnamine-6LU7 complex presented in Table 3, hydroxy moiety of pycnamine forms a hydrogen bond with the side chain of Glu166. Additionally, pycnamine forms *π*-cation, *π*-sulfur, *π*-sigma, and several hydrophobic interactions with the active site of 6LU7, as shown in Table 3.

DISCUSSION

Pycnamine is an alkaloid found in some species of Menispermaceae (*Triclisia patens* Oliv., *T. dictyophylla* Diels, *Pycnarrhena manillensis* Vidal, *P. ozantha* Diels) and Ranunculaceae families (*Thalictrum cultratum* Wall., *Isopyrum thalictroides* L.).[31-36] Pycnamine was reported to be a potential antimalarial, antiplasmodial, antiamoebic, and antimicrobial in previous studies.[36-40] It was evaluated against COVID-19 for the first time in this study.

Tetrahydrocannabinol, which has the second lowest binding free energy score (-9.10 kcal/mol) in this study, purified from *Cannabis sativa* L. was reported to inhibit macrophage extrinsic antiherpesvirus activity.[41]

Oleuropein, a secoiridoid monoterpene and the main component of *Olea europaea* L., is a potential inhibitor of the COVID-19 M^{pro} due to it is binding free energy score of -9.06 kcal/mol. It has antiviral activity against mononucleosis herpes, hepatitis, rota, bovine, parvo, HIV, leukemia, respiratory syncytial, parainfluenza-3, and salmonid rhabdoviruses.[42-46] In hepatitis B virus infected ducks, oleuropein reduced the virus entering the bloodstream.[47]

Quercetin, a flavonoid, is found abundantly in fruits and vegetables including onions, broccoli, buckwheat, peppers, *Brassica* species, apples, grapes, berries, tea, and wine as well as many nuts, seeds, barks, flowers, leaves, and spices.[48]

Quercetin also demonstrated a dose-dependent antiviral activity against poliovirus type 1, *Herpes simplex* virus (HSV-1, HSV-2), and respiratory syncytial virus, influenza virus strain, parainfluenza virus type-3, sindbis virus, rhinovirus, echovirus (types-7, -11, -12, and -19), coxsackievirus (A21 and B1), poliovirus (type-1 Sabin) and grouper iridovirus in cell cultures.[49-53] Early *in vivo* studies showed that oral treatment with quercetin-protected mice from lethal Mengo virus.[54] In mice infected with rhinovirus, quercetin treatment decreased viral replication and attenuates virus- induced airway cholinergic hyperresponsiveness.[55]

Kaempferol is another flavonoid derivative found in most edible plants such as tea, fruits, and vegetables consisting of *Allium cepa* L., *Camellia sinensis* (L.) Kuntze, *Citrus paradisi* Macfad., *Fragaria vesca* L., *Lactuca sativa* L., and in medicinal plants such as *Tilia tomentosa* Moench., *Aloe vera* L., *Crocus sativus* L., *Vitis vinifera* L., *Ginkgo biloba* L., *Hypericum perforatum* L., *Phyllanthus acidus* L., *Ribes nigrum* L., *Rosmarinus officinalis* L., *Hippophae rhamnoides* L., and *Sambucus nigra* L.[56] Antiviral activity of kaempferol on the influenza viruses (H1N1 and H9N2), HIV-1, flavivirus, two RNA viruses (murine norovirus and feline calicivirus), and human cytomegalovirus were mentioned.[14,48,51,57,58]

Primulic acid is a saponin found in some species of Primulaceae [*Primula officinalis* L., *P. elatior* (L.) Hill, *P. veris* L.] and Poaceae (*Panicum repens* L.),[59-63] and was reported to have antiviral activity by Helal and Melzig.[58]

Finally, cannabidiol, the potential inhibitor of COVID-19 M^{pro}, purified from the *C. sativa* L.,[64,65] and was reported to show high efficacy against viral hepatitis in previous studies.[64]

CONCLUSION

At currently, there is no antiviral drug for specific treatment of COVID-19, which is still a threat to global health. M^{pro} was used as a potential drug target to combat 2019-CoV. In this study, we evaluated several secondary metabolites obtained from medicinal plants against COVID-19 M^{pro} by molecular docking studies to identify a potential inhibitory compound that may be used to inhibit COVID-19 infection pathway. According to the results, pycnamine, tetrahydrocannabinol, oleuropein, quercetin, primulic acid, kaempferol, cannabidiol, lobeline, colchicine, piperidine, medicagenic acid, and narcotine are found to be potential inhibitors of COVID-19 M^{pro}. Among these compounds, pycnamine, which was evaluated against COVID-19 for the first time, showed high affinity to COVID-19 M^{pro} compared with other seconder metabolites and reference drugs. According to the results in this study, pycnamine has a binding free energy score of -11.30 kcal/mol, which is higher than nelfinavir used in clinics as the most potent inhibitor drug against COVID-19 M^{pro}. As a conclusion, this study has clearly shown that pycnamine may strongly inhibit COVID-19 M^{pro}. Our results obtained from the docking studies suggest that pycnamine should be examined *in vitro* to combat 2019-CoV. Moreover, pycnamine might be a promising lead compound for anti-CoV drugs.

Ethics

Ethics Committee Approval: Not applicable.

Informed Consent: Not applicable.

Peer-review: Externally peer-reviewed.

Authorship Contributions

Concept: S.G., S.B., Design: S.B., Data Collection or Processing: S.B., S.G., Z.G., Analysis or Interpretation: S.B., S.G., Literature Search: S.B., S.G., Z.G., Writing: S.B., S.G., Z.G.

Conflict of Interest: No conflict of interest was declared by the authors.

Financial Disclosure: The authors declared that this study received no financial support.

REFERENCES

1. Khaerunnisa S, Kurniawan H, Awaluddin R, Suhartati S, Soetjipto S. Potential inhibitor of COVID-19 main protease (M^{pro}) from several medicinal plant compounds by molecular docking study. Preprint. doi: 10.20944/preprints202003.0226.v1.
2. Bolelli K, Ertan-Bolelli T, Unsalan O, Altunayar-Unsalan C. Fenoterol and dobutamine as SARS-CoV-2 main protease inhibitors: a virtual screening study. J Mol Struct. 2021;1228:129449.
3. WHO. COVID-19 Weekly Epidemiological Update Report. World Health Organization; 11 May 2021. p. 1-2.
4. Wang Z, Chen X, Lu Y, Chen F, Zhang W. Clinical characteristics and therapeutic procedure for four cases with 2019 novel coronavirus pneumonia receiving combined Chinese and Western medicine treatment. Biosci Trends. 2020;14:64-68. Erratum in: Biosci Trends. 2020;14:E1.
5. Xu Z, Peng C, Shi Y, Zhu Z, Mu K, Wang X, Zhu W. Nelfinavir was predicted to be a potential inhibitor of 2019-nCov main protease by an integrative approach combining homology modelling, molecular docking and binding free energy calculation. BioRxiv. 2020. doi: https://doi.org/10.1101/2020.01.27.921627.
6. Chang YC, Tung YA, Lee KH, Chen TF, Hsiao YC, Chang HC, Hsieh TT, Su CH, Wang SS, Yu JY, Shih SS, Lin YH, Lin YH, Tu YCE, Chen CY. Potential therapeutic agents for COVID-19 based on the analysis of protease and RNA polymerase docking. Preprint. 2020. doi: 10.20944/preprints202002.0242.v2
7. Durdagi S, Orhan MD, Aksoydan B, Calis S, Dogan B, Sahin K, Shahraki A, Iyison NB, Avsar T. Screening of clinically approved and investigation drugs as potential inhibitors of SARS-CoV-2: a combined *in silico* and *in vitro* study. Mol Inform. 2022;41:e2100062.
8. Orhan IE, Senol Deniz FS. Natural products as potential leads against coronaviruses: could they be encouraging structural models against SARS-CoV-2? Nat Prod Bioprospect. 2020;10:171-186.
9. Kumar S, Maurya VK, Kabir R, Nayak D, Khurana A, Manchanda RK, Gadugu S, Shanker K, Saxena SK. Antiviral activity of belladonna during Japanese encephalitis virus infection *via* inhibition of microglia activation and inflammation leading to neuronal cell survival. ACS Chem Neurosci. 2020;11:3683-3696.
10. Yang CW, Lee YZ, Kang IJ, Barnard DL, Jan JT, Lin D, Huang CW, Yeh TK, Chao YS, Lee SJ. Identification of phenanthroindolizines and phenanthroquinolizidines as novel potent anti-coronaviral agents for porcine enteropathogenic coronavirus transmissible gastroenteritis virus and human severe acute respiratory syndrome coronavirus. Antiviral Res. 2010;88:160-168.
11. Kang KB, Ming G, Kim GJ, Ha TK, Choi H, Oh WK, Sung SH. Jubanines F-J, cyclopeptide alkaloids from the roots of *Ziziphus jujuba*. Phytochemistry. 2015;119:90-95.
12. Wu W, Li R, Li X, He J, Jiang S, Liu S, Yang J. Quercetin as an antiviral agent inhibits influenza A virus (IAV) entry. Viruses. 2015;8:6.
13. Behbahani M, Sayedipour S, Pourazar A, Shanehsazzadeh M. *In vitro* anti-HIV-1 activities of kaempferol and kaempferol-7-*O*-glucoside isolated from *Securigera securidaca*. Res Pharm Sci. 2014;9:463-469.
14. Fredrickson WR. Method and composition for antiviral therapy. Google Patents; 2000.
15. Lai WL, Chuang HS, Lee MH, Wei CL, Lin CF, Tsai YC. Inhibition of *Herpes simplex* virus type 1 by thymol-related monoterpenoids. Planta Med. 2012;78:1636-1638.
16. Ma SC, He ZD, Deng XL, But PP, Ooi VE, Xu HX, Lee SH, Lee SF. *In vitro* evaluation of secoiridoid glucosides from the fruits of *Ligustrum lucidum* as antiviral agents. Chem Pharm Bull (Tokyo). 2001;49:1471-1473.
17. Astani A, Reichling J, Schnitzler P. Comparative study on the antiviral activity of selected monoterpenes derived from essential oils. Phytother Res. 2010;24:673-679.
18. Bermejo P, Abad MJ, Díaz AM, Fernández L, De Santos J, Sanchez S, Villaescusa L, Carrasco L, Irurzun A. Antiviral activity of seven iridoids, three saikosaponins and one phenylpropanoid glycoside extracted from *Bupleurum rigidum* and *Scrophularia scorodonia*. Planta Med. 2002;68:106-110.
19. Efferth T, Romero MR, Wolf DG, Stamminger T, Marin JJ, Marschall M. The antiviral activities of artemisinin and artesunate. Clin Infect Dis. 2008;47:804-811.
20. Romero MR, Serrano MA, Vallejo M, Efferth T, Alvarez M, Marin JJ. Antiviral effect of artemisinin from *Artemisia annua* against a model member of the Flaviviridae family, the bovine viral diarrhoea virus (BVDV). Planta Med. 2006;72:1169-1174.
21. De Tommasi N, Conti C, Stein ML, Pizza C. Structure and *in vitro* antiviral activity of triterpenoid saponins from *Calendula arvensis*. Planta Med. 1991;57:250-253.
22. Pecetti L, Biazzi E, Tava A. Variation in saponin content during the growing season of spotted medic [*Medicago arabica* (L.) Huds.]. J Sci Food Agric. 2010;90:2405-2410.
23. Oso BJ, Adeoye AO, Olaoye IF. Pharmacoinformatics and hypothetical studies on allicin, curcumin, and gingerol as potential candidates against COVID-19-associated proteases. J Biomol Struct Dyn. 2022;40:389-400.
24. Patwardhan M, Morgan MT, Dia V, D'Souza DH. Heat sensitization of hepatitis A virus and Tulane virus using grape seed extract, gingerol and curcumin. Food Microbiol. 2020;90:103461.
25. Bilginer S, Gul HI, Anil B, Demir Y, Gulcin I. Synthesis and *in silico* studies of triazene-substituted sulfamerazine derivatives as acetylcholinesterase and carbonic anhydrases inhibitors. Arch Pharm (Weinheim). 2021;354:e2000243.
26. Samant L, Javle V. Comparative docking analysis of rational drugs against COVID-19 main protease. Biological Med. Chem 2020.
27. Hatada R, Okuwaki K, Mochizuki Y, Handa Y, Fukuzawa K, Komeiji Y, Okiyama Y, Tanaka S. Fragment molecular orbital based interaction

analyses on COVID-19 main protease - inhibitor N3 complex (PDB ID: 6LU7). J Chem Inf Model. 2020;60:3593-3602.

28. Li JY, You Z, Wang Q, Zhou ZJ, Qiu Y, Luo R, Ge XY. The epidemic of 2019-novel-coronavirus (2019-nCoV) pneumonia and insights for emerging infectious diseases in the future. Microbes Infect. 2020;22:80-85.
29. Yamamoto N, Yang R, Yoshinaka Y, Amari S, Nakano T, Cinatl J, Rabenau H, Doerr HW, Hunsmann G, Otaka A, Tamamura H, Fujii N, Yamamoto N. HIV protease inhibitor nelfinavir inhibits replication of SARS-associated coronavirus. Biochem Biophys Res Commun. 2004;318:719-725.
30. Spiff AI, Zabel V, Watson WH, Zemaitis MA, Ateya AM, Slatkin DJ, Knapp JE, Schiff PL Jr. Constituents of West African medicinal plants. XXX. Tridictyophylline, a new morphinan alkaloid from *Triclisia dictyophylla*. J Nat Prod. 1981;44:160-165.
31. Valentin A, Benoit-Vical F, Moulis C, Stanislas E, Mallié M, Fouraste I, Bastide JM. *In vitro* antimalarial activity of penduline, a bisbenzylisoquinoline from *Isopyrum thalictroides*. Antimicrob Agents Chemother. 1997;41:2305-2307.
32. Hernandez E, Santos A. Alkaloid of *Pycnarrhena manillensis* vidal. (family Menispermaceae). Constitution of Pycnamine. (Thesis) University of the Philippines. 28 pp., 1935. Jour. Philippine Pharm. 1946.
33. Gupta NC, Bhakuni DS, Dhar MM. Pendulin, a new biscoclaurine alkaloid from *Cocculus pendulus* Diels. Experientia. 1970;26:12-13.
34. Lin M. Part I. Isolation and identification of quaternary alkaloids from the roots of *Thalictrum cultratum* Wall. (Ranunculaceae). Part II. Isolation and identification of alkaloids from the roots and stems of *Pycnarrhena manillensis* Vidal (Menispermaceae) (1st ed). St. Petersburg; 1989:79-85.
35. Ragasa CY, Tepora MM, Rideout J. Antimicrobial activities of sterol from *Pycnarrhena manillensis*. ACGC Chemical Res Comm. 2009;23:31-34.
36. Simanjuntak P. Tumbuhan sebagai sumber zat aktif antimalaria. Repositori Riset Kesehatan Nasional. 2019;46:125-132.
37. Marshall SJ, Russell PF, Wright CW, Anderson MM, Phillipson JD, Kirby GC, Warhurst DC, Schiff PL Jr. *In vitro* antiplasmodial, antiamoebic, and cytotoxic activities of a series of bisbenzylisoquinoline alkaloids. Antimicrob Agents Chemother. 1994;38:96-103.
38. Sharma P, Sharma JD. A review of plant species assessed *in vitro* for antiamoebic activity or both antiamoebic and antiplasmodial properties. Phytother Res. 2001;15:1-17.
39. Kodi P. Antiplasmodial and toxicity activities and characterization of chemical compounds extracted from selected medicinal plants in Uganda (1st ed). Njero; Egerton University, 2018:87-95.
40. Cabral GA, Vasquez R. Delta 9-tetrahydrocannabinol suppresses macrophage extrinsic antiherpesvirus activity. Proc Soc Exp Biol Med. 1992;199:255-263.
41. Nediani C, Ruzzolini J, Romani A, Calorini L. Oleuropein, a bioactive compound from *Olea europaea* L., as a potential preventive and therapeutic agent in non-communicable diseases. Antioxidants (Basel). 2019;8:578.
42. Barbaro B, Toietta G, Maggio R, Arciello M, Tarocchi M, Galli A, Balsano C. Effects of the olive-derived polyphenol oleuropein on human health. Int J Mol Sci. 2014;15:18508-18524.
43. Karaboğa Arslan AK, Öztürk E, Yerer MB, Koşar M. Oleuropein in olive leaf and its pharmacologial effects. J Health Sci. 2017;26:89-93.
44. Micol V, Caturla N, Pérez-Fons L, Más V, Pérez L, Estepa A. The olive leaf extract exhibits antiviral activity against viral haemorrhagic septicaemia rhabdovirus (VHSV). Antiviral Res. 2005;66:129-136.
45. Omar SH. Oleuropein in olive and its pharmacological effects. Sci Pharm. 2010;78:133-154.
46. Zhao G, Yin Z, Dong J. Antiviral efficacy against hepatitis B virus replication of oleuropein isolated from *Jasminum officinale* L. var. *grandiflorum*. J Ethnopharmacol. 2009;125:265-268.
47. Bureau S, Ruiz D, Reich M, Gouble B, Bertrand D, Audergon JM, Renard CMGC. Rapid and non-destructive analysis of apricot fruit quality using FT-near-infrared spectroscopy. Food Chem. 2009;113:1323-1328.
48. Liu M, Yu Q, Xiao H, Li M, Huang Y, Zhang Q, Li P. The inhibitory activities and antiviral mechanism of medicinal plant ingredient quercetin against grouper iridovirus infection. Front Microbiol. 2020;11:586331.
49. Lyu SY, Rhim JY, Park WB. Antiherpetic activities of flavonoids against *Herpes simplex* virus type 1 (HSV-1) and type 2 (HSV-2) *in vitro*. Arch Pharm Res. 2005;28:1293-1301.
50. Zakaryan H, Arabyan E, Oo A, Zandi K. Flavonoids: promising natural compounds against viral infections. Arch Virol. 2017;162:2539-2551.
51. Debiaggi M, Tateo F, Pagani L, Luini M, Romero E. Effects of propolis flavonoids on virus infectivity and replication. Microbiologica. 1990;13:207-213.
52. De Palma AM, Vliegen I, De Clercq E, Neyts J. Selective inhibitors of picornavirus replication. Med Res Rev. 2008;28:823-884.
53. Agrawal PK, Agrawal C, Blunden G. Quercetin: antiviral significance and possible COVID-19 integrative considerations. Nat Prod Commun. 2020;15:1-10.
54. Ganesan S, Faris AN, Comstock AT, Wang Q, Nanua S, Hershenson MB, Sajjan US. Quercetin inhibits rhinovirus replication *in vitro* and *in vivo*. Antiviral Res. 2012;94:258-271.
55. Hossen MJ, Uddin MB, Ahmed SSU, Yu Z-L, Cho JY. Kaempferol: review on natural sources and bioavailability. Kaempferol: Biosynthesis, Food Sources and Therapeutic Uses; Nova Science Publishers: New York, NY, USA. 2016:101-150.
56. Jeong HJ, Ryu YB, Park SJ, Kim JH, Kwon HJ, Kim JH, Park KH, Rho MC, Lee WS. Neuraminidase inhibitory activities of flavonols isolated from *Rhodiola rosea* roots and their *in vitro* anti-influenza viral activities. Bioorg Med Chem. 2009;17:6816-6823.
57. Zhang W, Qiao H, Lv Y, Wang J, Chen X, Hou Y, Tan R, Li E. Apigenin inhibits enterovirus-71 infection by disrupting viral RNA association with trans-acting factors. PLoS One. 2014;9:e110429.
58. Helal R, Melzig MF. *In vitro* effects of selected saponins on the production and release of lysozyme activity of human monocytic and epithelial cell lines. Sci Pharm. 2011;79:337-349.
59. Czarnecki R, Librowski T. The effect of primulic acid on experimental, chronic venous insufficiency. Eur J Pharm Sci. 1996:121.
60. Grecu L, Cucu V. Saponine aus *Primula officinalis* and *Primula elatior*. Planta Med. 1975;27:247-253.
61. Morozowska M. Vegetative development, flowering, fruiting and saponin content in cultivated cowslip [*Primula veris* L.] plants. Herba Pol. 2004:2.

62. El-Tantawy WH, Temraz A, Hozaien HE, El-Gindi OD, Taha KF. Anti-hyperlipidemic activity of an extract from roots and rhizomes of *Panicum repens* L. on high cholesterol diet-induced hyperlipidemia in rats. Z Naturforsch C J Biosci. 2015;70:139-144.

63. Martinenghi LD, Jønsson R, Lund T, Jenssen H. Isolation, purification, and antimicrobial characterization of cannabidiolic acid and cannabidiol from *Cannabis sativa* L. Biomolecules. 2020;10:900.

64. Adams R, Pease DC, Clark JH. Isolation of cannabinol, cannabidiol and quebrachitol from red oil of Minnesota wild hemp. J Am Chem Soc. 1940;62:2194-2196.

65. Lowe HI, Toyang NJ, McLaughlin W. Potential of cannabidiol for the treatment of viral hepatitis. Pharmacognosy Res. 2017;9:116-118.

Turk J Pharm Sci 2022;19(4):442-446
DOI: 10.4274/tjps.galenos.2021.75317

ORIGINAL ARTICLE

Analysis of Fatty Acids of Some *Hyoscyamus*, *Datura*, and *Atropa* Species from Azerbaijan

Adila VALIYEVA[1]*, Eldar GARAEV[1], Amaliya KARAMLI[2], Nigar HUSEYNOVA[2]

[1]Azerbaijan Medical University, Deraptment of General and Toxicological Chemisrty, Baku, Azerbaijan
[2]Food Safety Agency of the Republic of Azerbaijan, Analitical Expertization Center, Section N1 of National Reference Laboratory, Baku, Azerbaijan

ABSTRACT

Objectives: *Datura stramonium* L., *D. stramonium* var. *tatula* (L.) Torr., *Hyoscyamus reticulatus* L., *H. niger* L., and *Atropa caucasica* Kreyer naturally found in Azerbaijan and their seeds possess 17-35% of oils. This study aims to evaluate and determine fatty acids of these plants special to Azerbaijan climate and geography. The presented study is the first to research into fatty acids of *A. caucasica*, which is an endemic species of Caucasus.

Materials and Methods: Fatty acid seed oils were derivatized to methyl esters and analyzed by gas chromatography equipped with a flame ionization detector, compared with a standard mixture of 37 fatty acid methyl esters.

Results: Linoleic (55-79%), oleic (11-26%), palmitic (4-12%), and stearic (2-3%) acids compose 97% of total fatty acids. Other minor compounds, including two *trans*-fatty acids, were determined in the samples. Significantly high concentration of a medicinally important polyunsaturated fatty acid, *e.g.* linoleic acid, was observed in all samples.

Conclusion: The results of this study showed that these oils are particularly valuable sources of linoleic and oleic acids, which have beneficial effects on cardiovascular diseases and are important compounds for the pharmaceutical and cosmetic industries in the manufacture of liposomes, nano- and microemulsions, soaps, *etc*.

Key words: Fatty acids, gas chromatography, *Datura*, *Hyoscyamus*, *Atropa*

INTRODUCTION

Hyoscyamus, Datura, and *Atropa* species are well-known natural sources of tropane alkaloids, primarily scopolamine, atropine, and hyoscyamine. Due to their biological activity, these plants and substances are widely used in medicine as mydriatics, antiasthmatics, spasmolytics, *etc*.[1,2] Furthermore, saponins, triterpenoids, phenolics, flavonoids, lignans, essential oils, sterols, and other compounds have been identified in the different organs of plants.[2-5] Fatty acids are the main components of seed oils. The quality, consumption, industrial and medicinal uses of oils are mainly related to their fatty acids. According to various references, the percentage of oil differs from 15 to 35% in the seeds of these species.[6,7]

Fatty acids play an essential role in the metabolic processes of human organisms - in the storage of energy, as basic components of cell membranes, *etc*. Scientists have reported that the replacement of saturated fatty acids with monounsaturated and polyunsaturated fatty acids in the diet reduces the risk of cardiovascular disease by decreasing total and low-density lipoprotein cholesterol levels in the blood.[7,8]

In the human body, linoleic acid is converted into docosahexaenoic and eicosapentaenoic acids, which are responsible not only for the reduction of cholesterol but also for inflammation, enhancement of brain functions, and prevention of cancers and autoimmune conditions.[9] Fatty acids are widely used in drug preparations as excipients and in the cosmetic

*Correspondence: adile.velieva1992baku@gmail.com, Phone: +994519370388 ORCID-ID: orcid.org/0000-0003-3459-4049
Received: 14.08.2021, Accepted: 27.09.2021

industry to prepare soaps, fat emulsions, liposomes, *etc*. They are essential components in some drugs due to their biological activities.[7,10] The seed oil of *Datura stramonium* is used as an analgesic in neurological practice, as well as for hair removal in cosmetology.[11] Biodiesel was prepared with the fatty acids of some *Datura* species and suggested as an alternative fuel source.[6,12,13] A scar cream is prepared with a Swiss recipe by using seed oil of *Hyoscyamus niger* under the brand name, *i.e.* Kelosoft®, and successfully sold in Europe.

In the present study, fatty acids of seed oils were analyzed in the accredited laboratory of the Food Safety Agency of the Republic of Azerbaijan.

MATERIALS AND METHODS

Plant collection

Plants were collected in the middle or end of vegetation periods, from various regions of Azerbaijan (Table 1). Species were authenticated at the Institute of Botany of the Azerbaijan National Academy of Sciences, Baku, where their voucher specimens were deposited (date: 01.09.2020, no: 01.04/1191).

Chemicals and solvents

Methanol, *n*-hexane and potassium hydroxide were purchased from Merck (Germany). 0.45 µm membrane filters were purchased from Isolab (Germany). A standard mix of fatty acid methyl esters (FAMEs) (Supelco 37 Component FAME mix, certified reference material, *TraceCERT*, in dichloromethane, ampule of 1 mL) was purchased from Sigma-Aldrich (Germany).

Extraction of oil

The seeds were dried and powdered. Extraction was carried out in a Soxhlet apparatus at 80°C for 6 h. 10 g of raw materials and 300 mL of *n*-hexane were used to obtain seed oils. After solvent evaporation, the percentage of oil was calculated by mass (w/w).

Preparation of fatty acid methyl esters

FAMEs for gas chromatography (GC) analysis. The oils (100 µL for each) and 5 mL of KOH-MeOH solution (0.5 M) were added to 10 mL-glass tubes. The mixtures were heated at 60°C for 15 min in the water bath under reflux, then, centrifuged in the closed tubes at 900 rpm for 8 min. After cooling to room temperature, 5 mL of *n*-hexane and 5 mL of distilled water were added and mixed thoroughly. The *n*-hexane phases were collected, filtered (membrane filter 0.45 µm), and applied to analysis.[14]

Gas chromatography conditions

Analysis of fatty acids was performed on an Aligent 7820A GC system equipped with a flame ionization detection (FID) detector and a capillary column HP-88 - 100 m × 0.25 mm × 0.25 µm. Helium was used as carrier gas with a flow rate of 1 mL/min. Oven temperature was initially programmed at 120°C, hold 1 min, and increased to 175°C with the rate of 10°C/min, hold 10 min. Temperature was elevated to 210°C, hold 5 min then 230°C and 5 min with a rate of 5°C/min. The total run time was 37.5 min. The injector and FID temperatures were set at 250°C and 280°C, respectively. The split ratio was 1:50. The injection volume was 1 µL.[15,16]

Standard sample

A standard mixture, which consists of 37 FAME components was applied. A 10 mg standard mixture was added to the volumetric flask, diluted to 10 mL with *n*-hexane. The injection volume was 1 µL.

Results calculation

The results were calculated compared with the retention times of standard samples. The concentrations of fatty acids were calculated using peak areas and expressed as percentages. Each analysis was repeated three times and mean values were reported. Statistical analysis has not been performed for evaluation of the results.

RESULTS

The percentages (w/w) of oils in the dried seeds are as follows: 22% in *D. stramonium*, 20% in *D. stramonium* var*. tatula,* 17% in *H. reticulatus*, 35% in *H. niger*, and 32% in *A. caucasica*. Results are presented individually for each fatty acid of five plant samples in Table 2.

Linoleic (55-79%), oleic (11-26%), palmitic (4-12%), and stearic (2-3%) acids compose 97% of total fatty acids. Percentage of unsaturated fatty acids are 83-91%. Changes of four main fatty acid concentrations are presented in Figure 1. Samples contained minor concentrations of *trans*-fatty acids.

Table 1. Collection times and places of plant species

No	Plant species	Location	Time of collection
1	*Datura stramonium*	Baku N 40°27'21.978" E 49°59'00.1752"	October, 2019
2	*Datura stramonium* var. *tatula*	Baku N 40°27'3.6072" E 49°56'47.4576"	September, 2018
3	*Hyoscyamus reticulatus*	Lerik - Zuvand N 38°40'21.1548" E 48°21'31.9428"	June, 2019
4	*Hyoscyamus niger*	Gusar N 41°30' 21.528" E 48°14'35.5992"	July, 2019
5	*Atropa caucasica*	Zagatala N 41°35'31.8156" E 46°44'36.5748"	July, 2019

Table 2. Concentrations of all fatty acids in the seed oils of plants

No	Fatty acids	t_R, min	*Datura stramonium*, %	*Datura stramonium* var. *tatula*, %	*Hyoscyamus reticulatus*, %	*Hyoscyamus niger*, %	*Atropa caucasica*, %
1	C4:0	4.43	0.02	0.07	-	0.06	-
2	C6:0	4.83	0.02	-	-	-	-
3	C8:0	5.46	0.02	-	-	-	-
4	C10:0	6.42	0.02	-	0.02	0.06	0.02
5	C12:0	7.77	0.02	0.02	0.07	0.03	0.01
6	C13:0	9.17	-	-	0.02	-	0.01
7	C14:0	9.55	0.15	0.12	0.06	0.05	0.03
8	C15:0	10.67	0.02	0.02	0.02	0.03	0.01
9	C15:1	11.42	0.02	-	0.02	-	-
10	C16:0	12.04	12.42	12.35	4.68	4.47	4.99
11	C16:1	13.00	0.39	0.36	0.14	0.04	0.06
12	C17:0	13.69	0.07	0.06	0.05	0.05	0.04
13	C17:1	14.76	0.05	0.06	0.06	0.03	0.02
14	C18:0	15.91	2.29	2.83	2.17	3.05	3.23
15	C18:1 *t*	16.84	0.05	0.03	0.06	0.03	0.01
16	C18:1 *c*	17.14	18.38	26.98	11.65	17.34	12.23
17	C18:2 *t*	18.62	0.06	0.04	0.05	0.08	0.05
18	C18:2 *c*	19.15	64.52	55.67	79.00	72.35	77.25
19	C20:0	20.44	0.27	0.35	0.31	0.34	0.18
20	C18:3, n6	21.32	0.04	0.02	0.02	0.03	0.35
21	C20:1	21.43	0.12	0.09	0.17	0.23	0.11
22	C18:3, n3	22.40	0.02	0.02	0.03	0.04	0.01
23	C21:0	22.96	0.02	0.02	0.08	0.08	0.07
24	C22:0	24.20	0.17	0.14	0.30	0.21	0.05
25	C20:3, n3	26.14	0.02	0.02	0.04	0.03	0.05
26	C23:0	26.36	0.06	0.05	0.02	0.03	-
27	C20:4	26.86	-	-	-	0.03	-
28	C24:0	28.31	0.09	0.11	0.15	0.13	0.03
29	C20:5, n3	28.81	0.14	0.06	0.08	0.21	-
30	C24:1	29.34	-	0.02	-	0.05	-
31	C22:6, n3	32.81	0.03	0.03	0.04	0.16	0.09
	Unsaturated FAs	-	83.8	83.4	91.4	90.6	90.2
	Saturated FAs	-	15.6	16.1	8.0	8.6	8.6
	Total number of FAs	-	28	25	26	27	23

t_R: Retention times

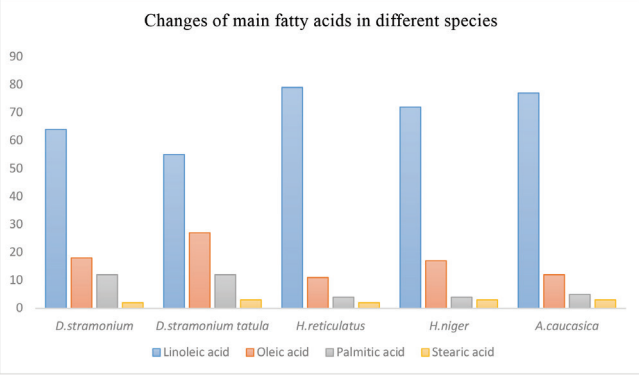

Figure 1. Concentrations (%) of four fatty acids in the plant species analyzed

Elaidic acid, a *trans* isomer of oleic acid (C18:1 *t*, <0.06%) and a *trans* isomer of linoleic acid (C18:2 *t*, <0.09%) are less than 1% of the total fatty acid mixtures. All other fatty acids are in the minor concentrations. The total number of fatty acids are varied - 28 in *D. stramonium*, 25 in *D. stramonium* var. *tatula*, 26 in *H. reticulatus*, 27 in *H. niger*, and 23 in *A. caucasica.*

The highest yield of oil was obtained from *H. niger* seeds. The maximum concentration of linoleic acid is observed in the seed oil of *H. reticulatus* (79%). *D. stramonium* var. *tatula* contains a higher amount of oleic acid (26%) than other samples. On the other hand, *Datura* species contain 20-22% oils as they are one of the optimal sources of plant oil, linoleic, and oleic acids because a whole plant produces at least 200-300 g seeds. 100 g of seeds were obtained from *Hyoscyamus* species, while approximately 40 g of seeds were gathered from *A. caucasica.* However, *Datura* species naturally grow in all regions of Azerbaijan. *Hyoscyamus* species were found in most parts of the country, but *A. caucasica* is rarely found in mountain forests.

DISCUSSION

The selected method, GC-FID is a useful and sensitive method for analyzing numerous compounds in a single run. Without wasting a long time, GC-FID method is successfully applied for routine analysis of fatty acids.[17]

Results of previous studies showed that 50-70% of polyunsaturated *cis*-linoleic acid (C18:2), 15-30% of monounsaturated oleic acid (C18:1) and 2-7% of saturated palmitic (C16:0) and stearic acids (C18:0) were found as major compounds in the seed oils of *Hyoscyamus* and *Datura* species.[8,9,11,15,18] 65% of monounsaturated fatty acids were reported by Koria and Nithya[12] in the seed oil of *D. stramonium* grown in India. Contrary to other studies, polyunsaturated fatty acids (18%) were lower than monounsaturated fatty acids.[11,12] Eicosanoic acid (C20:0) (34.55%), isomers of linoleic acid, (C18:2, n7) (4.56%) and (C18:2, n8) (3.61%), and eicosatrienoic acid (C20:3, n6) (4.39%), saturated - daturic acid $C_{17}H_{34}O_2$ were reported in *D. stramonium* oil.[11] Similar results were acquired compared with previous investigations. Total number of fatty acids was maximum in the present study.

CONCLUSION

The investigation evaluated the presence and concentrations of 37 fatty acids in five plant species from Azerbaijan. *Datura, Hyoscyamus,* and *Atropa* species are not harvested widely as oil and unsaturated fatty acid sources due to their toxicity. To the best of our knowledge, this is the first study on fatty acids in *A. caucasica.*

Depending on geographical and climate differences, components of the fatty acid mixture and their concentrations could be varied in the same species. An essential omega-6 fatty acid - linoleic acid dominates all investigated samples and gives them valuable nutritional and medicinal properties. Second major compound of oils is oleic acid. Another essential omega-3 fatty acid - linolenic acid, is found in trace amounts.

The results of the investigation might be useful for future researchers to evaluate these oils in medicinal, nutritional, cosmetic, fuel, and other industries.

ACKNOWLEDGEMENTS

The authors want to acknowledge the administration and laboratory members of the Food Safety Agency of the Republic of Azerbaijan.

Ethics

Ethics Committee Approval: Not applicable.

Informed Consent: Not applicable.

Peer-review: Externally peer-reviewed.

Authorship Contributions

Concept: A.V., Design: A.V., Data Collection or Processing: A.V., A.K., N.H., Analysis, or Interpretation: A.V., A.K., N.H., Literature Search: A.V., A.K., N.H., Writing: A.V., E.G.

Conflict of Interest: No conflict of interest was declared by the authors.

Financial Disclosure: The authors declared that this study received no financial support.

REFERENCES

1. Christen P, Bieri S, Berkov S. Methods of analysis: tropane alkaloids from plant origin. Natural Products, Springer, Berlin Heidelberg, 2013, chapter 31:1009-1048.
2. Jun L, Ji S, Xin-Wen Y, Jing-Kuan S, Qi-Ming M, Ting-Guo K. Chemical and pharmacological researches on *Hyoscyamus niger*. Chin Herb Med. 2011;3:117-126.
3. Rahmoune B, Zerrouk IZ, Morsli A, Khelifi-Slaoui M, Khelifi L, Do Amarante L. Phenylpropanoids and fatty acids levels in roots and leaves of *Datura stramonium* and *Datura innoxia*. Int J Pharm Pharm Sci. 2017;9:150-154.
4. Aboluwodi AS, Avoseh ON, Lawal OA, Ogunwande IA, Giwa AA. Chemical constituents and anti-inflammatory activity of essential oils of *Datura stramonium* L. J Med Plants Stud. 2017;5:21-25.
5. Kocór M, Pyrek JS, Atal CK, Bedi KL, Sharma BR. Triterpenes of *Datura innoxia* Mill. structure of daturadiol and daturaolone. J Org Chem. 1973;38:3685-3688.

6. Asilbekova DT, Bekker NP, Chernenko TV, Glushenkova AI, Ul'chenko. Lipids, lipophilic components and essential oils from plant sources. In: Azimova SS, Glushenkova AI, Vinogradova VI, eds. Springer-Verlag London; 2012:873-884.
7. Rustan AC, Drevon CA. Fatty acids: structures and properties. ELS. 2005;1-7.
8. Keskin C, Yavuz M, Kaçar S. Determination of fatty acid compositions of total lipid, phospholipid and triacylglycerol fractions of aboveground parts of four species of the genus *Hyoscyamus*. J Chem Res. 2016;1:1-8.
9. Doan LP, Nguyen TT, Pham MQ, Tran QT, Pham QL, Tran DQ, Than VT, Bach LG. Extraction process, identification of fatty acids, tocopherols, sterols and phenolic constituents and antioxidant evaluation of seed oils from five fabaceae species. Processes. 2019;7:456.
10. Pravst I. Biochemistry research trends. Whelan L, eds. Nova, Slovenia, 2014;3:35-54.
11. Yuldasheva NK, Kadirova DB, Ibotov SK, Gusakova SD, Aripova SF. Lipids from seeds of *Datura stramonium*. Chem Nat Compd. 2020;56:303-304.
12. Koria L, Nithya G. Analysis of *Datura stramonium* Linn. biodiesel by gas chromatography-mass spectrometry (GC-MS) and influence of fatty acid composition on the fuel related characteristics. J Phytol. 2012;4:6-9.
13. Gupta A. Experimental Investigation of *Datura stramonium* biodiesel. IJARIIT. 2020;6:1-5.
14. Wang J, Wu W, Wang X, Wang M, Wu F. An effective GC method for the determination of the fatty acid composition in silkworm pupae oil using a two-step methylation process. J Serb Chem Soc. 2015;80:9-20.
15. Ramadan MF, Zayed R, El-Shamy H. Screening of bioactive lipids and radical scavenging potential of some Solanaceae plants. Food Chem. 2007;103:885-890.
16. Jarukas L, Kuraite G, Baranauskaite J, Marksa M, Bezruk I, Ivanauskas L. Optimization and validation of the GC/FID method for the quantification of fatty acids in bee products. Appl. Sci. 2021;11:83.
17. Young KE, Quinn SM, Trumble SJ. Lipid studies in breath-hold diving mammals and obese, pre-diabetic mice. IJAST. 2012;2:11-21.
18. Al-Snafi AE. Therapeutic importance of *Hyoscyamus* species grown in Iraq (*Hyoscyamus albus*, *Hyoscyamus niger* and *Hyoscyamus reticulates*)- a review. IOSR J Pharm. 2018;8:8-32.

Turk J Pharm Sci 2022;19(4):447-454
DOI: 10.4274/tjps.galenos.2021.66066

ORIGINAL ARTICLE

Multidrug-Resistant and Extremely Drug-Resistant *Pseudomonas aeruginosa* in Clinical Samples From a Tertiary Healthcare Facility in Nigeria

Amaka Marian AWANYE[1]*, Chidozie Ngozi IBEZIM[1], Catherine Nonyelum STANLEY[1], Hannah ONAH[1], Iheanyi Omezurike OKONKO[2], Nkechi Eucharia EGBE[3]

[1]University of Port Harcourt, Faculty of Pharmaceutical Sciences, Department of Pharmaceutical Microbiology and Biotechnology, Rivers, Nigeria
[2]University of Port Harcourt, Faculty of Sciences, Department of Microbiology, Rivers, Nigeria
[3]Nigerian Defence Academy, Faculty of Science, Department of Biotechnology, Kaduna, Nigeria

ABSTRACT

Objectives: *Pseudomonas aeruginosa* has been globally implicated in healthcare-associated infection. The susceptibility pattern of clinical isolates of *P. aeruginosa* to anti-pseudomonal antibiotics is reported.

Materials and Methods: Clinical samples, namely blood, urine, tracheal aspirate, cerebrospinal fluid (CSF), wound swabs, high vaginal swabs, eye, and ear exudates were obtained from patients, processed and identified using standard microbiological protocols. Antibiotic susceptibility testing was undertaken using the Kirby Bauer Disc diffusion method. Results were reported following the Clinical and Laboratory Standards Institute guidelines.

Results: Of 104 *P. aeruginosa* isolates identified, males (52.88%) had a higher incidence of infection than female (47.11%) patients. The highest prevalence was recorded from wound swabs [46 (44.23%)] followed by ear exudates [23 (22.12%)], urine [22 (21.15%)], while eye exudates and samples from the CSF yielded the least [1 (0.96% each)]. From the antibiogram, imipenem had the highest antibiotic activity (91.3%) followed by polymyxin B (84.6%). The isolates exhibited the highest resistance to ceftazidime (73.1%) and piperacillin-tazobactam (61.5%). The antibiotic susceptibility pattern of *P. aeruginosa* isolates revealed 7.69% susceptible, 26% resistant, 61% multidrug resistance (MDR), 5% extremely drug resistance (XDR), and an absence (0%) of pandrug-resistant phenotypes.

Conclusion: The study recorded alarmingly high cases of MDR and some XDR phenotypes of *P. aeruginosa* in University of Port Harcourt Teaching Hospital. It will help identify existing gaps in antimicrobial resistance surveillance and assist in improving public health policies regarding antibiotic stewardship, initiatives, and interventions.

Key words: Antibiotics, antimicrobial resistance, multidrug resistance, extremely drug resistance, *Pseudomonas aeruginosa*, Nigeria

INTRODUCTION

Gram-negative bacteria account for many life-threatening hospital-associated infections.[1] *Pseudomonas aeruginosa* is an opportunistic Gram-negative bacterium implicated in many hospital infections especially in individuals with prolonged hospital stay, medical implants, weakened immune systems, or those with underlying conditions or disease states. Its ability to survive with minimal nutrition and tolerate various disinfectant conditions leads to its persistence on surfaces, where it can cause infection in the hospital and community settings.[2] Additionally, biofilms formed by *P. aeruginosa* enhance their capability of causing infection by protecting the bacteria from elimination by antibiotics and disinfectants.[3] Infections caused by *P. aeruginosa* include acute and chronic lung infections, urinary tract infections, ocular infections, and bacteremia, causing high mortality and morbidity.[4] They are usually difficult

*Correspondence: amaka.awanye@uniport.edu.ng, Phone: +2348025240014, ORCID-ID: orcid.org/0000-0003-4693-3722
Received: 02.07.2021, Accepted: 27.09.2021

to treat and are life-threatening due to the intrinsic susceptibility of *Pseudomonas* to few antimicrobial agents and their ability to readily acquire antimicrobial resistance genes from other bacteria and the environment. These factors contribute to the reason, why infections caused by antibiotic resistant *P. aeruginosa* usually result in a longer duration of treatment, increased costs of treatment and higher mortality rates.[5]

Antibiotic resistance constitutes a major health challenge, especially in people in critical care conditions such as those in intensive care units (ICU); those with implanted medical devices; those who have recently undergone surgery; those on broad spectrum antibiotics or those with pre-existing severe underlying conditions such as cancer, diabetes, renal insufficiency, heart failure, liver cirrhosis, and autoimmune diseases.[6] Cases of multiple-drug and extremely-drug resistance have been described for *P. aeruginosa* and this limit the efficacy of empirical treatment of infections caused by *P. aeruginosa*.[7-9] Antibiotics recommended for the treatment of infections caused by *P. aeruginosa* are grouped into eight antibiotic classes namely: Fluoroquinolones (ciprofloxacin and levofloxacin); aminoglycosides (gentamicin, tobramycin, amikacin, and netilmicin); beta-lactam antibiotics and beta-lactamase inhibitors (ticarcillin-clavulanate and piperacillin-tazobactam); cephalosporins (ceftazidime and cefepime); carbapenems (imipenem, meropenem, and doripenem); monobactams (aztreonam); polymyxins (colistin and polymyxin B), and phosphonic acids (fosfomycin). Increasing rates of drug resistance in *P. aeruginosa* to many antibiotics have been recorded[10] and is attributed to many chromosomes or plasmid-mediated mechanisms. These include the production of antibodies inactivating enzymes *e.g.* β-lactamase production; modification of target sites; overexpression of target molecules; overexpression of drug efflux pumps, reduced drug permeability through the loss of porin proteins.[11,12]

Ventilator-associated-pneumonia (VAP) is a common infectious disease in the ICU, caused by multidrug resistant (MDR) *P. aeruginosa*.[13] In 2016, Infectious Disease Society of America and the American Thoracic Society published a clinical practice guideline. In cases of VAP caused by *P. aeruginosa*, an empirical treatment consisting of imipenem, meropenem or aztreonam plus aminoglycoside, or colistin may be used.[14] As reported cases of carbapenem resistance (CR) increase, the guidelines have been updated to accommodate newer anti-pseudomonal antibiotics in the order of preference: Ceftolozane-tazobactam, ceftazidime-avibactam, meropenem, ceftazidime, or piperacillin-tazobactam plus amikacin or colistin.[15] Over the years, many countries have reported CR[2,16,17] and this has become a global health challenge. In 2016, World Health Organization (WHO) classified CR *P. aeruginosa* as a critical pathogen for new drug research, discovery and development.[18]

This study determined the incidence, prevalence, and resistance pattern of clinical isolates of *P. aeruginosa* obtained from a tertiary healthcare facility in Southern Nigeria. We report the prevalence of MDR and extremely drug resistant (XDR) phenotypes of clinical isolates of *P. aeruginosa* in Nigeria.

MATERIALS AND METHODS

Sample collection

The isolates used in this study were recovered from blood, urine, sputum, cerebrospinal fluid (CSF), wound swabs, high vaginal swabs, eye, and ear exudates. These were obtained from both in-patients and out-patients that presented to the University of Port Harcourt Teaching Hospital (UPTH), Nigeria. All samples that were collected were immediately transferred under aseptic conditions to the Pharmaceutical Microbiology Laboratory of the University of Port Harcourt for the isolation and identification of *P. aeruginosa*.

Isolation and identification of P. aeruginosa

P. aeruginosa was isolated and cultured on cetrimide agar (Himedia, India) using spread plate technique, and then, incubated at 37°C for 24 h. Identification followed the Clinical and Laboratory Standards Institute (CLSI) guidelines.[19,20] Species identification was determined based on differential growth characteristics; a Gram-negative reaction; pyocyanin production, and positive reactions to oxidase test, mannitol, and maltose fermentation.

Antimicrobial susceptibility tests

Antimicrobial susceptibility tests were carried out using the Kirby-Bauer disc diffusion method.[21] A colony of each isolate was grown in Muller Hinton broth. Broth cultures were diluted with normal saline to obtain similar turbidity as 0.05 McFarland standard. Standardized microbial cultures were spread on sterile Muller Hinton agar to generate a lawn culture. Single antibiotic disks (Oxoid, UK) namely: piperacillin-tazobactam (110 µg); cefepime (30 µg); aztreonam (30 µg); imipenem (10 µg); polymyxin B (300 units); ceftazidime (30 µg); gentamicin (10 µg); ciprofloxacin (5 µg), and levofloxacin (5 µg) were aseptically placed on agar plates 24 mm apart, the centre to centre between disks on the same plates. All plates were left to stand for 1 h on the bench at room temperature for pre-diffusion of the antibiotics before incubation at 37°C for 24 h. After incubation, the zones of inhibition were measured and interpreted as susceptible, intermediate, or resistant following the CLSI guidelines for antimicrobial susceptibility testing.[19,20]

Statistical analysis

Data analysis was carried out using the IBM Statistical Package for Social Science (SPSS) version 27.0 with values expressed as mean and percentage. Descriptive analysis was carried out on different isolates against the different antibiotics. The different inhibition-zone-diameter measurements in triplicate were compared by performing a one-way ANOVA. A significant difference at 95% of confidence level was set at $p<0.05$.

RESULTS

Prevalence of P. aeruginosa in clinical specimens

In total, 104 isolates of *P. aeruginosa* were recovered over the 3-month study period (Table 1). The age and gender distribution of patients from whom clinical specimens *P. aeruginosa* were recovered are shown in Tables 1 and 2, respectively.

The frequency of *Pseudomonas* infection was highest among children younger than 10 years of age (26.92%) with ear infections and least among the 11-20 age group (3.85%). The mean age of the patients was 31.94 years (range 0-70 years). More isolates were obtained from males (52.88%) than females (47.11%). *P. aeruginosa* was isolated mostly from wound swabs (44.23%), ear exudates (22.12%), and urine samples (21.15%). The least was obtained from eye exudates and CSF samples (0.96% each).

Antimicrobial susceptibility pattern of P. aeruginosa

A minimum of one antimicrobial agent for each anti-pseudomonal antibiotic category was tested on every isolate of *P. aeruginosa*. As shown in Table 3, the susceptibility pattern of *P. aeruginosa* to antibiotics showed the highest sensitivity to imipenem (91.3%) followed by polymyxin B (84.6%), gentamicin (78.8%), levofloxacin (75.0%), ciprofloxacin (68.3%), cefepime (47.1%), aztreonam (32.7%), piperacillin-tazobactam (27.9%), and least to ceftazidime (23.1%).

Patterns of antibiotic resistant phenotypes

The term "non-susceptible" describes those isolates showing resistant and intermediate levels of resistance following the CLSI guidelines.[19] The non-susceptible phenotype was further described as follows: Resistant when an isolate is unsusceptible to at least one drug in one or two antimicrobial classes; multi-drug-resistant when an isolate is unsusceptible to at least one drug in three or more antimicrobial categories; extremely-drug-resistant when an isolate is unsusceptible to at least one drug from six antibiotic categories and pandrug resistant when an isolate is unsusceptible to at least one drug in all antibiotic categories.

The susceptibility pattern of *P. aeruginosa* phenotypes is shown in Table 4. Our data show that 8% were susceptible, 26% were resistant, 61% were MDR and 5% were extremely-drug-resistant (Figure 1). No isolate showed resistance to all antibiotics tested. Figure 2 shows the response of individual isolates to anti-pseudomonal antibiotics. The antibiotic resistance profiles of individual isolates are shown in Table 5.

Table 1. Age distribution of sources of *Pseudomonas aeruginosa* isolates

Age group (years)	Frequency of cases	Relative frequency	Specimen site							
			Blood	CSF	Ear	Eye	HVS	Sputum	Urine	Wound
0 - 10	28	26.92	2	0	17	0	1	2	0	6
11-20	4	3.85	0	0	2	0	0	0	0	2
21-30	11	10.58	0	0	0	0	3	0	3	5
31-40	18	17.31	0	0	0	0	1	0	7	10
41-50	20	19.23	0	1	2	1	1	1	4	10
>51	23	22.12	0	0	2	0	0	0	8	13
Total	**104**	**100**	**2**	**1**	**23**	**1**	**6**	**3**	**22**	**46**

HVS: High vaginal swab, CSF: Cerebrospinal fluid

Table 2. Gender distribution of sources of *Pseudomonas aeruginosa* isolates

Specimen	Male	Female	Frequency (n)	Relative frequency (%)
Blood	0	2	2	1.92
CSF	0	1	1	0.96
Ear	11	12	23	22.12
Eye	1	0	1	0.96
HVS	0	6	6	5.77
Sputum	3	0	3	2.88
Urine	10	12	22	21.15
Wound	30	16	46	44.23
Total	**55**	**49**	**104**	**100.00**

HVS: High vaginal swab, CSF: Cerebrospinal fluid

Table 3. Antimicrobial categories and antibiotics used to classify *Pseudomonas aeruginosa* phenotypes

Antibiotic category	Anti-pseudomonal antibiotic	Antibiotic code	Antibiotic concentration	Number of isolates, n: 104		
				Susceptible	Intermediate	Resistant
β-Lactam + β-lactamase inhibitor	Piperacillin - tazobactam	TZP	110 µg	29 (27.9%)	11 (10.6%)	64 (61.5%)
Cephem	Ceftazidime	CAZ	30 µg	24 (23.1%)	4 (3.85%)	76 (73.1%)
Cephem	Cefepime	FEP	30 µg	49 (47.1%)	5 (4.81%)	50 (48.1%)
Monobactam	Aztreonam	ATM	30 µg	34 (32.7%)	28 (26.9%)	42 (40.4%)
Carbapenem	Imipenem	IMP	10 µg	95 (91.3%)	1 (0.96%)	8 (7.69%)
Polymyxin	Polymyxin B	PB	300 units	88 (84.6%)	-	16 (15.4%)
Aminoglycoside	Gentamicin	CN	10 µg	82 (78.8%)	3 (2.88%)	19 (18.3%)
Fluoroquinolone	Ciprofloxacin	CIP	5 µg	71 (68.3%)	7 (6.73%)	26 (25.0%)
Fluoroquinolone	Levofloxacin	LEV	5 µg	78 (75.0%)	1 (0.96%)	25 (24.0%)

Table 4. Phenotypic resistance pattern of *Pseudomonas aeruginosa*

Number of antibiotic categories	Number of isolates (frequency)	Relative frequency (%)	Antibiotic phenotype
0	8	7.69	Susceptible
1	12	11.54	Resistant
2	15	14.42	Resistant
3	35	33.65	Multi-drug resistant
4	16	15.38	Multi-drug resistant
5	13	12.50	Multi-drug resistant
6	5	4.81	Extremely drug resistant
7	0	0.00	Extremely drug resistant

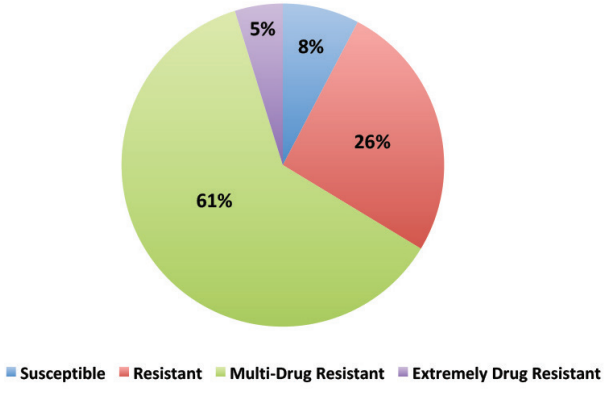

Figure 1. Prevalence of *Pseudomonas aeruginosa* drug-resistant phenotypes

DISCUSSION

MDR in microorganisms has raised much global concerns. Many factors contribute to the antibiotic resistance observed in *P. aeruginosa*.[11] This study reports the incidence, prevalence, and antibiotic resistance pattern of 104 isolates of *P. aeruginosa* recovered from various body fluids, swabs, and exudates. All clinical samples studied harbour this microorganism irrespective of age groups. Most isolates were obtained from wound swabs, ear exudates, and urine samples. The wound samples were mostly from adults above 30 years of age; urine samples from more than 20 years, while isolates from ear exudates were mostly children younger than 10 years of age.

The capability of some anti-pseudomonal antibiotics to clear infections caused by identified isolates was investigated *in vitro*. Our findings show that only 7.69% isolates were sensitive to all antibiotics tested, while others were unsusceptible to a minimum of one antibiotic. This is in agreement with similar studies that have shown a high incidence of antimicrobial resistance in *P. aeruginosa*.[8,9,22] Of all antibiotics tested, imipenem recorded the highest number of susceptibility (91.3%) followed by polymyxin B (84.6%). Our findings show that imipenem remains a potent drug for clearing infections caused by *P. aeruginosa*. However, the development of resistance to carbapenems has emerged, thus the need for research on new drugs. *P. aeruginosa* showed a high degree of resistance to penicillins and cephalosporins with ceftazidime expressing the highest level of resistance (73.1%). This is because *P. aeruginosa* is capable of acquiring genes encoding antimicrobial resistant determinants. The most common resistance mechanism is the

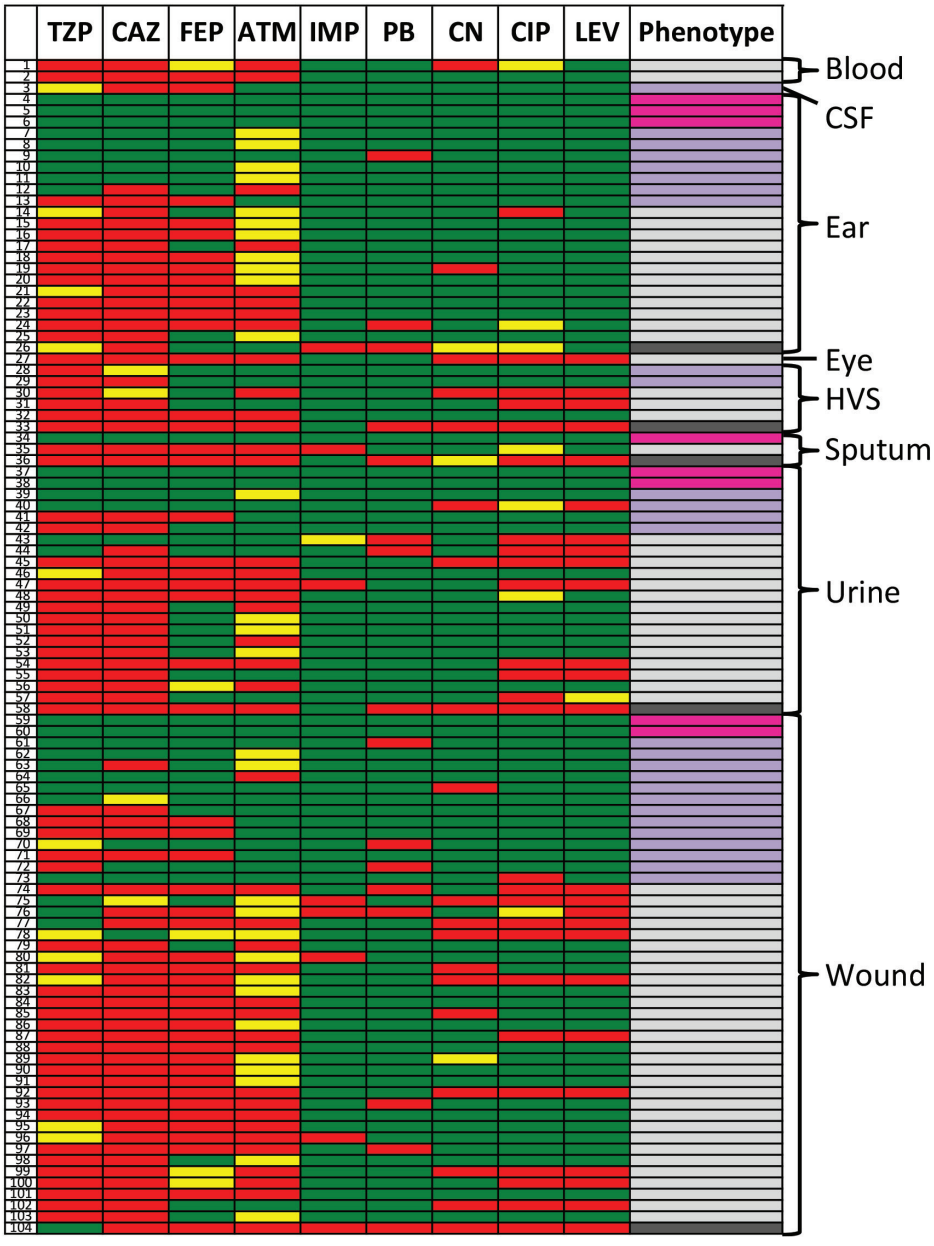

Figure 2. Heat map showing the response of individual isolates to anti-pseudomonal antibiotics

TZP: Piperacillin-tazobactam (110 µg), CAZ: Ceftazidime (30 µg), FEP: Cefepime (30 µg), ATM: Aztreonam (30 µg), IMP: Imipenem (10 µg), PB: Polymyxin B (300 units), CN: Gentamicin (10 µg), CIP: Ciprofloxacin (5 µg), LEV: Levofloxacin (5 µg), Green: Sensitive, Yellow: Intermediate, Red: Resistant, Pink: Susceptible phenotype (sensitive to all antibiotic categories), Lilac: Resistant phenotype (not susceptible to at least one drug in one or two antibiotic categories), Light grey: Multidrug-resistant phenotype (not susceptible to at least one drug in three or more antibiotic categories), Dark grey: Extremely-drug-resistant phenotype (not susceptible to at least one drug in all but one antibiotic category)

production of β-lactamase enzymes that inactivate penicillins and cephalosporins.[23] The next highest level of resistance was recorded for piperacillin-tazobactam (61.5%) showing that other mechanisms of resistance besides β-lactamase production contribute to the resistant phenotypes observed.

An international group of experts from the European Centre for Disease Prevention and Control and the Centers for Disease Control and Prevention came together to establish standardized terminologies that will define the resistance profiles in some selected bacteria associated with nosocomial infections, which are prone to MDR.[24] The selected bacteria include *P. aeruginosa, Acinetobacter* spp., *Enterobacteriaceae* (excluding *Salmonella* and *Shigella*), *Staphylococcus aureus*, and *Enterococcus* spp. An isolate is classified as MDR, when it is non-susceptible to at least one drug in three or more antimicrobial classes. Extremely-drug-resistant isolates are non-susceptible to at least one

agent in all but one or two anti-microbial categories. The pan-drug-resistant isolates are non-susceptible to all antimicrobial categories. An isolate is considered as non-susceptible to an antibiotic, when it tests resistant or intermediate using clinical breakpoints as interpretive criteria provided by Clinical & Laboratory Standards Institute (CLSI), European Committee on Antimicrobial Susceptibility Testing or US Food and Drug Administration. From this classification, *P. aeruginosa* were grouped based on the number of antibiotics they were resistant to. Our findings revealed a high prevalence (62%) of MDR strains. These isolates were resistant to at least one drug in 3-5 antibiotic categories. The highest recorded MDR occurred between piperacillin-tazobactam + ceftazidime and cefepime + aztreonam. The antibiotic categories, whose MDR patterns commonly occur, includes cephem » fluoroquinolone › monobactam= β-lactam/β-lactamase-inhibitor » aminoglycoside › polymyxin › carbapenem. Although the least amount of resistance was against imipenem, the incidence of resistance to this antibiotic class poses a global health concern. CR *P. aeruginosa* was ranked second after *Acinetobacter baumannii* as the most critical antimicrobial resistant bacteria, of which WHO placed it in the priority list for new drug R&D.[18] However, the lack of any new drugs and limited therapeutic options indicate that surveillance efforts

Table 5. Antibiotic resistance pattern of Pseudomonas aeruginosa clinical isolates

Antibiotic resistance patterns	Number of non-susceptible isolates	Drug resistance phenotype
CAZ/FEP	1	Resistant
ATM	7	Resistant
PB	2	Resistant
CN	1	Resistant
CIP/LEV	1	Resistant
TZP + CAZ/FEP	10	Resistant
TZP + PB	2	Resistant
CAZ/FEP + ATM	2	Resistant
CN + CIP/LEV	1	Resistant
TZP + CAZ/FEP + ATM	30	MDR
TZP + CAZ/FEP + CIP/LEV	3	MDR
PB + CAZ/FEP + CIP/LEV	1	MDR
PB + IMP + CIP/LEV	1	MDR
TZP + CAZ/FEP + ATM + IMP	2	MDR
TZP + CAZ/FEP + ATM + PB	2	MDR
TZP + CAZ/FEP + ATM + CN	4	MDR
TZP + CAZ/FEP + ATM + CIP/LEV	5	MDR
TZP + CAZ/FEP + CN + CIP/LEV	1	MDR
CAZ/FEP + ATM + CN + CIP/LEV	1	MDR
CAZ/FEP + IMP + CN + CIP/LEV	1	MDR
TZP + CAZ/FEP + ATM + PB + CIP/LEV	2	MDR
TZP + CAZ/FEP + ATM + IMP + CIP/LEV	2	MDR
TZP + CAZ/FEP + ATM + CN + CIP/LEV	8	MDR
CAZ/FEP + ATM + IMP + PB + CIP/LEV	1	MDR
TZP + CAZ/FEP + ATM + PB + CN + CIP/LEV	3	XDR
TZP + CAZ/FEP + IMP + PB + CN + CIP/LEV	1	XDR
CAZ/FEP + ATM + IMP + PB + CN + CIP/LEV	1	XDR

TZP: Piperacillin-tazobactam (110 µg), CAZ: Ceftazidime (30 µg), FEP: Cefepime (30 µg), ATM: Aztreonam (30 µg), IMP: Imipenem (10 µg), PB: Polymyxin B (300 units), CN: Gentamicin (10 µg), CIP: Ciprofloxacin (5 µg), LEV: Levofloxacin (5 µg), MDR: Multidrug resistant, XDR: Extremely drug resistant

and rigorous monitoring for MDR among *Pseudomonas* isolates is critical especially as given that *P. aeruginosa* has become a cause of many nosocomial infections.

CONCLUSION

In summary, we analyzed the incidence, prevalence, and antibiotic susceptibility pattern of *P. aeruginosa* in a healthcare facility in Nigeria. We report disturbingly high prevalence of MDR and some XDR phenotypes of *P. aeruginosa* in Nigeria. Our findings call for antimicrobial stewardship and improved public health policies regarding proper antibiotic use.

ACKNOWLEDGMENTS

The authors acknowledge the staff of the Department of Medical Microbiology, UPTH for access to patient's samples and Department of Pharmaceutical Microbiology and Biotechnology, University of Port Harcourt for their support throughout the study.

Ethics

Ethics Committee Approval: The Research and Ethics Committee of the University of Port Harcourt approved this study (reference number: UPH/CEREMAD/REC/MM76/053). Samples were taken from patients after they or their legal guardians had given their informed voluntary consent to partake in the study. Standard protocols were followed to ensure the confidentiality of patient information.

Informed Consent: Approval received.

Peer-review: Externally peer-reviewed.

Authorship Contributions

Concept: A.M.A., Design: A.M.A., Data Collection or Processing: C.N.I., C.N.S., H.O., I.O.O., N.E.E., Analysis, or Interpretation: A.M.A., C.N.I., C.N.S., H.O., I.O.O., N.E.E., Literature Search: A.M.A., C.N.I., C.N.S., H.O., I.O.O., N.E.E., Writing: A.M.A., C.N.I., C.N.S., H.O., I.O.O., N.E.E.

Conflict of Interest: No conflict of interest was declared by the authors.

Financial Disclosure: The authors declared that this study received no financial support.

REFERENCES

1. Driscoll JA, Brody SL, Kollef MH. The epidemiology, pathogenesis and treatment of *Pseudomonas aeruginosa* infections. Drugs. 2007;67:351-368.
2. Gill JS, Arora S, Khanna SP, Kumar KH. Prevalence of multidrug-resistant, extensively drug-resistant, and pandrug-resistant *Pseudomonas aeruginosa* from a tertiary level intensive care unit. J Glob Infect Dis. 2016;8:155-159.
3. Mulcahy LR, Isabella VM, Lewis K. *Pseudomonas aeruginosa* biofilms in disease. Microb Ecol. 2014;68:1-12.
4. Pérez A, Gato E, Pérez-Llarena J, Fernández-Cuenca F, Gude MJ, Oviaño M, Pachón ME, Garnacho J, González V, Pascual Á, Cisneros JM, Bou G. High incidence of MDR and XDR *Pseudomonas aeruginosa* isolates obtained from patients with ventilator-associated pneumonia in Greece, Italy and Spain as part of the MagicBullet clinical trial. J Antimicrob Chemother. 2019;74:1244-1252.
5. Thaden JT, Park LP, Maskarinec SA, Ruffin F, Fowler VG Jr, van Duin D. Results from a 13-year prospective cohort study show increased mortality associated with bloodstream infections caused by *Pseudomonas aeruginosa* compared to other bacteria. Antimicrob Agents Chemother. 2017;61:e02671.
6. Raman G, Avendano EE, Chan J, Merchant S, Puzniak L. Risk factors for hospitalized patients with resistant or multidrug-resistant *Pseudomonas aeruginosa* infections: a systematic review and meta-analysis. Antimicrob Resist Infect Control. 2018;7:79.
7. Morrissey I, Hackel M, Badal R, Bouchillon S, Hawser S, Biedenbach D. A review of ten years of the study for monitoring antimicrobial resistance trends (SMART) from 2002 to 2011. Pharmaceuticals (Basel). 2013;6:1335-1346.
8. Biswal I, Arora BS, Kasana D, Neetushree. Incidence of multidrug resistant *Pseudomonas aeruginosa* isolated from burn patients and environment of teaching institution. J Clin Diagn Res. 2014;8:DC26-29.
9. Raja NS, Singh NN. Antimicrobial susceptibility pattern of clinical isolates of *Pseudomonas aeruginosa* in a tertiary care hospital. J Microbiol Immunol Infect. 2007;40:45-49.
10. Obritsch MD, Fish DN, MacLaren R, Jung R. National surveillance of antimicrobial resistance in *Pseudomonas aeruginosa* isolates obtained from intensive care unit patients from 1993 to 2002. Antimicrob Agents Chemother. 2004;48:4606-4610.
11. Pang Z, Raudonis R, Glick BR, Lin TJ, Cheng Z. Antibiotic resistance in *Pseudomonas aeruginosa*: mechanisms and alternative therapeutic strategies. Biotechnol Adv. 2019;37:177-192.
12. Breidenstein EB, de la Fuente-Núñez C, Hancock RE. *Pseudomonas aeruginosa*: all roads lead to resistance. Trends Microbiol. 2011;19:419-426.
13. Ramírez-Estrada S, Borgatta B, Rello J. *Pseudomonas aeruginosa* ventilator-associated pneumonia management. Infect Drug Resist. 2016;9:7-18.
14. Kalil AC, Metersky ML, Klompas M, Muscedere J, Sweeney DA, Palmer LB, Napolitano LM, O'Grady NP, Bartlett JG, Carratalà J, El Solh AA, Ewig S, Fey PD, File TM Jr, Restrepo MI, Roberts JA, Waterer GW, Cruse P, Knight SL, Brozek JL. Management of adults with hospital-acquired and ventilator-associated pneumonia: 2016 Clinical Practice Guidelines by the infectious Diseases Society of America and the American Thoracic Society. Clin Infect Dis. 2016;63:e61-e111. Erratum in: Clin Infect Dis. 2017;64:1298. Erratum in: Clin Infect Dis. 2017;65:1435. Erratum in: Clin Infect Dis. 2017;65:2161.
15. Mensa J, Barberán J, Soriano A, Llinares P, Marco F, Cantón R, Bou G, González Del Castillo J, Maseda E, Azanza JR, Pasquau J, García-Vidal C, Reguera JM, Sousa D, Gómez J, Montejo M, Borges M, Torres A, Alvarez-Lerma F, Salavert M, Zaragoza R, Oliver A. Antibiotic selection in the treatment of acute invasive infections by *Pseudomonas aeruginosa*: Guidelines by the Spanish Society of Chemotherapy. Rev Esp Quimioter. 2018;31:78-100.
16. Labarca JA, Salles MJ, Seas C, Guzmán-Blanco M. Carbapenem resistance in *Pseudomonas aeruginosa* and *Acinetobacter baumannii* in the nosocomial setting in Latin America. Crit Rev Microbiol. 2016;42:276-292.

17. Cai B, Echols R, Magee G, Arjona Ferreira JC, Morgan G, Ariyasu M, Sawada T, Nagata TD. Prevalence of carbapenem-resistant gram-negative infections in the United States predominated by *Acinetobacter baumannii* and *Pseudomonas aeruginosa*. Open Forum Infect Dis. 2017;4:ofx176.

18. Tacconelli E, Carrara E, Savoldi A, Harbarth S, Mendelson M, Monnet DL, Pulcini C, Kahlmeter G, Kluytmans J, Carmeli Y, Ouellette M, Outterson K, Patel J, Cavaleri M, Cox EM, Houchens CR, Grayson ML, Hansen P, Singh N, Theuretzbacher U, Magrini N; WHO Pathogens Priority List Working Group. Discovery, research, and development of new antibiotics: the WHO priority list of antibiotic-resistant bacteria and tuberculosis. Lancet Infect Dis. 2018;18:318-327.

19. CLSI, Performance Standards for Antimicrobial Susceptibility Testing. 26th ed. CLSI supplement M100S. Wayne, PA: Clinical and Laboratory Standards Institute, 2016. Available from: https://clsi.org/media/2663/m100ed29_sample.pdf

20. Humphries RM, Ambler J, Mitchell SL, Castanheira M, Dingle T, Hindler JA, Koeth L, Sei K; CLSI Methods development and standardization working group of the subcommittee on antimicrobial susceptibility testing. CLSI methods development and standardization working group best practices for evaluation of antimicrobial susceptibility tests. J Clin Microbiol. 2018;56:e01934.

21. Biemer JJ. Antimicrobial susceptibility testing by the Kirby-Bauer disc diffusion method. Ann Clin Lab Sci (1971). 1973;3:135-140.

22. Alnimr AM, Alamri AM. Antimicrobial activity of cephalosporin-beta-lactamase inhibitor combinations against drug-susceptible and drug-resistant *Pseudomonas aeruginosa* strains. J Taibah Univ Med Sci. 2020;15:203-210.

23. Bonomo RA, Szabo D. Mechanisms of multidrug resistance in *Acinetobacter* species and *Pseudomonas aeruginosa*. Clin Infect Dis. 2006;43(Suppl 2):S49-S56.

24. Magiorakos AP, Srinivasan A, Carey RB, Carmeli Y, Falagas ME, Giske CG, Harbarth S, Hindler JF, Kahlmeter G, Olsson-Liljequist B, Paterson DL, Rice LB, Stelling J, Struelens MJ, Vatopoulos A, Weber JT, Monnet DL. Multidrug-resistant, extensively drug-resistant and pandrug-resistant bacteria: an international expert proposal for interim standard definitions for acquired resistance. Clin Microbiol Infect. 2012;18:268-281.

Turk J Pharm Sci 2022;19(4):455-461
DOI: 10.4274/tjps.galenos.2021.17702

ORIGINAL ARTICLE

Development of GC-MS/MS Method for Simultaneous Estimation of Four Nitrosoamine Genotoxic Impurities in Valsartan

Sambasiva Rao TUMMALA, Krishnamanjari Pawar AMGOTH*

Andhra University, College of Pharmaceutical Sciences, Department of Pharmaceutical Analysis, Andhra Pradesh, India

ABSTRACT

Objectives: Recently, *N*-nitrosamines were unexpectedly detected in valsartan and other generic sartan products. Taking into this account, we developed a sensitive and stable multiple reaction monitoring mode-based "gas chromatography-tandem mass spectrometry (GC-MS/MS)" approach for the quantification of "four *N*-nitrosamines" in valsartan, especially, *N*-nitrosodiisopropylamine, *N*-nitroso ethyl isopropylamine, *N*-nitrosodiethylamine, and *N*-nitrosodimethylamine.

Materials and Methods: GC and MS conditions were optimized with specificity, sensitivity, linearity, precision, and accuracy of the parameters. The approach was validated as *per* the "International Council for Harmonization" recommendations.

Results: The identification limits and limits of quantification of *N*-nitrosamines in valsartan varied between 0.02 and 0.03 ppm, and 0.06-0.09 ppm, respectively. The obtained values were satisfactory with limits established by the United States Food and Drug Administration for sensitivity requirements. The regression coefficients greater than 0.999 for four *N*-nitrosamines in the calibration curve demonstrated the strong linearity of the process. The retrievals of "*N*-nitrosamines" in valsartan between 91.9-122.7%. For the intra-day and inter-day accuracy studies, the (relative standard deviation) was less than 9.15%.

Conclusion: The proposed approach has rapid analysis capability, high precision, accuracy, and good sensitivity, which give a reliable approach for *N*-nitrosamines quality control in valsartan.

Key words: GC-MS/MS, valsartan, *N*-nitrosamine, genotoxic impurity

INTRODUCTION

In the production process of the "active pharmaceutical ingredients (APIs)", impurities are incorporated through various sources, like catalysts, solvents, reagents, intermediates, starting materials, and by-products. Compared to other impurities, genotoxic impurities (GTIs) are of a special kind that could inspire mutations at the genetic level, which lead to chromosomal breakage and rearrangements, and even present in low concentrations have increased the risk of cancer.[1] Considering into account the toxic effects of GTIs the international regulatory bodies had set an exposure limit thresholds for GTIs, specifically, 1.5 µg/day for long-run therapy with greater thresholds of clinical shorter intervals. As these GTIs are present in very low concentrations, the pharmaceutical industry faces an uphill task of developing robust analytical, sensitive, and high efficient methods for their determination.[2,3] Valsartan belongs to the category of antihypertensive drugs that selectively inhibit angiotensin receptor type II. It is used to treat mild-to-moderate essential hypertension. The angiotensin-II mediated unwanted effects are reduced to a significant extent by valsartan. Recalls for valsartan were issued between mid-to-late 2018. The cause of the recalls was due to the detection of GTIs such as "*N*-nitrosodiethylamine (NDEA)" or "*N*-nitrosodimethylamine (NDMA)" in valsartan in unacceptable limits.[4] The nitrosamine impurities were produced during the drug substance synthesis in which the sodium azide, which is applied in the production of the tetrazole moiety, was eliminated

*Correspondence: akmpawar@andhrauniversity.edu.in, Phone: +08912844941, ORCID-ID: orcid.org/0000-0002-2703-4505
Received: 24.04.2021, Accepted: 27.09.2021

using sodium nitrite and later under acidic circumstances would form nitrous acid, a powerful nitrosylating agent. Dimethylamine and diethylamine, which might be present as impurities in dimethylformamide may be *N*-nitrosylated in the synthesis might result in the formation of NDMA and NDEA. Likewise, in certain production processes for valsartan, the reagent triethylamine can degrade to produce diethylamine, and latter *N*-nitrosylated to produce NDEA. *N*-nitroso compounds are included in the "cohort of concern" as they exhibit great carcinogenic potency.[5,6] The appropriate regular intake limits for NDEA, NDMA, and other impurities in some products were published by the United States Food and Drug Administration (FDA). The limit of *N*-nitrosoethylisopropylamine (NEIA) and *N*-nitrosodiisopropylamine (NDIPA) is 96 ng/day.

Recently, for detecting *N*-nitrosamines in water, food, and personal care products, the analytical techniques widely used are gas chromatography (GC),[7-18] liquid chromatography (LC)[19,20] and supercritical fluid chromatography (SFC)-tandem mass spectrometry (MS).[21] FDA has determined the interim appropriate regular intake levels for *N*-nitrosamines in valsartan (Table 1) and employed GC-MS/MS by using liquid injection and headspace,[22,23] rapid fire-MS/MS,[24] and high performance liquid chromatography (HPLC)-high resolution mass spectrometry[25] for quantification of the *N*-nitrosamines in valsartan.

In the analysis of water, food, and personal care items, the extraction as well as purification measures are critical and important. However, in the pharmaceutical industry, these were much not much applicable. Liu et al.[26] reported a GC-MS/MS approach for detecting four "*N*-nitrosamines" in valsartan, but the method suffers from the drawback of long run time and less accuracy. Therefore, we established through direct injection for quantification of four "*N*-nitrosamines", as a simple, sensitive, precise, and rapid GC-MS/MS approach for valsartan. The limit of detections (LODs) and limit of quantification (LOQ) values were at acceptable limits as *per* the sensitivity requirements set by the FDA. The proposed GC-MS/MS approach validation was performed as *per* the International Council for Harmonization (ICH) guidelines.

MATERIALS AND METHODS

Chemicals and materials

Valsartan was found as a gift sample by the local pharma industry. NDMA (purity ≥98.3%), NDEA (purity ≥100.0%), NDIPA (purity ≥99.9%), and NEIA (purity ≥99.3%) standards were acquired by Sigma Aldrich. The solvents used methanol, acetonitrile, ethyl acetate, 1-methyl-2-pyrrolidinone, which were of all HPLC-grade, were purchased from Merck Ltd., Mumbai, India. The structures of valsartan and nitrosamine impurities are presented in Figure 1.

Instrumentation and optimized GC-MS/MS conditions

Agilent "7890B" "GC-MS/MS" equipped with an "Agilent 7693A" auto sampling device and 7697 a Headspace Sampler was used to examine *N*-nitrosamines. The analytical column used was DM-WAX (30 m x 0.25 mm, 0.5 µm). This detection was conducted at a 700°C triple quadrupole mass spectrometer consisting of electron ionization (EI) ion source. The temperature programming in GC oven was done by maintaining oven temperature of 70°C for 4 min, which first elevated at 20°C·min^{-1} to 240°C and maintained for 3 min. The run interval was fixed at 10 min. The flow rate was 3.0 mL/min for helium as the carrier gas. The injection temperature as well as injection interface were maintained at 240°C. The volume of injection in the split mode (1:2) was 1 µL. MS was run at 70 eV in EI mode with a 150°C "quadrupole temperature". The ion source has been adjusted to a temperature of 230°C. It was 4 min to delay the solvent. The data recovery mode for the quantitative estimation of "four *N*-nitrosamine GTIs" was chosen as the "multi-reaction monitoring (MRM)" mode. Table 2 provides a summary of the data for precursor ions, production and enhanced "collision energy" for four *N*-nitrosamine GTIs.

Preparation of samples and standard solutions

The standard stock solutions of NDMA, NDEA, NEIA, and NDIPA were prepared at 1 mg/mL concentrations through dissolving weighed reference standards in 1-methyl-2-pyrrolidinone, respectively, and stored at 4°C. A sequence of standard working

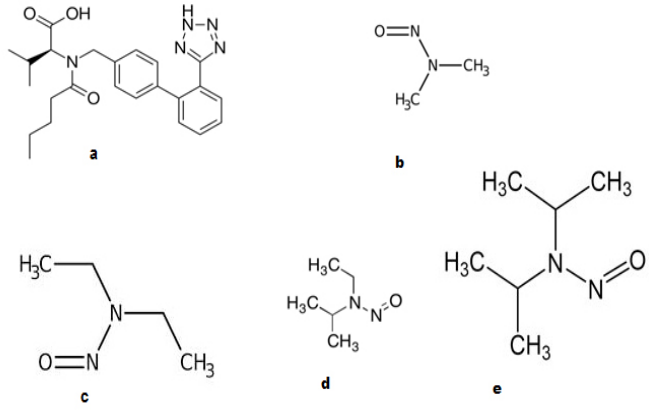

Figure 1. a) Structure of valsartan, b) *N*-Nitrosodimethylamine, c) *N*-Nitrosodiethylamine, d) *N*-Nitrosoethylisopropylamine, e) *N*-Nitrosodiisopropylamine

Table 1. Interim limits for NDMA and NDEA in valsartan set by FDA

Drug	Maximum daily dose (mg/day)	Acceptable intake NDMA (ng/day)	Acceptable intake NDMA (ppm)	Acceptable intake NDEA (ng/day)	Acceptable intake NDEA (ppm)
Valsartan	320	96	0.3	26.5	0.083

NDMA: *N*-nitrosodimethylamine, NDEA: *N*-nitrosodiethylamine, FDA: United States Food and Drug Administration

solutions of NDMA at the levels of 0.093, 0.155, 0.232, 0.309, 0.387, and 0.464 ppm (µg/g API) in 1-methyl-2-pyrrolidinone was found from a stock solution *via* the serial dilution process. The sequence of NDEA standard working solution was concentrated at 0.062, 0.154, 0.231, 0.308, 0.384, and 0.461 ppm (µg/g API), respectively. The working solution concentrations for NEIA were 0.090, 0.150, 0.224,0.299, 0.374, and 0.449 ppm (µg/g API), respectively. The concentrations of NDIPA were 0.088, 0.146, 0.220, 0.293, 0.366, and 0.439 ppm (µg/g API). Here, 1 ppm corresponds to 0.25 µg/mL of NDMA, NDEA, NEIA, and NDIPA, respectively. At 250 mg/mL concentration, valsartan was prepared. A mixed standard solution of NDIPA, NEIA, NDEA, and NDMA was prepared from the standard stock solution after subsequent dilution with 1-methyl-2-pyrrolidinone to obtain a concentration within the linearity range. The resulting mixture was sonicated for 30 min and kept in a centrifuge tube for around 1 min before being centrifuged for 10 min at 2500 rpm. The supernatant was passed to the chromatography injection vial through the 0.22 µm nylon syringe filter.

Method validation

The developed "GC-MS/MS" approach with MRM mode for detecting four *N*-nitrosamines was validated for parameters, as solution stability, precision, accuracy, LOQ, LOD, linearity, sensitivity, specificity, and system suitability. For LODs, signal-to-noise (S/N) ratio was 3 as well as LOQs were S/N: 10. To the accuracy of the proposed method, the recovery studies were conducted for evaluation. The precision studies were evaluated by inter-day and intra-day relative standard deviations (RSDs) of six specimens spiked across 3 continuous days at a single concentration. There was no statistical analysis performed in the developed method.

RESULTS AND DISCUSSION

Method development

Selection of solvents

Considering the trace level of *N*-nitrosamine GTIs NDMA, NDEA, NEIA, and NDIPA in valsartan and solubility parameter, 1-methyl-2-pyrrolidinone was selected as a solvent for the preparation of solutions for GC-MS/MS analysis.

Capillary column selection

Under the given temperature program, three different capillary columns were used to obtain the best chromatographic separation. The columns were HP-35MS, HP-5MS, and DM-WAX in the order of increasing polarity. A 10 µg/mL normal blend was inserted in all three cases. Identification of the compounds depended on the spectra EI using the National Institute of Standards and Technology library. Liu et al.[26] reported separation of four nitrosamines using DB-WAXetr capillary column without the inclusion of NDEA. We have used the DM-WAX column, which has sufficient polarity to isolate all nitrosamines with better peak shapes, resolution, less analysis time with applicable for the analysis of most polar and volatile compounds, such as NDMA and NDEA.The optimized chromatogram is shown in Figure 2.

Mass spectrometry

In the analysis of pharmaceuticals, the most crucial aspect is the trace detection method for GTIs. Considering the sensitivity criteria, MRM mode is superior to SIM mode for the quantification of *N*-nitrosamines. Consequently, the MRM mode was used to quantify four *N*-nitrosamine GTI in valsartan as MS approach. MS of valsartan and four *N*-nitrosamine GTIs with chromatograms are shown in Figure 3.

Method validation

The suggested approach for "four *N*-nitrosamine GTIs" was validated as *per* ICH recommendations.

Specificity

For the specificity of the recommended approach, 1-methyl-2-pyrrolidinone, the valsartan matrices and mixed standards of four *N*-nitrosamines were undergone by the "GC-MS/MS" examination. At the retention times of four *N*-nitrosamines there is no interference peaks from the 1-methyl-2-pyrrolidinone, and the valsartan matrices were observed, indicating the specificity of the approach for detecting four *N*-nitrosamines in valsartan.

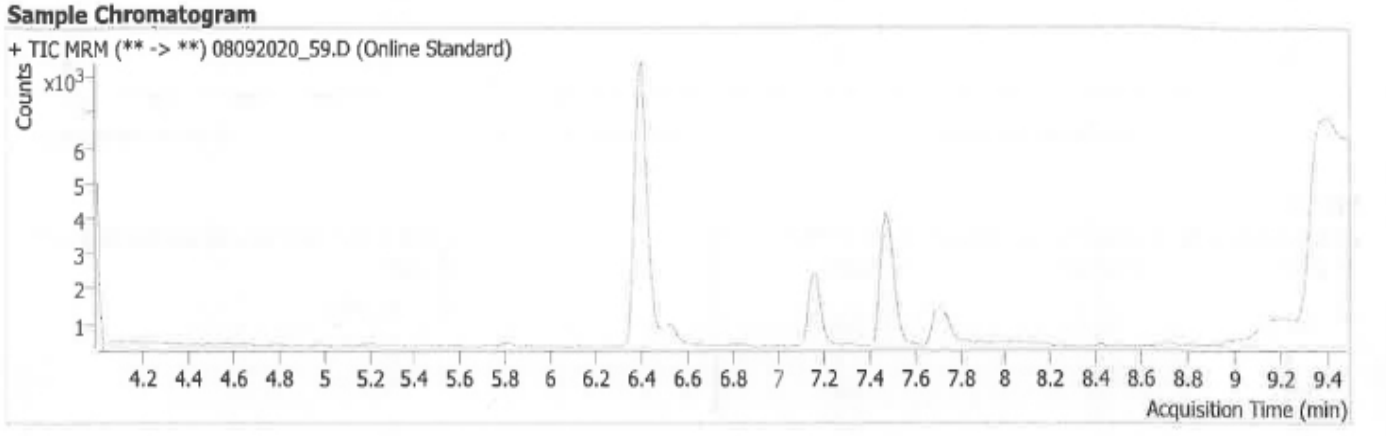

Figure 2. GC chromatograms of mixed standard solution of *N*-nitrosamines
GC: Gas chromatography

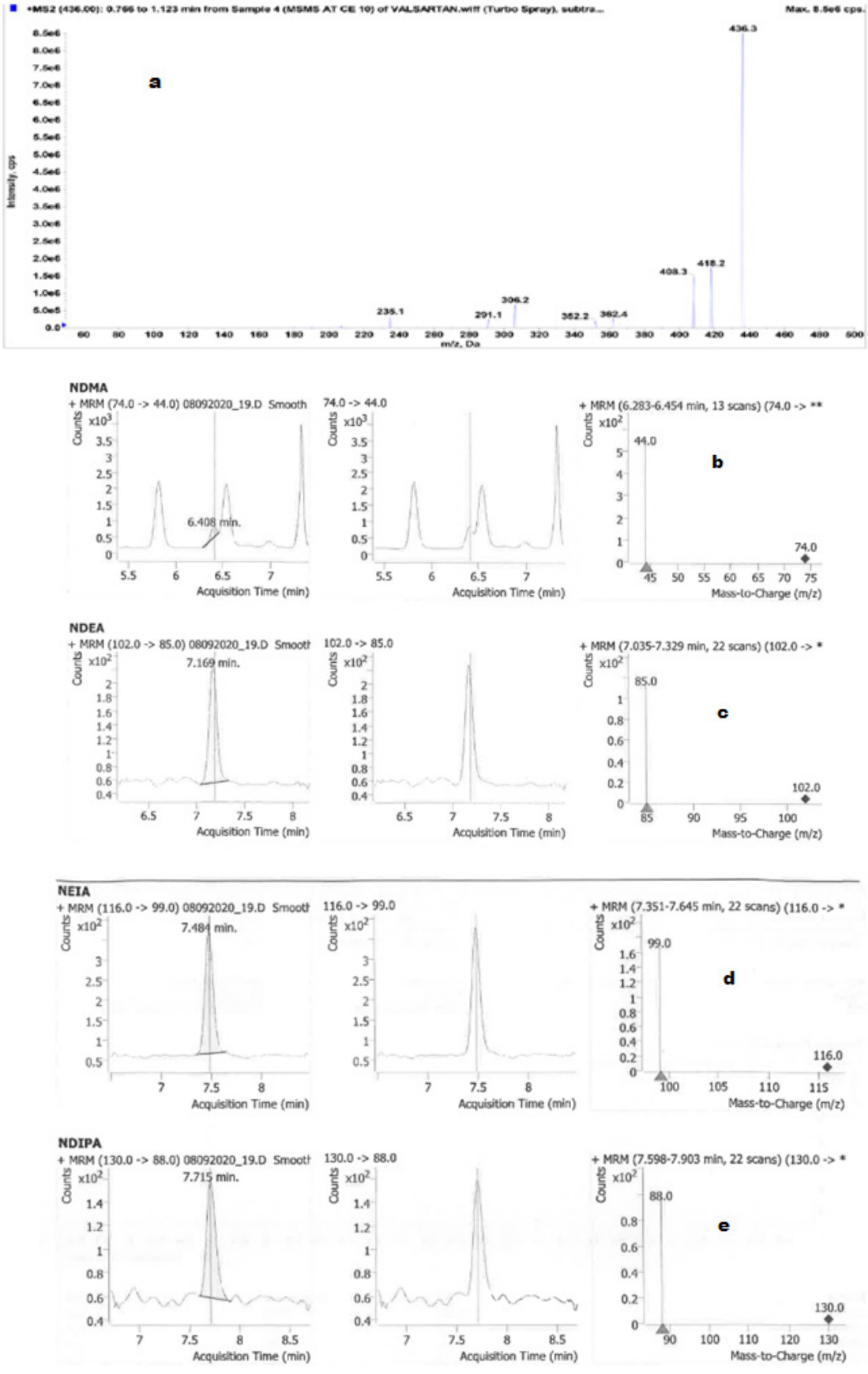

Figure 3. a) Mass spectra of valsartan, b) *N*-nitrosodimethylamine, c) *N*-nitrosodiethylamine, d) *N*-nitrosoethylisopropylamine, e) *N*-nitrosodiisopropylamine

Linearity and sensitivity

The data for linearity, LOQ, and LOD outcomes are summarized in Table 3. The standard curve (y= Ax + B, in which A signifies the slope and B signifies the intercept) was obtained by plotting the chromatographic peak area (*N*-nitrosamines, y) to normal *N*-nitrosamines (x) concentrations. To validate the linearity of the approach, six standard concentrations were used. The regression coefficients (R^2) of the standard curve for four *N*-nitrosamines were ›0.99 in the given concentration range, indicating better linearity and is appropriate for the quantitative examination, as shown in Figure 4. Therefore, based on LODs and LOQs, the sensitivity of the method was evaluated. In Table 3, LODs and LOQs for NDEA, NEIA, NDIPA, and NDMA in 1-methyl-2-pyrrolidinone are presented. The low values of LOQs and LODs for this GC-MS/MS approach were acceptable and suitable for detecting *N*-nitrosamines in valsartan.

Accuracy

The accuracy of the method was estimated from the recovery results of four *N*-nitrosamines. To evaluate the output of the recommended approach, improvements of four *N*-nitrosamines were determined after valsartan samples spiked with 3 separate levels of four *N*-nitrosamines at 50% (NDIPA-0.146 ppm, NDEA-0.154 ppm, NDMA-0.155 ppm, NEIA-0.150 ppm), 100% (NDIPA-0.293 ppm, NDEA-0.308 ppm ,NDMA-0.309 ppm, NEIA-0.299 ppm), and 150% (NDIPA-0.439 ppm, NDEA-0.461 ppm, NDMA-0.464 ppm, NEIA-0.449 ppm) of the limits, respectively. The recoveries for NDIPA, NDEA, NDMA, and NEIA in valsartan were in the range of 87.68 to 122.75%, as shown in Table 4. Considering the ultra-trace essence of the study, the recovery of *N*-nitrosamines was found in the acceptable range of 70-130%, indicating the accuracy of the proposed method for *N*-nitrosamines.

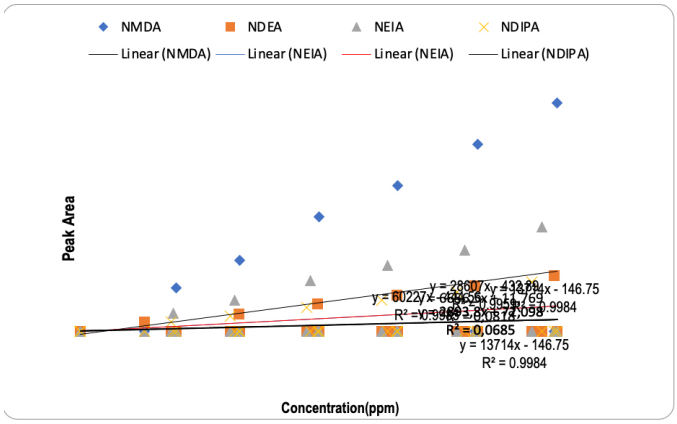

Figure 4. Calibration curve of four *N*-nitrosamines

Table 2. Multiple reactions monitoring transitions and optimized collision energy for four *N*-nitrosamine GTIs

Analyte	Precursor→product (*m/z*)	Dwell time (ms)	Collision energy (eV)
N-nitrosodimethylamine	74→44	200	5
N-nitrosodiethylamine	102→85	200	5
N-nitrosoethylisopropylamine	116→99	200	5
N-nitrosodiisopropylamine	130→88	200	5

GTIs: Genotoxic impurities

Table 3. Calibration curves, LODs, and LOQs for four *N*-nitrosamines

Analyte	Linearity range (ppm)	Regression equation	R^2	LOD (ppm)	LOQ (ppm)
N-nitrosodimethylamine	0.093-0.464	Y= 60227X - 444.56	0.9985	0.03	0.09
N-nitrosodiethylamine	0.062-0.461	Y= 13714X - 146.75	0.9984	0.02	0.06
N-nitrosoethylisopropylamine	0.09-0.449	Y= 28067X - 432.89	0.9959	0.03	0.09
N-nitrosodiisopropylamine	0.088-0.439	Y= 13714X - 146.75	0.9984	0.03	0.09

LODs: Limit of detections, LOQs: Limit of quantification, R^2: Regression coefficients

Table 4. Accuracy data of four nitrosoamines

Analyte	Valsartan concentration (mg/mL)	Mean % recovery at 50 % level ± SD	Mean % recovery at 100 % level ± SD	Mean % recovery at 150 % level ± SD
N-nitrosodimethylamine	250	103.21 ± 0.23	101.15 ± 0.98	102.29 ± 1.89
N-nitrosodiethylamine		91.93 ± 1.75	87.68 ± 0.76	101.6 4 ± 0.49
N-nitrosoethylisopropylamine		114.42 ± 0.31	112.21 ± 1.38	117.83 ± 1.66
N-nitrosodiisopropylamine		111.41 ± 1.73	113.62 ± 0.99	122.75 ± 0.26

SD: Standard deviation

Table 5. Precision results of four nitrosoamines

Drug (API)	Analyte	Concentration (ppm)* (µg/g API)	System precision (RSD %)	Method precision (RSD %)		Intermediate precision (RSD %)	
				Interday	Intraday	Analyst I	Analyst II
Valsartan (250 mg/mL)	*N*-nitrosodimethylamine	0.309	6.43	1.44	1.37	2.53	2.74
	N-nitrosodiethylamine	0.308	8.52	3.46	3.83	4.28	3.83
	N-nitrosoethylisopropylamine	0.299	7.02	2.26	2.69	6.35	5.97
	N-nitrosodiisopropylamine	0.293	9.21	2.79	2.93	6.41	7.27

*1 ppm corresponds to 0.25 µg/mL of *N*-nitrosodimethylamine, *N*-nitrosodiethylamine, *N*-nitrosoethylisopropylamine, and *N*-nitrosodiisopropylamine, respectively.
API: Active pharmaceutical ingredient, RSD: Relative standard deviation

Precision

To study the method precision, the inter-day and intra-day accuracy tests were performed. The intra-day precision measurements were carried out by comparison of the "SD" of the recovery proportions of the spiked specimens analyzed on the same day. For inter-day accuracy, spiked samples were tested for three distinct days. The intermediate precision was evaluated by results from the study on a different day with different analysts and with freshly prepared solutions. As reviewed in Table 5, this GC-MS/MS approach demonstrated acceptable percentage RSD values for the inter-day, intra-day precision as well as intermediate accuracy was between 1.45-6.38%, 2.88-9.15%, and 2.8-3.7%, respectively.

Stabilities of four N-nitrosamines in 1-methyl-2-pyrrolidinone

To study four *N*-nitrosamines solution stabilities in 1-methyl-2-pyrrolidinone, 0.3 ppm standard solutions were prepared and analyzed every 4 h for a recently prepared standard. Each solution was placed at 25˚C in the dark. The recovery percentage of *N*-nitrosamines from these stock solutions was between 97.51 and 105.04%, and the differential recoveries of *N*-nitrosamines at 0 h and 24 h at just 10%, indicate the stability of the stock solution for at least 24 h.

Applications in samples

This GC-MS/MS process was used in the determination of four *N*-nitrosamine GTIs in four batches of commercial valsartan-containing products and none of the four "*N*-nitrosamines" were observed in four batches of the commercially available formulation.

CONCLUSION

A simple and sensitive MRM mode-based GC-MS/MS approach was created for estimating four GTIs *i.e.* NEIA, NDIPA, NDEA, and NDMA in valsartan. The reported GC-MS/MS approach demonstrates satisfactory sensitivity and selectivity. The run time was under 10 min. The results of four *N*-nitrosamines in LOQs and LODs ranged 0.06-0.09 ppm and 0.02-0.03 ppm correspondingly, indicating the suitability of four *N*-nitrosamines in valsartan for sensitive quantification.

Ethics

Ethics Committee Approval: Not required.

Informed Consent: Not applicable as our study does not involve any human volunteers and animals.

Peer-review: Externally peer-reviewed.

Authorship Contributions

Concept: S.R.T., Design: S.R.T., K.P.A., Data Collection or Processing: S.R.T., Analysis or Interpretation: S.R.T., K.P.A., Literature Search: K.P.A., Writing: K.P.A.

Conflict of Interest: No conflict of interest was declared by the authors.

Financial Disclosure: The authors declared that this study received no financial support.

REFERENCES

1. Szekely G, Amores de Sousa MC, Gil M, Castelo Ferreira F, Heggie W. Genotoxic impurities in pharmaceutical manufacturing: sources, regulations, and mitigation. Chem Rev. 2015;115:8182-8229.
2. Raman NV, Prasad AV, Ratnakar Reddy K. Strategies for the identification, control and determination of genotoxic impurities in drug substances: a pharmaceutical industry perspective. J Pharm Biomed Anal. 2011;55:662-667.
3. Teasdale A, Elder DP. Analytical control strategies for mutagenic impurities: current challenges and future opportunities? Trends Anal Chem. 2014;103:2-28.
4. Scherf-Clavel O, Kinzig M, Besa A, Schreiber A, Bidmon C, Abdel-Tawab M, Wohlfart J, Sörgel F, Holzgrabe U. The contamination of valsartan and other sartans, part 2: untargeted screening reveals contamination with amides additionally to known nitrosamine impurities. J Pharm Biomed Anal. 2019;172:278-284.
5. Buist HE, Devito S, Goldbohm RA, Stierum RH, Venhorst J, Kroese ED. Hazard assessment of nitrosamine and nitramine by-products of amine-based CCS: alternative approaches. Regul Toxicol Pharmacol. 2015;71:601-623.
6. Ravnum S, Rundén-Pran E, Fjellsbø LM, Dusinska M. Human health risk assessment of nitrosamines and nitramines for potential application in CO_2 capture. Regul Toxicol Pharmacol. 2014;69:250-255.
7. Chen W, Li X, Huang H, Zhu X, Jiang X, Zhang Y, Cen K, Zhao L, Liu X, Qi S. Comparison of gas chromatography-mass spectrometry and gas chromatography-tandem mass spectrometry with electron ionization for determination of *N*-nitrosamines in environmental water. Chemosphere. 2017;168:1400-1410.

8. Hong Y, Kim KH, Sang BI, Kim H. Simple quantification method for *N*-nitrosamines in atmospheric particulates based on facile pretreatment and GC-MS/MS. Environ Pollut. 2017;226:324-334.

9. Luo YB, Chen XJ, Zhang HF, Jiang XY, Li X, Li XY, Zhu FP, Pang YQ, Hou HW. Simultaneous determination of polycyclic aromatic hydrocarbons and tobacco-specific *N*-nitrosamines in mainstream cigarette smoke using in-pipette-tip solid-phase extraction and on-line gel permeation chromatography-gas chromatography-tandem mass spectrometry. J Chromatogr A. 2016;1460:16-23.

10. McDonald JA, Harden NB, Nghiem LD, Khan SJ. Analysis of *N*-nitrosamines in water by isotope dilution gas chromatography-electron ionisation tandem mass spectrometry. Talanta. 2012;99:146-154.

11. Scheeren MB, Sabik H, Gariépy C, Terra NN, Arul J. Determination of *N*-nitrosamines in processed meats by liquid extraction combined with gas chromatography-methanol chemical ionisation/mass spectrometry. Food Addit Contam Part A Chem Anal Control Expo Risk Assess. 2015;32:1436-1447.

12. Sieira BJ, Carpinteiro I, Rodil R, Quintana JB, Cela R. Determination of *N*-nitrosamines by gas chromatography coupled to quadrupole-time-of-flight mass spectrometry in water samples. Separations. 2020;7:3.

13. Zhu M, Ye Q, Zhou T, Chen L, Yu L, Li B, Hu J, Zhou M. [Determination of 10 volatile *N*-nitrosamines in meat products by gas chromatography-tandem mass spectrometry]. Se Pu. 2019;37:207-215.

14. Hung HW, Lin TF, Chiu CH, Chang YC, Hsieh TY. Trace analysis of *N*-nitrosamines in water using solid-phase microextraction coupled with gas chromatograph–tandem mass spectrometry. Water Air Soil Pollut. 2010;213:459-469.

15. Pozzi R, Bocchini P, Pinelli F, Galletti GC. Determination of nitrosamines in water by gas chromatography/chemical ionization/selective ion trapping mass spectrometry. J Chromatogr A. 2011;1218:1808-1814.

16. Yoon S, Nakada N, Tanaka H. A new method for quantifying *N*-nitrosamines in wastewater samples by gas chromatography-triple quadrupole mass spectrometry. Talanta. 2012;97:256-261.

17. Wang Z, Zhai M, Xia X, Yang M, Han T, Huang M. A simple method for monitoring eight *N*-nitrosamines in Beef Jerkys by gas chromatography-tandem mass spectrometry with one-step treatment coupled to active carbon solid-phase extraction. Food Anal Methods. 2018;11:933-938.

18. Ma Q, Xi HW, Wang C, Bai H, Xi GC, Su N, Xu LY, Wang JB. Determination of ten volatile nitrosamines in cosmetics by gas chromatography tandem mass spectrometry. Chinese J Anal Chem. 2011;39:1201-1207.

19. Herrmann SS, Duedahl-Olesen L, Granby K. Simultaneous determination of volatile and non-volatile nitrosamines in processed meat products by liquid chromatography tandem mass spectrometry using atmospheric pressure chemical ionisation and electrospray ionisation. J Chromatogr A. 2014;1330:20-29.

20. Ngongang AD, Duy SV, Sauvé S. Analysis of nine *N*-nitrosamines using liquid chromatography-accurate mass high resolution-mass spectrometry on a Q-exactive instrument. Anal Methods. 2015;7:5748-5759.

21. Schmidtsdorff S, Schmidt AH. Simultaneous detection of nitrosamines and other sartan-related impurities in active pharmaceutical ingredients by supercritical fluid chromatography. J Pharm Biomed Anal. 2019;174:151-160.

22. U.S. Food & Drug Administration (FDA). Combined direct injection nnitrosodimethylamine (NDMA), *N*-nitrosodiethylamine (NDEA), *N*-nitrosoethylisopropylamine (NEIPA), *N*-nitrosodiisopropylamine (NDIPA), and *N*-nitrosodibutylamine (NDBA) impurity assay by GC-MS/MS. 2019.

23. U.S. Food & Drug Administration (FDA). Combined headspace *N*-nitrosodimethylamine (NDMA), *N*-nitrosodiethylamine (NDEA), *N*-nitrosoethylisopropylamine (NEIPA), and *N*-nitrosodiisopropylamine (NDIPA) impurity assay by GC-MS/MS. 2019.

24. U.S. Food & Drug Administration (FDA). Development and validation of a RapidFire-MS/MS method for screening of nitrosamine carcinogen impurities *N*-nitrosodimethylamine (NDMA), *N*-nitrosodiethylamine (NDEA), *N*-nitrosoethylisopropylamine (NEIPA), *N*-nitrosodiisopropylamine (NDIPA), *N*-nitrosodibutylamine (NDBA) and *N*-nitroso-*N*-methyl-4-aminobutyric acid (NMBA) in ARB drugs. 2019.

25. U.S. Food & Drug Administration (FDA). Liquid chromatography-high resolution mass spectrometry (LC-HRMS) method for the determination of six nitrosamine impurities in ARB drugs. 2019.

26. Liu J, Xie B, Mai B, Cai Q, He R, Guo D, Zhang Z, Fan J , Zhang W. Development of a sensitive and stable GC-MS/MS method for simultaneous determination of four *N*-nitrosamine genotoxic impurities in sartan substances. J Anal Sci Technol. 2021;12:1-8.

Turk J Pharm Sci 2022;19(4):462-475
DOI: 10.4274/tjps.galenos.2021.53533

REVIEW

Proniosome: A Promising Approach for Vesicular Drug Delivery

Marzina AJRIN*, Fahmida ANJUM

University of Science and Technology Chittagong, Department of Pharmacy, Chattogram, Bangladesh

ABSTRACT

Different types of drug delivery systems are intended to deliver therapeutic agents to the appropriate site of interest to get desired pharmacological effect. In the field of drug delivery, the advancement of nanotechnology helps develop novel dosage forms such as liposome, noisome, and proniosome. Proniosomes are promising drug carriers, that are dry formulations, and after hydration, are converted to noisome dispersion. Dry proniosomal powder can deliver a unit dose of the drug with improved drug stability and solubility. By using this formulation, both the hydrophilic and lipophilic drugs can be delivered through different routes like oral, topical, transdermal, vaginal, *etc*. This review revolves on different features of proniosomes such as their structure, formulation materials of proniosomes, preparation methods, evaluation, and application.

Key words: Proniosomes, vesicular drug delivery, evaluation of proniosome, application of proniosome

INTRODUCTION

A novel drug delivery system that delivers drugs at a preset rate set as *per* the need, pharmacologic aspects, drug profile, physiological conditions of the body, *etc*. In current times, no single drug delivery system meets all the standards; however, efforts are created through novel approaches.

The aim of novel drug delivery systems is targeted and controlled drug delivery. Colloidal delivery and nanotechnology have attracted the most interest because of promising systems for having a localized result.[1]

The delivery of drugs using colloidal particulate carriers such as proniosomes is dry and free-flowing preparation coated with a surfactant. To form a multi-lamellar noisome, proniosomes are rehydrated directly within minutes by transient agitation. Niosome suspension is appropriate for giving medication by different routes. They are promising candidates for industrial applications as they can transport, distribute, store, and process easily. Therefore, proniosomes can be another alternative to liposomal and other vesicular drug delivery systems for the entrapment of both polar and non-polar medications.[2]

Proniosomes improve effectivity, scale back or eliminate adverse effects and enhance therapeutic actions of medicine. They are accustomed to avoid the gastrointestinal tract incompatibility, pre-systemic metabolism, and unwanted adverse effects related to oral delivery. Additionally, they maintain therapeutic levels of drug for an extended time, decrease the frequency of administration and improve patient compliance.[3-5]

This article in brief reviews the types, fabrication, characterization, and pharmaceutical applications of proniosomes.

Structures of proniosomes

Proniosomes are microscopic lamellar structures, hexangular structures, and blackish structures, where their location is clear, semi-transparent, and semi-solid gel-like structures (Figure 1). Consistent with their methodology of preparation, proniosomes are unilamellar or multi-lamellar. They even have bilayer in their structure having hydrophilic ends that are exposed on the surface and hydrophobic chains that face one another within the bilayer inside the vesicles. Bilayer consists of non-ionic surface-active agents. To create a bilayer surfactant molecule,

*Correspondence: marzinaaj@gmail.com, Phone: +8801719234022, ORCID-ID: orcid.org/0000-0001-9331-8074
Received: 02.03.2021, Accepted: 04.06.2021

offers direction in such a way that hydrophilic ends of the non-ionic surfactant are arranged toward the outside, whereas the hydrophobic ends exist in the opposite direction. Hydrophilic drugs are placed at intervals in the area encircled within the vesicle and the hydrophobic medication is implanted within the bilayer. For association, in liquid media, proniosomes attach to cholesterol with different categories of non-ionic surfactant like alkyl radical or dialkyl polyglycerol ether.[6]

Materials used for the preparation of proniosomes

Surfactant: Surfactants, especially non-ionic surfactants are the key structural components in the preparation of proniosomes. These surfactants do not have any charge as they possess a polar head and non-polar tail. So, their stability, toxicity and compatibility is higher than other surfactants. The non-ionic surfactants have wet and emulsifying effects by which they improve the solubility and permeability of drugs. The hydrophilic-lipophilic balance (HLB) value is critical for selecting surfactants and HLB value between 4 and 8 is compatible with vesicle formation by proniosomes. It is difficult for hydrophilic surfactants to achieve a high concentration because of the high liquid solubility of hydrophilic surfactants. Therefore, aggregation and conglutination to form a proniosomal lamellar structure would be absent (Table 1).[7]

Cholesterol: Cholesterol can interact with non-ionic surfactants and regulates the physical and structural properties of proniosomes.[8] It improves the stability and rigidity of the proniosomal membrane and controls drug permeation through the membrane. Depending on the HLB value of the surfactants, the amount of cholesterol required for the preparation of proniosomes is determined. When the HLB value is above 10, the amount of cholesterol to be increased to cover the larger groups.[9] But entrapment efficiency (EE) of the prepared formulation is decreased[10] above a certain level of cholesterol, possibly due to a decrease in volume diameter.[11]

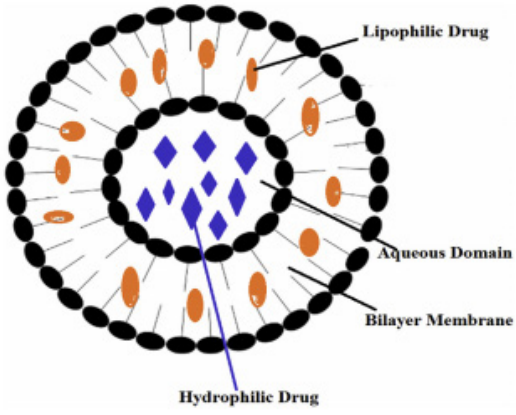

Figure 1. Structure of a proniosome

Lecithin: Lecithin is a phospholipid that acts as a membrane stabilizer in the formulation of proniosomes. The most common lecithins that are used in the formulation are soya and egg lecithin and it has been reported that hydrogenated-type lecithins have advantages over not hydrogenated lecithins, give increased rigidity of the cholesterol and help in the formation of tight vesicles.[12] Double bonds in non-hydrogenated lecithin allow the molecular chains to bend (conformational rotation), which prevents tight contact with the adjacent molecules on forming the niosomal membrane. This results in low rigidity and high permeability of the membrane.

Hydration medium: Generally, the hydration medium used in proniosomes is phosphate buffer. Depending on the solubility of the encapsulated drug, the pH of the buffer is selected.[13] Ruckmani and Sankar[14] ascertained that drug leakage increased with the increase in the volume of hydration medium but simultaneously, EE increases, when the hydration time was increased from 20 to 45 min.

Organic solvent: The solvent can act as a penetration enhancer. It also greatly affects the size of the vesicles formed. The size of the vesicle and permeation rate of the drug in a proniosomal formulation are influenced by the type of alcohol. Different sized vesicles are formed using different alcohols as they have the order: » isopropanol ‹ butanol ‹ propanol ‹ ethanol.[15]

Carrier material: Carrier materials accommodate the drug in the proniosomal formulations. Carriers should have safe, non-toxicity, free-flowing properties. They should possess low solubility in the solution of loaded, but good solubility in water for ease of hydration. They increase the surface area and impart flexibility to the proniosomes. The frequently used carrier materials are sorbitol, mannitol, maltodextrin, glucose monohydrate, spray-dried lactose, sucrose stearate, and lactose monohydrate.[16]

Table 1. Commonly used surfactants with their HLB values

Name of surfactant	M.W. (g/mol)	HLB value	Transition temperature
Span 20 (sorbitan monolaurate)	346.46	8.6	16°C
Span 40 (sorbitan monopalmitate)	402.57	6.7	42°C
Span 60 (sorbitan monostearate)	430.63	4.7	53°C
Tween 20 (polyoxyethylene sorbitan monolaurate)	522.68	16.7	-
Tween 60 (polyoxyethylene sorbitan monostearate)	648.92	14.9	-
Tween 80 (polyoxyethylene sorbitan monooleate)	604.82	15.0	-
Span 85 (sorbitan trioleate)	957.49	1.8	-

M.W.: Molecular weight, HLB: Hydrophilic-lipophilic balance

Preparation method of proniosomes

A drug that has poor aqueous solubility, low bioavailability and dissolution, poor membrane permeability, low absorption profile, excessive metabolism, variable plasma concentration, and poor patient efficiency is suitable to encapsulate into proniosomes.[17] Three methods are available for proniosomal drug formulation (Figure 2).

Slurry method

In this method, a single or a mixture of organic solvent is used in the preparation of a stock solution of surfactant and membrane stabilizer. The drug and carrier are dissolved in a membrane stabilizer solution and all the components are mixed until a slurry is formed. With the help of a rotary evaporator at specified conditions (*e.g.* 50-60 rpm, 45 ± 2°C temperature, and 600 mm of Hg pressure), the slurry is dried, and the free-flowing product is obtained. The obtained free-flowing dried material is further dried with the help of a desiccator at room temperature under vacuum to get proniosomes.[18]

Slow spray coating method

The slow spray-coating method is carried out by spraying organic solution, surfactant, cholesterol, and drug onto the carrier and then removing the solvent using a rotary evaporator under controlled conditions at 65-70°C for 15-20 min. Until the desired surfactant loading has been achieved, the process is continued and repeated. The vaporization should be carried on until the powder becomes completely dry.[19,20]

Coacervation phase separation method

Most of the proniosomal gel (PNG) is prepared by this method. In this method, exactly measured amounts of drugs, surfactants, and cholesterol are placed in a clean and dry glass vial having a wide opening. Then, the solvent is added and warmed in a water bath at 60-70°C until the surfactant and cholesterol is fully dissolved. To prevent the evaporation of the solvent, the open end of the vial should be covered with a lid. Followed by the addition of an aqueous phase in the vial, the mixture was warmed in the water bath to get a clear solution. It is then cooled at room temperature, between this time PNG is produced from the dispersion.[21]

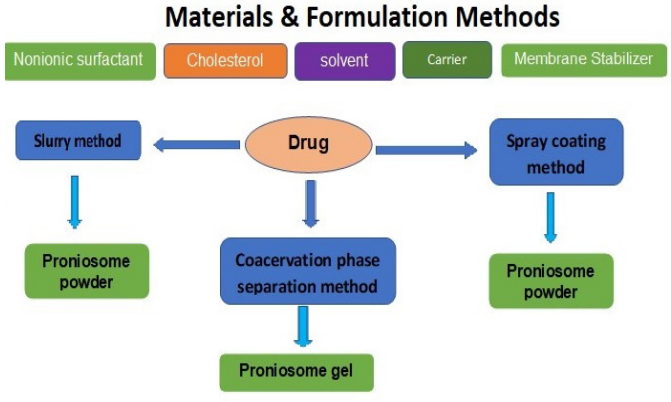

Figure 2. Schematic representation of materials and formulation methods of proniosomes

Evaluation of proniosomes

A group of properties of proniosomes can be evaluated using different methods. These methods are described below.

Vesicle size and shape

On hydration, proniosomes are converted to globular-shaped niosomes. The size and morphology of the niosomes can be determined by optical microscopy, scanning electron microscopy (SEM), photon correlation microscopy, transmission electron microscopy (TEM), and freeze-fracture electron microscopy.[22] Dynamic light scattering (DLS) method is applied to measure the vesicular size distribution. DLS essentially measure fluctuations in scattered light intensity due to diffusing particles, the diffusion coefficient of the particles can be determined. The vesicle size of the noisome is measured without agitation and with agitation. If hydration is performed without agitation, biggest size is formed.[23]

Angle of repose measurement

The angle of repose of dried proniosomes prepared using the slurry and spray coating method is measured by the funnel and cylinder technique.

Zeta potential (ZP)

The stability of the particle can be ensured with the value of ZP. This is ascribed to the electrostatic repulsion between particles with the same electric charge that causes the segregation of the particles. A high ZP value leads to increased repulsive interactions in charged particles and prevents the agglomerate formation between the particles. This ensured uniform size distribution in proniosomes. A proniosomal formulation having ZP value minimum ± 30 mV is considered a physically stable formulation. So, aggregation of particles can be avoided.[24,25]

Osmotic shock

An osmotic shock study helps in the determination of vesicle size changes. For this, the proniosomal formulations are incubated in different types of solution like hypertonic, isotonic, and hypotonic solutions for 3 h. Changes in vesicle size are detected by an optical microscope.[23]

Entrapment efficiency (EE)

To study EE, we should separate the free drug using several techniques like dialysis, gel filtration, ultracentrifugation, column chromatography, and freeze-thawing. Two techniques can be applied to measure EE. One is the destruction of the proniosomal vesicle with propane (50%) or triton (0.1%) and the entrapped drug is determined. Another method is that after the destruction of the vesicle, the un-entrapped drug is measured.[26]

The percentage of entrapment was calculated using the following formula:

$$\% \ Entrapment = \frac{ED}{TD} X\ 100$$

where ED is the amount of entrapped drug and TD is the initial amount of drug.

Drug content

The calibration curve is used to calculate drug content. For this, proniosomes are lysed with methanol in a volumetric flask by shaking for 15 min. Then, the stock solution is prepared with methanol. With the help of phosphate buffer, 10% solution is prepared from the stock solution. Aliquots are withdrawn and absorbance is measured followed by a drawing of calibration curve.[24]

Particle size (PS) measurement

One of the important criteria for prepared proniosomes is PS. With the help of SEM, the uniformity of PS and surface characteristics is measured. Optical microscopy is used to confirm the formed vesicles after hydration of proniosome.[26]

Rate of spontaneity

The rate of spontaneity is the measure of the number of niosomes formed following hydration of proniosomes. To determine the rate of spontaneity, PNG is transferred and spread uniformly along the walls of the small stoppered glass tube container. Then, NaCl (0.154 M) was added with caution and placed to one side without any turbulence. With the help of Neubauer's chamber, the number of niosomes eluted from proniosomes is calculated.[27]

In vitro dynamics study

The *in vitro* release study is a critical test to assess the safety, efficacy, and quality of nanoparticle-based drug delivery systems. *In vitro*, drug release kinetics of the prepared proniosomes can be determined using a Franz diffusion cell, Keshary-Chien diffusion cell, dialysis membrane, reverse dialysis, and United States Pharmacopeia dissolution apparatus type 1.[28]

Stability study

To ensure the stability of the prepared proniosomes, they are placed at a various temperatures, freezing temperature (2-8°C), normal temperature (25 ± 0.5°C) and elevated temperature (45 ± 0.5°C) for 1-3 months and the change in drug content and mean vesicle diameter is observed at a different time interval. The International Conference on harmonization (ICH) guidelines propose dry proniosomes powder should be studied for the accelerated stability at 75% relative humidity and 40°C as *per* international geographical zones and geographical conditions.[29]

Proniosomal drug delivery through different routes

Oral routes

The oral route of drug administration is the most preferred route for drug delivery. But bioavailability of the orally administered drug is sometimes affected by first-pass metabolism, instability in the gastric environment, low permeability through the intestinal epithelium. In some cases, absorption of the drug may be altered due to the presence of food. Thus, to improve the bioavailability of the oral drug, different nanocarriers are engaged. Oral proniosomes are one them that can solve the limitations of the conventional oral dosage form.[30] *In vitro* release kinetics of oral vinpocetine (VP) prepared using the slurry method indicated a faster release rate of reconstituted niosomes in contrast to VP suspension at pH 6.8 or 7.2 phosphate-buffered saline. *In vivo* pharmacokinetic study data also showed a better correlation with the *in vitro* data.[31] Oral acemetacin also prepared using the slurry method in proniosomal powder and tablet formulations, displayed better pharmacokinetic properties.[32] Lornoxicam is a widely used analgesic drug that belongs to the non-steroidal anti-inflammatory group. Proniosomal form of lornoxicam showed significantly higher (p<0.05) transmucosal flux across the oral mucosa than lornoxicam containing carbopol gel and the diffusion of lornoxicam was higher (more than two folds) in proniosomal formulation.[33] Proniosomal telmisartan tablets prepared with surfactants having different HLB values (span 40 and brij 35), cholesterol (20-50%), and phospholipids (egg yolk and soybean). *In vitro* as well *in vivo* comparative study showed extended drug release with a higher $C_{max.}$ The C_{max} was increased 1.5 fold while $AUC_{0-\infty}$ also increased significantly 3 fold compared with the commercial tablet. The sustained release pattern of telmisartan was indicated by t_{max}, which was increased 3 fold in contrast to conventional tablets. The relative bioavailability was also increased by 3.2 fold (Table 2).[34]

Ocular routes

Proniosomes are one of the promising methods in ocular drug delivery. In this route, PNGs in the ocular route provide several advantages like extended and sustained action, enhanced corneal residence time, prevented enzymatic degradation of drugs in tears, and ultimately improve ocular bioavailability.[35] Lomefloxacin HCl prepared using the coacervation phase separation method. The results showed that the area under the curve (AUC) of proniosomal formulation is higher (722.45 ± 0.01) than the marketed product (126.25 ± 0.049).[36] Li et al.[37] developed proniosomal formulation of tacrolimus, an immunosuppressive agent for topical ophthalmic delivery containing lecithin and poloxamer 188 as surfactants, cholesterol. *In vitro* studies in rabbit cornea of stable tacrolimus-loaded proniosomes showed enhanced precorneal permeation and retention of tacrolimus. The *in vivo* ocular irritation test of 0.1% tacrolimus-loaded proniosomes in rat eyes for 21 successive days (four times in a day) showed no irritation and good compatibility with the cornea. Proniosomes were also found to prolong the survival of corneal grafts and showed practical corneal anti-allograft rejection efficacy in the xenotransplantation model. Curcumin-loaded PNG was developed for treating ocular inflammation with the help of cremophore RH, lecithin, and cholesterol. Selected PNG showed 3.22 fold and 1.76 fold higher permeability rates than curcumin dispersion and its freeze-dried form, respectively.[38] This formulation could be an effective, better biofriendly alternative for the therapy of inflaming eyes.

Emad Eldeeb et al.[39] studied on brimonidine tartrate (BRT) proniosomal formulation used in glaucoma developed using the coacervation phase separation method. They used two surfactants having higher and lower HLB values, namely tween 80 (HLB 15) and span 60 (HLB 4.7), respectively. The results of BRT PNG showed a 7.90 fold increase in mean residence time compared to the marketed product.

Table 2. Proniosomal formulations delivered through different routes[31-58]

Route	Preparation method	*In vitro/in vivo* effects	References
Oral vinpocetine (VP)	Slurry method	VP-loaded proniosomes showed a significant improvement in the bioavailability	31
Oral acemetacin	Slurry method	Both proniosomal powder and tablet formulations showed better pharmacokinetic properties	32
Oral lornoxicam	Proliposome-liposome method	The transmucosal flux of proniosomal formulations lornoxicam across the oral mucosa was significantly higher (p<0.05) than lornoxicam containing carbopol gel and the percent drug diffused increased more than two folds	33
Oral telmisartan tablets	Slurry method	*In vitro* as well *in vivo* comparative study showed extended drug release	34
Ocular lomefloxacin HCl	Coacervation phase separation method	The results showed that the area under the curve of proniosomal formulation is higher than the marketed product	36
Ocular tacrolimus	The proliposome-liposome method	Showed enhanced precorneal permeation and retention of tacrolimus	37
Curcumin-loaded ocular proniosomal gels	Coacervation-phase method	Proniosomal gel showed enhanced permeability	38
Ocular Brimonidine tartrate (BRT)	Coacervation phase separation method	The *in vivo* pharmacodynamic study confirmed the improved ocular bioavailability of BRT selected formula compared with marketed products	39
Ocular dorzolamide-HCl	Coacervation phase separation method	*In vivo* performance of optimized dorzolamide-HCl showed sustained effect and a significant reduction in intraocular pressure	40
Cromolyn sodium nebulizer	Proniosomes were prepared according to the method developed by Hu and Rhodes[2]	High nebulization efficiency percentage and good physical stability	26
Aerosol beclometasone dipropionate (BDP) niosomes	Thin-film method	Entrapment of BDP in proniosome-derived niosomes was higher than that in conventional thin film-made niosomes	42
Vaginal tenofovir disoproxil fumarate	Coacervation phase separation	The results showed a controlled and sustained release rate	44
Vaginal terconazole	-	Results indicated that the selected formula showed good stability and provided higher mucoadhesion and retention time then the commercial product, which resulted in more efficient *in vitro* inhibition of *Candida albicans*	45
Parenteral flurbiprofen	Slurry method	Sustained anti-inflammatory activity and decreased dosing frequency	46
Parenteral letrozole (LTZ)	Slurry method	Drug release exhibited a biphasic pattern, being fast at the first 24 h (up to 65% released) followed by a very slow-release phase for one month, releasing at least 95%. Overall, in this study, a facile approach to generating niosomes incorporating LTZ using a slurry-based proniosome technology was demonstrated	47
Transdermal piroxicam	Coacervation phase separation method	Maximum flux achieved was 35.61 µg/cm^2/h, an enhancement of 7.39 times achieved for the transdermal system based on proniosomal gel as compared to control gel	48

Table 2. continued

Route	Preparation method	*In vitro/in vivo* effects	References
Transdermal ketoprofen	Slurry method	Showed significantly higher cumulative amount of drug permeated and steady-state transdermal flux compared to plain gel	49
Transdermal meloxicam	Coacervation phase separation method	The prepared proniosomes significantly improved drug permeation and reduced the lag time ($p<0.05$). Proniosomes prepared with span 60 provided a higher meloxicam flux across the rat skin than those prepared with tween 80. Testing of the anti-inflammatory effect of meloxicam proniosomal gel showed better pharmacological activity compared with the standard meloxicam gel	50
Transdermal celecoxib	Coacervation phase separation method	The selected proniosomal gel produced 100% inhibition of paw edema in rats up to 8 h after carrageenan injection. It produced 95% and 92% inhibition after 12 h and 24 h, respectively	51
Transdermal tenoxicam	Coacervation phase separation method	The investigated tenoxicam loaded proniosomal formula proved to be non-irritant, with significantly higher anti-inflammatory and analgesic effects compared to that of the oral market tenoxicam tablets	30
Transdermal fluconazole	Coacervation phase separation method	The results showed a well-defined spherical vesicle with sharp boundaries. Moreover, this formulation showed an excellent microbiological activity represented by a greater zone of inhibition (5.3 cm)	52
Transdermal estradiol	Coacervation phase separation method	The proniosome gel provided a higher permeation flux of estradiol across the skin compared with the noisome suspension	53
Dermal boswellic acid	Coacervation phase separation method	*In vitro*, skin permeation study showed the most sustained release in 24 h	54
Transdermal atorvastatin calcium (ATC)	Coacervation phase separation method	Results suggest a promising, easy-to-manufacture, and effective ATC proniosomal gel for the safe treatment of hyperlipidemia	55
Transdermal cilostazole (CLZ)	Coacervation phase separation method	The CLZ-loaded proniosomes showed promising results with high potential to delivery it across the skin	56
Transdermal CLZ	Coacervation phase separation method	The results suggested that clozapine could be effectively loaded into proniosomal gel for administration through the skin	57
Transdermal galantamine hydrobromide	Coacervation phase separation method	The *in vitro* drug diffusion studies revealed that the proniosomal gel containing tween 80 showed maximum drug diffusion (99.24%) and the gel containing span 20 showed minimum drug diffusion (71.74%)	58
Intranasal duloxetine	Coacervation phase separation method	Result showed significantly improved permeation enhancement and stability with better control over drug release for a longer period through intranasal administration	54

Simultaneously, the relative area under the plasma concentration-time curve over the last 24 h dosing interval (AUC_{0-24}) value was also increased to 5.024 folds. Draize test also ensured that the formulations had no ocular irritation.[39] Dorzolamide-HCl (Dorz) is an anti-glaucoma drug soluble in water. The PNG of this drug was developed to sustain its effect and to reduce dosing frequency. Here, the gel was developed by using L-α-lecithin, cholesterol, span 40 using the coacervation phase separation method. *In vivo* results showed a maximum reduction in intraocular pressure (IOP) of 32.6 ± 2.7 at 1.5 h. On the contrary, the PNG showed a sustained decrease in IOP with a maximum value of 45.4 ± 8.2 at 6 h, which was significantly

higher than standard formulation. Even after completion of the experimental period (8 h), the % dec in IOP was 19.5 ± 9.2. This implies a prolonged release of Dorz PNG from the optimized formulation.[40]

Pulmonary routes

With the aid of the pulmonary route, one can easily treat respiratory diseases than other delivery methods. Through this route, drugs can be directly applied within the lungs. Drug-loaded particles like liposomes dispensed through aerosol can easily distribute to the bronchi and lungs and prolong the release of the drug. Liposomal delivery also has minimum systemic side effects due to localized action to the lungs. But liposomes may be degraded by oxidation or hydrolysis. So, the proniosome can be an option to overcome the limitations of the liposome.[41]

For pulmonary drug delivery, the air-jet nebulizer is known very well. Proniosome-derived niosomes of cromolyn sodium were prepared by Abd-Elbary et al.[26] They used sucrose stearates in the formulation. The results exhibited a controlled release of drugs from the proniosome-derived niosomes compared to standard drug solution. Furthermore, high nebulization efficiency and physical stability were also achieved.[26]

Likewise, aerosol properties of beclometasone dipropionate (BDP) niosomes using Aeroneb Pro and Omron Micro Air vibrating mesh nebulizers and Pari LC Sprint air-jet nebulizer were investigated by Elhissi et al.[42] The study demonstrated that the satisfactory EE of BDP in proniosome-derived niosomes and the value was higher than that in conventional thin film-made niosomes.[42]

Vaginal routes

Vaginal drug delivery is one of the favorable routes to target the disease associated with female health issues. It offers both the local and systemic delivery of drugs. Usually, different categories of drugs like antibiotics, antifungal, antiprotozoal, antiviral, labor-inducing agents, spermicidal agents, steroids, *etc.* are delivered through the vaginal route.[43] PNG has excellent mucoadhesive properties and provides a constant release pattern, which is very useful for vaginal drug delivery. Tenofovir disoproxil fumarate (TDF) is an antiretroviral drug (a nucleotide analog) that works through the inhibition of viral reverse transcriptase. PNG of TDF was prepared with the help of cholesterol, surfactants (span 20, 40, 60, 80, tween 20 and 80), lecithin by coacervation phase separation method. A comparative *in vivo* dissolution study was conducted between proniosomes suppository, drug suppository and PNG formulations for 24 h using cellophane membrane, our results indicated the proniosomal suppository. Another result revealed a controlled and sustained release rate compared to the other two formulations.[44] Terconazole, an antifungal drug, PNGs were developed on the basis of span 60 and brij 76 in different molar ratios (1:1, 1:1.5, and 1:2) relative to cholesterol. The results displayed that increased concentration of cholesterol relative to the surfactant affected both EE and vesicle size of niosomes prepared by incorporating into 1% carbopol gel. Drug release profiles from different prepared PNG formulations in simulated vaginal fluid studied in comparison with the commercial product of terconazole for 24 h. Depending on the high EE % and *in vitro* release profile, selected formulation was further evaluated for stability, mucoadhesion to the vaginal mucosa and inhibition of candida growth. Results indicated that the selected formula was in good stability and provided higher mucoadhesion and retention time than the commercial product, which resulted in more efficient *in vitro* inhibition of *Candida albicans*.[45]

Parenteral routes

In parenteral drug delivery, targeted and sustained drug release at a predetermined rate can be achieved due to remarkable advancement in pharmaceutical technology. Flurbiprofen[46] and letrozole[47] are prepared by the slurry method. Both drugs showed sustained activity and reduced dosing frequency.

Dermal and transdermal routes

The dermal route is employed for local action only to treat different types of skin disease. This route can avoid systemic effects and therefore offers fewer side effects. However, through transdermal delivery, we can deliver drugs for systemic action. But in both the dermal and transdermal drug delivery, the skin prevents the penetration of drugs. Vesicular drug delivery can be used to overcome this problem.

Non-steroidal anti-inflammatory drugs (NSAIDs) such as piroxicam,[48] ketoprofen,[49] meloxicam,[50] celecoxib,[51] and tenoxicam[30] are planned to avoid gastrointestinal adverse effects. Here, all the NSAIDs except ketoprofen are prepared by the coacervation phase separation method, whereas ketoprofen is prepared by the slurry method.

Fluconazole-loaded PNGs were prepared by the coacervation phase separation method using different non-ionic surfactants (spans and tweens). The prepared fluconazole PNGs were evaluated for various parameters such as PS, drug EE %, and *in vitro* drug release. The experimental results showed that the EE % for the prepared formulae are acceptable (85.14-97.66%) and they are size (19.8-50.1 nm). The planned gel also showed sustained drug release. The formulation, which was prepared from span 60:tween 80 (1:1), and cholesterol showed highest EE % and gave slow release (40.50 ± 1.50% after 6 h), was subjected to ZP test, TEM as well as microbiological study. The results indicated a well-defined spherical vesicle with sharp boundaries and good physical stability of fluconazole within the prepared gel. Moreover, this formulation showed an excellent microbiological activity represented by a greater zone of inhibition (5.3 cm) compared with control gel (fluconazole in 2% hydroxy propyl methyl cellulose gel formula) (4.2 cm) and plain gel with no drug (0 cm) against *C. albicans*.[52] Fang et al.[53] studied transdermal estradiol gel and the results provided a higher permeation flux of estradiol across the skin. *In vitro* skin permeation study of dermal boswellic acid gel, was studied for 24 h, and a sustained release pattern was observed (84.83 ± 0.153 mg/cm^2). Inhibition of inflammation of the proniosomal patch was also significantly (p<0.001) higher compared to the marketed gel at the same dose.[54]

In an attempt to modify the anti-hyperlipidemic effect and to reduce statins-induced hepatotoxicity, atorvastatin calcium (ATC) transdermal PNG was developed by a coacervation phase separation method. Different non-ionic surfactants (spans, tweens, cremophor RH 40, and brij 52) were incorporated in the vesicle's lipid bilayer, along with lecithin. PNG gel was characterized for encapsulation EE %, vesicle size, polydispersity index (PDI), and ZP. The results revealed nano-sized (≤350 nm) range vesicles with relatively high ATC EE (70.12-88%). *Ex vivo* results of the selected formulation demonstrated the permeation superiority of ATC proniosomes over free drugs. The selected PNGs showed significantly high flux ranging from 4.23 to 8.46 μg/cm^2 h - 1 with permeability coefficient values (P) (0.004-0.008 cm/h) when compared to free ATC dispersion, which significantly possessed lower flux and permeability coefficient results (2.92 μg/cm^{2}h - 1 and 0.003 cm/h respectively). The pharmacodynamic study revealed that transdermal administration of ATC-PNG succeeded in retaining the antihyperlipidemic efficacy of orally administered ATC without elevating liver biomarkers. Histological examination signified the role of optimized ATC-PNG in hindering statin-induced hepatocellular damage.[55] Transdermal cilostazole (CLZ) proniosomes were prepared by a coacervation phase separation technique. The optimum formula composed of 540 mg span 60 and 59.7 mg of cholesterol, had the highest EE % of (75.125 ± 0.125%), PS of (300.3 ± 0.2 nm), ZP of (-39.35 ± 0.15 mV), the percentage of the drug released after 2 h was (24.32 ± 0.13%) and after 24 h was (81.175 ± 0.325%). The safety of the proniosomes for topical application was confirmed by the histopathological examination. The CLZ-loaded proniosomes showed promising results with high potential to delivery it across the skin.[56] CLZ loaded PNG was prepared by the coacervation phase separation method using span 60, cholesterol, and lecithin. The optimized formulation had the highest EE of 90% and an average PS of approximately 325 nm PDI reflected homogeneity in the formulation. ZP was -59.76 mV, high enough to indicate a stable formulation. The *in vitro* release studies manifested a sustained release behavior of clozapine from the PNG. The *ex vivo* permeation demonstrated noteworthy permeation of the drug through *stratum corneum* with a steady state flux of 18.26 ug/cm^2/hr.[57] Galantamine hydrobromide (HBr) is used for treating Alzheimer's disease and is described as proniosome gel by coacervation phase separation method to overcome the side effects of oral delivery. Microscopical observations of the gels showed vesicles of optimum size from 3.030 - 3.735 mm. The gel also showed an optimum rate of spontaneity in the range 9.60 mm^3 x 1000 to 11.80 mm^3 x 1000 and EE of vesicles in the range 66.15% to 86.92%. The gels had pH in suitable range of skin (5.92-6.9). The *in vitro* drug diffusion studies revealed that the PNG containing tween 80 showed maximum drug diffusion (99.24%), whereas the gel containing span 20 showed minimum drug diffusion (71.74%).[58]

Intranasal routes

The nasal drug delivery method has some limitations like mucociliary clearance, degradation of drugs by the enzyme. Vesicular drug delivery systems can circumvent these limitations. Duloxetine (DX) is a new norepinephrine reuptake inhibitor used for treating depression. But it has high first-pass metabolism and low bioavailability (<50%) following oral administration, eventually leading to low cerebrospinal fluid concentrations. Khatoon et al.[59] designed mucoadhesive thiolated chitosan (TCS) gel containing proniosomes of DX for intranasal drug delivery to enhance the drug's contact time with nasal mucosa, bypass the first-pass effect and target the brain possibly using the olfactory pathway. Here, soya lecithin, cholesterol, and tween 80 was used in the preparation of the gel. pH of the DX-loaded proniosomal gel (D-MPNG) was 5.67 ± 0.145, indicating the compatibility of formulations within the nasal cavity without producing irritation. Notably, D-MPNG exhibited better control, releasing only 24% DX at pH 7.4 over 24 h compared to 78% release at pH 5.5. The presence of thiol groups of TCS significantly controls water uptake, resulting in moderate swelling and higher viscosity; thus, providing a sustained effect for a longer period.[59]

Cosmeceuticals application of proniosomes

Cosmeceuticals are generally used to refer to skincare products that contain active ingredients that are beneficial for improving the skin's appearance and promoting healthy skin.[60] Anti-aging cosmeceuticals are most frequently recommended by physicians, who use them as an integral part of a comprehensive skin rejuvenation program. Moisturizers and serum containing ingredients such as vitamin C, niacinamide, retinol, peptides, growth factors, and botanicals can all be used in this regard. Additionally, patients undergoing cosmetic procedures such as laser resurfacing and chemical peels may be given cosmeceuticals to prime the skin for procedures, encourage healing, and reduce complications after. Cosmeceuticals are also recommended for patients with acne, rosacea, eczema, and other skin conditions, where they are commonly used along with prescription medications. For example, moisturizers containing anti-inflammatory botanical ingredients may be used in conjunction with prescription medications for treating rosacea. Cosmeceuticals containing soy can be used to provide added skin lightening benefits when paired with hydroquinone.

Applying therapeutic and cosmetic agents onto or through skin requires a non-toxic, dermatologically acceptable carrier, which not only controls the release of the agent for prolonging action but also enhances the penetration to the skin layer.[61] Proniosome gel meets such criteria, which are useful for the delivery of cosmetics and cosmeceuticals. The therapeutic agents which can be used for incorporation into proniosomal carrier systems include, moisturizing, nutritional, anti-wrinkle, anti-aging, cleansing, sunscreen particles, *etc*.

Proniosome is a potentially scalable method to produce niosomes for the delivery of hydrophobic or amphiphilic drugs.[62] Anti-aging cream containing the methanolic purple glutinous rice extract loaded in niosomes was developed by Manosroi et al.[63] Anthocyanin present in purple glutinous rice extract is responsible for the anti-aging activity. After 6 cycles of heating and cooling test, the formulation with 1% w/v of the purple glutinous rice extract contained 52.28% anthocyanin of

the initial. For *in vivo* antiaging activities, a cream containing niosomes loaded with the extract gave significantly decreased melanin index and skin roughness reduction of 14.05 and 9.95% of the initial, respectively. The percentage changes of the increased skin hydration, skin elastic extension, and skin elastic recovery when applied on human volunteers' skin with this formulation were +48.73, 24.51, and +35.98%, respectively

Tretinoin (TRT) is a widely used retinoid for the topical treatment of acne, photo-aged skin, psoriasis, and skin cancer. TRT-loaded proniosomes were prepared by the slurry method with the help of span 60 and D-sorbitol, span 40, cholesterol 95% stabilized, and tween 20.[64] prepared hydrated proniosomes were characterized by an evaluation of PS, the effect of drug concentration, EE, *etc*. EE of all hydrated proniosomal dispersions ranged from 76.6 ± 0.001% prepared to use span 40 to 94.15 ± 0.041% prepared using span 60. *In vitro* drug release was increased till 5th hour.

Diferuloylmethane or curcumin is obtained from turmeric, which possesses infiammatory properties blocking the formation of reactive oxygen species.[65] Proniosomes of curcumin were prepared using non-ionic surfactants (tween 80, span 60) either solely or in combination with cholesterol. The highest encapsulation efficiency of curcumin in niosomal formulations was 99.74%. Kinetically, niosomes fitted to the Korsmeyer-Peppas model with non-Fickian transport. The anti-inflammatory activity of curcumin in various formulations was evaluated using a rat hind paw edema method and the percentage of swelling was 17.5% following 24 h in the group treated with curcumin niosomal emulgel.[66]

Coenzyme Q10 (CoQ10) also known as ubiquinone, an essential compound is found in every cell of the human body. CoQ10, an essential compound of cellular bioenergetics, also acts as a strong antioxidant and protects the body against aging.[67] CoQ10 proniosomes were prepared using the standard method with the help of Q10, span 85, soya lecithin, and cholesterol. *In vitro* drug release of CoQ10 followed a special cubic model, as the statistics of the chosen model were found significant (p= 0.0006). The change in the levels of soy lecithin had a great impact and showed a synergistic effect on the release characteristics. A skin permeation study showed that the cumulative amount of CoQ10 permeated in 12 h was found to be 515.85, 463.25, and 507.49 mg/cm^2, respectively for selected PNG formulations. Animal skin was treated with UV radiation followed by treatment of PNG CoQ10 and conventional CoQ10 present in a gel base. The effectiveness of the treatment was evaluated based on biochemical estimation and histopathological studies. By using CoQ10 PNG formulation, levels of superoxide dismutase, catalase, glutathione, and total proteins were restored by 81.3%, 72.1%, 74.8%, and 77.1%, respectively to that of the control group. Histopathological studies revealed better protection of skin treated with CoQ10 PNG compared to free CoQ10. The prepared PNG did not interact with the normal histology and, hence, tolerated by the animal skin compared to conventional gel. Assessments of the formulations for various enzymatic and non-enzymatic estimations in animal skin after UV irradiation proved the efficacy of the developed formulation.

Proniosomal formulations containing the natural antioxidant resveratrol (*trans*-3,5,4′-trihydroxystilbene, RSV) were prepared by Schlich et al.[68] RSV is a polyphenol compound having anti-inflammatory,[69] neuroprotective,[70] anti-aging,[71] and anticancer effects.[72] Proniosomal powders were prepared by the slurry method and characterized. The hydration and sonication of proniosomes resulted in the formation of lipid nanoparticles with a mean diameter in the range 180-300 nm and a highly negative surface charge. RSV release from proniosome-derived niosomes was investigated in simulated gastric and intestinal fluid. biocompatibility assay carried out on intestinal cells (Caco2) demonstrated that proniosomes prepared with an HLB of 13.5 were significantly less toxic than their HLB16.7 counterpart. All the tested formulations could be employed safely at the doses commonly administered by the oral route.

Canthaxanthin (CTX) is a xanthophyll (a subclass of carotenoids) with widespread applications in pharmaceutical and cosmetic industries. It is a superior antioxidant and scavenger of free radicals compared with carotenoids such as β-carotene.[73] CTX was encapsulated in proniosome powders, which were were prepared with an equimolar ratio of span 60/cholesterol and four different carriers, namely, maltodextrin, mannitol, lactose, and pullulan.[74] The study showed that the niosomes produced by hydration and sonication of the proniosomes were small (≤200 nm) and quite homogeneously dispersed (PDI ≤0.3). The encapsulation efficiency of CTX in formulations varied between 55.3 ± 1.8% and 74.1 ± 2.7% after hydration and sonication. Although light and high temperatures affected the stability of CTX drastically, encapsulation in proniosomes retarded its degradation. This formulation can provide convenient, non-toxic, and inexpensive vehicles for dissolving and stabilizing CTX in functional food products.

O-padimate is a UV-B filter widely used as a sunscreen agent. A study investigated the combined influence of 3 independent variables in the preparation of *O*-padimate proniosomes, which were prepared by the slurry method with span: Brij, surfactant. The developed gels were characterized for vesicle size, morphology and EE, skin permeation studies, rheological properties, and sun protection factor (SPF). Results reveal that optimized *O*-padimate proniosomal formulations showed high SPF and low transepidermal water loss.[75]

Rutin (Rut) is a natural flavonol that has various therapeutic properties including antioxidant and antitumor activities. Rut PNG for cutaneous applications was designed to improve the poor aqueous solubility of Rut. The gel was prepared by the coacervation phase-separation method and complies with the standard requirements in terms of PS (140.5 ± 2.56 nm), ZP (-27.33 ± 0.09 mV), encapsulation capacity (>50%), pH (7.002 ± 0.18), and rheological properties. The results showed high biocompatibility of the gel on the 3D reconstructed human epidermis model characterized by increased viability of the cells and lack of irritant and phototoxic potential. The values on 2D cells confirmed the preferential cytotoxic effect of Rut on melanoma cells (IC_{50} value: 8.601 µM, nuclear fragmentation) compared with normal keratinocytes. Our data suggest that the

PNG is a promising drug carrier for Rut in the management and prevention of skin disorders.[76]

Clinical trials with proniosomes

Selected proniosomal formulation of VP was tested *in vivo* to compare the pharmacokinetics of VP from a proniosomal patch containing VP (treatment A) to an oral commercial tablet containing the same dose of VP (treatment B) using a non-blind, two treatment, two-period, randomized, crossover design.[77] Twelve healthy non-smoking male volunteers (26-37 years, 78-96 kg) participated in the study and were randomly assigned to one of the two treatment groups of equal size. The study results showed significant differences in the shape of the concentration-time courses between the two treatments. For VP oral tablet a rapid sharp peak was found at 1.5 h followed by a fast decline in plasma drug levels. However, for the VP proniosomal patch, the absorption was much slower and extended over a longer period. Moreover, the patch exhibited higher drug levels in the plasma from 6 to 12 h compared to the tablet. The average C_{max} was significantly lower (p<0.05) for the patch (12.44 ± 1.87 ng/mL) compared with the oral tablet (63.69 ± 8.32 ng/mL), while t_{max} was significantly higher (p<0.05) in the case of the transdermal patch (12 h) compared with the oral tablet (1.5 h). The extent of absorption of VP from the patch expressed by AUC_{0-t} was determined to be about 101% larger and statistically significantly different compared to the oral tablet. The relative bioavailability of VP proniosomal patch to the oral tablet was estimated to be on average 206%. The elimination half-lives of VP after oral and transdermal administration were 1.36 ± 0.27 h and 13.94 ± 1.2 h, respectively, and were statistically significant (p<0.01).[77]

TRT-loaded proniosomes were prepared by the slurry method with the help of span 60 and D-sorbitol, span 40, cholesterol 95% stabilized, and tween 20. The planned PNG was studied clinically on 12 Egyptian patients aged more than 18 years [2 males and 10 females; with an average of 20 (± 4 years) with acne (papules, closed comedones, and open comedones)] on their face.[64] The result showed only very slight erythema (score: 0.143 ± 0.377) for TRT PNG compared to 0.025% TRT gel (score: 1.70 ± 0.755). Similarly, the marketed product displayed an erythema score of 1.50 ± 0.534 and could not diminish the irritation caused by topical application of TRT. The overall improvement of the individual lesions was also better than the marketed product during the 4 week study period.

Niosomal (hydrated form of proniosome) benzoyl peroxide (BPO) and clindamycin (CL) lotion was prepared and compared with niosomal CL in *acne vulgaris*. In both cases, the concentration of the drug was 1%. A double-blind clinical trial study on 100 patients with *acne vulgaris* was conducted in Afzalipour Hospital in Kerman (Iran).[72] The efficacy of treatment protocols was evaluated in the 2nd, 4th, 8th, and 12th weeks of treatment by counting lesions (severity and grading acne lesions) and quality of life. Furthermore, the side effects were evaluated at each treatment visits. The reduction in the mean percentage of acne lesions in the case group (treated with BPO 1% and CL 1%) (64.21%) was higher than that the control group (treated with niosomal CL 1%) (59.04%), but the statistical difference was not significant. A sum of excellent and good results was found in 80% and 76.1% of the case and control groups, respectively (p= 0.377). Also, adding BPO to the treatment formulation in the case group did not increase adverse effects, as the statistical difference between the 2 groups was not significant (Table 3).[78]

Table 3. Brief description of patents on proniosomes

Patent application IDs	Inventors	Title	Patent description in brief	References
CN103340823A	Qiang L, Bin Z, Li L, Hongxia Z, Shasha L, Xiao J	Formulation of paeonol proniosomes and preparing method thereof	Paeonol proniosomes are an effective method for solving the problems of easy aggregation and easy fusion of niosomes and leakage of drugs in a solution state and a storage process of the non-ionic surfactant noisomes. The paeonol proniosomes can be directly applied to skins, and also can be prepared into a gel agent, an ointment, a patch and other transdermal drug delivery formulations	79
1288/DEL/2012	Yadav K, Yadav D, Nanda S, Saroha K	Curcumin proniosomal/ niosomal formulation, method for it is preparation and use thereof	Niosomal/proniosomal vesicular system can improve the dispersibility of curcumin and thus providing advantage to make curcumin in administrable or applicable form for it is cosmetic/therapeutic/medical purposes	80
3228/DEL/2012	Garg M, Joon M	Novel proniosomal gel of *Withania somnifera*	This invention relates to preparation of proniosomal gel of standardised *Withania somnifera* leaves extract, for better bioavailability, anti-inflammatory activity, to be used as transdermal application	81

Table 3. continued

Patent application IDs	Inventors	Title	Patent description in brief	References
3231/DEL/2012	Garg M, Garg P	Novel ursolic acid loaded proniosomal gel and method of preparation thereof	Ursolic acid is a well-known anti-inflammatory bioactive compound. This invention relates to the preparation of ursolic acid loaded proniosomal gel by coacervation phase separation method	82
U.S. Patent US 6051250A	Ribier A, Jean-Thierry S	Process for the stabilization of vesicles of amphiphilic lipid(s) and composition for topical application containing the said stabilized vesicles	This invention relates to a process for stabilization of vesicles formed from a lipid-phase membrane containing at least one ionic and/or non-ionic amphiphilic lipid encapsulating an aqueous phase, in the form of a dispersion in an aqueous phase, by addition of at least one stabilizing agent to the aqueous dispersion phase	83
U.S. Patent US 4830857A, 1989	Handjani R, Ribier A, Vanlerberghe G, Zabotto S, Griat J	Cosmetic and pharmaceutical compositions containing niosomes and a water-soluble polyamide, and a process for preparing these compositions	This invention relates to a composition consisting of a dispersion in an aqueous medium of niosome and/or liposome spherules, within which an aqueous phase is encapsulated, at least one portion of the spherules being niosomes. The formulation is usable in cosmetics or pharmaceuticals	84
CN105311638A	Jianfang F, Kaili H, Helong L, Mei L, Luting W	Drug-carrying precursor vesicle, preparation method and application thereof	In this invention drug-carrying precursor vesicle can form homogeneous and mono-dispersed vesicles after hydration, has excellent stability, can significantly promote oral absorption and improve the bioavailability of poorly soluble drugs, and also has significant slow-releasing effect and is suitable for large-scale production	85
WO2000042987A8	Singh A and Jain R	Targeted vesicular constructs for cytoprotection and treatment of *Helicobacter pylori* infections	A novel composition for targeted vesicular constructs for treatment of *H. pylori* infections and for protection of the cell is disclosed	86
KR20040058196A	Young C, Lee W, Keith, Kwang-Ho	Pro-micelle pharmaceutical compositions	The present invention provides a composition containing a pharmaceutically active drug encapsulated with an esterified C_l-C_{i8} fatty acid membrane. The result of the conversion of the micelles (pro-micelle) - are pharmaceutically that effectively deliver the active drug in systemic circulation procedure	87
EG24388A	Abd-Elbary A, El-laithy HM, Tadros MI	A method for the preparation of nebulizable micronized niosomes of cromolyn sodium using non-ionic surfactants	This invention involves the controlling the rate of drug release after inhalation so that biological half-life could be increased, consequently number of doses (4 - 6 daily) should be reduced	88

CONCLUSION

Proniosomes could be a promising vesicular drug delivery method for the future. They are one of the drug carriers in vesicular drug delivery methods, which is a better alternative to liposomal drug delivery due to its controlled and sustained action and provide better physical, chemical stability, and potentially scalable for commercial viability. They offer excellent potential for improved drug delivery through versatile routes such as oral, parenteral, dermal, transdermal, ocular, vaginal, pulmonary, and nasal by overcoming the permeation barriers faced by several drugs. Different types of unit dosages form like tablets, capsules, and beads can be prepared with the dry form of proniosomes. Due to the versatility of proniosomes, they are widely investigated as drug carriers. There is a lot of scope to investigate new carrier materials for the preparation of proniosomes and their potential remains to be investigated to the full extent.

Ethics

Peer-review: Externally and internally peer-reviewed.

Authorship Contributions

Concept: M.A., Design: M.A., F.A., Data Collection or Processing: F.A., Analysis or Interpretation: M.A., F.A., Literature Search: M.A., F.A., Writing: M.A., F.A.

Conflict of Interest: No conflict of interest was declared by the authors.

Financial Disclosure: The authors declared that this study received no financial support.

REFERENCES

1. Singla S, Harikumar S, Aggarwal G. Proniosomes for penetration enhancement in transdermal system. Int J Drug Dev Res. 2012;4:1-13
2. Hu C, Rhodes DG. Proniosomes: a novel drug carrier preparation. Int J Pharm. 1999;185:23-35. Corrected and republished in: Int J Pharm. 2000;206:110-22.
3. Naik A, Kalia YN, Guy RH. Transdermal drug delivery: overcoming the skin's barrier function. Pharm Sci Technol Today. 2000;3:318-326.
4. Hiroyuki O, Makino K, eds. Colloid and interface science in pharmaceutical research and development. Elsevier, 2017.
5. Prausnitz MR, Langer R. Transdermal drug delivery. Nat Biotechnol. 2008;26:1261-1268.
6. Walve JR, Rane BR, Gujrathi NA, Bakaliwal SR, Pawar SP. Proniosomes: a surrogate carrier for improved transdermal drug delivery system. Int J Res Ayurveda Res. 2011;2:743-750.
7. Sivaprasad SN, Kumar PL, Srinivas M, Brahmaiah B, Nama S. Proniosome: a novel approach to vesicular drug delivery system. Int J Drug Discov. 2013;3:85-90.
8. Nasseri B. Effect of cholesterol and temperature on the elastic properties of niosomal membranes. Int J Pharm. 2005;300:95-101.
9. Uchegbu IF, Vyas SP. Non-ionic surfactant-based vesicles (niosomes) in drug delivery. Int J Pharm. 1998;172:33-70.
10. Bouwstra JA, van Hal DA, Hofland HEJ, Junginger HE. Preparation and characterization of nonionic surfactant vesicles. Colloids Surf A Physicochem Eng Asp. 1997;123-124:71-80.
11. Pardakhty A, Varshosaz J, Rouholamini A. *In vitro* study of polyoxyethylene alkyl ether niosomes for delivery of insulin. Int J Pharm. 2007;328:130-141.
12. Morakul B, Junyaprasert VB. Proniosomes: an effective carrier for dermal and transdermal delivery. Songklanakarin J Sci Technol. 2020;42:1171-1186.
13. Bhardwaj P, Tripathi P, Gupta R, Pandey S. Niosomes: a review on niosomal research in the last decade. J Drug Deliv Sci Technol. 2020;56:Part A:101581.
14. Ruckmani K, Sankar V. Formulation and optimization of zidovudine niosomes. AAPS PharmSciTech. 2010;11:1119-1127.
15. Sahoo RK, Biswas N, Guha A, Kuotsu K. Maltodextrin based proniosomes of nateglinide: bioavailability assessment. Int J Biol Macromol. 2014;69:430-434.
16. Akhilesh D, Faishal G, Kamath JV. Comparative study of carriers used in proniosomes. Int J Pharm Chem Sci. 2012;1:164-173.
17. Ahmad MZ, Akhter S, Mohsin N, Abdel-Wahab BA, Ahmad J, Warsi MH, Rahman M, Mallick N, Ahmad FJ. Transformation of curcumin from food additive to multifunctional medicine: nanotechnology bridging the gap. Curr Drug Discov Technol. 2014;11:197-213.
18. Blazek-Welsh AI, Rhodes DG. SEM imaging predicts quality of niosomes from maltodextrin-based proniosomes. Pharm Res. 2001;18:656-661.
19. Mishra A, Kapoor A, Bhargava S. Proniosomal gel as a carrier for improved transdermal drug delivery. Asian J Pharm Life Sci. 2011;1:370-379.
20. Jadhav KR, Pawar AY, Bachhav AA, Ahire SA. Proniosomes: a novel non-ionic pro-vesicles as potential drug carrier. Asian J Pharm Sci. 2016;10(Suppl):S210.
21. Azeem A, Jain N, Iqbal Z, Ahmad FJ, Aqil M, Talegaonkar S. Feasibility of proniosomes-based transdermal delivery of frusemide: formulation optimization and pharmacotechnical evaluation. Pharm Dev Technol. 2008;13:155-163.
22. Malhotra M, Jain NK. Niosomes as drug carriers. Indian Drugs. 1994;31:81-86.
23. Biju SS, Talegaonkar S, Mishra PR, Khar RK. Vesicular systems: an overview. Indian J Pharm Sci. 2006;68:141-153.
24. Keservani RK, Sharma AK, Ayaz MD. Novel drug delivery system for the vesicular delivery of drug by the niosomes. Int J Res Control Release. 2011;1:1-8.
25. Kumar GP, Rao PR. Nonionic surfactant vesicular systems for effective drug delivery – an overview. Acta Pharm Sinica B. 2011; 1:208-219.
26. Abd-Elbary A, El-Laithy HM, Tadros MI. Sucrose stearate-based proniosome-derived niosomes for the nebulisable delivery of cromolyn sodium. Int J Pharm. 2008;357:189-198.
27. Vardhani S, Nirosha M, Chandrashekar KB. Proniosomal gel- an effective approach for topical and transdermal drug delivery. Int J Res Pharm Sci. 2016;7:179-183.
28. Radha GV, Rani TS, Sarvani B. A review on proniosomal drug delivery system for targeted drug action. J Basic Clin Pharm. 2013;4:42-48.
29. Yasam VR, Jakki SL, Natarajan J, Kuppusamy G. A review on novel vesicular drug delivery: proniosomes. Drug Deliv. 2014;21:243–249.
30. Ammar HO, Ghorab M, El-Nahhas SA, Higazy IM. Proniosomes as a carrier system for transdermal delivery of tenoxicam. Int J Pharm. 2011;405:142-152.

31. Song S, Tian B, Chen F, Zhang W, Pan Y, Zhang Q, Yang X, Pan W. Potentials of proniosomes for improving the oral bioavailability of poorly water-soluble drugs. Drug Dev Ind Pharm. 2015;41:51-62.
32. Shehata TM, Abdallah MH, Ibrahim MM. Proniosomal oral tablets for controlled delivery and enhanced pharmacokinetic properties of acemetacin. AAPS PharmSciTech. 2015;16:375-383.
33. Abdelbary GA, Aburahma MH. Oro-dental mucoadhesive proniosomal gel formulation loaded with lornoxicam for management of dental pain. J Liposome Res. 2015;25:107-121.
34. Teaima MH, Yasser M, El-Nabarawi MA, Helal DA. Proniosomal telmisartan tablets: formulation, *in vitro* evaluation and *in vivo* comparative pharmacokinetic study in rabbits. Drug Des Devel Ther. 2020;14:1319-1331.
35. Kuzmov A, Minko T. Nanotechnology approaches for inhalation treatment of lung diseases. J Control Release. 2015;219:500-518.
36. Khalil RM, Abdelbary GA, Basha M, Awad GE, El-Hashemy HA. Design and evaluation of proniosomes as a carrier for ocular delivery of lomefloxacin HCl. J Liposome Res. 2017;27:118-129.
37. Li Q, Li Z, Zeng W, Ge S, Lu H, Wu C, Ge L, Liang D, Xu Y. Proniosome-derived niosomes for tacrolimus topical ocular delivery: *in vitro* cornea permeation, ocular irritation, and *in vivo* anti-allograft rejection. Eur J Pharm Sci. 2014;62:115-123.
38. Aboali FA, Habib DA, Elbedaiwy HM, Farid RM. Curcumin-loaded proniosomal gel as a biofreindly alternative for treatment of ocular inflammation: *in-vitro* and *in-vivo* assessment. Int J Pharm. 2020;589:119835.
39. Emad Eldeeb A, Salah S, Ghorab M. Proniosomal gel-derived niosomes: an approach to sustain and improve the ocular delivery of brimonidine tartrate; formulation, *in-vitro* characterization, and *in-vivo* pharmacodynamic study. Drug Deliv. 2019;26:509-521.
40. Fouda NH, Abdelrehim RT, Hegazy DA, Habib BA. Sustained ocular delivery of dorzolamide-HCl *via* proniosomal gel formulation: *in-vitro* characterization, statistical optimization, and *in-vivo* pharmacodynamic evaluation in rabbits. Drug Deliv. 2018;25:1340-1349.
41. Hao Y, Zhao F, Li N, Yang Y, Li K. Studies on a high encapsulation of colchicine by a niosome system. Int J Pharm. 2002;244:73-80.
42. Elhissi A, Hidayat K, Phoenix DA, Mwesigwa E, Crean S, Ahmed W, Faheem A, Taylor KM. Air-jet and vibrating-mesh nebulization of niosomes generated using a particulate-based proniosome technology. Int J Pharm. 2013;444:193-199.
43. Harrison PF. Microbicides: forging scientific and political alliances. AIDS Patient Care STDS. 2000;14:199-205.
44. Radha GV, Vinisha V, Rajkumar J, Ghosh A. Design and evaluation of topical vaginal proniosomal formulations of tenofovir disoproxil fumarate for HIV prevention. Int J Pharm Res. 2019;10:94-102.
45. Abdou EM, Ahmed NM. terconazole proniosomal gels: effect of different formulation factors, physicochemical and microbiological evaluation. J Pharm Drug Deliv Res. 2016;5:1.
46. Verma P, Prajapati SK, Yadav R, Senyschyn D, Shea PR, Trevaskis NL. Single intravenous dose of novel flurbiprofen-loaded proniosome formulations provides prolonged systemic exposure and anti-inflammatory effect. Mol Pharm. 2016;13:3688-3699.
47. Khudair N, Agoun A, Elrayess MA, Najlah M, Younes HM, Elhissi A. Letrozole-loaded nonionic surfactant vesicles prepared *via* a slurry-based proniosome technology: formulation development and characterization. J Drug Deliv Sci Technol. 2020;58:101721.
48. Chandra A, Sharma PK. Proniosome based drug delivery system of piroxicam. Afr J Pharm. Pharmacol. 2008;2:184-190.
49. Solanki AB, Parikh JR, Parikh RH. Preparation, optimization and characterization of ketoprofen proniosomes for transdermal delivery. Int J Pharm Sci. Nanotech. 2009;2:413-420.
50. Mahrous GM. Proniosomes as a drug carrier for transdermal delivery of meloxicam. Bull Pharm Sci. 2010;33:131-140.
51. Alam MI, Baboota S, Kohli K, Ali J, Ahuja A. Pharmacodynamic evaluation of proniosomal transdermal therapeutic gel containing celecoxib. ScienceAsia. 2010;36:305-311.
52. Abu El-Enin ASM, Khalifa MKA, Dawaba AM, Dawaba HM. Proniosomal gel-mediated topical delivery of fluconazole: development, *in vitro* characterization, and microbiological evaluation. J Adv Pharm Technol Res. 2019;10:20-26.
53. Fang JY, Yu SY, Wu PC, Huang YB, Tsai YH. *In vitro* skin permeation of estradiol from various proniosome formulations. Int J Pharm. 2001;215:91-99.
54. Mehta M, Dureja H, Garg M. Development and optimization of boswellic acid-loaded proniosomal gel. Drug Deliv. 2016;23:3072-3081.
55. Eltellawy YA, El-Kayal M, Abdel-Rahman RF, Salah S, Shaker DS. Optimization of transdermal atorvastatin calcium - loaded proniosomes: restoring lipid profile and alleviating hepatotoxicity in poloxamer 407-induced hyperlipidemia. Int J Pharm. 2021;593:120163.
56. Nemr AA, El-Mahrouk GM, Badie HA. Development and evaluation of proniosomes to enhance the transdermal delivery of cilostazole and to ensure the safety of its application. Drug Dev Ind Pharm. 2021;47:403-415.
57. Tareen FK, Shah KU, Ahmad N, Ur Rehman A, Shah SU, Ullah N. Proniosomes as a carrier system for transdermal delivery of clozapine. Drug Dev Ind Pharm. 2020:1-24.
58. Sarfaraz M, Goel T, Doddayya H. Formulation and evaluation of galantamine hydrobromide proniosome gel for Alzheimer's disease. JDDTAO. 2020;10(Suppl):68-74.
59. Khatoon M, Sohail MF, Shahnaz G, Ur Rehman F, Fakhar-Ud-Din, Ur Rehman A, Ullah N, Amin U, Khan GM, Shah KU. Development and evaluation of optimized thiolated chitosan proniosomal gel containing duloxetine for intranasal delivery. AAPS PharmSciTech. 2019;20:288.
60. Farris PK. Cosmeceuticals and cosmetic practice. Oxford, UK: Wiley-Blackwell; 2014.
61. Souto EB, Müller RH. Cosmetic features and applications of lipid nanoparticles (SLN, NLC). Int J Cosmet Sci. 2008;30:157-165.
62. Blazek-Welsh AI, Rhodes DG. Maltodextrin-based proniosomes. AAPS PharmSci. 2001;3:E1.
63. Manosroi J, Chankhampan C, Kitdamrongtham W, Zhang J, Abe M, Akihisa T, Manosroi W. *In vivo* anti-ageing activity of cream containing niosomes loaded with purple glutinous rice (*Oryza sativa* Linn.) extract. Int J Cosmet Sci. 2020;42:622-631.
64. Rahman SA, Abdelmalak NS, Badawi A, Elbayoumy T, Sabry N, El Ramly A. Formulation of tretinoin-loaded topical proniosomes for treatment of acne: *in-vitro* characterization, skin irritation test and comparative clinical study. Drug Deliv. 2015;22:731-739.

65. Chainani-Wu N. Safety and anti-inflammatory activity of curcumin: a component of tumeric (*Curcuma longa*). J Altern Complement Med. 2003;9:161-168.

66. Shehata TM, Ibrahim MM, Elsewedy HS. Curcumin niosomes prepared from proniosomal gels: *in vitro* skin permeability, kinetic and *in vivo* studies. Polymers (Basel). 2021;13:791.

67. Yadav NK, Nanda S, Sharma G, Katare OP. Systematically optimized coenzyme q10-loaded novel proniosomal formulation for treatment of photo-induced aging in mice: characterization, biocompatibility studies, biochemical estimations and anti-aging evaluation. J Drug Target. 2016;24:257-271.

68. Schlich M, Lai F, Pireddu R, Pini E, Ailuno G, Fadda AM, Valenti D, Sinico C. Resveratrol proniosomes as a convenient nanoingredient for functional food. Food Chem. 2020;310:125950.

69. de Sá Coutinho D, Pacheco MT, Frozza RL, Bernardi A. Anti-inflammatory effects of resveratrol: mechanistic insights. Int J Mol Sci. 2018;19:1812.

70. Salehi B, Mishra AP, Nigam M, Sener B, Kilic M, Sharifi-Rad M, Fokou PVT, Martins N, Sharifi-Rad J. Resveratrol: a double-edged sword in health benefits. Biomedicines. 2018;6:91.

71. Smoliga JM, Baur JA, Hausenblas HA. Resveratrol and health-a comprehensive review of human clinical trials. Mol Nutr Food Res. 2011;55:1129-1141.

72. Zupančič Š, Lavrič Z, Kristl J. Stability and solubility of t*rans*-resveratrol are strongly influenced by pH and temperature. Eur J Pharm Biopharm. 2015;93:196-204.

73. Tanaka T, Shnimizu M, Moriwaki H. Cancer chemoprevention by carotenoids. Molecules. 2012;17:3202-3242.

74. Ravaghi M, Sinico C, Razavi SH, Mousavi SM, Pini E, Fadda AM. Proniosomal powders of natural canthaxanthin: preparation and characterization. Food Chem. 2017;220:233-241.

75. Sandeep G, Raju J, Subba Rao D, Vamshi Krishna M. Proniosomal sunscreen gel-based formulation: a promising approach for improving quality of life (QOL). Reconstructive Surgery and Anaplastology. Longdom Publishing SL; -1 [cited 2021May19]. Available from: https://www.longdom.org/proceedings/proniosomal-sunscreen-gel-based-formulation--a-promising-approach-for-improving-quality-of-life-qol-613.html

76. Pinzaru I, Tanase A, Enatescu V, Coricovac D, Bociort F, Marcovici I, Watz C, Vlaia L, Soica C, Dehelean C. Proniosomal gel for topical delivery of rutin: preparation, physicochemical characterization and *in vitro* toxicological profile using 3D reconstructed human epidermis tissue and 2D cells. Antioxidants (Basel). 2021;10:85.

77. El-Laithy HM, Shoukry O, Mahran LG. Novel sugar esters proniosomes for transdermal delivery of vinpocetine: preclinical and clinical studies. Eur J Pharm Biopharm. 2011;77:43-55.

78. Mohammadi S, Pardakhty A, Khalili M, Fathi R, Rezaeizadeh M, Farajzadeh S, Mohebbi A, Aflatoonian M. Niosomal benzoyl peroxide and clindamycin lotion *versus* niosomal clindamycin lotion in treatment of acne vulgaris: a randomized clinical trial. Adv Pharm Bull. 2019;9:578-583.

79. Qiang L, Bin Z, Li L, Hongxia Z, Shasha L, Xiao J. Formulation of paeonol proniosomes and preparing method thereof. CN103340823A.

80. Yadav K, Yadav D, Nanda S, Saroha K. Curcumin proniosomal/niosomal formulation, method for its preparation and use thereof. Indian Patent. 1288/DEL/2012.

81. Garg M, Joon M. Novel Proniosomal gel of *Withania somnifera*. Indian Patent. 3228/DEL/2012.

82. Garg M, Garg P. Novel ursolic acid loaded proniosomal gel and method of preparation thereof. Indian Patent. 3231/DEL/2012.

83. Ribier A, Jean-Thierry S. Process for the stabilization of vesicles of amphiphilic lipid(s) and composition for topical application containing the said stabilized vesicles. U.S. Patent. US 6051250A

84. Handjani R, Ribier A, Vanlerberghe G, Zabotto S, Griat J. Cosmetic and pharmaceutical compositions containing niosomes and a water soluble polyamide, and a process for preparing these compositions. U.S. Patent. US 4830857A.

85. Jianfang F, Kaili H, Helong L, Mei L, Luting W. Drug-carrying precursor vesicle, preparation method and application thereof. CN105311638A.

86. Singh A, Jain R. Targeted vesicular constructs for cytoprotection and treatment of *H. pylori* infections. WO2000042987A8.

87. Young C, Lee W, Keith, Kwang-Ho. Pro-micelle pharmaceutical compositions. KR20040058196A.

88. Abd-Elbary A, El-laithy HM, Tadros MI. A method for the preparation of nebulizable micronized niosomes of cromolyn sodium using nonionic surfactants. EG24388A.

Turk J Pharm Sci 2022;19(4):476-487
DOI: 10.4274/tjps.galenos.2021.44959

REVIEW

Features and Facts of a Gastroretentive Drug Delivery System-A Review

Kuldeep VINCHURKAR[1,2*], Jitendra SAINY[2], Masheer Ahmed KHAN[2], Sheetal MANE[2], Dinesh K MISHRA[1], Pankaj DIXIT[1]

[1]Indore Institute of Pharmacy, Department of Pharmaceutics, Indore, India
[2]Devi Ahilya Vishwavidyalaya University, School of Pharmacy, Department of Pharmaceutics, Indore, India

ABSTRACT

English oral delivery of drug was the commonly used modality because of patient compliance and ease of administration. After oral administration of any drug, its bioavailability is affected by its residence time in stomach. Recently, gastroretentive drug delivery systems (GRDDS) have gained wide acceptance for drugs with a narrow absorption window, decreased stability at high alkaline pH, and increased solubility at low pH. This approach develops a drug delivery system, which gets retained within gastric fluid, thereby releasing its active principles in the stomach. Some methods used to achieve gastric retention of drugs include the use of effervescence agents, mucoadhesive polymers, magnetic material, bouncy enhancing excipient, and techniques that form plug-like devices that resist gastric emptying. This review provides a concise account of various attributes of recently developed approaches for GRDDS.

Key words: Bioavailability, bio/mucoadhesive system, therapeutic window, gastric emptying

INTRODUCTION

Oral administration is popular despite continuous improvement in drug delivery approaches owing to patient comfort and ease of administration. Controlled release drug delivery systems are designed for oral administration. These drug delivery systems release the medication in a predetermined, predictable, and controlled way. They are not suitable for drugs with low bioavailability due to stability or absorption issues.[1] These problems can get better through modern approaches, which are designed to increase the residence of such drugs in the stomach for an extended time. Such drug delivery systems are called gastroretentive drug delivery systems (GRDDS). GRDDS are suitable for those drugs, which are absorbed from the stomach (*e.g.* albuterol),[2] labile at alkaline pH (*e.g.* ranitidine and metformin),[3] poorly soluble at alkaline pH (*e.g.* furosemide and diazepam),[4] and having a narrow window of absorption (*e.g.* riboflavin and levodopa).[5]

Some of the common advantages associated with use of GRDDS include improved patient compliance by reducing the frequency of dosing; improved therapeutic efficacy of drugs with a short half-life; site-specific delivery of medications; sustained and controlled release of drugs in the stomach; enhanced residence time of drugs at the absorption site; improved bioavailability from the gastrointestinal tract; avoiding dose dumping of medicines.[6]

To develop GRDDS, different materials like ion-exchange resins, mucoadhesives, high-density materials, raft forming substances, magnetic substances, and super porous hydrogels are used.[7,8]

This review provides a concise account of various attributes of recently developed approaches for GRDDS.

Anatomy and physiology of the stomach

Knowledge about the anatomy and physiology of the stomach is essential for the successful formulation of gastroretentive

*Correspondence: kuldeepvinchurkar@gmail.com, Phone: +917387527076, ORCID-ID: orcid.org/0000-0002-9206-9587
Received: 10.03.2021, Accepted: 18.06.2021

dosage forms. Anatomically, the stomach is divided into three areas: the proximal portion toward the esophagus is fundus, followed by the body, which serves as a storage site for engulfed food, and the antrum, last part that connects the body to the small intestine. Antrum helps in churning action and in gastric emptying.[9] In fasting state, a sequence of contractions occurs cyclically through the stomach and intestine every 120-180 min, called the migrating myoelectric cycle. It is further divided into four phases. The pattern of contraction changes in a fed state is termed as the digestive motility pattern.[10] This pattern comprises phase 1- (basal phase); phase 2- (preburst phase); phase 3- (burst phase); and phase 4.[11] Figure 1 depicts the motility pattern in the gastrointestinal tract.

Physicochemical properties of GRDDS

Physicochemical properties of GRDDS include density, size, and shape of the dosage form, which play major roles in the formulation of GRDDS. The dosage forms having a density lower than the gastric contents can float to the surface, while high-density systems sink to the bottom of the stomach. For an ideal formulation, the density should be in the range of 1.0-2.5 g/cm^3. Dosage forms having a diameter of more than 7.5 mm show better gastric residence time (GRT). Circular, spherical or tetrahedron-shaped devices show excellent gastroretentive properties.[12]

Physiological factors affecting retention of GRDDS in the stomach

The most important factors controlling the gastric retention time of dosage forms include fed or unfed state, nature of the meal, caloric content, and frequency of feeding. In the case of a fasting environment, gastric retention time is less due to the increase in GI motility. Emptying of gastric content occurs due to peristalsis. If peristalsis coincides with dosage form administration, the gastric residence is short. However, after meals, peristalsis is delayed and may help increase the gastric residence of the formulation. A high-calorie meal containing proteins, fats, and fibrous compounds increases gastric retention time. In the case of multiple meals, the gastric retention is more than a single meal due to persistent inhibition of peristalsis.

Also, some other factors, such as sex and age, affect gastric retention. Compared with males, females have a slower gastric emptying time irrespective of height, weight, and body surface. A person at the age of more than 70 exhibits longer GRT. In comparison, neonates show less GRT compared with geriatric patients.[13-15]

Gastroretentive dosage form approaches

Continuous research and advancements in various approaches to gastroretentive dosage forms over the last few years are as presented in Figure 2. These approaches to GRDDS help in delivering the medicament in a sustained and restrained way through the gastrointestinal tract.

Classification of GRDDS

GRDDS are classified into mainly two types: floating and non-floating systems. Floating systems are further classified into effervescent system and non-effervescent systems based on the mechanism of floating, while non-floating systems classified into four different classes based on the mechanism used for gastroretention. Figure 3 depicts the classification of the GRDDS.

I- High-density system

The density of dosage form plays an important factor in the formulation of the GRDDS. A high-density system uses its weight as a retention mechanism. To enhance the gastric residence of a drug in the stomach, its density must exceed the normal stomach content (1.004 g/mL).[16] Figure 4A depicts the principle of a high-density system. Clarke et al.[17] compared

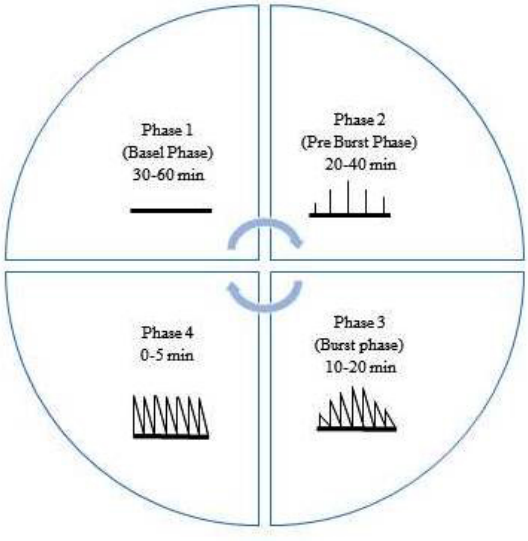

Figure 1. Motility pattern in gastrointestinal tract

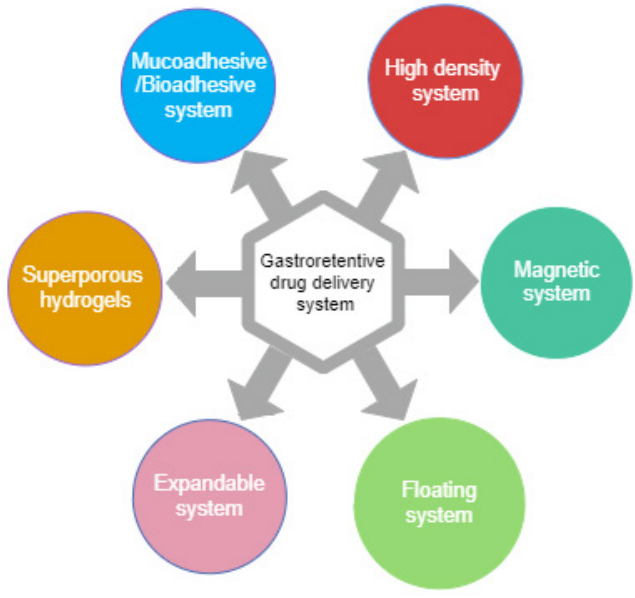

Figure 2. Approaches of gastroretentive drug delivery system

gastrointestinal transit of placebo pellet systems of varying densities using gamma scintigraphy. They reported that GRT of such a formulation can be extended from an average of 5.8 h to 25 h, depending more on density than on the diameter of the pellets.

II- Floating or low-density system

Another approach to increase gastric residence is to lower the density of dosage form than the normal gastric content. These systems remain buoyant due to lower density and provide continuous drug release. In this way, they increase GRT of the drug and improve its bioavailability.[18] Figure 4B depicts the principle of floating or low-density systems.

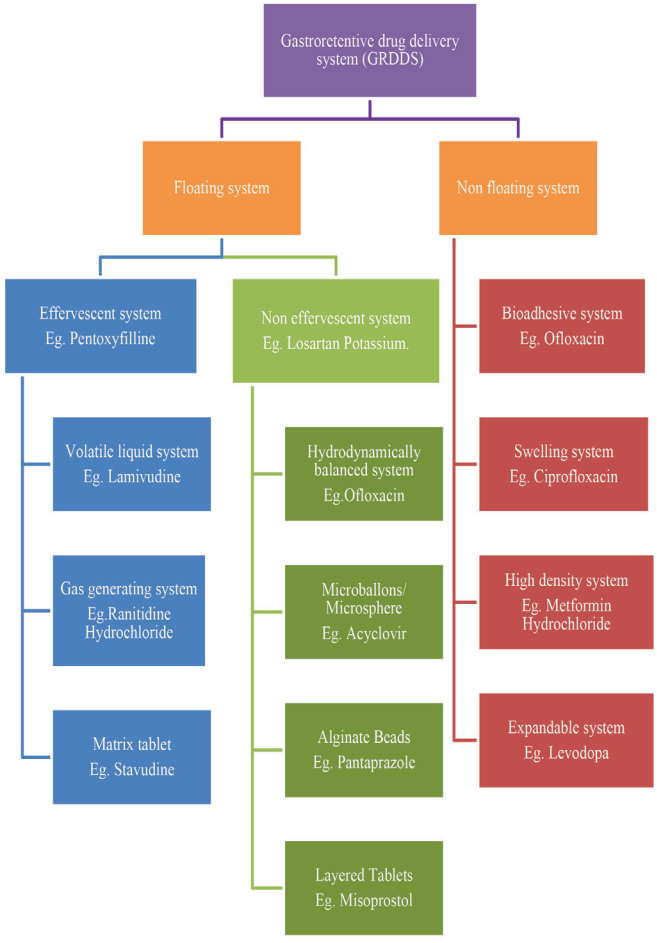

Figure 3. Classification of gastroretentive drug delivery system

(A) Effervescent system

This system uses carbonates (*e.g.* sodium bicarbonate) to generate *in situ* carbon dioxide (CO_2).[19,20] Organic acids (*e.g.* citric and tartaric acids) are added to speed up the reaction, thus reducing the density of dosage form and remaining buoyant in the stomach.[20] It is categorized into two classes:

a) Volatile liquid/vacuum type: These are further classified into three types.

i) Inflatable system

It consists of a pullout system having a space filled with volatile liquids that evaporate at body temperature. Thus, when these systems are introduced into the stomach, the chamber inflates, and the system floats. The inflatable chamber comprises a bioerodible polymer filament that is made from polymers like polyvinyl alcohol and polyethylene. When the inflatable chamber floats in the gastrointestinal fluid, the polymer gradually dissolves and releases the drug. After some time, due to polymer dissolution, the inflatable section collapses.[19,20] Figure 4C depicts a floating effervescent type of inflatable system.

ii) Intragastric floating system

It contains a chamber filled with a vacuum and includes a microporous compartment serving as a drug reservoir.[20] Figure 5 depicts a floating type of intragastric system. Patel et al.[21] developed intragastric floating tablets of verapamil HCl using hydroxypropyl methylcellulose (HPMC), carbopol, and xanthan

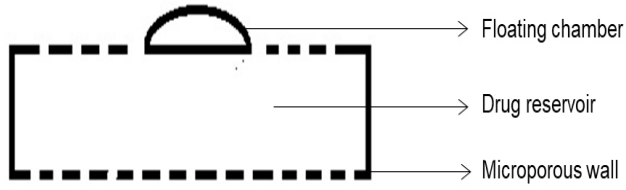

Figure 5. Intragastric floating gastrointestinal drug delivery system.

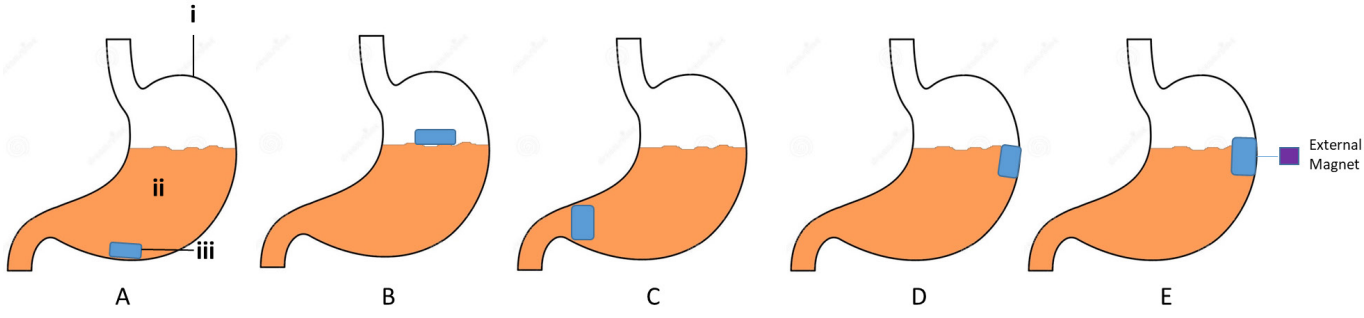

Figure 4. Different types of gastroretentive drug delivery system. A) High density system, B) floating/low density system, C) inflatable system, D) mucoadhesive system, E) magnetic system (i- stomach, ii- gastric fluid, iii- dosage form)

gum as gel-forming agents. Buoyancy was achieved by adding an effervescent mixture of sodium bicarbonate and anhydrous citric acid. Optimized formulation exhibited satisfactory results with a short buoyancy lag time of 36 sec, a total buoyancy time of more than 24 h, and controlled drug release for up to 24 h.

iii) Intragastric-osmotically controlled system

Osmotic control can be achieved using a biodegradable capsule comprising inflatable floating support congestion with an osmotic pressure-controlled drug delivery device.[22,23] Zhao et al.[24] used fenofibrate-loaded mesoporous silica nanoparticles to prepare an oral push-pull osmotic pump. Polyethylene oxide (100,000) and polyethylene oxide (6,000,000) were selected as suspending agents and expanding agents, respectively. Cellulose acetate was used as a semipermeable membrane along with polyethylene glycol 6,000 to increase flexibility and control the membrane permeability. The prepared system is reported to stay in the stomach for a period of 21.72 h rather than 12.48 h of the reference tablet and delivers the drug in an approximately zero-order manner for 24 h.

b) Matrix tablets: They are of two types, *i.e.* single-layer and bilayer matrix tablets. The single-layer matrix tablets are prepared using a drug and a hydrocolloid forming gel, while the bilayer matrix tablet contains one immediate-release layer and another sustained release layer. Saisivam et al.[25] developed single-layer floating matrix tablets of losartan potassium using different proportions of HPMC-K4M and karaya gum as retarding polymer and sodium bicarbonate as an effervescent agent by direct compression method. Results of an *in vivo* study of optimized formulation displayed the floatability of tablet in gastric content and prolonged the GRT to approximately 12 h. X-ray imaging study in albino rabbits indicated the residence of tablet in the stomach even after a period of 12 h.

c) Gas generating systems: Gas-generating systems are prepared using effervescent compounds along with hydrophilic polymers.

i) Floating capsules

These dosage forms involve encapsulation of drugs in hydrophilic polymers like ethyl cellulose and eudragit RS-100 with effervescent agents such as sodium bicarbonate, calcium carbonate, *etc.* Moursy et al.[26] developed a hydrodynamically balanced capsule containing a mixture of nicardipine hydrochloride and hydrocolloids. Upon contact with gastric fluid, the capsule shell dissolves with subsequent swelling, forming a gelatinous barrier, which remains buoyant in the gastric juice for an extended period.

ii) Floating pills

Multiple unit types of oral floating dosage forms have been developed using a hydrophilic polymer in the outer layer and an effervescent agent in the inner layer. When it comes in contact with the gastric fluid, the outer layer of hydrophilic polymer starts to swell and then sinks, but as the effervescent agent meets gastric content, it releases CO_2, and the system starts to float.[27,28] Meka et al.[29] prepared multiple-unit minitab of captopril based on a gas formation technique to prolong the GRT and to increase the overall bioavailability of the drug. They developed drug-containing core units using the direct compression process, which were coated with three successive layers of an inner seal coat, effervescent layer (sodium bicarbonate), and an outer gas-entrapped polymeric membrane of polymethacrylates (eudragit RL30D, RS30D, and combinations of them). They found that increasing the coating level of gas-entrapped polymeric membrane decreased the drug release.

iii) Floating systems with ion exchange resins

These floating systems are mainly developed to prolong the GRT of dosage forms using ion exchange resin. They consist of drug resin complex beads loaded with bicarbonate ions, and they are coated with hydrophilic polymers.[30] It results in the generation of CO_2 gas when it comes in contact with the gastric fluid and causes the beads to float. Atyabi et al.[31] developed a floating system based on an ion exchange resin, which consists of resin beads, loaded with bicarbonate and a negatively charged drug that was bound to the resin. Two resins, *i.e.* Amberlite IRA-400 and Dowex 2 x 10, were investigated and both exhibited *in vitro* floating times of over 24 h using a standardized procedure. The coated dosage form remained for over 3 h in the stomach with the non-coated system and demonstrated a marked increase in retention over conventional formulation.

(B) Non-effervescent systems

In non-effervescent floating systems, the drug comes in contact with gastric fluid and it swells. It maintains its shape, and its density remains less than one, hence it floats in gastric juice.[32] Matrix forming polymer, gel-forming, or swellable type hydrocolloids are used for these types of floating systems. They are further classified as follows:

i. Hydrodynamically balanced systems (HBS)

These systems mainly consist of a mixture of drugs and hydrocolloids that forms a gelatinous barrier, when it comes in contact with gastric fluid due to swelling of the combination. It remains buoyant in the stomach for an extended period as its bulk density is less than one in gastric fluid. Nayak and Malakar[33] developed gastroretentive theophylline HBS capsules using HPMC, polyethylene oxide, polyvinylpyrrolidone, ethylcellulose, liquid paraffin, and lactose to control the delivery of theophylline for a longer period in the stomach with a minimum floating time of 6 h.

ii. Microballoons

Microballoons are described by the gradual addition of drug-containing emulsion into a volatile solvent. On evaporation of the solvent, gas is generated in a dispersed polymer droplet, which results in the formation of an interior orifice in the microsphere of the drug with polymer. It is also called emulsion solvent diffusion method.[22] The floating time of microspheres depends upon the type and amount of polymer used in the formulation. Gupta et al.[34] developed pantoprazole sodium-loaded microspheres using eudragit L100 by adopting an emulsion solvent diffusion method with a non-effervescent approach. The results of *in vitro* and *in vivo* studies exhibited a suitable drug-release pattern in terms of increased bioavailability and

efficient ulcer healing effect. Figure 6 depicts the steps involved in the preparation of microballoons by solvent diffusion method.

iii. Alginate beads

These systems are prepared using a hydrocolloid gel-forming agent and sodium alginate as the interlocking agents. In the presence of gastric fluid, the hydrocolloid absorbs water and forms a barrier that results in entrapment of air in the polymer, which causes swelling of the polymer, and hence the dosage form starts to float, and results in releasing the drug for a prolonged period. Ghareeb and Radhi[35] developed trimetazidine calcium alginate floating beads using sodium alginate solution (2, 3, and 4% w/v), HPMC, and peppermint oil (15, 20, and 25% v/v) using emulsion gelation method. They found that oil entrapped floating beads gave promising results for sustaining the release of the drug over 10 h.

iv. Layered tablets

Layered tablets are more popular due to ease of their preparation, low cost, and high stability.

a. Single-layered floating tablets: These tablets were developed by mixing drug and gas generating agents within the matrix tablet. These formulations have lower bulk density than gastric fluid, and thus they remain buoyant in the stomach by increasing GRT.[36] Kim et al.[37] developed non-effervescent gastroretentive tablets of pregabalin once a day using wet granulation and compaction. They found that the amounts of HPMC and crospovidone were found be critical factors affecting *in vitro* dissolution and floating properties of the prepared tablets. Figure 7 depicts a schematic of single-layered floating tablets.

b. Double-layered floating tablets: It comprises of two formulations separated by layering, one on top of the other, having two different release profiles.[3,38] Kuldeep et al.[39] developed a bilayer floating tablet of metoprolol succinate (sustained-release layer) and rosuvastatin calcium (immediate-release layer) by direct compression method. HPMC K100, K4M, and K15M were used as gel-forming agents, while cross carmellose sodium, sodium starch glycolate, and crospovidone were used as super disintegrant. Sodium bicarbonate is used as an effervescent agent. From the *in vitro* buoyancy study, it was observed that as the concentration of gas-generating agents increases, floating lag time decreases. Also, the polymer gas generating agent ratio was found to influence the floating lag time and the total duration of floating.

III- Mucoadhesive and bioadhesive systems

A mucoadhesive and bioadhesive system uses its adhesive properties to target a drug to a specific region of the body for an extended period. Figure 4D displays a mucoadhesive system of GRDDS. For this, bioadhesive or mucoadhesive polymers

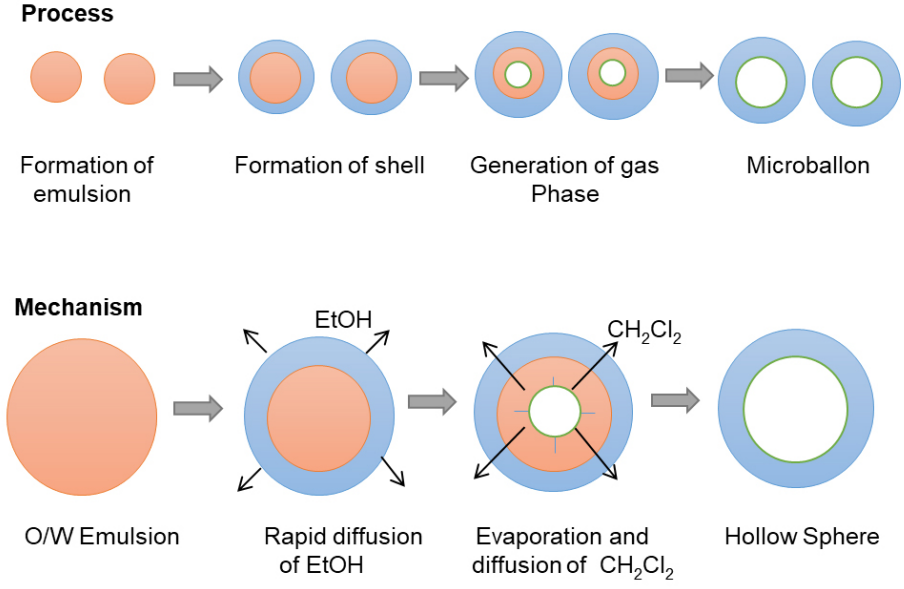

Figure 6. Preparation technique and mechanism of microballoons formation

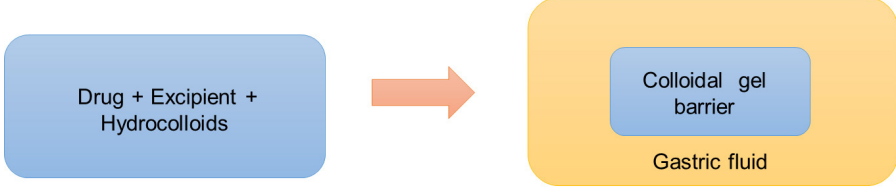

Figure 7. Mechanism of single layer tablet

are mainly used.[40] Natural polymers such as sodium alginate, gelatin, guar gum, *etc*., and semisynthetic polymers such as HPMC, lectins, carbopol, and sodium carboxymethyl cellulose are widely used for mucoadhesion. The adhesion is mediated by hydration, bonding, or receptor interactions.[41,42] Madgulkar et al.[43] developed sustained-release tablets of itraconazole using mucoadhesive polymer carbopol 934P and HPMC K4M. They confirmed sustained drug release and gastric retention for six hours in albino rats. Figure 8 depicts the principle of mucoadhesive drug delivery systems.

IV- Swelling system

These systems, when come in contact with gastric fluid, their size increases significantly than that of the pyloric sphincter and thus, after swelling, remain logged in the stomach. These are also called a "plug type system".[44] Controlled and sustained drug release is achieved using an appropriate excipient. The swelling ability of polymer mainly depends upon the degree of cross-linking of hydrophilic polymer network. The high degree of cross-linking maintains the integrity of the system, while a low degree of cross-linking causes extensive swelling resulting in rapid dissolution of the polymer.[45]

V- Superporous hydrogels

Superporous hydrogels are a three-dimensional network of hydrophilic polymers that have numerous super-size pores inside them. The swelling of superporous hydrogels occurs by the mechanism of capillary wetting through interconnected open pores. To develop superporous hydrogels, certain ingredients like initiators and cross-linkers are used to initiate the cross-linking.[46] Other ingredients were foam stabilizers, foaming aids, and foaming agents. Desu et al.[47] developed a superporous hydrogel system using *N′*, *N′*-methylene bisacrylamide as the cross-linking operator and polyvinyl alcohol as a composite specialist, ammonium persulfate and *N*, *N*-tetramethylenediamine as an initiator pair and Span 80 as a surfactant. They are used as a froth stabilizer to make a permeable structure using the gas-forming method.

VI- Magnetic system

In this system, by using a strong magnet with a powerful magnetic field onto the body surface, the movement of gastroretentive formulation with a small internal magnet is controlled. Several reports tell about the positive results of this system, but the success of this system depends upon the selection of the magnet position with very high precision.[48] Gröning et al.[49] developed peroral acyclovir depot tablets with an internal magnet. An extracorporeal magnet was used to prolong the GRT of the dosage form and to influence the duration of absorption of acyclovir. They performed an *in vivo* study with five healthy male subjects and determined the plasma concentration-time profiles of acyclovir. Computer simulations were carried out to display the influence of GRT of acyclovir depot preparations on the plasma concentration-time profiles of acyclovir. Figure 4E displays a magnetic system of GRDDS.

In vitro assessment

For GRDDS, *in vitro* assessment is very essential to predict gastric transit behavior. Following are the parameters, which should be considered for designing novel gastroretentive formulations.

i. Buoyancy lag time

It is the time taken for gastroretentive formulations to move onto the surface of the dissolution medium. It is determined using a USP dissolution apparatus containing 900 mL of 0.1 N HCl solution as a testing medium maintained at 37°C. The time required to float different dosage forms noted as floating lag time.[50]

ii. Floating time

This determines the buoyancy of dosage form. In this test, a specific dissolution apparatus is used depending upon the type of dosage form with 900 mL of dissolution medium kept at 37°C. The floating time or floating duration of the dosage form is determined by visual observation.[51,52]

iii. Specific gravity/density

Specific gravity estimates are essential for both low-density and high-density GRDDS. Specific gravity is determined using the displacement method.[53]

iv. Swelling index

Swelling index is determined by immersing the tablets in 0.1 N HCl at 37°C and their periodic removal at regular intervals.[54]

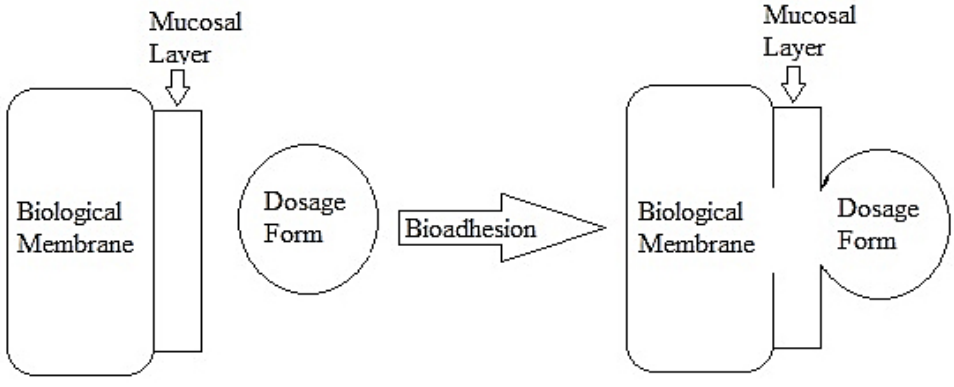

Figure 8. Principle of mucoadhesive drug delivery system

v. Water uptake

In this study, the dosage form is removed from the dissolution medium after the regular interval and a weight change is determined.[55]

Water uptake (WU) = $(W_t - W_o) * 100/W_o$

where W_t= weight of the dosage form at time t, W_o= initial weight of the dosage form

vi. Weight variation

Various official methods are recommended by pharmacopeias to calculate the weight variation. Usually, the individual and average weight of 20 tablets are recorded. From these data, average weight and weight variation is calculated.[56,57]

iii. Hardness and friability

Hardness or crushing strength is determined using a Monsanto tester, Strong cobb tester, Pfizer tester, *etc.* Friability (strength) of tablets is determined using a Roche friabilator.[58,59]

viii. In vitro dissolution tests

This test is performed to determine drug release from GRDDS in gastric fluid and intestinal fluid maintained at 37°C at a definite time using USP dissolution type II apparatus (paddle).[59,60]

Here, after *in vitro* assesment, Table 1 represents the recent trends in GRDDS, while Table 2 represents the names of drug candidates for GRDDS.

Evaluation of microsphere and beads

An optical microscope was used to measure the particle size of beads and microspheres. Surface morphology and cross-sectional morphology are evaluated with the help of a scanning electron microscope.

In vivo assessment

a. Radiology

This technique is mainly used to determine the position of gastroretentive dosage form filled with barium sulfate (radio-opaque marker) inside the body system concerning time using

Table 1. Showing some recent trends in GRDDS

Drug	Requirements for development	Dosage forms	References
Diltiazem HCl	a) Low solubility b) Short half-life c) Low bioavailability (40-50%)	Osmotic tablet (pump)	63
Theophylline	a) Short half-life b) Low bioavailability	Floating capsule	64
Metformin HCl	a) Short half-life b) Low bioavailability	Beads	65
Ciprofloxacin hydrochloride	a) Low bioavailability b) Short elimination half-life	CR floating tablet	66
Acyclovir	a) Short half-life b) Oral bioavailability is poor (15-30%) due to poor water solubility c) Degrade at high pH	SR floating microsphere	67
Ranitidine HCl	a) Short half-life b) Absorption window in a part of GIT c) Poor bioavailability	Floating (pulsatile) DDS	68
Ciprofloxacin HCl	a) Short elimination half-life (about 4 h) b) Narrow absorption window and absorbed in proximal SI c) Freely soluble in water	Floating tablet (matrix)	69
Ziduvudine	a) Dose dependant solubility b) Short biological half-life c) Poor bioavailability	Tablet	72
Cephalexin	a) Acidic drug b) Short half-life c) Poor bioavailability	Floating tablet	73

GRDDS: Gastroretentive drug delivery systems

X-ray. X-ray pictures are taken at different intervals to record the correct position of the dosage form.[61,62]

b. Scintigraphy

Similar to radiology, it is used to determine *in vivo* floating behavior of the gastroretentive dosage form. In scintigraphy, 99mTc pertechnetate is used as an emitting material instead of an X-ray to engulf the formulation to record the image.[63,64]

c. Gastroscopy

Gastroscopy is widely used for visual examinations of gastroretentive dosage forms. In this technique, an illuminate optical, tubular, and slender instrument called "endoscope" is used to look deep inside the body parts such as the stomach, esophagus, and small intestine.[65,66]

d. Ultrasonography

It is a diagnostic imaging technique, in which ultrasound is used for imaging internal body structures. The main disadvantage of this test is non-detectability at entrails.[1,66,67]

e. ^{13}C octanoic acid breath test

Radioactive ^{13}C octanoic acid is used to assess the extent of absorption of drugs from GRDDS. This compound gets absorbed

Table 2. Some of the drug candidates for GRDDS

Drug	Pharmacological and/or therapeutic class	Solubility	Stability in gastric and intestinal	Absorption and oral bioavailability	Half-life (h)	References
Itraconazole	Antibiotics	Low water solubility	-	70-80% absolute bioavailability	4	66
Acyclovir	Antiviral	Slightly soluble in water	-	Rapidly absorbed	3.0 ± 1.4	67
Ranitidine	Histamine H2-receptor antagonist	Low solubility at alkaline Ph	Colonic metabolism	50% absolute bioavailability	2.5-3	68
Ciprofloxacin	Fluoroquinoline	Freely soluble in water	-	Mainly absorbed in proximal areas	4	69
Furosemide	Loop diuretic	Poor water solubility	-	Mainly absorbed from stomach	1.3 ± 0.8	70
Tacrolimus	Immunosuppressant	Poor water solubility	-	Low oral availability	-	71
Captopril	Angiotensin converting enzyme inhibitor	Freely soluble in water	Stable at gastric pH but unstable in intestine	-	2	72
Repaglinide	Oral hypoglycemic agent	Poorly soluble in water	-	Low bioavailability	1	73
Metformin hydrochloride	Antidiabetic	Freely soluble in water	-	Absolute bioavailability (50-60%)	1.5-1.6	74
Alfuzocin HCL	Alpha adrenergic receptor blocker	Highly water soluble	-	Absorbed from upper GIT	5	75
Cephalexin	Cephalosporin type antibiotic	-	Degrade in alkaline pH	-	1	76
Ofloxacin	Fluoroquinoline	-	-	Highly soluble in Absorption occurs	9	77
	Antidiabetic	-	-	Acidic media and precipitate in upper GIT alkaline media	-	-
Verapamil hydrochloride	Calcium channel blocker	Soluble in water	-	Low bioavailability (10-20%) due to first pass effect	4	78
Domperidone	Prokinetic agent	Good solubility in acidic pH but reduced	-	Rapidly absorbed from stomach & upper part of GIT	7	79

GRDDS: Gastroretentive drug delivery systems

from the duodenum, and, when it is radiolabelled, then after its metabolism, the CO_2 exhaled in breath can be correlated with the amount of octanoic acid absorbed. The radiolabelled CO_2 was measured by isotope ratio mass spectroscopy.[65,66]

f. Magnetic marker monitoring

Compared with radiology and scintigraphy, this method is radiation-less, and thus is non-hazardous.[67,68] It involves real-time tracking of the dosage form in the gastrointestinal tract.[69,70] This technique is mainly used for the determination of the gastrointestinal motility and dissolution behavior of pharmaceuticals. In this technique, the dosage form is labeled as a magnetic dipole by incorporating a trace of ferromagnetic particles and recording the magnetic dipole field by an apparatus responsive to bio-magnetic measurement.[71-73]

Advantages and applications of gastroretentive delivery systems

Gastroretentive dosage forms release the drug in a controlled manner to their specific site of action.[74] These systems help increase the bioavailability of drugs that get metabolized in the upper part of the gastrointestinal tract, such as riboflavin and levodopa, *etc*.[75,76] For drugs that have a short half-life, gastroretentive dosage forms help reduce the dosing frequency and improve patient compliance by enhancing GRT. Also, they provide a sustained and prolonged release of drugs in the stomach and intestine, which are helpful in local therapy.[77-79] Lastly, Table 3 depicts the gastroretentive technologies adopted by various pharmaceutical companies, and Table 4 represents the list of commonly used drugs for various floating systems.

Table 3. Gastroretentive technologies adopted by various pharmaceutical companies

Technology	Company	Product	API	References
Bioadhesive tablets	Lupin, India	Xifaxan	Rifaximin	80
			Ofloxacin	
Effervescent floating system	Ranbaxy, India	Zanocin OD	Metformin HCl	81
		Riomet OD	Ciprofloxacin	
	-	Cifran OD		
Colloidal gel forming floating system	Ranbaxy, India	Conviron	Ferrous sulphate	82
Foam-based floating system	Sato Pharma, Japan	Inon ace tablets	Simethicone	83
	-	-	Gabapentin	
Polymer-based swelling technology: AcuFormTM	Depomed, USA	Gabapentin GR	Ciprofloxacin	84
	-	ProQuin XR	Metformin HCl	
Effervescent and swelling-based floating system	Sun Pharma	Prazopress XL	Prazosin HCl	85
Swelling-based floating system	Japan	Metformin Hcl	Metformin HCl	86
	Galenix, France	Cafeclor LP	Cefaclor	
	-	Tramadol LP	Tramadol	
Floating CR capsule	Roche, UK	Madopar	Levodopa and benserzide	86
	-	Valrelease	Diazepam	
Expandable system (unfloading)	Intec Pharma, Israel	Accordion PillTM	Carbidopa/levodopa	86
Erodible matrix-based system	Bayer, USA	Cipro XR	Ciprofloxacin HCl and betaines	87
Coated multi-layer and swelling system	Sun Pharma, India	Baclofen GRS	Baclofen	88
Gastroretention with osmotic system	GlaxoSmithKline, UK	Coreg CR	Carvedilol	89
Effervescent floating liquid alginate preparation	Reckitt Benckiser Healthcare,UK	Liquid gaviscon	Alginic acid and sodium bicarbonate	89
Bilayer-floating capsule	Pfizer, UK	Cytotec	Misoprostol	90
Raft-forming system	Pierre Fabre	Topalkan	Aluminium magnesium	90
	Medicament, France	Almagate flatcoat	Aluminium magnesium antacid	

Table 4. List of commonly used drugs for various floating system[82,83,85,87-90]

Type of system	Drugs used
Microspheres tablets/pills	Rosiglitazone maleate, verapamil, orlistat, aspirin, griseofulvin, acetylsalicylic acid, ibuprofen, ampicillin, captopril, sotalol, isosorbide dinitrate, terfanadine
Tablets	Losartan, furosemide, ciprofloxacin, captopril, cinnarazine, sotalol, ampicillin, florouracil, metformin hydrochloride, atenolol, baclofen
Films	Cinnarizine, peritanide, quinidine gluconate, albendazole, *p*-aminobenzoic acid, prednisolone
Granules	Ranitidine HCl, diclofenac sodium, cinnarizine, indomethacin, fluorouracil, diltiazem, isosorbide dinitrate
Powders	Riboflavin, sotalol, theophylline
Capsules	Verapamil HCl, chlordizepoxide, diazepam, misoprostol, furosemide, L-DOPA, pepstatin, nicardipine

CONCLUSION

GRDDS are unique systems and have become important in the last three decades. It offers various advantages, *viz*., site-specific, slow, and controlled release of drugs from different types of gastroretentive dosage forms, thus improving patient compliance and reducing the side effects by minimizing dosing frequency. Therefore, it is expected that in the future, various pharmaceutical companies will come forward to initialize gastroretentive drug delivery technology to create excellent advantages, prolonging patents, and a better outcome for their marketed formulations.

Ethics

Peer-review: Externally peer-reviewed.

Authorship Contributions

Concept: K.V., S.M., P.D., Design: K.V., S.M., J.S., P.D., Data Collection or Processing: K.V., S.M., P.D., Analysis or Interpretation: K.V., S.M., Literature Search: K.V., S.M., Writing: K.V., S.M., M.A.K., D.K.M.

Conflict of Interest: No conflict of interest was declared by the authors.

Financial Disclosure: The authors declared that this study received no financial support.

REFERENCES

1. Schneider F, Koziolek M, Weitschies W. *In vitro* and *in vivo* test methods for the evaluation of gastroretentive dosage forms. Pharmaceutics. 2019;11:416.
2. Boulton DW, Fawcett JP. Enantioselective disposition of albuterol in humans. Clin Rev Allergy Immunol. 1996;14:115-138.
3. Chandira RM, Palanisamy P, Jaykar B. Formulation and evaluation of bilayered floating tablets of metformin hydrochloride. Int Res J Pharm. 2012;3:257-267.
4. Menon A, Ritschel WA, Sakr A. Development and evaluation of a monolithic floating dosage form for furosemide. J Pharm Sci. 1994;83:239-245.
5. Levy G, Jusko WJ. Factors affecting the absorption of riboflavin in man. J Pharm Sci. 1966;55:285-289.
6. Badoni A, Ojha A, Gnanarajan G, Kothiyal P. Review on gastroretentive drug delivery system. J Pharm Innov. 2012;1:32-42.
7. Malpure PS, Chavan BR, Maru AD, Bhadhane JS, Thakare EB, Sonawane PS. Gastroretentive drug delivery systems. World J Pharm Pharm Sci. 2019;8:506-528.
8. Kumar M, Kaushik D. An Overview on various approaches and recent patents on gastroretentive drug delivery systems. Recent Pat Drug Deliv Formul. 2018;12:84-92.
9. Pund AU, Shendge R, Pote AK. Current approaches on gastroretentive drug delivery system. J Drug Deliv Ther. 2020;10:139-146.
10. Gunda RK. Formulation development and evaluation of gastroretentive drug delivery system. A review. J Pharm Res. 2017;8:11-20.
11. More S, Gavali K, Doke O, Kasgawadek P. Gastroretentive drug delivery system. J Drug Deliv Ther. 2018;8:24-35.
12. Tomar A, Upadhyay A, Gupta S, Kumar S. An overview on gastroretentive drug delivery system: current approaches and advancements. Res Pharm Sci. 2019;9:12-16.
13. Taylor K, Aulton M. Aulton's Pharmaceutics. The design and manufacture of medicines (4th ed). Churchill Livingstone; London; 2007:397.
14. Gandhi A, Verma S, Imam SS, Vyas M. A review on techniques for grafting of natural polymers and their applications. Plant Arch. 2019;19:972-978.
15. Chudiwal V, Shahi S, Chudiwal S, Ahale D. Innovative technologies for gastro-retentive. Asian J Pharm Res 2017;6:22-28.
16. Devkant S, Anjali S. Gastro retentive drug delivery system. A review. Asian Pac J Health Sci. 2014;1:80-89.
17. Clarke GM, Newton JM, Short MB. Comparative gastrointestinal transit of pellet systems of varying density. Int J Pharm. 1995;114;1-11.
18. Streubel A, Siepmann J, Bodmeier R. Gastroretentive drug delivery system. Expert Opin Drug Deliv. 2006;3:217-233.
19. Garg R, Gupta GD. Progress in controlled gastroretentive delivery systems. Trop J Pharm Res. 2008;7:1055-1066.
20. Thapa P, Jeong SH. Effects of formulation and process variables on gastroretentive floating tablets with a high-dose soluble drug and experimental design approach. Pharmaceutics. 2018;10:161.
21. Patel A, Modasiya M, Shah D, Patel V. Development and *in vivo* floating behavior of verapamil HCl intragastric floating tablets. AAPS PharmSciTech. 2009;10:310-315.
22. Nayak AK, Maji R, Das B. Gastroretentive drug delivery systems: a review. Asian J Pharm Clin Res. 2010;3:2-10.

23. Nasa P, Mahant S, Sharma D. Floating systems: a novel approach towards gastro retentive drug delivery systems. Int J Pharm Pharm Sci. 2010;2:2-7.
24. Zhao Z, Wu C, Zhao Y, Hao Y, Liu Y, Zhao W. Development of an oral push-pull osmotic pump of fenofibrate-loaded mesoporous silica nanoparticles. Int J Nanomedicine. 2015;10:1691-1701. Erratum in: Int J Nanomedicine. 2022;17:15-16.
25. Saisivam S, Ulla MR, Shakeel F. Development of floating matrix tablet of losartan potassium: *in vitro* and *in vivo* evaluation. J Drug Deliv Sci Technol. 2013;23:611-617.
26. Moursy NM, Afifi NN, Ghorab DM, El-Saharty Y. Formulation and evaluation of sustained release floating capsules of nicardipine hydrochloride. Pharmazie. 2003;58:38-43.
27. Samal HB, Dey S, Kumar D, Kumar DS, Sreenivas SA, Rahul V. Formulation, characterization and *in-vitro* evaluation of floating microspheres of nateglinide. Int J Pharm Bio Sci. 2011;2:147-157.
28. Pal P, Sharma V, Singh L. A review on floating type gastroretentive drug delivery system. Int Res J Pharm. 2012;3:37-43.
29. Meka L, Kesavan B, Chinnala KM, Vobalaboina V, Yamsani MR. Preparation of a matrix type multiple-unit gastro retentive floating drug delivery system for captopril based on gas formation technique: *in vitro* evaluation. AAPS PharmSciTech. 2008;9:612-619.
30. Verma R, Kumar A, Purohit S, Bhandari A. Overview of gastro-retentive drug delivery system. J Natura Conscientia. 2011;2:423-436.
31. Atyabi F, Sharma HL, Mohammad HAH, Fell JT. *In vivo* evaluation of novel gastric retentive formulation based on ion exchange resin. J Control Release. 1996;42:105-113.
32. Ali A, Shahid MA, Hossain MD, Islam MN. Antibacterial bi-layered polyvinyl alcohol (PVA)-chitosan blend nanofibrous mat loaded with *Azadirachta indica* (neem) extract. Int J Biol Macromol. 2019;138:13-20.
33. Nayak AK, Malakar J. Formulation and *in vitro* evaluation of hydrodynamically balanced system for theophylline delivery. J Basic Clin Pharm. 2011;2:133-137.
34. Gupta P, Kumar M, Kaushik D. Pantoprazole sodium loaded microballoons for the systemic approach: *in vitro* and *in vivo* evaluation. Adv Pharm Bull. 2017;7:461-467.
35. Ghareeb MM, Radhi ZA. Formulation and *in vitro* evaluation of trimetazidine dichloride floating beads. Int J Pharm Pharm Sci. 2014;6:456-440.
36. Vinchurkar K, Balekar N. Formulation and evaluation of floating multilayered coated tablets. J Adv Pharm Technol Res. 2015;212-222.
37. Kim S, Hwang KM, Park YS, Nguyen TT, Park ES. Preparation and evaluation of non-effervescent gastroretentive tablets containing pregabalin for once-daily administration and dose proportional pharmacokinetics. Int J Pharm. 2018;550:160-169.
38. Soni RP, Patel AV, Patel RB. Patel NM. Gastroretentive drug delivery systems. A review. Int J Pharm World Res. 2011;2:1-24.
39. Kuldeep V, Sheetal M, Jitendra S, Masheer K. Formulation and evaluation of once a day dual component gastroretentive drug delivery system. Asian J Sci Technol. 2019;10:10247-10254.
40. Shep S, Dodiya S, Lahoti SR, Mayee R. Swelling system: a novel approach towards gastroretentive drug delivery system. Indo Global J Pharm Sci. 2011;1:234-242.
41. Rocca DJ, Omidian H, Shah K. Progresses in gastroretentive drug delivery systems. Business Briefing Pharmatech. 2003;152-156.
42. Zate SU, Mahale GH, Kapse KP, Anantwar SP. Gastroretentive bioadhesive drug delivery system: a review. Int J PharmTech Res. 2010;2:1227-1235.
43. Madgulkar A, Kadam S, Pokharkar V. Studies on formulation development of mucoadhesive sustained release itraconazole tablet using response surface methodology. AAPS PharmSciTech. 2008;9:998-1005.
44. Yeole PG, Khan S, Patel VF. Floating drug delivery systems. Need and development. Indian J Pharm Sci. 2005;67:265-272.
45. Dolas RT, Hosmani A, Bhandari A, Kumar B, Somvanshi S. Novel sustained release gastroretentive drug delivery system: a review. Int J Pharm Res Dev. 2004;2:26-41.
46. Hardenia SS, Jain A, Patel R, Kaushal A. Floating drug delivery systems. A review. Asian J Pharm Life Sci. 2011;1:284-293.
47. Desu P, Paasam V, Kotra V. Formulation and *in vitro* evaluation of superporous hydrogel based gastroretentive drug delivery system of vildagliptin. J Pharm Res. 2019;23:873-885.
48. Joshi P, Patel P, Modi H, Patel MR, Patel KR, Patel NM. A review on gastro retentive drug delivery system. J Pharm Sci Bio-Sci Res. 2012;2:123-128.
49. Gröning R, Berntgen M, Georgarakis M. Acyclovir serum concentrations following peroral administration of magnetic depot tablets and the influence of extracorporal magnets to control gastrointestinal transit. Eur J Pharm Biopharm. 1998;46:285-291.
50. Hilton AK, Deasy PB. *In vitro* and *in vivo* evaluation of an oral sustained-release floating dosage form of amoxycillin trihydrate. Int J Pharm. 1992;86:79-88.
51. Sangekar S, Vadino WA, Chaudhary I, Parr A, Beinh R, Digenis G. Evaluation of the effect of food and specific gravity of tablets, on gastric retention time. Int J Pharm. 1987;35:187-191.
52. Patel N, Nagesh C, Chandrashekhar S, Jinal P, Devdatt J. Floating drug delivery system: an innovative acceptable approach in gastroretentive drug delivery. Asian J Pharm Res. 2012;2:7-18.
53. Pham AT, Lee PI. Probing the mechanisms of drug release from hydroxypropylmethyl cellulose matrices. Pharm Res. 1994;11:1379-1384.
54. Sharma N, Agarwal D, Gupta MK, Mahaveer PK. A comprehensive review on floating drug delivery system. Int Res J Pharm. 2011; 2:428-441.
55. Caldwell LJ, Gardner CR, Cargill RC. Drug delivery device which can be retained in the stomach for a controlled period of time. US patent no: 4735804. April 05, 1988.
56. Shivkumar HG, Vishakante GD, Pramodkumar TM. Floating controlled drug delivery systems for prolong gastric residence. Indian J Pharm Edu Res. 2004;38:172-179.
57. Singh BN, Kim KH. Floating drug delivery systems: an approach to oral controlled drug delivery *via* gastric retention. J Control Release. 2000;63:235-259.
58. Burns SJ, Corness D, Hay G, Higginbottom S, Whwlan I, Attwood D, Barnwell SG. Development and validation of an *in vitro* dissolution method for a floating dosage form with biphasic release characteristics. Int J Pharm. 1995;121:37-34.
59. Timmermans J, Moës AJ. Factors controlling the buoyancy and gastric retention capabilities of floating matrix capsules: new data for reconsidering the controversy. J Pharm Sci. 1994;83:18-24.

60. Hendee WR. In: Textbook of diagnostic imaging. Fundamentals of diagnostic imaging: Characteristic of radiographic image. WB Saunders Co, Philadelphia (1th ed). 1994;1:9-10.
61. Koner P, Saudagar RB, Dharwal SJ. Gastro-retentive drugs: a novel approach towards floating therapy. J Novel Drug Deliv. 2007;1:2211-2215.
62. Biller S, Baumgarten D, Haueisen J. Magnetic marker monitoring: a novel approach for magnetic marker design. Ifmbe Proceedings. 2010;29:260:263.
63. Bathool A, Gowda DV, Khan MS, Ahmed A, Vasudha SL, Rohitash K. Development and evaluation of microporous osmotic tablets of diltiazem hydrochloride. J Adv Pharm Technol Res. 2012;3:124-133.
64. Bhise SB, Aloorkar NH. Formulation and *in vitro* evaluation of floating capsule of theophylline. Indian J Pharm Sci. 2008;70:224-227.
65. Savale S. Formulation and evaluation of metformin HCl microbeads by ionotropic gelation method. Der Pharmacia Lettre. 2016;8:189-196.
66. Arza RA, Gonugunta CS, Veerareddy PR. Formulation and evaluation of swellable and floating gastroretentive ciprofloxacin hydrochloride tablets. AAPS PharmSciTech. 2009;10:220-226.
67. Vinodbhai PK, Gohel M, Suthar S. Sustained release floating microspheres of acyclovir: formulation, optimization, characterization and *in vitro* evaluation. Int J Drug Dev. 2011;3:242-251.
68. Suthakaran R, Akkala M. Formulation and evaluation of sustained release floating matrix tablet of an antiretroviral drug. JPSBR. 2016;5:82-83.
69. Yin L, Qin C, Chen K, Zhu C, Cao H, Zhou J, He W, Zhang Q. Gastro-floating tablets of cephalexin: preparation and in *vitro*/*in vivo* evaluation. Int J Pharm. 2013;452:241-248.
70. Munir R, Massud A, Inam S, Umber A. Development and evaluation of gastroretentive tablet of furesomide. Int J Adv Pharm Res. 2013;4:2362-2370.
71. Wang YP, Gan Y, Zhang XX. Novel gastroretentive sustained-release tablet of tacrolimus based on self-microemulsifying mixture: *in vitro* evaluation and *in vivo* bioavailability test. Acta Pharmacol Sin. 2011;32:1294-1302.
72. Jiménez-Martínez I, Quirino-Barreda T, Villafuerte-Robles L. Sustained delivery of captopril from floating matrix tablets. Int J Pharm. 2008;362:37-43.
73. Sharma M, Kohli S, Dinda A. *In-vitro* and *in-vivo* evaluation of repaglinide loaded floating microspheres prepared from different viscosity grades of HPMC polymer. Saudi Pharm J. 2015;23:675-682.
74. Wadher KJ, Kakde RB, Umekar MJ. Formulation and evaluation of a sustained-release tablets of metformin hydrochloride using hydrophilic synthetic and hydrophobic natural polymers. Indian J Pharm Sci. 2011;73:208-215.
75. Rudraswamy-Math NR, Gupta VR. Formulation and evaluation of gastroretentive controlled release tablets of alfuzosin hydrochloride. Pak J Pharm Sci. 2015;28:2147-2152.
76. Sonani NG, Hiremath SP, Dasankoppa FS, Jamakandi VG, Sreenivas SA. Design and evaluation of gastroretentive mucoadhesive cephalexin tablets. Pharm Dev Technol. 2010;15:178-183.
77. Gangurde HH, Chordiya MA, Tamizharasi S, Senthilkumaran K, Sivakumar T. Formulation and evaluation of sustained release bioadhesive tablets of ofloxacin using 3(2) factorial design. Int J Pharm Investig. 2011;1:148-156.
78. Gattani SG, Londhe SG, Chalikwar SS, Amrutkar JR. Formulation and evaluation of gastroretentive drug delivery of verapamil hydrochloride. Eur J Parenter Pharm Sci. 2010;15:125-129.
79. Saritha D, Sathish D, Rao YM. Formulation and evaluation of gastroretentive floating tablets of domperidone maleate. J Appl Pharm Sci. 2012;2:68-73.
80. Jahagirdar HA, Kulkarni R, Kulkarni S. Pharmaceutical composition of rifaximin. U.S. patent 8383151. 2008; June 23.
81. Mandal UK, Chatterjee B, Senjoti FG. Gastro-retentive drug delivery systems and their *in vivo* success: a recent update. Asian J Pharm Sci. 2016;11:575-584.
82. Gautam CS, Saha L, Sekhri K, Saha PK. Iron deficiency in pregnancy and the rationality of iron supplements prescribed during pregnancy. Medscape J Med. 2008;10:283.
83. Tripathi J, Thapa P, Maharjan R, Jeong SH. Current state and future perspectives on gastroretentive drug delivery systems. Pharmaceutics. 2019;11:193.
84. Pawar VK, Kansal S, Garg G, Awasthi R, Singodia D, Kulkarni GT. Gastroretentive dosage forms: a review with special emphasis on floating drug delivery systems. Drug Deliv. 2011;18:97-110.
85. Lopes CM, Bettencourt C, Rossi A, Buttini F, Barata P. Overview on gastroretentive drug delivery systems for improving drug bioavailability. Int J Pharm. 2016;510:144-158.
86. Prinderre P, Sauzet C, Fuxen C. Advances in gastro retentive drug-delivery systems. Expert Opin Drug Deliv. 2011;8:1189-1203.
87. Achi AA, Gupta MR, Stagner WC. Integrated pharmaceutics: applied preformulation, Product design, and Regulatory science (1st ed). John Wiley & Sons: New York, 2013:1;1024.
88. Mishra A, Shahiwala A. *In-vitro* and *in-vivo* tools in drug delivery research for optimum clinical outcomes (1st ed). CRC Press, New York, 2018:1;350.
89. Kotreka UK, Adeyeye MC. Gastroretentive floating drug-delivery systems: a critical review. Crit Rev Ther Drug Carrier Syst. 2011;28:47-99.
90. Waterman KC. A critical review of gastric retentive controlled drug delivery. Pharm Dev Technol. 2007;12:1-10.